

## Response to Referee #1

The paper “Spatial-scale dependence of aerosol indirect effects over land in eastern China: A comparative analysis” by Yuqin Liu et al. investigates the effect of spatial scale on the sensitivity of cloud droplet effective radius (CER) to aerosol optical depth (AOD) and on the sensitivity of cloud droplet number ( $N_d$ ) concentration to AOD, for two different time periods (2008–2014 and 2015–2022) in the eastern region of China. The present study is of scientific interest, falls within the scope of ACP, the manuscript is really well-written and even better well-structured, the presentation clear, the language fluent. I recommend publication in ACP; however, I recommend to the authors the following revisions and modifications. Since the study is already at a good level, I would argue the authors to see the comments in a positive way as made, raised by an approach and a view point of an external reader, as modifications that would improve the flow, and help other readers to better understand the outcomes and the scope of the study, improving also specific points that it seems that there are gaps to fill.

The authors are grateful to Referee #1 for the valuable time spent on thorough reading our manuscript and providing expert views to guide us for improving the manuscript with the main and specific points and the references. We have taken notice of all comments, listed below in black, and made many changes to the manuscript to address these, together with the comments from the other referees. All modifications in the revised manuscript have been highlighted for your convenience. We address each of your comments below and refer to our responses in the revised manuscript and provide line numbers (**clean version**) and copy text in “quotes”. Finally, relevant references have been added to the reference list.

### Main points

1) Abstract: The suggestion here is to re-write it in a different concept. The suggestion is to add somewhere in the beginning a sentence delineating the objective to the study, something like “... aims to reveal the sensitivity patterns of aerosol indirect effects to spatial scales, ...” and then referring to the datasets used to facilitate the results and the basic outcomes. In addition, please re-visit the sentence “decreases, reflecting the weaker of aerosol-cloud interactions for declining aerosol concentrations.”. It needs to be written clearer.

**Answer:** Thank you for this constructive comment. The abstract has been fully rewritten following the suggested conceptual framework. A clear statement of the study objective has been added at the beginning of the abstract as recommended. Subsequent content of the abstract is reorganized to sequentially introduce the utilized datasets, analytical methods, key results and main conclusions, to ensure a logical and coherent narrative that closely links data application to outcome derivation.

“This study aims to reveal patterns of the sensitivity of aerosol indirect effects to spatial scales and investigate the regulatory role of the liquid water path (LWP) in aerosol-cloud interactions over land in eastern China. Using MODIS and CALIOP satellite observations, we systematically analyzed the relationships between aerosol optical depth (AOD) and cloud properties (cloud droplet effective radius, CER; cloud droplet number concentration,  $N_d$ ) during two periods: 2008–2014 (period 1, high AOD) and 2015–2022 (period 2, decreasing AOD). The results show two distinct regimes of CER variation with LWP: a rapid growth regime ( $LWP < 55/50 \text{ g/m}^2$ ) and a decreasing regime ( $LWP = 55\text{-}135/50\text{-}100 \text{ g/m}^2$ ) (thresholds vary by period). The sensitivity of CER to AOD ( $S_{CER}$ ) exhibited a negative correlation, with stronger sensitivity in the decreasing LWP regime than in the rapid growth regime. Spatial

scale (characterized by buffer size and study area) significantly modulated these sensitivities:  $|S_{CER}|$  and the positive sensitivity of  $N_d$  to AOD ( $S_{N_d}$ ) both decreased with increasing spatial scale. Optimal buffer sizes range from  $6^\circ \times 6^\circ$  to  $10^\circ \times 10^\circ$ : increasing with study area in period 2 but decreasing in period 1 for the decreasing LWP regime. Compared with period 1,  $|S_{CER}|$  in period 2 significantly reduced, reflecting the weakened aerosol-cloud interactions due to declining aerosol concentrations. Additionally, the optimal buffer sizes for  $S_{N_d}$  are larger in the  $8^\circ \times 8^\circ$  and  $10^\circ \times 10^\circ$  study areas than in  $4^\circ \times 4^\circ$  and  $6^\circ \times 6^\circ$  areas. This study reveals the scale-dependence of aerosol-cloud interactions, providing critical observational support for optimizing climate model parameterization schemes.”

The ambiguous sentence “decreases, reflecting the weaker of aerosol-cloud interactions for declining aerosol concentrations” has been revised for clarity and grammatical accuracy. The revised version is: “Compared with period 1,  $|S_{CER}|$  in period 2 significantly reduced, reflecting the weakened aerosol-cloud interactions due to declining aerosol concentrations.”, to explicitly clarify the causal relationship and eliminate the grammatical flaw in the original expression.

2) “Buffer size”: Though the authors have tried to delineate the concept, it needs further improvements. From the reviewer’s point of view, and since this is a core-element of the study, I would suggest further effort on explaining this concept. I would argue the authors to address this as a constructive point, improvement is needed.

**Answer:** We sincerely appreciate the reviewer’s constructive comment on the clarification of “buffer size”, which is indeed a core concept of this study. We have further refined and supplemented the explanation of this concept in the revised manuscript to enhance its clarity and comprehensibility. We have also ensured the consistency of the concept’s expression throughout the manuscript to avoid any potential ambiguity for readers. See the text in the Section 2.4 lines 331-333 and 338-364.

The text “Here, the spatial scales are described by two parameters: study area size (the geographic scope of the analysis) and buffer size (the local spatial extent around each observation point for aggregating aerosol and cloud data).” in Section 2.4 lines 331-333.

The text “Buffer size refers here to a circular spatial domain centered at each CALIOP-detected point in the study area where CALIOP detected the presence of aerosols. Within this circular domain, MODIS-retrieved cloud and aerosol data (AOD, CER,  $N_d$ , LWP) are spatially averaged to construct matched aerosol-cloud datasets at different local scales. This approach assumes that aerosol properties are reasonably homogeneous between adjacent clear and cloudy regions (Anderson et al., 2003; Quaas et al., 2008), which is a plausible considering the short-range transport of aerosols (e.g., 10-300 km) and the near-simultaneous observations (1-2 minutes) by MODIS and CALIOP within the A-Train constellation.

Buffer zones with sizes increasing from 10 to 300 km (10 km, 20 km, 30 km, 40 km, 50 km, 60 km, 70 km, 80 km, 90 km, 100 km, 120 km, 140 km, 150 km, 160 km, 180 km, 200 km, 250 km, and 300 km) were determined within the whole study area by using CALIOP data. Previous observations indicate that the typical horizontal scale of cloud clusters ranges from tens to hundreds of kilometers (Zhang et al., 2024; Cai et al., 2022), supported by CloudSat/CALIPSO satellite data showing power-law distributed cloud scales (10-1000 km fitting range) covering major cloud types (Zhang et al., 2024) and regional evidence of consistent multi-season, multi-latitude cloud extents (Cai et al., 2022). Meanwhile, aerosol spatial homogeneity varies with distance: local-scale aerosols ( $\leq 50$  km) exhibit high homogeneity due to consistent sources and stable diffusion, while regional-scale aerosols ( $>$

100 km) show enhanced heterogeneity from multi-source mixing and atmospheric transport (Hassan et al., 2024; Mohebalhojeh et al., 2026). Thus, the 10–300 km buffer range covers both cloud characteristic scales and the aerosol homogeneity transition range, ensuring that MODIS data averaging effectively captures cloud-aerosol coupling. This range avoids insufficient MODIS pixel coverage due to excessively small buffer sizes (< 10 km). It also prevents conflation between regional meteorological variations and local aci signals arising from overly large buffer sizes (> 300 km), as synoptic-scale circulation and other regional meteorological changes may interfere with local aci signals (Quaas et al., 2010). Meanwhile, this range aligns with the 50–150 km buffer sizes widely adopted in regional aci studies (Wang et al., 2015; Liu et al., 2017; 2024), enabling cross-validation of results and ensuring that MODIS data averaging effectively captures cloud-aerosol coupling.” in Section 2.4 lines 338-364.

3. A basic comment is that frequently the manuscript needed references that were missing. In the following part of the review suggestions on parts that need a reference-or-two will follow. For instance:

3.1) at the end of the sentence in lines 43, 44, and 45, references are needed.

**Answer:** Added. See the text in the Introduction lines 46-49.

“An increase in CCN concentrations results in a larger number of cloud droplets ( $N_d$ ), and if the cloud liquid water path (LWP) remains constant, it leads to a reduction in the cloud droplet effective radius (CER) (Twomey, 1977; Feingold et al., 2001).”

3.2) for the arguments in lines 55, 56, and 57: for each of the “satellite observations”, “aircraft measurements”, “ground-based monitoring”, and “numerical simulations” add one-or-two references, to show the importance of the research on atmospheric dust.

**Answer:** Added. See the text in the Introduction lines 59-62.

“Extensive research on the impact of aerosols on the microphysical properties of clouds has been conducted utilizing satellite observations (Liu et al., 2017; Jia et al., 2022), aircraft measurements (Jia et al., 2019; Zheng et al., 2024), ground-based monitoring (Sarna et al., 2016; Zheng et al., 2020), and numerical simulations (Lee et al., 2025; Li et al., 2008).”

4. 3.3) line 60 and “MODIS”. When referencing to instruments, references are required.

**Answer:** Added. See the text in the Introduction lines 64-66.

“However, optical satellite sensors such as the Moderate Resolution Imaging Spectroradiometer (MODIS) cannot effectively penetrate cloud layers (King et al., 2003; Kaufman et al., 2005; Remer et al., 2005), making it difficult to directly retrieve the optical properties of aerosols underneath clouds.”

3.4) line 97 and “CALIOP”. Similar comment with the above.

**Answer:** Added. See the text in the Introduction lines 108-110.

“In addition, significant progress has been made in research based on Cloud-Aerosol Lidar with Orthogonal Polarization (CALIOP) data (Winker et al., 2007).”

3.5) line 142 and “particularly during spring”: add references on dust climatology over the region of interest.

**Answer:** Added. See the text in the Section 2.1 line 182.

“Eastern China presents a unique atmospheric laboratory due to its complex aerosol composition - featuring both anthropogenic pollutants from industrial emissions and natural mineral dust transported from Central Asian deserts, particularly during the spring (Proestakis et al., 2018; Liu et al., 2021).”

3.6) line 155 and “cloud systems”: add references.

**Answer:** Added. See the text in the Section 2.2 line 195-197.

“The satellite’s equator crossing time is 13:30 (Local time, i.e. in the early afternoon, coinciding with optimal development conditions for continental warm cloud systems (Wang et al., 2014; Liu et al., 2024).”

3.7) lines 204-206: add references.

**Answer:** Added. See the text in the Section 2.3 lines 288-290.

“Under specific environmental conditions, aerosol particles can transform into CCN or INP, a process primarily determined by their chemical composition and ambient temperature (Bellouin et al., 2020).”

3.8) lines 361-363: add references.

**Answer:** Added. See the text in the Section 3.2.2 lines 504-506.

4) line 82 and “exhibited positive values over land and negative values over oceans”: complete the sentence on positive and negative values of what.

**Answer:** Corrected. See the text in the Introduction lines 87-90.

“They concluded that the sensitivity of retrieved CER to AOD generally exhibited positive values over land and negative values over oceans, and pointed out that using grids larger than  $4^{\circ}\times 4^{\circ}$  could introduce significant errors due to the spatial variability of aerosol and cloud parameters.”

5) line 91 and “only two of these”: add which regions.

**Answer:** Corrected. See the text in the Introduction lines 101-102.

“Their results indicated that only two of these regions, near the coasts of the Gulf of Mexico and the South China Sea, exhibited a positive correlation between CER and AOD.”

6) lines 93 and 94 and “aerosol and cloud properties”: it would be good to add information on the kind on properties (e.g., physical, chemical, optical, ...), naming them.

**Answer:** Corrected. See the text in the Introduction lines 102-105.

“Similarly, Jones et al. (2009) utilized multi-source remote sensing data and applied a point spread function to derive the mean AOD within a 20 km range, which was designed to match the native 20 km resolution of the corresponding cloud properties (cloud optical thickness, COT; LWP; CER; cloud top pressure, CTP).”

7) line 98 and “calculating aerosol”: calculating aerosols what? AOD? a532nm, CCN, ...? Please be more specific.

**Answer:** Corrected. See the text in the Introduction lines 110-115.

“For instance, Costantino et al. (2010) used CALIOP data to investigate the aerosol influence on CER in stratocumulus clouds over the coastal regions of Namibia and Angola. They performed the analysis by co-locating an aerosol index (based on AOD and the Ångström exponent) with CER within a 150 km buffer zone around CALIOP observations. They found that there was no correlation between aerosol load and CER when aerosol and cloud layers were clearly separated, but a strong correlation when lidar profiles indicated mixing.”

8) General the comment on the introduction: frequently in the paragraph studies are mentioned to support the necessity of the study, and this is the approach of the present study. However, in this paper, there are studies that are referencing without properly mentioning the core outcomes and conclusions of the studies, to pave the road for the present study. This leaves a potential reader confused on which is the point of mentioning them if not for also fulfilling the point of delineating the scientific gap. It would be towards the right direction if the authors revisit the introduction and work more on the studies that are mentioned, to bring everything together in the end.

**Answer:** Thank you for this constructive comment. We fully agree that clarifying the core findings of cited studies and linking them explicitly to the scientific gaps addressed in our work is critical for strengthening the logical flow of the introduction.

To address this issue, we have revised the introduction as follows (See the text in the Introduction lines 84-157):

“Currently, researchers usually use grid methods (such as  $1^\circ \times 1^\circ$ ,  $2^\circ \times 2^\circ$ , etc.) to study the aerosol indirect effects in large areas (Bréon, 2002; Kaufman et al., 2005; Bulgín et al., 2008; Quaas et al., 2008). For instance, Grandey and Stier (2010) estimated the relationship between aerosols and CER on a global scale ( $60^\circ\text{N}$ – $60^\circ\text{S}$ ) using multiple spatial resolutions ( $1^\circ \times 1^\circ$ ,  $4^\circ \times 4^\circ$ ,  $8^\circ \times 8^\circ$ ,  $15^\circ \times 15^\circ$ , and  $60^\circ \times 60^\circ$ ). They concluded that the sensitivity of retrieved CER to AOD generally exhibited positive values over land and negative values over oceans, and pointed out that using grids larger than  $4^\circ \times 4^\circ$  could introduce significant errors due to the spatial variability of aerosol and cloud parameters. Additionally, the study highlighted that, when using grids larger than  $4^\circ \times 4^\circ$  to investigate the relationship between aerosols and CER, significant errors could be introduced in calculating the aerosol indirect effect index due to the spatial variability of aerosol and cloud parameters.

For studies focusing on smaller regions, researchers often employ a moving window or a fixed area referred to as a buffer zone, within which the distribution of aerosol concentrations is assumed to be uniform. Spatially matched samples are constructed by averaging AOD and

cloud parameters within the window or buffer zone. The choice of the window or buffer size is often arbitrary, and existing studies rarely systematically explore how the detection of aci signals is influenced by the size of the area. For example, Yuan et al. (2008) used a 100 km × 100 km moving window to calculate the mean values of AOD and cloud properties to investigate the relationship between aerosols and CER across seven global regions. Their results indicated that only two of these regions, near the coasts of the Gulf of Mexico and the South China Sea, exhibited a positive correlation between CER and AOD. Similarly, Jones et al. (2009) utilized multi-source remote sensing data and applied a point spread function to derive the mean AOD within a 20 km range, which was designed to match the native 20 km resolution of the corresponding cloud properties (cloud optical thickness, COT; LWP; CER; cloud top pressure, CTP). Their study examined the influence of aerosol types, cloud conditions, and atmospheric factors on aerosol indirect effects across six different oceanic regions globally, finding that the sensitivity of cloud properties to AOD varied substantially with regional characteristics. In addition, significant progress has been made in research utilizing observations from the Cloud-Aerosol Lidar with Orthogonal Polarization (CALIOP) data (Winker et al., 2007). For instance, Costantino et al. (2010) used CALIOP data to investigate the aerosol influence on CER in stratocumulus clouds over the coastal regions of Namibia and Angola. They performed the analysis by co-locating an aerosol index (based on AOD and the Ångström exponent) with CER within a 150 km buffer zone around CALIOP observations. They found that there was no correlation between aerosol load and CER when aerosol and cloud layers were clearly separated, but a strong correlation when lidar profiles indicated mixing. Costantino et al. (2013) further analyzed the statistical relationship between aerosol concentrations and cloud physical parameters by examining aerosol and cloud properties within a 20 km buffer zone around CALIOP samples, integrating vertical profiles of aerosol and cloud data. Their statistics also clearly showed that cloud micro-physical properties were affected by aerosols when aerosol and cloud layers were mixed, decreasing the CER. It is noted that these two studies by Costantino et al. (2010, 2013) reached consistent conclusions about aci (i.e., aerosols modulate CER when layers interact), by adopting different buffer sizes (150 km vs. 20 km) to target distinct study areas. This demonstrates that the buffer size is tailored to the research objectives rather than through a systematic sensitivity analysis. Wang et al. (2015) revealed an inverse “Twomey” effect between aerosols and CER in eastern China by analyzing aerosol concentrations and CER within a 50 km buffer zone around CALIOP samples. Their results showed that larger CER was associated with high AOD, which was attributed to the feedback of microphysical processes from intense competition for vapor in the presence of high aerosol concentrations and the evaporation of smaller, less hygroscopic, droplets. Similarly, Liu et al. (2017) systematically examined the response mechanisms of warm cloud macro- and microphysical parameters to increasing AOD in the Yangtze River Delta region, also using CALIOP samples within a 50 km buffer zone. They found that the relation between cloud properties and AOD depended on the aerosol abundance, with a different behavior for low and high AOD (i.e.  $AOD < 0.35$  and  $AOD > 0.35$ ). However, both Wang et al. (2015) and Liu et al. (2017) used a fixed 50 km buffer zone without justifying the choice or exploring how varying buffer sizes might alter the strength or robustness of their findings—a common limitation in regional aci studies. More recently, Liu et al. (2024) quantified the relative importance of aerosols, meteorological parameters and their interactions for cloud properties in the eastern coastal and inland regions of China, utilizing MODIS  $1^\circ \times 1^\circ$  aerosol and cloud product data. Their study confirmed that CER decreased with the increase in AOD in the moderately polluted atmosphere ( $0.1 < AOD < 0.3$ ) over the East China Sea, whereas, in contrast, CER increased with increasing AOD in the polluted atmosphere ( $AOD > 0.3$ ) over the Yangtze River Delta. These studies have provided critical scientific insights into aci at regional scales, but the lack of systematic scale sensitivity analysis—especially for varying

window/buffer sizes within the same regional domain—leaves uncertainties about the generalizability of their conclusions.

However, the properties and interaction processes of aerosols and clouds are spatially significantly heterogeneous and scale dependent (McComiskey et al., 2009; McComiskey and Feingold, 2012; Chen et al., 2015; Glotfelty et al., 2020). McComiskey and Feingold (2012) explicitly pointed out that the “scale problem” is a major challenge in quantifying aerosol indirect effects, as the spatial scale of observation can mask or exaggerate the true interaction signals. In previous studies, the definitions of window size and buffer size have often been subjective, inadvertently introducing uncertainties into the research on aci. Although studies have explored the relationship between aerosols and CER across different observational scales, these investigations have primarily focused on larger spatial scales, leaving a gap in sensitivity analysis of aerosol indirect effects at smaller regional scales. For example, Grandey and Stier (2010) focused on global-scale grid resolutions but did not explore the scale dependence within regional domains; Wang et al. (2015) and Liu et al. (2017) used fixed buffer sizes (50 km) without investigating how varying buffer sizes affect the results. Therefore, utilizing multi-source remote sensing data to explore whether and how the aerosol indirect effect depends on observational spatial scales in eastern China is of great significance for developing parameterization schemes that align with the regional characteristics of aci.”

These revisions will ensure that each cited study serves a clear purpose in justifying the scientific rationale of our research, helping readers better understand the motivation and novelty of the present work.

9) Section 2.2. and Data used. It would be towards the right direction to add a paragraph describing the degree of uncertainties behind the products used, especially of the CDR, LWP, COT, CTP, and CPI, this addition would be of particular importance, since the uncertainties of the aforementioned products are significantly higher than MODIS AOD.

**Answer:** Thank you for pointing out this important aspect. We fully agree that explicitly describing the uncertainties of AOD and key cloud products (CER, LWP, COT, CTP, and CPI) is critical for enhancing the transparency and rigor of our study, especially given their relatively higher uncertainty compared to MODIS AOD.

To address this comment, we will add the following paragraph to Section 2.2 “Data used” (lines 201-204 and lines 216-233) to clarify the uncertainty characteristics of the involved products, based on existing validation studies and official product documentation:

“The MODIS AOD (at 550 nm) Level 2 product (10 km × 10 km) has been validated against ground-based remote sensing data and the results show that 69.40% of the MODIS AOD data fall within the expected uncertainty of  $\pm (0.05 + 15 \%)$  over land (Levy et al., 2013).”

“Uncertainties in the MODIS C6.1 cloud parameters over land originate from instrument calibration, atmospheric correction, land surface properties, and model assumptions (Platnick et al., 2017, 2018). For COT, these include scene-dependent Level 1B data errors (1.5%–30%), land surface albedo errors ( $\pm 15\%$ ), and atmospheric correction errors ( $\pm 20\%$ ). The C6.1 algorithm addresses some prior limitations by inheriting C6’s optimized lookup table design, which reduces interpolation errors to 0.1%–0.2% for near-nadir views and corrects C5’s overestimation of thin-cloud COT (Platnick et al., 2017). CER uncertainties, stemming from solar irradiance error ( $\sim 4\%$  at 3.7  $\mu\text{m}$ ), atmospheric correction, and scattering differences, are

mitigated as C6.1 retains C6's separate multi-band reporting, thereby eliminating C5's systematic bias (Platnick et al., 2017). LWP uncertainty is linked to COT/CER retrieval errors and cloud-phase classification accuracy; the latter is improved by C6's voting-based phase algorithm (preserved in C6.1), which reduces misclassification over complex surfaces like vegetation and deserts (Marchant et al., 2015; Platnick et al., 2017). For CTP (1 km resolution), uncertainties from viewing angles and cloud structure are partially countered in C6.1 by assigning fill values when the 1 km retrieval fails, avoiding surface parameter defaults. For land clouds above 3 km, CTP accuracy reaches ~50 hPa (Baum et al., 2012). Finally, CPI adopts C6's weighted voting logic (replacing C5's sequential tree), with C6.1 maintaining an enhanced Phase Agreement Fraction against CALIOP/POLDER data, which reduces uncertainties from weak thin-cloud signals and complex land interference (Marchant et al., 2015; Platnick et al., 2017)"

This revision will provide readers with a clear understanding of the data quality and potential limitations, further strengthening the credibility of our study's findings.

10) line 160: The authors need to add a justification on the reason behind applying the threshold on 1.5, and not for instance 1.4, or 1.6? Add references or as a supplement the analysis made supporting this upper limit.

**Answer:** Thank you for this insightful comment. To address this concern, we will revise Line 160 and add the following justification in Section 2.2 "Data used" (lines 204-211):

"In this study, AOD larger than 1.5 was excluded from further analysis to mitigate potential retrieval overestimation. This threshold was selected based on two key considerations: (1) Christensen et al. (2017) used MOD06 C6 data (1 km × 1 km) and reported that "large aerosol optical depths remain in the MODIS-observed pixels near cloud edges, due primarily to 3D effects (Varnai and Marshak, 2009) and the swelling of aerosols by higher relative humidity"; (2) the threshold of 1.5 aligns with widely adopted thresholds in regional aerosol-cloud interaction studies over eastern China, where high AOD often coincides with complex surface conditions (e.g., urbanization, heterogeneous land cover) that exacerbate retrieval biases (Wang et al., 2015; Liu et al., 2017, 2021)."

This revision ensures the AOD threshold is not arbitrary but grounded in product characteristics, literature consensus, and data sensitivity, enhancing the transparency and rigor of our data processing steps.

10) Paragraph in lines 180-188: Please revisit the paragraph, the references are not so suitable. When referring to CALIOP and CALIPSO the Winker et al., 2009, 2010, and 2013 are the most suitable ones, the Winker et al., 2003 should change. Moreover, the Stephens et al., 2002 is at the early steps of the A-Train and the authors should possibly add more updated references. Finally, CALIOP is not the "first" space-based lidar in space, so remove please correct this part.

**Answer:** Corrected. See the text in the Section 2.2 lines 249-255.

"CALIPSO (Cloud-Aerosol Lidar and Infrared Pathfinder Satellite Observations) operates within the A-Train constellation alongside the Aqua satellite and other NASA Earth-observing platforms. The primary instrument aboard CALIPSO is the Cloud-Aerosol Lidar with Orthogonal Polarization (CALIOP). CALIOP is a two-wavelength, polarization-sensitive lidar specifically designed to provide high-resolution vertical profiles of aerosols and clouds on a

global scale (Winker et al., 2009). The mission and its lidar instrument are described in Winker et al. (2009), and the associated Level 1 data products are detailed in Winker et al. (2010).”

11) Table 1: add more information on the products used, especially in terms of CALIOP, the list is not complete I guess, I am left of the impression that more observations and products were applied than just the coordinates.

**Answer:** Thanks for your reminder! Just to clarify: In this study, we only used latitude, longitude, and time information from CALIOP. This is because CALIOP and MODIS are both part of the A-Train satellite constellation, and their observation time difference is controlled within 1–2 minutes. This coordinated observation ensures that the MODIS aerosol (AOD) and cloud parameter data corresponding to the CALIOP positioning buffer are “quasi-simultaneous”, which effectively avoids interferences such as aerosol diffusion and cloud physical state evolution caused by observation time lags—an advantage that positioning methods like random grid points or ground stations cannot match. Subsequently, we calculated the mean values of MODIS AOD and cloud parameters within each CALIOP positioning buffer to conduct correlation analysis of aerosol indirect effects. We also added the text in the Section 2.2 lines 261-263.

“This temporal synchronization guarantees data consistency when extracting coincident measurements, avoiding interferences such as aerosol diffusion and cloud evolution caused by observational time lags—an advantage unparalleled by positioning methods like random grid points and ground-based stations.”

12) end of section 2.3: It would be fair to the approach and the readers to provide a paragraph reporting the assumptions and uncertainties of the methods/equations, and as such the limitations, in order to facilitate also future studies.

**Answer:** Thank you for this valuable suggestion. We fully agree that explicitly outlining the key assumptions, inherent uncertainties, and limitations of the data processing methods in Section 2.3 is essential for enhancing the transparency of our study and providing meaningful references for future research.

To address this comment, we have added the following paragraph at the end of Section 2.3 lines 316-327:

“This method quantifies the sensitivity of CER and  $N_a$  to AOD variations via linear regression in log-log space, using Eq. 1 and Eq. 2, respectively. Its core assumptions, uncertainties, and limitations are highly consistent: both rely on AOD as an aerosol proxy variable, assume constant cloud liquid water content and a linear sensitivity relationship, and depend on the reliability of satellite-retrieved parameters (Feingold et al., 2001; Gryspeerdt et al., 2023). However, AOD cannot distinguish aerosol size and hygroscopicity, retrieval errors are substantial in clean conditions, and linear fitting fails to capture nonlinear/non-monotonic responses. Both methods are constrained by satellite retrieval biases, limited scenario applicability (only valid for specific homogeneous clouds and aerosol types), the omission of key modulating factors (dynamical conditions, aerosol type) and feedback processes, and can only assess first-order direct effects. Reliability requires scenario constraints and uncertainty analysis; the only nuances come from the target variable (CER vs.  $N_a$ ), which do not alter the shared methodological limitations.”

13) Section 2.4 line 236: at some point the comparison of clouds' horizontal extent with the spatial homogeneity of aerosols should be discussed.

**Answer:** Thank you for highlighting this critical point. We fully agree that discussing the relationship between cloud horizontal extent and aerosol spatial homogeneity is essential for justifying the multi-scale analysis framework in Section 2.4, as it directly affects the validity of assuming aerosol homogeneity within buffer zones.

To address this comment, we will add the following discussion in Section 2.4 lines 348-364:

“Previous observations indicate that the typical horizontal scale of cloud clusters ranges from tens to hundreds of kilometers (Zhang et al., 2024; Cai et al., 2022), supported by CloudSat/CALIPSO satellite data showing power-law distributed cloud scales (10-1000 km fitting range) covering major cloud types (Zhang et al., 2024) and regional evidence of consistent multi-season, multi-latitude cloud extents (Cai et al., 2022). Meanwhile, aerosol spatial homogeneity varies with distance: local-scale aerosols ( $\leq 50$  km) exhibit high homogeneity due to consistent sources and stable diffusion, while regional-scale aerosols ( $> 100$  km) show enhanced heterogeneity from multi-source mixing and atmospheric transport (Hassan et al., 2024; Mohebalhojeh et al., 2026). Thus, the 10–300 km buffer range covers both cloud characteristic scales and the aerosol homogeneity transition range, ensuring that MODIS data averaging effectively captures cloud-aerosol coupling. This range avoids insufficient MODIS pixel coverage due to excessively small buffer sizes ( $< 10$  km). It also prevents conflation between regional meteorological variations and local aci signals arising from overly large buffer sizes ( $> 300$  km), as synoptic-scale circulation and other regional meteorological changes may interfere with local aci signals (Quaas et al., 2010). Meanwhile, this range aligns with the 50–150 km buffer sizes widely adopted in regional aci studies (Wang et al., 2015; Liu et al., 2017; 2024), enabling cross-validation of results and ensuring that MODIS data averaging effectively captures cloud-aerosol coupling.”

14) Central hypothesis of the comparison between the two periods is that LWP is more or less similar, allowing comparison between AOD and CER/ $N_d$  in terms of spatial sensitiveness. Please add at some point discussion on the degree that this hypothesis holds.

**Answer:** Thank you for this critical observation. We fully agree that verifying the similarity of LWP characteristics between the two study periods (2008–2014 and 2015–2022) is essential to validate the core hypothesis of our comparative analysis—ensuring that differences in aerosol-cloud sensitivity ( $S_{CER}/S_{N_d}$ ) are primarily driven by changes in AOD rather than variations in LWP.

To address this comment, we will add the following discussion in Section 4.1 lines 636-651:

“The central hypothesis of this study—that LWP is relatively consistent between the two periods (2008–2014 and 2015–2022), supporting valid comparisons of the spatial sensitivity of AOD-CER relationships—is well-supported by the following analysis. The differences in the mean, median, 25th, and 50th percentiles of LWP between the two periods are all less than 5%, indicating a stable overall water vapor supply level. The spatial patterns of high-LWP regions (e.g., southeastern areas) and low-LWP regions (e.g., the mountainous areas in northern Shanxi) remained stable across the two periods (see Supplement Figure S1), demonstrating LWP spatial distribution characteristics are highly consistent. The sample proportions of LWP in the rapid growth regime are 59.30% (period 1: 0–55 g/m<sup>2</sup>) and 55.36% (period 2: 0–50 g/m<sup>2</sup>),

while those in the decreasing regime are 29.64% (period 1: 55–135 g/m<sup>2</sup>) and 24.59% (period 2: 50–100 g/m<sup>2</sup>), suggesting that there is no systematic temporal shift in the LWP distribution. Meanwhile, short-term fluctuations are smoothed by multi-year averaging and large-sample statistics, resulting in a weak indirect impact of aerosols on LWP (LWP only increased by 5.6%, much smaller than the 24% decrease in AOD). Additionally, LWP-stratified analysis further isolates interference. The validation of the core hypothesis provides a reliable premise for accurately quantifying the impact of aerosol concentration changes on the sensitivity of cloud parameters and their spatial scale dependence.”

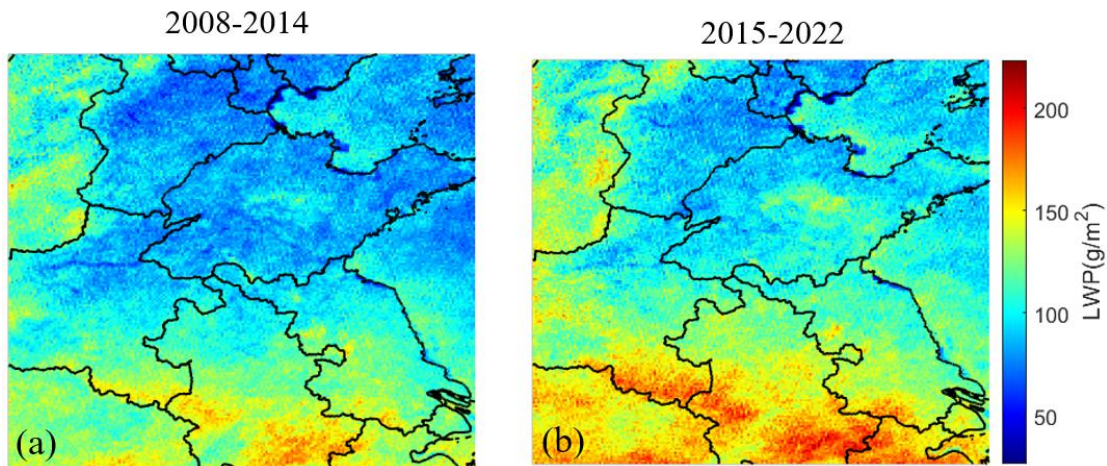


**Figure S1. Spatial distributions of LWP averaged over the years 2008-2014 (a) and 2015-2022 (b) over the study area. The lines are provincial borders and the names of provinces mentioned in the text are indicated in Fig. 3(f).**

15) Lines 261-262 and lines 269-270: please add at least at one map the Hebei, Shandong, Shanxi, and Anhui provinces at a map, not everyone is familiar with the geographical areas and provinces in terms of where they are located.

**Answer: Corrected.**

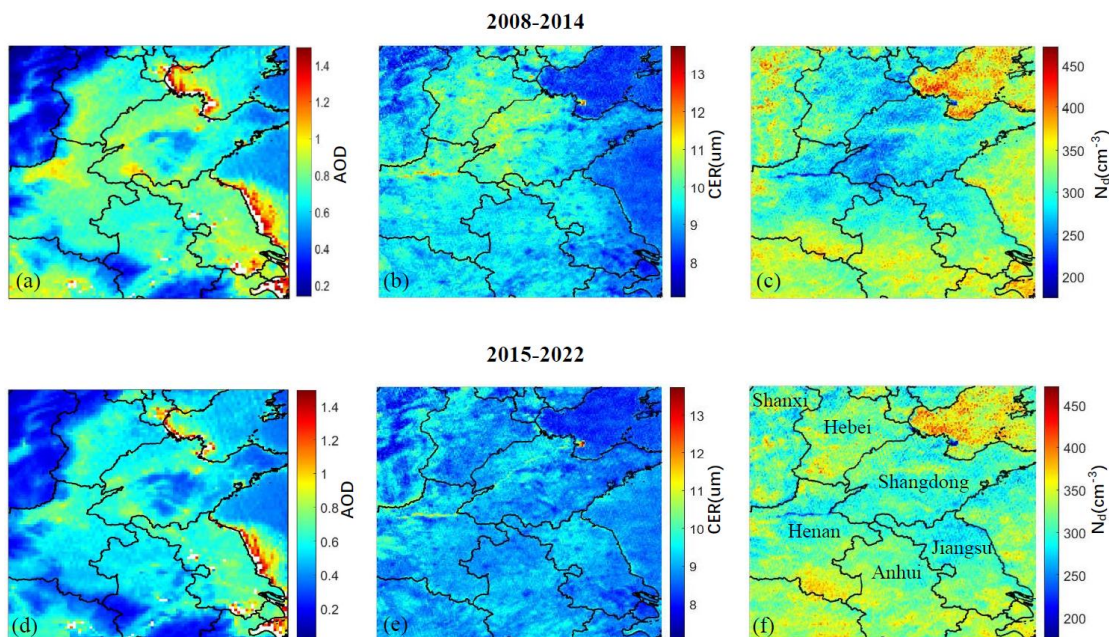


Figure 3. Spatial distributions of AOD (a, d), CER (b, e) and  $N_d$  (c, f), averaged over the years 2008-2014 (top row) and 2015-2022 (bottom row) over the study area.

16) line 268: correct “.,”.

**Answer:** Corrected.

17) Lines 314-318: When providing results of the analysis discuss on the reasons “why” behind the results is of significance. A connection with theory is missing in this section. The paper would benefit by adding a few lines at the end of the section.

**Answer:** Thank you for this valuable suggestion. We fully agree that explaining the “why” behind the results—by linking them to aerosol-cloud interaction theory — is critical for deepening the scientific insight of Section 3.2.1 (Rapid CER growth regime) and enhancing the paper’s rigor.

To address this, we will add the following lines at the end of Section 3.2.1 lines 461-463 and Section 4.2 lines 662-673, connecting the observed scale-dependent  $SCER$  patterns to theoretical mechanisms:

“The decrease of  $|SCER|$  with increasing study area is mechanistically tied to scale-dependent aerosol indirect effect theory and meteorological confounding (Quaas et al., 2009; McComiskey & Feingold, 2012).”

“The results from this study suggest that AOD-cloud property correlations in large study areas are susceptible to meteorological confounding effects (Quaas et al., 2010; Boucher and Quaas, 2012; Gryspeerdt et al., 2014; Liu et al., 2024). Theoretically, aerosol regulation of cloud microphysics is strongly local: smaller domains (e.g.,  $4^\circ \times 4^\circ$ ) feature homogeneous meteorological conditions (humidity, updrafts), preserving undiluted aerosol-cloud interaction signals and yielding larger  $|SCER|$  (pronounced Twomey effect). In contrast, expanded domains (e.g.,  $10^\circ \times 10^\circ$ ) encompass heterogeneous meteorological conditions (circulation differences, boundary layer variability) that independently modulate cloud droplet growth. For example, strong updrafts enhance liquid water supply, offsetting aerosol-induced radius reduction (Altartatz et al., 2014), weakening aerosol-CER correlations and reducing  $|SCER|$ . Consistent with Grandey & Stier (2010), large-scale domains introduce “dilution bias” via non-target meteorological variability. This scale-dependent confounding mechanism elucidates uncertainties in aerosol indirect effect assessments at regional scales.”

18) Lines 369-371: In general it is missing an explanation on the mechanisms resulting to the observed patterns, here are results provided without any connection with theory or at least some brief discussion. The section can be significantly improved.

**Answer:** Thank you for this constructive feedback. We fully agree that supplementing mechanistic explanations—linking the observed  $SCER$  patterns in the decreasing LWP regime to aerosol-cloud interaction theories and physical processes—is critical for enhancing the scientific depth of Section 3.2.2 and addressing the “why” behind the results.

To address this gap, we will add the following discussion at the end of Section 3.2.2 lines 514-516 and Section 4.1 lines 602-624, integrating theoretical mechanisms with the observed results:

“This pattern highlights the dominant role of LWP in regulating aerosol-cloud interaction sensitivity, with AOD variations further modulating the magnitude of such differences.”

“Comparative analysis of scale-conditioned  $S_{CER}$  across LWP regimes in periods 1 and 2 revealed markedly enhanced sensitivity of  $S_{CER}$  to AOD in the second LWP regime. There is a trade-off between AOD and LWP when the amount of water vapor is insufficient and CER becomes smaller. As suggested by Costantino et al. (2013), the LWP response to aerosol invigoration is influenced by two competing mechanisms: a drying effect caused by enhanced entrainment of dry air at cloud top (dominant in optically thin clouds) and a moistening effect from precipitation suppression (dominant in optically thick clouds). For larger LWP, the supply of cloud water is sufficient, and the increase in aerosol number concentrations significantly affects the distribution of cloud droplet number concentrations and sizes, enhancing the sensitivity of CER to AOD. For small aerosol concentrations, the values of  $|S_{CER}|$  (Figure 5b, 7b) decreased overall with expanding buffer size within the same study area. For fixed buffer size,  $|S_{CER}|$  decreased as the study area increased, and the ranges of  $|S_{CER}|$  values across different study area showed a convergent pattern, typically remaining small (close to zero). During the high AOD period (2008–2014), anthropogenic emissions and dust transport provided abundant CCN, laying the material foundation for aerosol-cloud interactions. This enhanced the synergistic effect of “sufficient liquid water + abundant CCN” in the second LWP regime, amplifying the difference in  $S_{CER}$  between the two LWP regimes. In the period of decreasing AOD (2015–2022), following the implementation of clean air policies (de Leeuw et al., 2021; 2023), CCN concentration decreased (Wang et al, 2023), weakening the direct impact of aerosols on CER. However, the LWP-driven microphysical differences persisted, so  $S_{CER}$  in the second regime remained significantly smaller than that in the first regime, albeit with a smaller difference. Additionally, the complexity of aerosol types during the high AOD period (e.g., mixing of anthropogenic pollutants and natural dust) may have adjusted the value of  $S_{CER}$ , but did not alter the dominant role of LWP. This aligns with the theory that “aerosol indirect effects are jointly regulated by concentration and type” (Liu et al., 2017).”

19) Section 3.3: At some point discussion of AOD has to be included, in terms of composition. The aerosol composition resulting to the AOD over the two periods may have significantly changed due to the policies imposed, therefore the impact of AOD on clouds may be very different, even for exact same AOD values, since the relative percentage of different aerosol species will be different. Add at least some discussion on this aspect, to be fair with the analysis, the hypothesis that are made, and the readers.

**Answer:** Thank you for highlighting this important aspect. We fully agree that discussing potential changes in aerosol composition between the two periods (2008–2014 and 2015–2022) is critical for contextualizing the observed  $S_{Nd}$  patterns—since aerosol composition directly affects CCN activity and thus the impact of AOD on cloud microphysics, even for identical AOD values.

To address this gap, we will add the following discussion in Section 3.3 lines 560-575, linking aerosol composition changes to policy impacts and cloud sensitivity:

“The chemical composition of aerosols, which directly affects AOD and CCN activation efficiency, underwent significant changes between the two periods due to policy interventions. During 2008–2014, aerosols over eastern China were dominated by sulfate, which accounted for 30%–40% of the  $PM_{2.5}$  mass (Huang et al., 2014; Zheng et al., 2018). Given the strong hygroscopicity of sulfate-dominated aerosols (Zhang et al., 2012; Liu et al., 2023), their CCN

activation efficiency was likely high, which may have provided a critical physical basis for the aerosol-cloud indirect effect (Lee et al., 2009). In the period of 2015–2022, driven by policies such as the Air Pollution Prevention and Control Action Plan (Zheng et al., 2018), the chemical composition of aerosols underwent a structural transition. Specifically, the mass fraction of sulfate dropped sharply to 15%–25% with an absolute concentration reduction of more than 50%, while the relative proportions of nitrate, carbonaceous aerosols (i.e., organic carbon (OC) and black carbon (BC)), and secondary organic aerosols (SOA) showed an increasing trend (Huang et al., 2014; Zheng et al., 2018). As these components generally exhibit weaker hygroscopicity compared with sulfate (Zhang et al., 2012; Liu et al., 2023), such a compositional shift might have led to a decrease in CCN activation efficiency under the same AOD conditions, thereby potentially weakening the sensitivity of cloud droplet number concentration to AOD and altering the intensity and mode of aerosol-cloud interactions to a certain extent (Lee et al., 2009).”

20) Section 4. The discussion is well-written. However, some of the points raised should also appear accompanying the results and the discussion on the figures, and not appearing in this section for the first time.

**Answer:** We thank the reviewer for the positive feedback on the discussion and for this constructive suggestion. We have carefully integrated the key discussion points raised in Section 4 into the corresponding results sections and figure captions throughout the manuscript to ensure a more logical flow. The revisions are now reflected in the updated manuscript for the reviewer’s inspection.

## **4 Discussion**

### **4.1 The importance of liquid water path constraint**

LWP is a critical parameter governing cloud radiative properties (Murray-Watson et al., 2022). The quantification of albedo effects strongly depends on the spatial scale and the LWP. Neglecting LWP constraints in aerosol-cloud interaction studies can weaken microphysical signals, leading to underestimation of radiative forcing (McComiskey et al., 2012). To address this, we first systematically investigated the dynamic relationship between CER and LWP before analyzing CER sensitivity to AOD. The results demonstrate pronounced CER sensitivity to LWP variations, which can be categorized into three distinct regimes (Figure 4):

In the first LWP regime, CER increases rapidly with LWP, i.e. the evolution of CER is predominantly driven by changes in LWP. This dominance may lead to overestimation of the influence of the AOD on CER (Liu et al., 2021).

In the second LWP regime, CER decreases with increasing LWP. In this regime, the regulatory effect of LWP on CER weakens significantly, and CER variations become increasingly governed by aerosol-related processes, indicating the growing dominance of aerosol indirect effects.

The third regime contains an insufficient number of CER observations to yield statistically significant results, which excludes the analysis of the sensitivity of CER to AOD.

Comparative analysis of scale-conditioned  $S_{CER}$  across LWP regimes in periods 1 and 2 revealed markedly enhanced sensitivity of  $S_{CER}$  to AOD in the second LWP regime. There is a trade-off between AOD and LWP when the amount of water vapor is insufficient and CER becomes smaller. As suggested by Costantino et al. (2013), the LWP response to aerosol

invigoration is influenced by two competing mechanisms: a drying effect caused by enhanced entrainment of dry air at cloud top (dominant in optically thin clouds) and a moistening effect from precipitation suppression (dominant in optically thick clouds). For larger LWP, the supply of cloud water is sufficient, and the increase in aerosol number concentrations significantly affects the distribution of cloud droplet number concentrations and sizes, enhancing the sensitivity of CER to AOD. For small aerosol concentrations, the values of  $|S_{CER}|$  (Figure 5b, 7b) decreased overall with expanding buffer size within the same study area. For fixed buffer size,  $|S_{CER}|$  decreased as the study area increased, and the ranges of  $|S_{CER}|$  values across different study area showed a convergent pattern, typically remaining small (close to zero). During the high AOD period (2008–2014), anthropogenic emissions and dust transport provided abundant CCN, laying the material foundation for aerosol-cloud interactions. This enhanced the synergistic effect of “sufficient liquid water + abundant CCN” in the second LWP regime, amplifying the difference in  $S_{CER}$  between the two LWP regimes. In the period of decreasing AOD (2015–2022), following the implementation of clean air policies (de Leeuw et al., 2021; 2023), CCN concentration decreased (Wang et al., 2023), weakening the direct impact of aerosols on CER. However, the LWP-driven microphysical differences persisted, so  $S_{CER}$  in the second regime remained significantly smaller than that in the first regime, albeit with a smaller difference. Additionally, the complexity of aerosol types during the high AOD period (e.g., mixing of anthropogenic pollutants and natural dust) may have adjusted the value of  $S_{CER}$ , but did not alter the dominant role of LWP. This aligns with the theory that “aerosol indirect effects are jointly regulated by concentration and type” (Liu et al., 2017).

The larger  $S_{CER}$  observed at larger spatial scales (Figures 5 and 7) may be attributed to meteorological confounding effects. In addition, clouds with larger LWP are usually associated with strong updrafts (such as convective clouds), and stronger turbulence and vertical transport will bring more aerosols into the clouds, increasing CCN concentration and a decrease in particle size, making them more sensitive to changes in AOD (Jones et al., 2009; Han et al., 2022; Fan et al., 2025). Therefore, this phenomenon is the result of the combined action of cloud microphysical processes (CCN activation, cloud droplet competition growth) and dynamic processes (updrafts, turbulent mixing). If the characteristics of aerosols (such as composition) change in the second LWP regime, this sensitivity may be further amplified. Consequently, the LWP-stratified  $S_{CER}$  quantification framework enables precise characterization of scale-dependent aerosol-cloud interactions, providing robust physical insights for climate effect assessments and effectively reducing uncertainties in future climate projections.

The central hypothesis of this study—that LWP is relatively consistent between the two periods (2008–2014 and 2015–2022), supporting valid comparisons of the spatial sensitivity of AOD-CER relationships—is well-supported by the following analysis. The differences in the mean, median, 25th, and 50th percentiles of LWP between the two periods are all less than 5%, indicating a stable overall water vapor supply level. The spatial patterns of high-LWP regions (e.g., southeastern areas) and low-LWP regions (e.g., the mountainous areas in northern Shanxi) remained stable across the two periods (see Supplement Figure S1), demonstrating LWP spatial distribution characteristics are highly consistent. The sample proportions of LWP in the rapid growth regime are 59.30% (period 1: 0–55 g/m<sup>2</sup>) and 55.36% (period 2: 0–50 g/m<sup>2</sup>), while those in the decreasing regime are 29.64% (period 1: 55–135 g/m<sup>2</sup>) and 24.59% (period 2: 50–100 g/m<sup>2</sup>), suggesting that there is no systematic temporal shift in the LWP distribution. Meanwhile, short-term fluctuations are smoothed by multi-year averaging and large-sample statistics, resulting in a weak indirect impact of aerosols on LWP (LWP only increased by 5.6%, much smaller than the 24% decrease in AOD). Additionally, LWP-stratified analysis further isolates interference. The validation of the core hypothesis provides a reliable premise for

accurately quantifying the impact of aerosol concentration changes on the sensitivity of cloud parameters and their spatial scale dependence.

## 4.2 Scale dependence of cloud parameters sensitivities to aerosol variations

Extensive studies have demonstrated a significant spatial scale dependence of aerosol indirect effects (McComiskey et al., 2012; Possner et al., 2016; Glotfelty et al., 2020; Ekman et al., 2023). Failure to explicitly define the scale-dependent behavior of aerosol indirect effects may introduce systematic biases and inconsistencies in subsequent process analyses. Based on satellite observations, this study confirms statistically significant negative correlations between CER and AOD, as well as positive correlations between  $N_d$  and AOD during periods with different aerosol concentrations, aligning with classical aerosol-cloud interaction theory (Quaas et al., 2009). Analysis of scale-conditioned  $SCER$  and  $SN_d$  reveals that for fixed buffer size, an increase in the size of the study area leads to a systematic reduction in  $SCER$  (less negative) and  $SN_d$ , corroborating the nonlinear attenuation of aerosol signals with spatial domain expansion (Quaas et al., 2009). The results from this study suggest that AOD-cloud property correlations in large study areas are susceptible to meteorological confounding effects (Quaas et al., 2010; Boucher and Quaas, 2012; Gryspeerdt et al., 2014; Liu et al., 2024). Theoretically, aerosol regulation of cloud microphysics is strongly local: smaller domains (e.g.,  $4^\circ \times 4^\circ$ ) feature homogeneous meteorological conditions (humidity, updrafts), preserving undiluted aerosol-cloud interaction signals and yielding larger  $|SCER|$  (pronounced Twomey effect). In contrast, expanded domains (e.g.,  $10^\circ \times 10^\circ$ ) encompass heterogeneous meteorological conditions (circulation differences, boundary layer variability) that independently modulate cloud droplet growth. For example, strong updrafts enhance liquid water supply, offsetting aerosol-induced radius reduction (Altaratz et al., 2014), weakening aerosol-CER correlations and reducing  $|SCER|$ . Consistent with Grandey & Stier (2010), large-scale domains introduce “dilution bias” via non-target meteorological variability. This scale-dependent confounding mechanism elucidates uncertainties in aerosol indirect effect assessments at regional scales.

Multi-scale spatial analysis identifies different optimal buffer sizes for  $SCER$  and  $SN_d$  in different periods. These findings align closely with satellite-based aerosol indirect effect studies (Wang et al., 2015; Liu et al., 2017), providing critical scale benchmarks for satellite product validation. Wang et al. (2015) reported an inverse “Twomey” effect between aerosols and CER in eastern China by analyzing aerosol and CER within a 50 km buffer zone around CALIOP samples. Similarly, Liu et al. (2017) systematically examined the response mechanisms of warm cloud macro- and microphysical parameters to increasing AOD in the Yangtze River Delta region, also using CALIOP samples within a 50 km buffer zone. Present study further shows that, as aerosol concentrations decrease,  $SCER$  values across different study areas with the same buffer size exhibit convergence characteristics, with generally smaller  $SCER$  (closer to zero). This indicates a significant weakening of aerosol-cloud interaction intensity and reduced spatial extent dependency in low aerosol loading conditions. This phenomenon is consistent with the simulated behavior of aerosol-limited cloud regimes, where aerosol-cloud interactions are quantitatively modulated by moisture availability and lose their sensitivity to large-scale dynamical stability, leading to a weaker and more homogeneous effect (Zhao et al., 2025).

By systematically quantifying the scale-response characteristics of aerosol indirect effects, this work not only elucidates the dynamic scale behavior of aerosol-cloud interactions but, more critically, establishes criteria for determining optimal buffer size in regional aerosol indirect effect studies. Such advancements provide actionable insights for refining parameterization schemes in climate models, thereby enhancing their predictive reliability.

### 4.3 Contrasting sensitivity patterns of cloud parameters in response to AOD

A comprehensive comparison of the sensitivity  $S_{CER}$  and  $S_{Nd}$  reveals that the responses of CER and  $N_d$  to AOD exhibit distinct yet inherently interconnected characteristics. These characteristics are jointly modulated by spatial scale and LWP regimes (Figs. 5, 7, 8; Supplements Tables 1–2), which profoundly reflect the core microphysical mechanisms of aerosol-cloud interactions. Details are elaborated as follows:

#### 4.3.1 Core differences in response modes between $S_{CER}$ and $S_{Nd}$ to AOD

$S_{CER}$  is consistently negative across both periods and all LWP regimes ( $-0.33 < S_{CER} < 0$ ) (Figs. 5, 7; Supplement Table 1), indicating that an increase in AOD leads to a decrease in CER. This aligns with the core principle of the Twomey effect (Twomey, 1977; Feingold et al., 2001). The values of  $|S_{CER}|$  are larger in the second LWP regime than in the first regime, reflecting stronger aerosol modulation of cloud microphysical properties when liquid water is abundant (McComiskey & Feingold, 2012). In contrast,  $S_{Nd}$  maintains a significant positive correlation with AOD across all scenarios ( $0 < S_{Nd} < 1$ ) (Fig. 8; Supplement Table 2), confirming that higher AOD directly promotes CCN activation and thereby increases cloud droplet number concentration (Andreae, 2009).  $S_{Nd}$  is larger in small-scale study areas (e.g.,  $4^\circ \times 4^\circ$ ) and small buffer zones, with a maximum value of 0.45 in the first period, indicating greater sensitivity of cloud droplet number to aerosol loading at fine spatial scales.

#### 4.3.2 Synergistic modulation of AOD and spatial scale

Using the LWP interval corresponding to  $S_{Nd}$  ( $0 < LWP \leq 200 \text{ g/m}^2$ ) as a benchmark, comparisons between the two periods (incorporating average values of  $S_{CER}$  across two LWP regimes) reveal distinct characteristics:

For the small-scale study area ( $4^\circ \times 4^\circ$ ): In period 1, the average  $|S_{CER}|$  across two LWP regimes is 0.271 (0.2232 for the 0–55  $\text{g/m}^2$  LWP regime, 0.3189 for the 55–135  $\text{g/m}^2$  LWP regime) and  $S_{Nd}=0.4496$ , both significantly higher than those in period 2 (average  $|S_{CER}|=0.154$ , with 0.0863 for 0–50  $\text{g/m}^2$  LWP regime and 0.2212 for 50–100  $\text{g/m}^2$  LWP regime;  $S_{Nd}=0.2903$ ). The negative correlation between AOD and CER is more significant in period 1, as sufficient CCN in small-scale areas amplifies both cloud droplet number increase and size reduction, enhancing the Twomey effect.

For the medium-to-large scale study areas ( $6^\circ \times 6^\circ$ ,  $8^\circ \times 8^\circ$ ,  $10^\circ \times 10^\circ$ ): In period 1, the average  $|S_{CER}|$  across two LWP regimes is 0.1683 (0.1305 for 0–55  $\text{g/m}^2$ , 0.2061 for 55–135  $\text{g/m}^2$ ), 0.13065 (0.1026 for 0–55  $\text{g/m}^2$ , 0.1587 for 55–135  $\text{g/m}^2$ ), and 0.1067 (0.0858 for 0–55  $\text{g/m}^2$ , 0.0885 for 55–135  $\text{g/m}^2$ ), respectively, all higher than the corresponding values in period 2 (0.1516, 0.1246, 0.0985). However,  $S_{Nd}$  in period 1 (0.2430, 0.2050, 0.1430) is lower than that in period 2 (0.2960, 0.2680, 0.1740), with no significant difference in the negative correlation between AOD and CER between the two periods.

This characteristic indicates that meteorological confounding effects are enhanced at larger scales, weakening the regulation of  $S_{Nd}$  by aerosols, while at small scales the aci is directly driven by AOD levels.

#### 4.3.3 Implications for aerosol indirect effects

The differences and interconnections between  $S_{CER}$  and  $S_{Nd}$  highlight that aerosol indirect effects are dominated by coupled microphysical processes: Aerosol-induced increases in CCN first enhance  $N_d$  through positive  $S_{Nd}$ , and then reduce CER through negative  $S_{CER}$  under constant LWP conditions. The scale-dependent attenuation of both sensitivities and their modulation by LWP indicate that quantifying aerosol indirect effects requires full consideration of spatial scales and the key role of liquid water, providing observational basis for optimizing climate model parameterization schemes.

#### 4.4 Limitations and future perspectives

This study has three significant limitations. Firstly, similar to most previous studies (Wang et al., 2015; Liu et al., 2021), this study only utilized MODIS data with a resolution of 10 km to explore scale effects, ignoring finer or coarser resolution data. Therefore, using a 10 km buffer size as the minimum observation unit, this limitation makes the indirect effects of aerosols on smaller scales still unknown, which may lead to inaccurate evaluation of aerosol indirect effects. Therefore, future research can improve the sensitivity of aerosol indirect effects to scale changes by using observation data with higher accuracy or model simulations. Secondly, the current research focuses on the influence of buffer size and study areas, the potential impact of spatial aggregation methods (especially zoning directionality) on the quantitative results of aerosol indirect effects has not been systematically evaluated. Future research should further investigate the sensitivity of aerosol indirect effects to zoning direction. Moreover, the current study employs a uniform buffer size for both aerosol and cloud parameters, failing to account for potential interaction effects arising from discrepancies of buffer size between them. Therefore, clarifying scale dependence will avoid directly extrapolating local observation results to a larger study area when downscaling climate models or formulating regional environmental policies.

#### References

- Dagan, G., Yeheskel, N., Williams, A. I. L.: Radiative forcing from aerosol–cloud interactions enhanced by large-scale circulation adjustments, *Nature geoscience*, 16, 1092–1098, 2023.
- Twomey, S. Pollution and the planetary albedo, *Atmos. Environ.*, 1974, 41, 120–125.
- Feingold, G. Modeling of the first indirect effect: analysis of measurement requirements, *Geophys. Res. Lett.*, 30, 1997, doi:10.1029/2003GL017967, 2003.
- Jia, H., Quaas, J., Gryspeerdt, E., Böhm, C., & Sourdeval, O.: Addressing the difficulties in quantifying droplet number response to aerosol from satellite observations, *Atmospheric Chemistry and Physics*, 22(11), 7353–7372. <https://doi.org/10.5194/acp-22-7353-2022>, 2022.
- Sarna, K. and Russchenberg, H. W. J.: Ground-based remote sensing scheme for monitoring aerosol–cloud interactions, *Atmos. Meas. Tech.*, 9, 1039–1050, <https://doi.org/10.5194/amt-9-1039-2016>, 2016.
- Zheng, X., Xi, B., Dong, X., Logan, T., Wang, Y., and Wu, P.: Investigation of aerosol–cloud interactions under different absorptive aerosol regimes using Atmospheric Radiation Measurement (ARM) southern Great Plains (SGP) ground-based measurements, *Atmos. Chem. Phys.*, 20, 3483–3501, <https://doi.org/10.5194/acp-20-3483-2020>, 2020.

Lee, H.-H., Zheng, X., Qiu, S., and Wang, Y.: Numerical case study of the aerosol–cloud interactions in warm boundary layer clouds over the eastern North Atlantic with an interactive chemistry module, *Atmos. Chem. Phys.*, 25, 6069–6091, <https://doi.org/10.5194/acp-25-6069-2025>, 2025.

Li, G. H., Wang, Y., Zhang, R. Y.: Implementation of a two-moment bulk microphysics scheme to the WRF model to investigate aerosol-cloud interaction, *Journal of Geophysical Research-Atmospheres*, 113, D15, <https://doi.org/10.1029/2007JD009361>, 2008.

Kaufman, Y. J., Remer, L., Tanré, D., Li, R., Kleidman, R., Mattoo, S., Levy, R., Eck, T., Holben, B., Ichoku, C., Martins, J., and Koren, I.: A critical examination of the residual cloud contamination and diurnal sampling effects on MODIS estimates of aerosol over ocean, *IEEE Trans. Geosci. Remote Sens.*, 43, 2886–2897, 2005.

Winker, D. M., Hunt, W. H., and McGill, M. J.: Initial performance assessment of CALIOP, *Geophys. Res. Lett.*, 34, L19803, [doi:10.1029/2007GL030135](https://doi.org/10.1029/2007GL030135), 2007.

Proestakis, E., Amiridis, V., Marinou, E., Georgoulas, A. K., Solomos, S., Kazadzis, S., Chimot, J., Che, H., Alexandri, G., Biniotoglou, I., Daskalopoulou, V., Kourtidis, K. A., de Leeuw, G., and van der A, R. J.: Nine-year spatial and temporal evolution of desert dust aerosols over South and East Asia as revealed by CALIOP, *Atmos. Chem. Phys.*, 18, 1337–1362, <https://doi.org/10.5194/acp-18-1337-2018>, 2018.

Li, Z., et al.: Aerosol and monsoon climate interactions over Asia, *Rev. Geophys.*, 54, 866–929, [doi:10.1002/2015RG000500](https://doi.org/10.1002/2015RG000500), 2016.

Leung, G. R., Saleeby, S. M., Sokolowsky, G. A., Freeman, S. W., and van den Heever, S. C.: Aerosol–cloud impacts on aerosol detrainment and rainout in shallow maritime tropical clouds, *Atmos. Chem. Phys.*, 23, 5263–5278, <https://doi.org/10.5194/acp-23-5263-2023>, 2023.

Levy, R. C., Mattoo, S., Munchak, L. A., Remer, L. A., Sayer, A. M., Patadia, F., and Hsu, N. C.: The Collection 6 MODIS aerosol products over land and ocean, *Atmos. Meas. Tech.*, 6, 2989–3034, <https://doi.org/10.5194/amt-6-2989-2013>, 2013.

Platnick, S., et al.: MODIS Cloud optical properties: User guide for the Collection 6/6.1 level-2 MOD06/MYD06 product and associated level-3 data sets. v1.1, July 2018.

Platnick, S., K. G. Meyer, M. D. King, G. Wind, N. Amarasinghe, B. Marchant, G. T. Arnold, Z. Zhang, Hubanks, P. A., Holz, R. E., Yang, P., Ridgway, W. L., and Riedi, J.: The MODIS cloud optical and microphysical products: Collection 6 updates and examples from Terra and Aqua, *IEEE Trans. Geosci. Remote Sens.*, 55, 502–525, 2017.

Marchant, B., et al.: MODIS Collection 6 shortwave-derived cloud phase classification algorithm and comparisons with CALIOP, *Atmos. Meas. Tech. Discuss.*, 8, 11893–11924, 2015.

Baum, B. A., et al.: MODIS cloud-top property refinement for Collection 6, *J. Appl. Meteorol. Climatol.*, 51(6), 1145–1163, 2012.

Winker, D. M., Vaughan, M. A., Omar, A., Hu, Y., Powell, K. A., Liu, Z. Y., Hunt, W. H., Young, S. A.: Overview of the CALIPSO Mission and CALIOP Data Processing Algorithms, *Journal of Atmospheric and Oceanic Technology*, 26 (11), 2310–2323, 2009. [doi:10.1175/2009JTECHA1281.1](https://doi.org/10.1175/2009JTECHA1281.1).

Winker, D. M., Pelon, J., Coakley Jr, J. A., Ackerman, S. A., Charlson, R. J., Colarco, P. R., Flamant, P., Fu, Q., Hoff, R. M., Kittaka, C., Kubar, T. L., Le Treut, H., McCormick, M. P.,

Mégie, G., Poole, L., Powell, K., Trepte, C., Vaughan, M. A., and Wielicki, B. A.: The CALIPSO Mission. *Bulletin of American Meteorological Society*, 91(9), 1211-1230, 2010.

Zhang, L., Li, J., Li, J., Li, R., Zhang, W., Lei, M., et al.: Studying the impacts of meteorological factors on distribution of cloud horizontal scales based on active satellite, *Journal of Geophysical Research: Atmospheres*, 129, e2024JD041844, <https://doi.org/10.1029/2024JD041844>, 2024.

Cai, H., Yang, Y., Chen, Q.: Distribution Characteristics of Cloud Types and Cloud Phases over China and Their Relationship with Cloud Temperature, *Remote Sensing*, 14(21), 2022. <https://doi.org/10.3390/rs14215601>

Hassan, T., Zhang, K., Li, J., Singh, B., Zhang, S., Wang, H., and Ma, P.: Impacts of spatial heterogeneity of anthropogenic aerosol emissions in a regionally refined global aerosol–climate model, *Geosci. Model Dev.*, 17, 3507-3532, 2024.

Mohebalhojeh, M., Frederick, S., Riemer, N., & West, M. (2026). A Metric for Quantifying Spatial Heterogeneity in Gridded Atmospheric Fields. *Earth and Space Science* (preprint).

Li, Y., Liu, X., and Cai, H.: Numerical simulation of aerosol concentration effects on cloud droplet size spectrum evolutions of warm stratiform clouds in Jiangxi, China, *Atmos. Chem. Phys.*, 24, 13525–13540, <https://doi.org/10.5194/acp-24-13525-2024>, 2024.

Zhao, J., Ma, X., Quaas, J., and Yang, T.: How meteorological conditions influence aerosol–cloud interactions under different pollution regimes, *Atmos. Chem. Phys.*, 25, 17701–17723, <https://doi.org/10.5194/acp-25-17701-2025>, 2025.

Wang, Y., Wang, Y., Song, X., Shang, Y., Zhou, Y., Huang, X., Li, Z.: The impact of particulate pollution control on aerosol hygroscopicity and CCN activity in North China, *Environmental Research Letters*, 18, 074028, 2023.

Han, X., Zhao, B., Lin, Y., Chen, Q., Shi, H., Jiang, Z., et al.: Type-dependent impact of aerosols on precipitation associated with deep convective cloud over East Asia, *Journal of Geophysical Research: Atmospheres*, 127, e2021JD036127. <https://doi.org/10.1029/2021JD036127>, 2022.

Fan, J., Zhang, Y., Li, Z., Yan, H., Prabhakaran, T., Rosenfeld, D., & Khain, A.: Unveiling aerosol impacts on deep convective clouds: Scientific concept, modeling, observational analysis, and future direction, *Journal of Geophysical Research: Atmospheres*, 130, e2024JD041931. <https://doi.org/10.1029/2024JD041931>, 2025.

Zhang, Q., Meng, J., Quan, J., et al. Impact of aerosol composition on cloud condensation nuclei activity, *Atmos. Chem. Phys.*, 12, 3783–3790, 2012.

Lee, S. S., Donner, L. J., Phillips, V. T. J. Impacts of aerosol chemical composition on microphysics and precipitation in deep convection, *Atmospheric Research*, 94, 220–237, 2009.

Huang, R. J., Zhang, Y. L., Bozzetti, C., et al. High secondary aerosol contribution to particulate pollution during haze events in China, *Nature*, 514, 218–222, 2014.

Liu, Q., Shen, X., Li, L., et al. Impacts of Aerosol Chemical Composition on Cloud Condensation Nuclei (CCN) Activity during Wintertime in Beijing, China. *Remote Sens.*, 15, 4119, 2023.

Zheng, B., Tong, D., Li, M., Liu, F., Hong, C., Geng, G., Li, H., Li, X., Peng, L., Qi, J., Yan, L., Zhang, Y., Zhao, H., Zheng, Y., He, K., and Zhang, Q.: Trends in China's anthropogenic

emissions since 2010 as the consequence of clean air actions, *Atmos. Chem. Phys.*, 18, 14095–14111, <https://doi.org/10.5194/acp-18-14095-2018>, 2018.

## Response to Referee #2

Using aerosol and cloud parameter data derived from MODIS and CALIPSO satellite observations over the land areas of eastern China, this study systematically investigated the regulatory role of liquid water path (LWP) in cloud droplet effective radius (CER), and the interaction between aerosol optical depth (AOD) and cloud properties during Period 1 (2008–2014) and Period 2 (2015–2022). This manuscript is well planned and written, and I think that the analysis of data is well conducted. However, in my opinion, the current version of the manuscript has some problems which need to be addressed before the work can be considered suitable for publication.

The authors are grateful to Referee #2 for the valuable time spent on thorough reading our manuscript and providing expert views to guide us for improving the manuscript with the main and specific points and the references. We have taken notice of all comments, listed below in black, and made many changes to the manuscript to address these, together with the comments from the other referees. All modifications in the revised manuscript have been highlighted for your convenience. We address each of your comments below and refer to our responses in the revised manuscript and provide line numbers (**clean version**) and copy text in “quotes”. Finally, relevant references have been added to the reference list.

### General comments

Comments (1): Discussion: This study explores the responses of two cloud parameters (CER and  $N_d$ ) to AOD and the sensitivity of these responses to scales, but lacks an in-depth analysis of the differences and correlations between the two parameters' responses to AOD. It would be helpful if the authors make comparisons between them.

**Answer:** Thank you for this valuable suggestion. We fully agree that an in-depth comparison of the differences and correlations between CER and  $N_d$  responses to AOD—including their scale-dependent characteristics—will enrich the discussion and deepen the understanding of aerosol-cloud interaction mechanisms.

To address this gap, we will add a dedicated subsection (e.g., “4.3 Contrasting sensitivity patterns of cloud parameters in response to AOD”) in the Discussion section lines 693-733, focusing on the following key aspects:

#### 4.3 Contrasting sensitivity patterns of cloud parameters in response to AOD

A comprehensive comparison of the sensitivity  $S_{CER}$  and  $S_{N_d}$  reveals that the responses of CER and  $N_d$  to AOD exhibit distinct yet inherently interconnected characteristics. These characteristics are jointly modulated by spatial scale and LWP regimes (Figs. 5, 7, 8; Supplements 1–2), which profoundly reflect the core microphysical mechanisms of aerosol-cloud interactions. Details are elaborated as follows:

##### 4.3.1 Core differences in response modes between $S_{CER}$ and $N_d$ to AOD

$S_{CER}$  is consistently negative across both periods and all LWP regimes ( $-0.33 < S_{CER} < 0$ ) (Figs. 5, 7; Supplement 1), indicating that an increase in AOD leads to a decrease in CER. This aligns with the core principle of the Twomey effect (Twomey, 1977; Feingold et al., 2001). The values of  $|S_{CER}|$  are larger in the second LWP regime than in the first regime, reflecting stronger

aerosol modulation of cloud microphysical properties when liquid water is abundant (McComiskey & Feingold, 2012). In contrast,  $S_{Nd}$  maintains a significant positive correlation with AOD across all scenarios ( $0 < S_{Nd} < 1$ ) (Fig. 8; Supplement Tables 1-2), confirming that higher AOD directly promotes CCN activation and thereby increases cloud droplet number concentration (Andreae, 2009).  $S_{Nd}$  is larger in small-scale study areas (e.g.,  $4^\circ \times 4^\circ$ ) and small buffer zones, with a maximum value of 0.45 in the first period, indicating greater sensitivity of cloud droplet number to aerosol loading at fine spatial scales.

### 4.3.2 Synergistic modulation of AOD and spatial scale

Using the LWP interval corresponding to  $S_{Nd}$  ( $0 < LWP \leq 200 \text{ g/m}^2$ ) as a benchmark, comparisons between the two periods (incorporating average values of  $S_{CER}$  across two LWP regimes) reveal distinct characteristics:

For the small-scale study area ( $4^\circ \times 4^\circ$ ): In period 1, the average  $|S_{CER}|$  across two LWP regimes is 0.271 (0.2232 for the  $0\text{--}55 \text{ g/m}^2$  LWP regime, 0.3189 for the  $55\text{--}135 \text{ g/m}^2$  LWP regime) and  $S_{Nd}=0.4496$ , both significantly higher than those in period 2 (average  $|S_{CER}|=0.154$ , with 0.0863 for  $0\text{--}50 \text{ g/m}^2$  LWP regime and 0.2212 for  $50\text{--}100 \text{ g/m}^2$  LWP regime;  $S_{Nd}=0.2903$ ). The negative correlation between AOD and CER is more significant in period 1, as sufficient CCN in small-scale areas amplifies both cloud droplet number increase and size reduction, enhancing the Twomey effect.

For the medium-to-large scale study areas ( $6^\circ \times 6^\circ$ ,  $8^\circ \times 8^\circ$ ,  $10^\circ \times 10^\circ$ ): In period 1, the average  $|S_{CER}|$  across two LWP regimes is 0.1683 (0.1305 for  $0\text{--}55 \text{ g/m}^2$ , 0.2061 for  $55\text{--}135 \text{ g/m}^2$ ), 0.13065 (0.1026 for  $0\text{--}55 \text{ g/m}^2$ , 0.1587 for  $55\text{--}135 \text{ g/m}^2$ ), and 0.1067 (0.0858 for  $0\text{--}55 \text{ g/m}^2$ , 0.0885 for  $55\text{--}135 \text{ g/m}^2$ ), respectively, all higher than the corresponding values in period 2 (0.1516, 0.1246, 0.0985). However,  $S_{Nd}$  in period 1 (0.2430, 0.2050, 0.1430) is lower than that in period 2 (0.2960, 0.2680, 0.1740), with no significant difference in the negative correlation between AOD and CER between the two periods.

This characteristic indicates that meteorological confounding effects are enhanced at larger scales, weakening the regulation of  $S_{Nd}$  by aerosols, while at small scales the aci is directly driven by AOD levels.

### 4.3.3 Implications for aerosol indirect effects

The differences and interconnections between  $S_{CER}$  and  $S_{Nd}$  highlight that aerosol indirect effects are dominated by coupled microphysical processes: Aerosol-induced increases in CCN first enhance  $N_d$  through positive  $S_{Nd}$ , and then reduce CER through negative  $S_{CER}$  under constant LWP conditions. The scale-dependent attenuation of both sensitivities and their modulation by LWP indicate that quantifying aerosol indirect effects requires full consideration of spatial scales and the key role of liquid water, providing observational basis for optimizing climate model parameterization schemes.

This revision will systematically clarify the links and differences between CER and  $N_d$  responses to AOD, providing a more holistic understanding of aerosol-cloud interaction processes and strengthening the scientific depth of the discussion.

Comments (2): Discussion: This study conducts a comparative analysis using two periods with different atmospheric pollution concentrations. Although AOD exerts a significant impact on

cloud parameters, the role of meteorological conditions cannot be overlooked. Therefore, when comparing the differences in cloud parameters' responses to aerosols between different periods, explanations of meteorological conditions should be incorporated.

**Answer:** Thank you for this critical suggestion. We fully agree that meteorological conditions are a key confounding factor in aerosol-cloud interaction studies, and explicitly integrating their role into the inter-period comparison of cloud parameter responses is essential for enhancing the robustness of our conclusions.

To address this gap, we have added the text in the Discussion 4.2 lines 662-673 to incorporate meteorological condition analyses, linking them to the observed differences in  $S_{CER}$  and  $S_{Nd}$  between 2008–2014 (high AOD) and 2015–2022 (decreasing AOD).

“The results from this study suggest that AOD-cloud property correlations in large study areas are susceptible to meteorological confounding effects (Quaas et al., 2010; Boucher and Quaas, 2012; Gryspeerd et al., 2014; Liu et al., 2024). Theoretically, aerosol regulation of cloud microphysics is strongly local: smaller domains (e.g.,  $4^\circ \times 4^\circ$ ) feature homogeneous meteorological conditions (humidity, updrafts), preserving undiluted aerosol-cloud interaction signals and yielding larger  $|S_{CER}|$  (pronounced Twomey effect). In contrast, expanded domains (e.g.,  $10^\circ \times 10^\circ$ ) encompass heterogeneous meteorological conditions (circulation differences, boundary layer variability) that independently modulate cloud droplet growth. For example, strong updrafts enhance liquid water supply, offsetting aerosol-induced radius reduction (Altartatz et al., 2014), weakening aerosol-CER correlations and reducing  $|S_{CER}|$ . Consistent with Grandey & Stier (2010), large-scale domains introduce “dilution bias” via non-target meteorological variability. This scale-dependent confounding mechanism elucidates uncertainties in aerosol indirect effect assessments at regional scales.”

Comments (3): Abstract: It would greatly enhance the abstract (as well as the conclusion section) if the authors could emphasize the overall significance and potential implications of this study at the abstract's conclusion.

**Answer:** Thank you for this valuable suggestion. We fully agree that emphasizing the overall scientific significance and practical implications of the study at the end of the abstract (and corresponding conclusion section) will better highlight the work's contribution and improve its impact.

To address this, we have revised the **Abstract** as follows:

“This study aims to reveal patterns of the sensitivity of aerosol indirect effects to spatial scales and investigate the regulatory role of the liquid water path (LWP) in aerosol-cloud interactions over land in eastern China. Using MODIS and CALIOP satellite observations, we systematically analyzed the relationships between aerosol optical depth (AOD) and cloud properties (cloud droplet effective radius, CER; cloud droplet number concentration,  $N_d$ ) during two periods: 2008–2014 (period 1, high AOD) and 2015–2022 (period 2, decreasing AOD). The results show two distinct regimes of CER variation with LWP: a rapid growth regime ( $LWP < 55/50 \text{ g/m}^2$ ) and a decreasing regime ( $LWP = 55-135/50-100 \text{ g/m}^2$ ) (thresholds vary by period). The sensitivity of CER to AOD ( $S_{CER}$ ) exhibited a negative correlation, with stronger sensitivity in the decreasing LWP regime than in the rapid growth regime. Spatial scale (characterized by buffer size and study area) significantly modulated these sensitivities:  $|S_{CER}|$  and the positive sensitivity of  $N_d$  to AOD ( $S_{Nd}$ ) both decreased with increasing spatial

scale. Optimal buffer sizes range from  $6^\circ \times 6^\circ$  to  $10^\circ \times 10^\circ$ : increasing with study area in period 2 but decreasing in period 1 for the decreasing LWP regime. Compared with period 1,  $|SCER|$  in period 2 significantly reduced, reflecting the weakened aerosol-cloud interactions due to declining aerosol concentrations. Additionally, the optimal buffer sizes for  $S_{Nd}$  are larger in the  $8^\circ \times 8^\circ$  and  $10^\circ \times 10^\circ$  study areas than in  $4^\circ \times 4^\circ$  and  $6^\circ \times 6^\circ$  areas. This study reveals the scale-dependence of aerosol-cloud interactions, providing critical observational support for optimizing climate model parameterization schemes.”

These revisions will clearly articulate the study’s unique contributions to the field, its relevance to climate modeling and policy, and its value for guiding future research—strengthening the abstract’s impact and aligning the conclusion with the broader scientific and practical context.

We will ensure the abstract remains concise (within typical word limits) while the conclusion expands on implications in sufficient detail, maintaining consistency between the two sections.

Comments (4): It would be beneficial to include a figure or table illustrating the availability of satellite retrievals across the analyzed domain. Additionally, the sample size should be reported for all figures presented in the study.

**Answer:** Thank you for this constructive suggestion. We fully agree that supplementing satellite retrieval availability across the study domain and explicitly reporting sample sizes for all figures will enhance the transparency, reproducibility, and rigor of our study.

To address this, we have reported sample sizes of CER and AOD for the first LWP regime across both study periods, all buffer sizes and study areas in Supplement Tables S3–S8.

**Table S3. Sample sizes of cloud droplet effective radius (CER) and aerosol optical depth (AOD) across different buffer sizes, study areas (LWP regime 1, 2008–2014).**

Buffer sizes	Sample sizes of CER in LWP regime 1				Sample sizes of AOD in LWP regime 1			
	$10^\circ \times 10^\circ$	$8^\circ \times 8^\circ$	$6^\circ \times 6^\circ$	$4^\circ \times 4^\circ$	$10^\circ \times 10^\circ$	$8^\circ \times 8^\circ$	$6^\circ \times 6^\circ$	$4^\circ \times 4^\circ$
10	25054	16133	8551	3879	47846	32406	18711	8808
20	41667	26507	14077	6376	64878	42949	24462	11377
30	54960	34885	18421	8346	76569	50055	28274	13047
40	66170	42147	22136	9966	86291	56006	31523	14482
50	76207	48769	25738	11593	94726	61227	34272	15664
60	85194	54539	28946	12979	102262	65860	36741	16695
70	93413	59681	31788	14192	108792	69756	38749	17519
80	100728	64370	34330	15317	114357	73103	40498	18246
90	107291	68535	36552	16270	119187	76077	42016	18893
100	113457	72525	38761	17155	123607	78839	43496	19469
120	124793	79882	42945	18964	131449	83807	46217	20534
140	134597	86324	46525	20462	138140	88001	48518	21557

150	138760	89086	48145	21141	141012	89985	49570	21991
160	142693	91808	49602	21734	143725	91767	50570	22436
180	150015	96789	52326	22860	148480	94870	52385	23155
200	156655	101246	54894	23983	153084	97946	53963	23921
250	169423	109475	59449	26008	162530	104346	56987	25388
300	178015	115051	62656	27442	170117	109006	59332	26453

**Table S4. Sample sizes of cloud droplet effective radius (CER) and aerosol optical depth (AOD) across different buffer sizes, study areas (LWP regime 2, 2008–2014).**

Buffer sizes	Sample sizes of CER in LWP regime 2				Sample sizes of AOD in LWP regime 2			
	10°×10°	8°×8°	6°×6°	4°×4°	10°×10°	8°×8°	6°×6°	4°×4°
10	22338	14357	7737	3715	47846	32406	18711	8808
20	35406	22471	11964	5697	64878	42949	24462	11377
30	45473	28805	15162	7187	76569	50055	28274	13047
40	54074	34078	17839	8368	86291	56006	31523	14482
50	61579	38732	20290	9444	94726	61227	34272	15664
60	68173	43017	22553	10424	102262	65860	36741	16695
70	74272	46909	24584	11230	108792	69756	38749	17519
80	79999	50507	26412	11950	114357	73103	40498	18246
90	85339	53806	28177	12654	119187	76077	42016	18893
100	90440	56944	29812	13329	123607	78839	43496	19469
120	99758	62598	32673	14486	131449	83807	46217	20534
140	108723	68273	35600	15795	138140	88001	48518	21557
150	112740	70969	36864	16426	141012	89985	49570	21991
160	116558	73463	38046	16974	143725	91767	50570	22436
180	123653	78031	40203	17917	148480	94870	52385	23155
200	129864	81813	42186	18674	153084	97946	53963	23921
250	142429	89112	46079	20120	162530	104346	56987	25388
300	152460	95213	49452	21369	170117	109006	59332	26453

**Table S5. Sample sizes of cloud droplet effective radius (CER) and aerosol optical depth (AOD) across different buffer sizes, study areas (LWP regime 1, 2015–2022).**

Buffer sizes	Sample sizes of CER in LWP regime 1				Sample sizes of AOD in LWP regime 1			
	10°×10°	8°×8°	6°×6°	4°×4°	10°×10°	8°×8°	6°×6°	4°×4°

10	25054	16133	8551	3879	47846	32406	18711	8808
20	41667	26507	14077	6376	64878	42949	24462	11377
30	54960	34885	18421	8346	76569	50055	28274	13047
40	66170	42147	22136	9966	86291	56006	31523	14482
50	76207	48769	25738	11593	94726	61227	34272	15664
60	85194	54539	28946	12979	102262	65860	36741	16695
70	93413	59681	31788	14192	108792	69756	38749	17519
80	100728	64370	34330	15317	114357	73103	40498	18246
90	107291	68535	36552	16270	119187	76077	42016	18893
100	113457	72525	38761	17155	123607	78839	43496	19469
120	124793	79882	42945	18964	131449	83807	46217	20534
140	134597	86324	46525	20462	138140	88001	48518	21557
150	138760	89086	48145	21141	141012	89985	49570	21991
160	142693	91808	49602	21734	143725	91767	50570	22436
180	150015	96789	52326	22860	148480	94870	52385	23155
200	156655	101246	54894	23983	153084	97946	53963	23921
250	169423	109475	59449	26008	162530	104346	56987	25388

**Table S6. Sample sizes of cloud droplet effective radius (CER) and aerosol optical depth (AOD) across different buffer size, study areas (LWP regime 2, 2015–2022).**

Buffer sizes	Sample sizes of CER in LWP regime 2				Sample sizes of AOD in LWP regime 2			
	10°×10°	8°×8°	6°×6°	4°×4°	10°×10°	8°×8°	6°×6°	4°×4°
10	6548	6548	5449	2803	12892	12892	12892	5961
20	24886	16258	8833	4421	46067	30536	17623	8079
30	32260	20786	11214	5490	55767	36685	20780	9408
40	38784	24739	13284	6440	63457	41493	23310	10474
50	44831	28399	15176	7183	70030	45443	25423	11419
60	50181	31609	16909	7816	75667	48900	27138	12122
70	54865	34476	18456	8415	80872	51807	28559	12723
80	58946	37042	19776	8901	85308	54361	29846	13245
90	62835	39437	21006	9359	89202	56659	31024	13706
100	66623	41757	22165	9796	92939	58931	32143	14126
120	73427	46010	24248	10605	99298	62674	34081	14927
140	79486	49854	26210	11312	104540	65994	36013	15617

150	82336	51650	26988	11633	107089	67545	36876	15939
160	85055	53440	27893	11942	109626	69104	37718	16261
180	89669	56388	29401	12520	114187	72088	39380	16889
200	93898	58986	30700	13034	117969	74508	40596	17401
250	102933	64417	33649	14040	125590	79489	43005	18271
300	109964	68913	35755	14701	132000	83404	45012	18913

**Table S7. Sample sizes of cloud droplet number concentration (Na) and aerosol optical depth (AOD) across different buffer sizes and study areas during 2008-2014.**

Buffer sizes	Sample sizes of Na				Sample sizes of AOD			
	10°×10°	8°×8°	6°×6°	4°×4°	10°×10°	8°×8°	6°×6°	4°×4°
10	47846	32406	18711	8808	50686	32611	17320	8053
20	64878	42949	24462	11377	70102	45066	23944	11084
30	76569	50055	28274	13047	84442	54334	28822	13435
40	86291	56006	31523	14482	96186	62056	32857	15309
50	94726	61227	34272	15664	106166	68620	36473	16906
60	102262	65860	36741	16695	114950	74328	39638	18292
70	108792	69756	38749	17519	122840	79508	42510	19478
80	114357	73103	40498	18246	129763	84048	45038	20599
90	119187	76077	42016	18893	135810	87931	47225	21548
100	123607	78839	43496	19469	141407	91543	49256	22436
120	131449	83807	46217	20534	151353	98040	53031	24145
140	138140	88001	48518	21557	159758	103516	56167	25517
150	141012	89985	49570	21991	163180	105820	57561	26100
160	143725	91767	50570	22436	166373	108000	58769	26661
180	148480	94870	52385	23155	172007	111773	60981	27665
200	153084	97946	53963	23921	176658	114922	62862	28696
250	162530	104346	56987	25388	185393	120627	66331	30409
300	170117	109006	59332	26453	191138	124592	68823	31481

**Table S8. Sample sizes of cloud droplet number concentration (Na) and aerosol optical depth (AOD) across different buffer sizes and study areas during 2015-2022.**

Buffer sizes	Sample sizes of Na				Sample sizes of AOD			
	10°×10°	8°×8°	6°×6°	4°×4°	10°×10°	8°×8°	6°×6°	4°×4°

10	37182	23994	13048	6149	31621	21503	12892	5961
20	51313	32990	17755	8252	46067	30536	17623	8079
30	61921	39800	21327	9788	55767	36685	20780	9408
40	70663	45351	24213	11063	63457	41493	23310	10474
50	78059	50080	26808	12118	70030	45443	25423	11419
60	84354	53975	28967	13015	75667	48900	27138	12122
70	89675	57448	30881	13832	80872	51807	28559	12723
80	94620	60671	32636	14556	85308	54361	29846	13245
90	99042	63497	34138	15155	89202	56659	31024	13706
100	102936	65993	35444	15703	92939	58931	32143	14126
120	110590	70884	38002	16787	99298	62674	34081	14927
140	116487	74472	40007	17549	104540	65994	36013	15617
150	119140	76230	41049	17958	107089	67545	36876	15939
160	121506	77846	41958	18265	109626	69104	37718	16261
180	125788	80845	43582	18935	114187	72088	39380	16889
200	129613	83370	44887	19538	117969	74508	40596	17401
250	136752	87967	47756	20784	125590	79489	43005	18271
300	141896	91273	49807	21431	132000	83404	45012	18913

Comments (5): There are a number of statements that I could not understand. I cannot list them all here, but I will list some under Specific Comments. I think editing for English grammar and style would help with readability a great deal.

**Answer:** Thank you for this important feedback. We fully agree that refining the English grammar, style, and clarity of the manuscript is critical for improving readability and ensuring that all statements are easily understandable. To address this, we have implemented a comprehensive editorial revision of the entire manuscript.

### Specific comments

Comments: (1) Page 1, Line 31: change “significantly...weaker of aerosol” to “significant...weaker aerosol...”

**Answer:** Corrected. As the abstract has been revised comprehensively, the sentence has been revised as follow (lines 34-35):

“Compared with period 1, |SCER| in period 2 significantly reduced, reflecting the weakened aerosol-cloud interactions due to declining aerosol concentrations.”

Comments: (2) Page 5, Line 144: Please replace them with more recent literature citations.

**Answer:** Corrected.

The text “The multitude of sources and the persistent nature of these aerosol particles, which can remain suspended for days to weeks and be transported over long distances in the absence of precipitation (Costantino et al., 2013; Li et al., 2021; Leung et al., 2023), makes eastern China an ideal study area for investigating aci.” in Section 2.1 lines 182-185.

Comments: (3) Page 6, Line 149: change “30–40 N and 112–122 E” to “30°–40°N and 112°–122°E”

**Answer:** Corrected.

Comments: (4) Page 6, Line 154: change “LT” to “Local time”

**Answer:** Corrected in lines 195-196.

“The satellite’s equator crossing time is 13:30 (Local time, i.e. in the early afternoon, coinciding with optimal development conditions for continental warm cloud systems (Wang et al., 2014; Liu et al., 2024).”

Comments: (5) Page 6, Line 159-160: The selection of AOD values greater than 1.5 requires literature support.

**Answer:** Thank you for this insightful comment. To address this concern, we have added the following justification in Section 2.2 “Data used” (lines 204-211):

“In this study, AOD larger than 1.5 was excluded from further analysis to mitigate potential retrieval overestimation. This threshold was selected based on two key considerations: (1) Christensen et al. (2017) used MOD06 C6 data (1 km × 1 km) and reported that “large aerosol optical depths remain in the MODIS-observed pixels near cloud edges, due primarily to 3D effects (Varnái and Marshak, 2009) and the swelling of aerosols by higher relative humidity”; (2) the threshold of 1.5 aligns with widely adopted thresholds in regional aerosol-cloud interaction studies over eastern China, where high AOD often coincides with complex surface conditions (e.g., urbanization, heterogeneous land cover) that exacerbate retrieval biases (Wang et al., 2015; Liu et al., 2017, 2021).”

Comments: (6) Page 6, Line 161: CDR appears in multiple places throughout the manuscript and should be corrected.

**Answer:** Corrected.

Comments: (7) The clarity of Figure 7 in the manuscript needs to be improved.

**Answer:** Corrected.

Comments: (8): Explanations should be provided for the abnormal values of  $SCER$  and  $S_{Nd}$  (which do not conform to general conditions) under the larger buffer zones in the figures.

**Answer:** Thank you for this perceptive comment. We fully agree that explicitly explaining the abnormal  $SCER$  and  $S_{Nd}$  values (deviating from general theoretical expectations) under larger

buffer zones (>150–200 km) is critical for clarifying potential mechanisms and avoiding misinterpretation of the results.

To address this, we will supplement targeted explanations in the Section 3.3 lines 557-559.

“It is noted that  $S_{CER}$  and  $N_d$  exhibit distinct anomalies in large buffer zones, which may be associated with key factors including aerosol distribution, meteorological heterogeneity, cloud type transitions, and satellite retrieval limitations.”

Comments: (9): The usage of “period” and “P” when referring to the two different periods in the manuscript should be consistent.

**Answer:** The terms have been standardized to “period” throughout the manuscript and figures for consistency.

Comments: (10) Page 11, Line 268: delete ‘.’

**Answer:** Corrected.

Comments: (11) Lines 288, 294, and many others: Present tense is used where past tense should be (are vs. were, is vs. was). When describing what was done and what was found, the past tense should be used.

**Answer:** We have corrected the verb tenses throughout the manuscript, changing present tense to past tense where appropriate when describing methods and results.

Comments: (12) Lines 295, It is necessary to supplement the findings of Liu et al. (2021).

**Answer:** Added.

“These results show that CER is very sensitive to the changes in LWP, which is consistent with the study of Liu et al. (2021). Their results showed that CER was very sensitive to the changes in LWP, which was consistent with the study of Liu et al. (2021). Specifically, CER exhibited a three-stage variation with LWP: rapid growth when  $LWP < 50 \text{ g/m}^2$  (with the fastest change rate), a stable state during  $50\text{--}150 \text{ g/m}^2$ , and slow growth when  $LWP > 150 \text{ g/m}^2$  (at a rate much lower than the first stage). This highlighted the necessity of fixing LWP conditions to accurately investigate the impact of AOD on CER.” in Section 3.2 lines 432-437.

Comments: (13) Lines 308-311, The “Twomey effect” is mentioned in multiple places throughout the manuscript; it should be simplified when referenced for the second time.

**Answer:** Corrected.

“For the first LWP regime, the  $S_{CER}$  is negative (as shown in Figure 5). This aligns with the Twomey effect (Twomey, 1977): an increase in aerosols raises the number of CCN, and with constant LWP, less water vapor is available per cloud droplet, reducing CER, increasing cloud albedo, and ultimately cooling the atmosphere.” in Section 3.2.1 lines 450-453.

Comments: (14) Lines 316, change “much stronger” to “much more strongly”.

**Answer:** Corrected.

Comments: (15) Lines 322-323, It is necessary to clarify why this definition is adopted.

**Answer:** Thank you for this important comment. We fully agree that explicitly justifying the definition of “optimal scale” (the buffer size with the highest correlation coefficient R between SCER and AOD) is critical for ensuring the methodological transparency and rationale of our scale-dependent analysis. We have further refined and supplemented the explanation of this concept in the revised manuscript to enhance its clarity and comprehensibility. We have also ensured the consistency of the concept’s expression throughout the manuscript to avoid any potential ambiguity for readers. See the text in the Section 2.4 lines 331-333 and 338-364.

The text “Here, the spatial scales are described by two parameters: study area size (the geographic scope of the analysis) and buffer size (the local spatial extent around each observation point for aggregating aerosol and cloud data).” in Section 2.4 lines 331-333.

The text “Buffer size refers here to a circular spatial domain centered at each CALIOP-detected point in the study area where CALIOP detected the presence of aerosols. Within this circular domain, MODIS-retrieved cloud and aerosol data (AOD, CER,  $N_d$ , LWP) are spatially averaged to construct matched aerosol-cloud datasets at different local scales. This approach assumes that aerosol properties are reasonably homogeneous between adjacent clear and cloudy regions (Anderson et al., 2003; Quaas et al., 2008), which is plausible considering the short-range transport of aerosols (e.g., 10-300 km) and the near-simultaneous observations (1-2 minutes) by MODIS and CALIOP within the A-Train constellation.

Buffer zones with sizes increasing from 10 to 300 km (10 km, 20 km, 30 km, 40 km, 50 km, 60 km, 70 km, 80 km, 90 km, 100 km, 120 km, 140 km, 150 km, 160 km, 180 km, 200 km, 250 km, and 300 km) were determined within the whole study area by using CALIOP data. Previous observations indicate that the typical horizontal scale of cloud clusters ranges from tens to hundreds of kilometers (Zhang et al., 2024; Cai et al., 2022), supported by CloudSat/CALIPSO satellite data showing power-law distributed cloud scales (10-1000 km fitting range) covering major cloud types (Zhang et al., 2024) and regional evidence of consistent multi-season, multi-latitude cloud extents (Cai et al., 2022). Meanwhile, aerosol spatial homogeneity varies with distance: local-scale aerosols ( $\leq 50$  km) exhibit high homogeneity due to consistent sources and stable diffusion, while regional-scale aerosols ( $> 100$  km) show enhanced heterogeneity from multi-source mixing and atmospheric transport (Hassan et al., 2024; Mohebalhojeh et al., 2026). Thus, the 10–300 km buffer range covers both cloud characteristic scales and the aerosol homogeneity transition range, ensuring that MODIS data averaging effectively captures cloud-aerosol coupling. This range avoids insufficient MODIS pixel coverage due to excessively small buffer sizes ( $< 10$  km). It also prevents conflation between regional meteorological variations and local aci signals arising from overly large buffer sizes ( $> 300$  km), as synoptic-scale circulation and other regional meteorological changes may interfere with local aci signals (Quaas et al., 2010). Meanwhile, this range aligns with the 50–150 km buffer sizes widely adopted in regional aci studies (Wang et al., 2015; Liu et al., 2017; 2024), enabling cross-validation of results and ensuring that MODIS data averaging effectively captures cloud-aerosol coupling.” in Section 2.4 lines 338-364.

Comments: (16) Lines 327, change “decreases” to “also decreases”

**Answer:** Corrected.

Comments: (17) Lines 362, change “cloud-aerosol” to “aerosol-cloud”

**Answer:** Corrected.

Comments: (18) Lines 378,392,419, change “Supplement” to “Appendices”

**Answer:** Corrected.

Comments: (19) Lines 409, The expression suffers from ambiguous reference.

**Answer:** Thank you for comment. We have revised the sentence in Lines 551-554 in the revised manuscript to clarify the intended meaning and remove any ambiguity.

“The variation of R with buffer size for each of the two periods shows that the optimal buffer sizes are larger when the study area is larger, Specifically, these optimal sizes in the 8°×8° and 10°×10° study areas are larger than those in the 4°×4° and 6°×6° areas (Figure 9).”

Comments: (20) Lines 431, The descriptions of “regime” and “phase” in the manuscript need to be consistent.

**Answer:** The terms have been standardized to “regime” throughout the manuscript for consistency.

Comments: (21) Lines 449, The logical expression of the sentence is unclear.

**Answer:** Corrected. See the text in Section 4.1 Lines 631-632.

“If the characteristics of aerosols (such as composition) change in the second LWP regime, this sensitivity may be further amplified.”

Comments: (22) Lines 450-453, It is necessary to add supplementary literature to support this point.

**Answer:** Added. See the text in Section 4.1 Lines 626-629.

“In addition, clouds with larger LWP are usually associated with strong updrafts (such as convective clouds), and stronger turbulence and vertical transport will bring more aerosols into the clouds, increasing CCN concentration and a decrease in particle size, making them more sensitive to changes in AOD (Jones et al., 2009; Han et al., 2022; Fan et al., 2025).”

## References

Dagan, G., Yeheskel, N., Williams, A. I. L.: Radiative forcing from aerosol–cloud interactions enhanced by large-scale circulation adjustments, *Nature geoscience*, 16, 1092-1098, 2023.

Twomey, S. Pollution and the planetary albedo, *Atmos. Environ.*, 1974, 41, 120-125.

Feingold, G. Modeling of the first indirect effect: analysis of measurement requirements, *Geophys. Res. Lett.*, 30, 1997, doi:10.1029/2003GL017967, 2003.

- Jia, H., Quaas, J., Gryspeerdt, E., Böhm, C., & Sourdeval, O.: Addressing the difficulties in quantifying droplet number response to aerosol from satellite observations, *Atmospheric Chemistry and Physics*, 22(11), 7353–7372. <https://doi.org/10.5194/acp-22-7353-2022>, 2022.
- Sarna, K. and Russchenberg, H. W. J.: Ground-based remote sensing scheme for monitoring aerosol–cloud interactions, *Atmos. Meas. Tech.*, 9, 1039–1050, <https://doi.org/10.5194/amt-9-1039-2016>, 2016.
- Zheng, X., Xi, B., Dong, X., Logan, T., Wang, Y., and Wu, P.: Investigation of aerosol–cloud interactions under different absorptive aerosol regimes using Atmospheric Radiation Measurement (ARM) southern Great Plains (SGP) ground-based measurements, *Atmos. Chem. Phys.*, 20, 3483–3501, <https://doi.org/10.5194/acp-20-3483-2020>, 2020.
- Lee, H.-H., Zheng, X., Qiu, S., and Wang, Y.: Numerical case study of the aerosol–cloud interactions in warm boundary layer clouds over the eastern North Atlantic with an interactive chemistry module, *Atmos. Chem. Phys.*, 25, 6069–6091, <https://doi.org/10.5194/acp-25-6069-2025>, 2025.
- Li, G. H., Wang, Y., Zhang, R. Y.: Implementation of a two-moment bulk microphysics scheme to the WRF model to investigate aerosol-cloud interaction, *Journal of Geophysical Research-Atmospheres*, 113, D15, <https://doi.org/10.1029/2007JD009361>, 2008.
- Kaufman, Y. J., Remer, L., Tanré, D., Li, R., Kleidman, R., Mattoo, S., Levy, R., Eck, T., Holben, B., Ichoku, C., Martins, J., and Koren, I.: A critical examination of the residual cloud contamination and diurnal sampling effects on MODIS estimates of aerosol over ocean, *IEEE Trans. Geosci. Remote Sens.*, 43, 2886–2897, 2005.
- Winker, D. M., Hunt, W. H., and McGill, M. J.: Initial performance assessment of CALIOP, *Geophys. Res. Lett.*, 34, L19803, [doi:10.1029/2007GL030135](https://doi.org/10.1029/2007GL030135), 2007.
- Proestakis, E., Amiridis, V., Marinou, E., Georgoulas, A. K., Solomos, S., Kazadzis, S., Chimot, J., Che, H., Alexandri, G., Biniotoglou, I., Daskalopoulou, V., Kourtidis, K. A., de Leeuw, G., and van der A, R. J.: Nine-year spatial and temporal evolution of desert dust aerosols over South and East Asia as revealed by CALIOP, *Atmos. Chem. Phys.*, 18, 1337–1362, <https://doi.org/10.5194/acp-18-1337-2018>, 2018.
- Li, Z., et al.: Aerosol and monsoon climate interactions over Asia, *Rev. Geophys.*, 54, 866–929, [doi:10.1002/2015RG000500](https://doi.org/10.1002/2015RG000500), 2016.
- Leung, G. R., Saleeby, S. M., Sokolowsky, G. A., Freeman, S. W., and van den Heever, S. C.: Aerosol–cloud impacts on aerosol detrainment and rainout in shallow maritime tropical clouds, *Atmos. Chem. Phys.*, 23, 5263–5278, <https://doi.org/10.5194/acp-23-5263-2023>, 2023.
- Levy, R. C., Mattoo, S., Munchak, L. A., Remer, L. A., Sayer, A. M., Patadia, F., and Hsu, N. C.: The Collection 6 MODIS aerosol products over land and ocean, *Atmos. Meas. Tech.*, 6, 2989–3034, <https://doi.org/10.5194/amt-6-2989-2013>, 2013.
- Platnick, S., et al., MODIS Cloud optical properties: User guide for the Collection 6/6.1 level-2 MOD06/MYD06 product and associated level-3 data sets. v1.1, July 2018.
- Platnick, S., K. G. Meyer, M. D. King, G. Wind, N. Amarasinghe, B. Marchant, G. T. Arnold, Z. Zhang, Hubanks, P. A., Holz, R. E., Yang, P., Ridgway, W. L., and Riedi, J.: The MODIS cloud optical and microphysical products: Collection 6 updates and examples from Terra and Aqua, *IEEE Trans. Geosci. Remote Sens.*, 55, 502–525, 2017.

Marchant, B., et al.: MODIS Collection 6 shortwave-derived cloud phase classification algorithm and comparisons with CALIOP, *Atmos. Meas. Tech. Discuss.*, 8, 11893–11924, 2015.

Baum, B. A., et al.: MODIS cloud-top property refinement for Collection 6, *J. Appl. Meteorol. Climatol.*, 51(6), 1145-1163, 2012.

Winker, D. M., Vaughan, M. A., Omar, A., Hu, Y., Powell, K. A., Liu, Z. Y., Hunt, W. H., Young, S. A.: Overview of the CALIPSO Mission and CALIOP Data Processing Algorithms, *Journal of Atmospheric and Oceanic Technology*, 26 (11), 2310-2323, 2009. doi:10.1175/2009JTECHA1281.1.

Winker, D. M., Pelon, J., Coakley Jr, J. A., Ackerman, S. A., Charlson, R. J., Colarco, P. R., Flamant, P., Fu, Q., Hoff, R. M., Kittaka, C., Kubar, T. L., Le Treut, H., McCormick, M. P., Mégie, G., Poole, L., Powell, K., Trepte, C., Vaughan, M. A., and Wielicki, B. A.: The CALIPSO Mission. *Bulletin of American Meteorological Society*, 91(9), 1211-1230, 2010.

Zhang, L., Li, J., Li, J., Li, R., Zhang, W., Lei, M., et al.: Studying the impacts of meteorological factors on distribution of cloud horizontal scales based on active satellite, *Journal of Geophysical Research: Atmospheres*, 129, e2024JD041844, <https://doi.org/10.1029/2024JD041844>, 2024.

Cai, H., Yang, Y., Chen, Q.: Distribution Characteristics of Cloud Types and Cloud Phases over China and Their Relationship with Cloud Temperature, *Remote Sensing*, 14(21), 2022. <https://doi.org/10.3390/rs14215601>

Hassan, T., Zhang, K., Li, J., Singh, B., Zhang, S., Wang, H., and Ma, P.: Impacts of spatial heterogeneity of anthropogenic aerosol emissions in a regionally refined global aerosol–climate model, *Geosci. Model Dev.*, 17, 3507-3532, 2024.

Mohebalhojeh, M., Frederick, S., Riemer, N., & West, M. (2026). A Metric for Quantifying Spatial Heterogeneity in Gridded Atmospheric Fields. *Earth and Space Science* (preprint).

Li, Y., Liu, X., and Cai, H.: Numerical simulation of aerosol concentration effects on cloud droplet size spectrum evolutions of warm stratiform clouds in Jiangxi, China, *Atmos. Chem. Phys.*, 24, 13525–13540, <https://doi.org/10.5194/acp-24-13525-2024>, 2024.

Zhao, J., Ma, X., Quaas, J., and Yang, T.: How meteorological conditions influence aerosol–cloud interactions under different pollution regimes, *Atmos. Chem. Phys.*, 25, 17701–17723, <https://doi.org/10.5194/acp-25-17701-2025>, 2025.

Wang, Y., Wang, Y., Song, X., Shang, Y., Zhou, Y., Huang, X., Li, Z.: The impact of particulate pollution control on aerosol hygroscopicity and CCN activity in North China, *Environmental Research Letters*, 18, 074028, 2023.

Han, X., Zhao, B., Lin, Y., Chen, Q., Shi, H., Jiang, Z., et al.: Type-dependent impact of aerosols on precipitation associated with deep convective cloud over East Asia, *Journal of Geophysical Research: Atmospheres*, 127, e2021JD036127. <https://doi.org/10.1029/2021JD036127>, 2022.

Fan, J., Zhang, Y., Li, Z., Yan, H., Prabhakaran, T., Rosenfeld, D., & Khain, A.: Unveiling aerosol impacts on deep convective clouds: Scientific concept, modeling, observational analysis, and future direction, *Journal of Geophysical Research: Atmospheres*, 130, e2024JD041931. <https://doi.org/10.1029/2024JD041931>, 2025.

Zhang, Q., Meng, J., Quan, J., et al. Impact of aerosol composition on cloud condensation nuclei activity, *Atmos. Chem. Phys.*, 12, 3783–3790, 2012.

Lee, S. S., Donner, L. J., Phillips, V. T. J. Impacts of aerosol chemical composition on microphysics and precipitation in deep convection, *Atmospheric Research*, 94, 220–237, 2009.

Huang, R. J., Zhang, Y. L., Bozzetti, C., et al. High secondary aerosol contribution to particulate pollution during haze events in China, *Nature*, 514, 218–222, 2014.

Liu, Q., Shen, X., Li, L., et al. Impacts of Aerosol Chemical Composition on Cloud Condensation Nuclei (CCN) Activity during Wintertime in Beijing, China. *Remote Sens.*, 15, 4119, 2023.

Zheng, B., Tong, D., Li, M., Liu, F., Hong, C., Geng, G., Li, H., Li, X., Peng, L., Qi, J., Yan, L., Zhang, Y., Zhao, H., Zheng, Y., He, K., and Zhang, Q.: Trends in China's anthropogenic emissions since 2010 as the consequence of clean air actions, *Atmos. Chem. Phys.*, 18, 14095–14111, <https://doi.org/10.5194/acp-18-14095-2018>, 2018.

# Spatial-scale dependence of aerosol indirect effects over land in eastern China: A comparative analysis

Yuqin Liu<sup>1,2</sup>, Tao Lin<sup>1,2</sup>, Jiahua Zhang<sup>3</sup>, Fu Wang<sup>4</sup>, Meixia Lin<sup>1,2</sup>, Yuan Chen<sup>1,2</sup>, Yiyi Huang<sup>1,2</sup>, Hongkai Geng<sup>1,2</sup>, Xin Cao<sup>1,2</sup>, Gerrit de Leeuw<sup>5,6</sup>

1 State Key Laboratory of Regional and Urban Ecology, Institute of Urban Environment, Chinese Academy of Sciences, Xiamen 361021, China

2 Fujian Key Laboratory of Digital Technology for Territorial Blank Analysis and Simulation, Fuzhou 350108, China

3 Key Laboratory of Digital Earth Sciences, The Aerospace Information Research Institute, Chinese Academy of Sciences, Beijing 100094, China

4 CMA Earth System Modeling and Prediction Centre (CEMC), Beijing 100081, China

5 Royal Netherlands Meteorological Institute (KNMI), R&D Satellite Observations, 3730AE De Bilt, The Netherlands

6 State Key Laboratory of Remote Sensing and Digital Earth & Key Laboratory of Satellite Remote Sensing of Ministry of Ecology and Environment, Aerospace Information Research Institute, Chinese Academy of Sciences, Beijing 100101, China

Correspondence to: Tao Lin ([tlin@iue.ac.cn](mailto:tlin@iue.ac.cn)); Gerrit de Leeuw ([gerrit.de.leeuw@knmi.nl](mailto:gerrit.de.leeuw@knmi.nl), ORCID: 0000-0002-1649-6333)

## Abstract

This study aims to reveal patterns of the sensitivity of aerosol indirect effects to spatial scales and investigate the regulatory role of the liquid water path (LWP) in aerosol-cloud interactions over land in eastern China. Using MODIS and CALIOP satellite observations, we systematically analyzed the relationships between aerosol optical depth (AOD) and cloud properties (cloud droplet effective radius, CER; cloud droplet number concentration,  $N_d$ ) during two periods: 2008–2014 (period 1, high AOD) and 2015–2022 (period 2, decreasing AOD). The results show two distinct regimes of CER variation with LWP: a rapid growth regime ( $LWP < 55/50$  g/m<sup>2</sup>) and a decreasing regime ( $LWP = 55-135/50-100$  g/m<sup>2</sup>) (thresholds vary by period). The sensitivity of CER to AOD ( $S_{CER}$ ) exhibited a negative correlation, with stronger sensitivity in the decreasing LWP regime than in the rapid growth regime. Spatial scale (characterized by buffer size and study area) significantly modulated these sensitivities:  $|S_{CER}|$  and the positive sensitivity of  $N_d$  to AOD ( $S_{N_d}$ ) both decreased with increasing spatial scale. Optimal buffer sizes range from  $6^\circ \times 6^\circ$  to  $10^\circ \times 10^\circ$ : increasing with study area in period 2 but decreasing in period 1 for the

34 decreasing LWP regime. Compared with period 1,  $|S_{CER}|$  in period 2 significantly reduced, reflecting the  
35 weakened aerosol-cloud interactions due to declining aerosol concentrations. Additionally, the optimal  
36 buffer sizes for  $S_{Nd}$  are larger in the  $8^\circ \times 8^\circ$  and  $10^\circ \times 10^\circ$  study areas than in  $4^\circ \times 4^\circ$  and  $6^\circ \times 6^\circ$  areas. This  
37 study reveals the scale-dependence of aerosol-cloud interactions, providing critical observational support  
38 for optimizing climate model parameterization schemes.

39 **Keywords:** Aerosol, Cloud, Liquid water path, Scale effect, Satellite, Eastern China

40

## 41 1 Introduction

42 Aerosol particles, depending on their chemical composition and size, can serve as cloud condensation  
43 nuclei (CCN) in liquid clouds or as ice nucleating particles (INP) in ice clouds. When CCN are activated,  
44 they can alter the microphysical properties of clouds and affect precipitation, indirectly impacting the  
45 Earth's radiative budget through aerosol-cloud interactions (aci) (Tao et al., 2012; Fan et al., 2016;  
46 Rosenfeld et al., 2019; Rao and Dey, 2020; Bellouin et al., 2020; Dagan et al., 2023). An increase in CCN  
47 concentrations results in a larger number of cloud droplets ( $N_d$ ), and if the cloud liquid water path (LWP)  
48 remains constant, it leads to a reduction in the cloud droplet effective radius (CER) (Twomey, 1974;  
49 Feingold et al., 2003). The reduced CER leads to an increased reflection of solar radiation, i.e. a higher  
50 cloud albedo, and enhances radiative forcing due to aerosol-cloud interaction (RFaci). The impact of  
51 increasing aerosol particle numbers on cloud properties, while maintaining a constant LWP, is commonly  
52 known as the "Twomey" effect (Twomey, 1977; Feingold, et al., 2001; Matheson et al., 2005; Koren et  
53 al., 2005; Meskhidze and Nenes, 2010; Costantino et al., 2010; 2013). Another aspect of RFaci involves  
54 quick adjustments, which could also cause changes in other cloud characteristics due to the rise in  $N_d$  and  
55 the decrease of CER. For example, this may lead to a reduction in precipitation efficiency, causing an  
56 increase in the LWP and cloud cover. As a result, the reflection of solar radiation is intensified (Albrecht,  
57 1989). These two effects of aci are often categorized as the cloud albedo effect and the cloud lifetime  
58 effect (Quaas et al., 2008).

59 Extensive research on the impact of aerosols on the microphysical properties of clouds has been  
60 conducted utilizing satellite observations (Liu et al., 2017; Jia et al., 2022), aircraft measurements (Jia et  
61 al., 2019; Zheng et al., 2024), ground-based monitoring (Sarna et al., 2016; Zheng et al., 2020), and  
62 numerical simulations (Lee et al., 2025; Li et al., 2008). Among these, satellite-based instruments have

63 become a vital observational tool for studying aerosol-cloud interactions due to their wide spatial  
64 coverage and high spatiotemporal resolution. However, optical satellite sensors such as the Moderate  
65 Resolution Imaging Spectroradiometer (MODIS) cannot effectively penetrate cloud layers (King et al.,  
66 2003; Kaufman et al., 2005; Remer et al., 2005), making it difficult to directly retrieve the optical  
67 properties of aerosols underneath clouds. Currently, aerosol data are mainly obtained in cloud-free  
68 conditions as determined using cloud detection methods. This limitation results in significant spatial  
69 mismatches between aerosol and cloud properties, often requiring aggregation of satellite data over large-  
70 scale grids for statistical analysis to determine relationships between aerosol and cloud parameters. The  
71 discrepancy between this large-scale analysis and the actual process scale frequently leads to biases in  
72 quantifying aerosol indirect effects, thereby significantly increasing the uncertainty in radiative forcing  
73 estimates (Lebsock et al., 2013; Altaratz et al., 2014; Ma et al., 2015; Possner et al., 2016; Bender et al.,  
74 2018).

75 In recent years, studies based on multi-source satellite data or multi-instrument joint observations have  
76 demonstrated that aerosol particles significantly influence cloud microphysical properties (Saponaro et  
77 al., 2017; Liu et al., 2018; Pandey et al., 2020). Numerous studies have validated the existence of the  
78 Twomey effect (Jones et al., 2009; Christensen et al., 2016; Jia et al., 2019). However, also studies have  
79 been published with findings that contradict the Twomey effect, particularly over land, where an increase  
80 in aerosol optical depth (AOD) results in an increase in CER (Feingold et al., 2001; Yuan et al., 2008;  
81 Grandey and Stier, 2010; Tang et al., 2014; Wang et al., 2015; Ma et al., 2018; Jia et al., 2019; Liu et al.,  
82 2020). These inconsistent findings highlight the complexity and regional variability of aci mechanisms,  
83 and further in-depth research is needed to reveal the underlying processes.

84 Currently, researchers usually use grid methods (such as  $1^\circ \times 1^\circ$ ,  $2^\circ \times 2^\circ$ , etc.) to study the aerosol indirect  
85 effects in large areas (Bréon, 2002; Kaufman et al., 2005; Bulgin et al., 2008; Quaas et al., 2008). For  
86 instance, Grandey and Stier (2010) estimated the relationship between aerosols and CER on a global  
87 scale ( $60^\circ\text{N}\sim 60^\circ\text{S}$ ) using multiple spatial resolutions ( $1^\circ \times 1^\circ$ ,  $4^\circ \times 4^\circ$ ,  $8^\circ \times 8^\circ$ ,  $15^\circ \times 15^\circ$ , and  $60^\circ \times 60^\circ$ ). They  
88 concluded that the sensitivity of retrieved CER to AOD generally exhibited positive values over land and  
89 negative values over oceans, and pointed out that using grids larger than  $4^\circ \times 4^\circ$  could introduce significant  
90 errors due to the spatial variability of aerosol and cloud parameters. Additionally, the study highlighted  
91 that, when using grids larger than  $4^\circ \times 4^\circ$  to investigate the relationship between aerosols and CER,

92 significant errors could be introduced in calculating the aerosol indirect effect index due to the spatial  
93 variability of aerosol and cloud parameters.

94 For studies focusing on smaller regions, researchers often employ a moving window or a fixed area  
95 referred to as a buffer zone, within which the distribution of aerosol concentrations is assumed to be  
96 uniform. Spatially matched samples are constructed by averaging AOD and cloud parameters within the  
97 window or buffer zone. The choice of the window or buffer size is often arbitrary, and existing studies  
98 rarely systematically explore how the detection of aci signals is influenced by the size of the area. For  
99 example, Yuan et al. (2008) used a 100 km × 100 km moving window to calculate the mean values of  
100 AOD and cloud properties to investigate the relationship between aerosols and CER across seven global  
101 regions. Their results indicated that only two of these regions, near the coasts of the Gulf of Mexico and  
102 the South China Sea, exhibited a positive correlation between CER and AOD. Similarly, Jones et al.  
103 (2009) utilized multi-source remote sensing data and applied a point spread function to derive the mean  
104 AOD within a 20 km range, which was designed to match the native 20 km resolution of the  
105 corresponding cloud properties (cloud optical thickness, COT; LWP; CER; cloud top pressure, CTP).

106 Their study examined the influence of aerosol types, cloud conditions, and atmospheric factors on aerosol  
107 indirect effects across six different oceanic regions globally, finding that the sensitivity of cloud  
108 properties to AOD varied substantially with regional characteristics. In addition, significant progress has  
109 been made in research utilizing observations from the Cloud-Aerosol Lidar with Orthogonal Polarization  
110 (CALIOP) data (Winker et al., 2007). For instance, Costantino et al. (2010) used CALIOP data to  
111 investigate the aerosol influence on CER in stratocumulus clouds over the coastal regions of Namibia  
112 and Angola. They performed the analysis by co-locating an aerosol index (based on AOD and the  
113 Ångström exponent) with CER within a 150 km buffer zone around CALIOP observations. They found  
114 that there was no correlation between aerosol load and CER when aerosol and cloud layers were clearly  
115 separated, but a strong correlation when lidar profiles indicated mixing. Costantino et al. (2013) further  
116 analyzed the statistical relationship between aerosol concentrations and cloud physical parameters by  
117 examining aerosol and cloud properties within a 20 km buffer zone around CALIOP samples, integrating  
118 vertical profiles of aerosol and cloud data. Their statistics also clearly showed that cloud micro-physical  
119 properties were affected by aerosols when aerosol and cloud layers were mixed, decreasing the CER. It  
120 is noted that these two studies by Costantino et al. (2010, 2013) reached consistent conclusions about aci

121 (i.e., aerosols modulate CER when layers interact), by adopting different buffer sizes (150 km vs. 20 km)  
122 to target distinct study areas. This demonstrates that the buffer size is tailored to the research objectives  
123 rather than through a systematic sensitivity analysis. Wang et al. (2015) revealed an inverse “Twomey”  
124 effect between aerosols and CER in eastern China by analyzing aerosol concentrations and CER within  
125 a 50 km buffer zone around CALIOP samples. Their results showed that larger CER was associated with  
126 high AOD, which was attributed to the feedback of microphysical processes from intense competition  
127 for vapor in the presence of high aerosol concentrations and the evaporation of smaller, less hygroscopic,  
128 droplets. Similarly, Liu et al. (2017) systematically examined the response mechanisms of warm cloud  
129 macro- and microphysical parameters to increasing AOD in the Yangtze River Delta region, also using  
130 CALIOP samples within a 50 km buffer zone. They found that the relation between cloud properties and  
131 AOD depended on the aerosol abundance, with a different behavior for low and high AOD (i.e.  $AOD <$   
132  $0.35$  and  $AOD > 0.35$ ). However, both Wang et al. (2015) and Liu et al. (2017) used a fixed 50 km buffer  
133 zone without justifying the choice or exploring how varying buffer sizes might alter the strength or  
134 robustness of their findings—a common limitation in regional aci studies. More recently, Liu et al. (2024)  
135 quantified the relative importance of aerosols, meteorological parameters and their interactions for cloud  
136 properties in the eastern coastal and inland regions of China, utilizing MODIS  $1^\circ \times 1^\circ$  aerosol and cloud  
137 product data. Their study confirmed that CER decreased with the increase in AOD in the moderately  
138 polluted atmosphere ( $0.1 < AOD < 0.3$ ) over the East China Sea, whereas, in contrast, CER increased  
139 with increasing AOD in the polluted atmosphere ( $AOD > 0.3$ ) over the Yangtze River Delta. These studies  
140 have provided critical scientific insights into aci at regional scales, but the lack of systematic scale  
141 sensitivity analysis—especially for varying window/buffer sizes within the same regional domain—  
142 leaves uncertainties about the generalizability of their conclusions.  
143 However, the properties and interaction processes of aerosols and clouds are spatially significantly  
144 heterogeneous and scale dependent (McComiskey et al., 2009; McComiskey and Feingold, 2012; Chen  
145 et al., 2015; Glotfelty et al., 2020). McComiskey and Feingold (2012) explicitly pointed out that the  
146 “scale problem” is a major challenge in quantifying aerosol indirect effects, as the spatial scale of  
147 observation can mask or exaggerate the true interaction signals. In previous studies, the definitions of  
148 window size and buffer size have often been subjective, inadvertently introducing uncertainties into the  
149 research on aci. Although studies have explored the relationship between aerosols and CER across

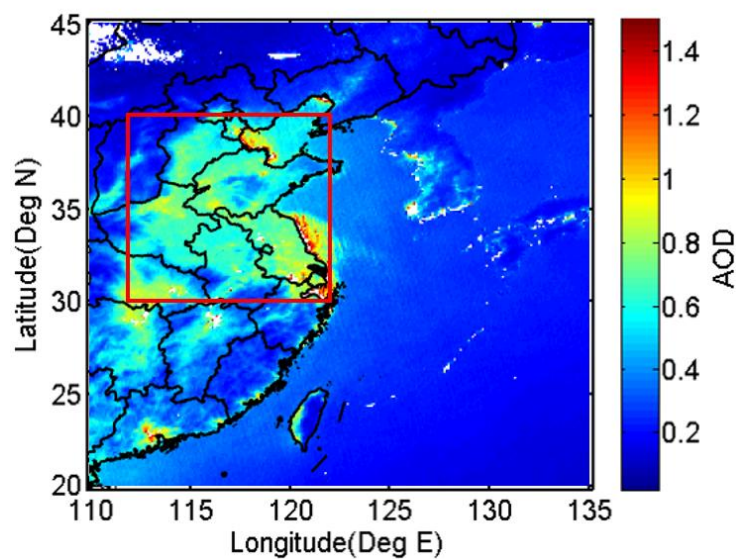
150 different observational scales, these investigations have primarily focused on larger spatial scales, leaving  
151 a gap in sensitivity analysis of aerosol indirect effects at smaller regional scales. For example, Grandey  
152 and Stier (2010) focused on global-scale grid resolutions but did not explore the scale dependence within  
153 regional domains; Wang et al. (2015) and Liu et al. (2017) used fixed buffer sizes (50 km) without  
154 investigating how varying buffer sizes affect the results. Therefore, utilizing multi-source remote sensing  
155 data to explore whether and how the aerosol indirect effect depends on observational spatial scales in  
156 eastern China is of great significance for developing parameterization schemes that align with the  
157 regional characteristics of aci.

158 Aerosol properties in China have significantly changed between 2008 and 2022 due to economic  
159 development and the implementation of emission reduction policies. The AOD over China increased  
160 until 2007 to become among the highest worldwide and remained high between 2008 and 2014 with large  
161 interannual variations. The enforcement of emission reduction measures, in particular the implementation  
162 of the 2013-2017 Clean Air Action Plan, resulted in the decline of the AOD between 2014 and 2018 (de  
163 Leeuw et al., 2021; 2022; 2023) and a further decrease resulted in an AOD lower than that in 2000 (de  
164 Leeuw et al., 2023). This distinct two-period variation (high AOD vs. decreasing AOD) provides a unique  
165 opportunity to investigate how changes in aerosol loading modulate the scale dependence of aerosol  
166 indirect effects, a topic that has not been systematically addressed in previous studies. Based on these  
167 observations, in this study we conduct a comparative analysis of the sensitivity of cloud parameters (CER  
168 and  $N_d$ ) to AOD variation using data from two distinct periods: 2008-2014 (period 1, high AOD) and  
169 2015-2022 (period 2, decreasing AOD). The main objectives of this study are to: (1) reveal patterns of  
170 the sensitivity of aerosol indirect effects to spatial scales by investigating how spatial scale modulates  
171 the sensitivity of CER to AOD ( $S_{CER}$ ) and the sensitivity of  $N_d$  to AOD ( $S_{N_d}$ ) over eastern China during  
172 the two periods; and (2) clarify the regulatory role of LWP in cloud-aerosol interaction by examining the  
173 LWP-stratified responses of  $S_{CER}$  and  $S_{N_d}$  to spatial scale and AOD variations. The study aims to reveal  
174 the patterns of the sensitivity of aerosol indirect effects to spatial scales, provides support for optimizing  
175 parameterization schemes and accurate assessment of regional aerosol effects.

176 **2 Method**

177 **2.1 Study area**

178 Eastern China (30°N-40°N, 112°E-122°E; Figure 1) has undergone remarkable economic expansion over  
179 the past three decades, which was accompanied by a substantial increase in AOD. Eastern China presents  
180 a unique atmospheric laboratory due to its complex aerosol composition - featuring both anthropogenic  
181 pollutants from industrial emissions and natural mineral dust transported from Central Asian deserts,  
182 particularly during the spring (Proestakis et al., 2018; Liu et al., 2021). The multitude of sources and the  
183 persistent nature of these aerosol particles, which can remain suspended for days to weeks and be  
184 transported over long distances in the absence of precipitation (Costantino et al., 2013; Li et al., 2021;  
185 Leung et al., 2023), makes eastern China an ideal study area for investigating aci. Our research leverages  
186 satellite observations to systematically evaluate the sensitivity of cloud properties ( $S_{CER}$  and  $S_{Nd}$ ) to the  
187 AOD variation, thereby revealing the scale-sensitive patterns of aerosol indirect effects and clarifying  
188 the regulatory role of LWP in cloud-aerosol interactions over this region.



189  
190 **Figure 1.** Map of annual averaged MODIS/AQUA level 2 AOD for all years during the period from 2008 to  
191 2022. The red rectangle (30°–40°N, 112°–122°E) indicates the study area.

192 **2.2 Data used**

193 Data used in this study were acquired by the MODIS instrument aboard NASA’s Aqua satellite, which  
194 features an extensive swath width of approximately 2300 km and comprehensive spectral coverage across  
195 multiple bands (King et al., 2003). The satellite’s equator crossing time is 13:30 (Local time, i.e. in the

196 early afternoon, coinciding with optimal development conditions for continental warm cloud systems  
197 (Wang et al., 2014; Liu et al., 2024). For aerosol characterization, we utilized the MODIS Collection 6.1  
198 aerosol product (MOD04), generated from cloud-screened pixels with a native resolution of 500 m at  
199 nadir and subsequently aggregated to 10 km grid cells (Remer et al., 2005; Levy et al., 2010). AOD  
200 retrieval over land uses radiances measured at the top of the atmosphere (TOA) at wavelengths of 0.47,  
201 0.66, and 2.13  $\mu\text{m}$  (Remer et al., 2005). The MODIS AOD (at 550 nm) Level 2 product (10 km  $\times$  10  
202 km) has been validated against ground-based remote sensing data and the results show that 69.40% of  
203 the MODIS AOD data fall within the expected uncertainty of  $\pm (0.05 + 15 \%)$  over land (Levy et al.,  
204 2013). In this study, AOD larger than 1.5 was excluded from further analysis to mitigate potential  
205 retrieval overestimation. This threshold was selected based on two key considerations: (1) Christensen  
206 et al. (2017) used MOD06 C6 data (1 km  $\times$  1 km) and reported that “large aerosol optical depths remain  
207 in the MODIS-observed pixels near cloud edges, due primarily to 3D effects (Varnáí and Marshak, 2009)  
208 and the swelling of aerosols by higher relative humidity”; (2) the threshold of 1.5 aligns with widely  
209 adopted thresholds in regional aerosol-cloud interaction studies over eastern China, where high AOD  
210 often coincides with complex surface conditions (e.g., urbanization, heterogeneous land cover) that  
211 exacerbate retrieval biases (Wang et al., 2015; Liu et al., 2017, 2021).

212 The cloud properties used in this study, including CER, LWP, COT, CTP, and cloud phase infrared (CPI)  
213 index, were derived from the Collection 6.1 MODIS Level 2 cloud product (MYD06) (King et al., 2003).  
214 The retrieval of these cloud characteristics utilizes six spectral channels spanning wavelengths from the  
215 visible to the near-infrared (0.66, 0.86, 1.24, 1.64, 2.12, and 3.75  $\mu\text{m}$ ) as described by King et al. (1997).  
216 Uncertainties in the MODIS C6.1 cloud parameters over land originate from instrument calibration,  
217 atmospheric correction, land surface properties, and model assumptions (Platnick et al., 2017, 2018). For  
218 COT, these include scene-dependent Level 1B data errors (1.5%–30%), land surface albedo errors  
219 ( $\pm 15\%$ ), and atmospheric correction errors ( $\pm 20\%$ ). The C6.1 algorithm addresses some prior limitations  
220 by inheriting C6’s optimized lookup table design, which reduces interpolation errors to 0.1%–0.2% for  
221 near-nadir views and corrects C5’s overestimation of thin-cloud COT (Platnick et al., 2017). CER  
222 uncertainties, stemming from solar irradiance error ( $\sim 4\%$  at 3.7  $\mu\text{m}$ ), atmospheric correction, and  
223 scattering differences, are mitigated as C6.1 retains C6’s separate multi-band reporting, thereby  
224 eliminating C5’s systematic bias (Platnick et al., 2017). LWP uncertainty is linked to COT/CER retrieval

225 errors and cloud-phase classification accuracy; the latter is improved by C6's voting-based phase  
226 algorithm (preserved in C6.1), which reduces misclassification over complex surfaces like vegetation  
227 and deserts (Marchant et al., 2015; Platnick et al., 2017). For CTP (1 km resolution), uncertainties from  
228 viewing angles and cloud structure are partially countered in C6.1 by assigning fill values when the 1 km  
229 retrieval fails, avoiding surface parameter defaults. For land clouds above 3 km, CTP accuracy reaches  
230 ~50 hPa (Baum et al., 2012). Finally, CPI adopts C6's weighted voting logic (replacing C5's sequential  
231 tree), with C6.1 maintaining an enhanced Phase Agreement Fraction against CALIOP/POLDER data,  
232 which reduces uncertainties from weak thin-cloud signals and complex land interference (Marchant et  
233 al., 2015; Platnick et al., 2017).

234 Following the methodology of Platnick et al. (2017), CER and COT measurements at  $3.7 \mu\text{m}$  were used  
235 to estimate  $N_d$  through adiabatic approximation principles (Quaas et al., 2006). Previous investigations  
236 have demonstrated that implementing filters based on cloud adiabaticity produced minimal effects on  
237  $S_{Nd}$  estimates while significantly reducing the available dataset by up to 63.00% (Gryspeerd et al., 2022).  
238 Therefore, such filtering procedures were not adopted in the current analysis. Instead,  $N_d$  calculations are  
239 initially performed at the native pixel resolution (approximately 1 km) prior to spatial aggregation,  
240 thereby avoiding potential biases associated with deriving  $N_d$  from nonlinear combinations of CER and  
241 COT at coarser resolutions (Feingold et al., 2022). To maintain data quality, the analysis incorporated  
242 several quality control measures: only single-phase liquid clouds (CPI = 1) with CTP exceeding 700 hPa  
243 and LWP smaller than  $200 \text{ g m}^{-2}$  are considered, consistent with the typical atmospheric distribution of  
244 aerosols in the lower troposphere (Michibata et al., 2014). Pixels with CER values smaller than  $4 \mu\text{m}$  or  
245 COT values smaller than 4 were excluded due to increased retrieval uncertainties (Sourdeval et al., 2016).  
246 Additionally, observations were restricted to solar zenith angles  $<65.00^\circ$  and sensor zenith angles  
247  $<41.40^\circ$ . This constraint was intended to reduce the influence of well-documented biases, as elaborated  
248 in Grosvenor et al. (2018).

249 CALIPSO (Cloud-Aerosol Lidar and Infrared Pathfinder Satellite Observations) operates within the A-  
250 Train constellation alongside the Aqua satellite and other NASA Earth-observing platforms. The primary  
251 instrument aboard CALIPSO is the Cloud-Aerosol Lidar with Orthogonal Polarization (CALIOP).  
252 CALIOP is a two-wavelength, polarization-sensitive lidar specifically designed to provide high-  
253 resolution vertical profiles of aerosols and clouds on a global scale (Winker et al., 2009). The mission

254 and its lidar instrument are described in Winker et al. (2009), and the associated Level 1 data products  
255 are detailed in Winker et al. (2010). This advanced sensor features an exceptionally narrow ground  
256 footprint of 70 m diameter for each laser pulse. The vertical resolution of CALIOP's products varies with  
257 altitude: 30 m within 0-8.2 km, 60 m between 8.2-20.2 km, and 180 m from 20.2-30.1 km, while  
258 maintaining a consistent 5 km horizontal resolution along the track direction (Liu et al., 2009).  
259 The coordinated A-Train configuration ensures near-simultaneous observations (within 1-2 minutes)  
260 between MODIS/Aqua and CALIOP/CALIPSO for identical atmospheric targets (Stephens et al., 2002).  
261 This temporal synchronization guarantees data consistency when extracting coincident measurements,  
262 avoiding interferences such as aerosol diffusion and cloud evolution caused by observational time lags—  
263 an advantage unparalleled by positioning methods like random grid points and ground-based stations.  
264 For spatial compatibility, we resampled the higher-resolution MODIS cloud products (CER, LWP, and  
265  $N_d$  at 1 km native resolution) to match CALIOP's 5 km along-track scale, while directly utilizing the 5  
266 km-resolution CTP and CPI parameters. In cases where CALIOP detected aerosol presence, we  
267 computed spatial averages of MODIS aerosol and cloud retrieval products across multiple observation  
268 scales (detailed in Section 2.4) centred on CALIOP targets. This approach assumes reasonable  
269 homogeneity of aerosol properties between adjacent clear and cloudy regions (Anderson et al., 2003;  
270 Quaas et al., 2008). Table 1 provides a comprehensive overview of the aerosol and cloud datasets  
271 including the parameters used from each product, the resolution, and the data source, used in this study.

272  
273  
274  
275  
276  
277  
278  
279  
280  
281  
282  
283

284 **Table 1. Aerosol and cloud products, parameters, horizontal resolutions, and their sources applied in the**  
 285 **present study.**

<b>Product</b>	<b>Parameters</b>	<b>Horizontal resolution</b>	<b>Data source</b>		
Aerosol (MYD04 Level 2 Collection 6)	Latitude	10 km	MODIS		
	Longitude	10 km			
	Scan_Start_Time	10 km			
	AOD at 550 nm	10 km			
Cloud (MYD06 Level 2 Collection 6)	Latitude	5 km			
	Longitude	5 km			
	Scan_Start_Time	5 km			
	CER at 3.7 um and 2.1 um	1 km			
	LWP at 3.7 um	1 km			
	COT at 3.7 um	1 km			
	Cloud multi-layer flag	1 km			
	Cloud_Phase_Infrared_Day	5 km			
	Cloud_TOP_Pressure_Day	5 km			
	Sensor_Zenith_Day	5 km			
	Solar_Zenith_Day	5 km			
	Aerosol (05kmALay)	Latitude		5 km	CALIOP
		Longitude		5 km	
Profile_Time		5 km			

286 **2.3 Calculation of sensitivities**

287 Variations in aerosol loading significantly influence cloud optical properties (such as COT) and  
 288 microphysical parameters (such as CER). Under specific environmental conditions, aerosol particles can  
 289 transform into CCN or INP, a process primarily determined by their chemical composition and ambient  
 290 temperature (Bellouin et al., 2020). When these nuclei are activated, water vapor condenses on their  
 291 surfaces to form cloud droplets or ice particles. As the concentration of aerosol particles increases, the  
 292 number of CCN or INP may rise correspondingly, leading to an increase in the number of cloud droplets.  
 293 Notably, under conditions where the liquid water content in clouds remains constant (i.e., LWP), the same  
 294 amount of water vapor is distributed across more cloud droplets, resulting in a reduction in the size of  
 295 individual droplets. Specifically, as aerosol concentration increases, the CER decreases, while cloud  
 296 albedo increases. On the basis of findings of Kaufman and Fraser (1997), Feingold et al. (2001) pointed  
 297 out that the sensitivity of cloud microphysical properties (e.g., CER) to changes in the number  
 298 concentration of aerosol particles (e.g., using AOD as a measure) can be described by the following  
 299 formula:

300 
$$S_{\text{CER}} = \left. \frac{d \ln r_e}{d \ln \alpha} \right|_{\text{LWP}} \quad -0.33 < S < 0 \quad (1)$$

301 Where  $r_e$  represents the CER and  $\alpha$  represents the AOD. Following Andreae (2009), AOD and CCN  
 302 are correlated and AOD varies with CCN following a power law relationship. Eq. (1) describes the  
 303 relative change of CER with the relative change of the AOD for constant LWP. It is noted that this  
 304 formulation differs from that used in recent studies (e.g., Bellouin et al., 2020) where S is expressed in  
 305 terms of  $N_d$  with no restriction in LWP. The sensitivity S of CER to AOD can be determined as the slope  
 306 of a linear fit to a log-log plot of CER versus AOD. The effect of aerosols on CER is analyzed by  
 307 comparing the difference in  $S_{\text{CER}}$  and correlation coefficients between AOD and CER under different  
 308 spatial scales (Section 2.4) and LWPs (Section 3.2).

309 In this study, the variation in  $N_d$  with CCN is referred to as the susceptibility  $S_{N_d}$ . Following the method  
 310 of Gryspeerdt et al. (2023), the sensitivity,  $S_{N_d}$ , of a cloud property,  $N_d$ , to  $\alpha$  is defined here as

311 
$$S_{N_d} = d \ln N_d / d \ln \alpha \quad 0 < S < 1 \quad (2)$$

312 Relations between CER and  $N_d$  and AOD are determined through Eq. 1 and Eq. 2 and correlation  
 313 coefficients R. The significance of these relations is determined by using the student's t test, i.e. the  
 314 results are statistically significant when the p value is smaller than 0.01, where p is defined as the  
 315 probability of obtaining a result equal to or "more extreme" than what was actually observed.

316 This method quantifies the sensitivity of CER and  $N_d$  to AOD variations via linear regression in log-log  
 317 space, using Eq. 1 and Eq. 2, respectively. Its core assumptions, uncertainties, and limitations are highly  
 318 consistent: both rely on AOD as an aerosol proxy variable, assume constant cloud liquid water content  
 319 and a linear sensitivity relationship, and depend on the reliability of satellite-retrieved parameters  
 320 (Feingold et al., 2001; Gryspeerdt et al., 2023). However, AOD cannot distinguish aerosol size and  
 321 hygroscopicity, retrieval errors are substantial in clean conditions, and linear fitting fails to capture  
 322 nonlinear/non-monotonic responses. Both methods are constrained by satellite retrieval biases, limited  
 323 scenario applicability (only valid for specific homogeneous clouds and aerosol types), the omission of  
 324 key modulating factors (dynamical conditions, aerosol type) and feedback processes, and can only assess  
 325 first-order direct effects. Reliability requires scenario constraints and uncertainty analysis; the only  
 326 nuances come from the target variable (CER vs.  $N_d$ ), which do not alter the shared methodological  
 327 limitations.

328

## 329 2.4 Research design for scale effects analysis

330 This study was conducted at multiple spatial scales to examine the scale dependence of  $S_{CER}$  and  $S_{Nd}$  in  
331 delineating aci (Fig. 2). Here, the spatial scales are described by two parameters: study area size (the  
332 geographic scope of the analysis) and buffer size (the local spatial extent around each observation point  
333 for aggregating aerosol and cloud data). To this end, the study area was divided into four congruent square  
334 research areas all centered at the same geographical location (35°N, 117°E) over Eastern China. Hence,  
335 spatial extent varies from the whole study area as defined in Section 2.1 (30°N-40°N, 112°E-122°E) to  
336 successively smaller areas simulated by decreasing the study area in steps of 2° to 4°×4° as illustrated in  
337 Figure 2a.

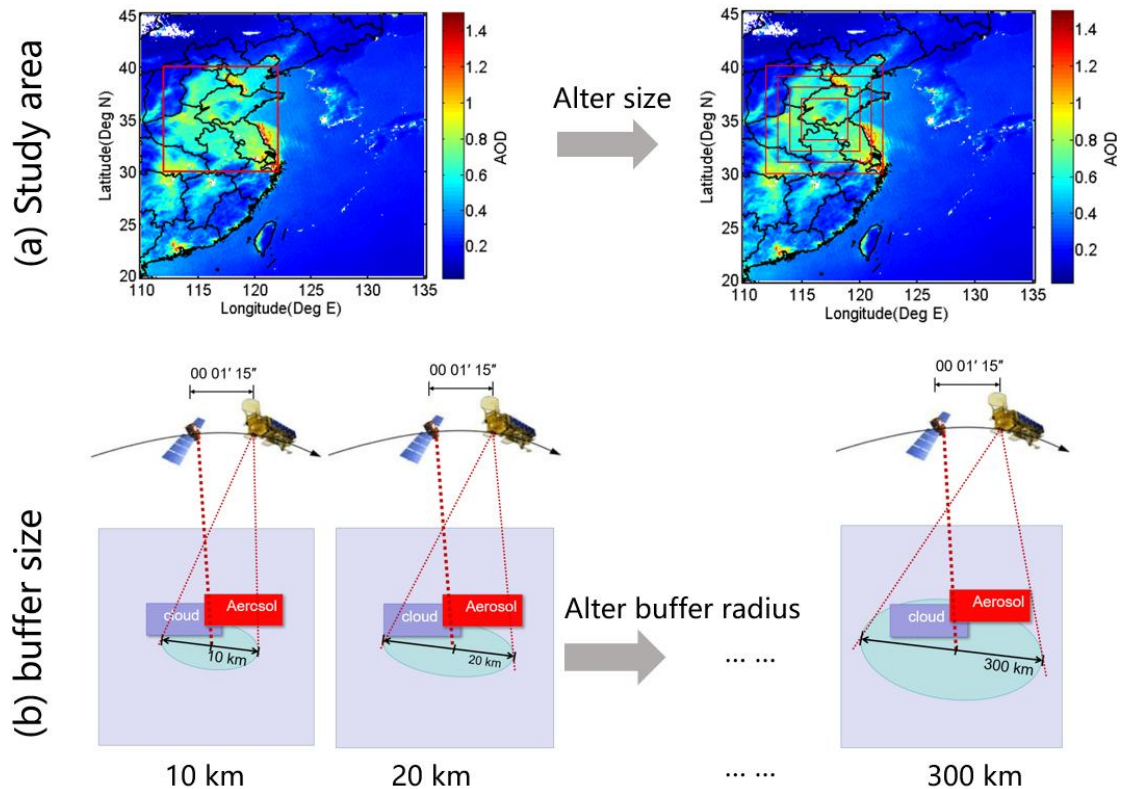
338 Buffer size refers here to a circular spatial domain centered at each CALIOP-detected point in the study  
339 area where CALIOP detected the presence of aerosols. Within this circular domain, MODIS-retrieved  
340 cloud and aerosol data (AOD, CER,  $N_d$ , LWP) are spatially averaged to construct matched aerosol-cloud  
341 datasets at different local scales. As previously noted, this approach relies on the assumption that aerosol  
342 properties are reasonably homogeneous between adjacent clear and cloudy regions (Anderson et al., 2003;  
343 Quaas et al., 2008), and this premise is supported by the short-range transport of aerosols (e.g., 10–300  
344 km) and the near-simultaneous observations (1–2 minutes) by MODIS and CALIOP within the A-Train  
345 constellation.

346 Buffer zones with sizes increasing from 10 to 300 km (10 km, 20 km, 30 km, 40 km, 50 km, 60 km, 70  
347 km, 80 km, 90 km, 100 km, 120 km, 140 km, 150 km, 160 km, 180 km, 200 km, 250 km, and 300 km)  
348 were determined within the whole study area by using CALIOP data. Previous observations indicate that  
349 the typical horizontal scale of cloud clusters ranges from tens to hundreds of kilometers (Zhang et al.,  
350 2024; Cai et al., 2022), supported by CloudSat/CALIPSO satellite data showing power-law distributed  
351 cloud scales (10-1000 km fitting range) covering major cloud types (Zhang et al., 2024) and regional  
352 evidence of consistent multi-season, multi-latitude cloud extents (Cai et al., 2022). Meanwhile, aerosol  
353 spatial homogeneity varies with distance: local-scale aerosols ( $\leq 50$  km) exhibit high homogeneity due  
354 to consistent sources and stable diffusion, while regional-scale aerosols ( $> 100$  km) show enhanced  
355 heterogeneity from multi-source mixing and atmospheric transport (Hassan et al., 2024; Mohebalhojeh  
356 et al., 2026). Thus, the 10–300 km buffer range covers both cloud characteristic scales and the aerosol  
357 homogeneity transition range, ensuring that MODIS data averaging effectively captures cloud-aerosol

358 coupling. This range avoids insufficient MODIS pixel coverage due to excessively small buffer sizes (<  
359 10 km). It also prevents conflation between regional meteorological variations and local aci signals  
360 arising from overly large buffer sizes (> 300 km), as synoptic-scale circulation and other regional  
361 meteorological changes may interfere with local aci signals (Quaas et al., 2010). Meanwhile, this range  
362 aligns with the 50 - 150 km buffer sizes widely adopted in regional aci studies (Wang et al., 2015; Liu et  
363 al., 2017; 2024), enabling cross-validation of results and ensuring that MODIS data averaging effectively  
364 captures cloud-aerosol coupling.

365 MODIS-retrieved cloud and aerosol data were averaged over a buffer area around each CALIOP data  
366 point with a radius varying from 10 km to 300 km. Thus, a dataset including aerosol and cloud properties  
367 was constructed with different buffer sizes. The effect of buffer size on the sensitivity of CER and  $N_d$  to  
368 variations in AOD was determined in each study area varying from  $4^\circ \times 4^\circ$  to  $10^\circ \times 10^\circ$ . To this end, for  
369 each buffer size, the averaged AOD and cloud parameters were paired to calculate the sensitivities  $S_{CER}$   
370 (Eq. 1) and  $S_{N_d}$  (Eq. 2), as well as their correlation coefficients (R) between cloud properties (e.g., CER,  
371  $N_d$ ) and AOD. The optimal buffer size for each study area is defined as the one maximizing the R. This  
372 definition is adopted based on two core considerations. Firstly, it aligns with the statistical principle that  
373 a higher R value indicates a stronger linear correlation between the two variables in the log-log space,  
374 minimizing the interference of random noise and non-aerosol confounding factors on the sensitivity  
375 estimation (Quaas et al., 2006; Gryspeerd et al., 2022). This ensures that the derived  $S_{CER}$  can reliably  
376 reflect the intrinsic relationship between aerosol loading and cloud droplet effective radius, rather than  
377 spurious correlations caused by inappropriate spatial scales. Secondly, this definition also facilitates  
378 comparability with existing literature, as it aligns with the methodological framework of satellite-based  
379 aerosol-cloud interaction studies (Saponaro et al., 2017; Liu et al., 2021). In these studies, the optimal  
380 spatial scale is typically identified by maximizing the statistical robustness of variable correlations.

381 The dataset was used to study the characteristics of aerosol indirect effects as function of buffer size and  
382 study area, for two different periods: one with a high aerosol content (2008-2014) and another one with  
383 a decreasing aerosol content (2015-2022). This approach enabled the determination of the optimal buffer  
384 size for aerosol indirect effects as function of the size of the study area, ultimately leading to the  
385 development of a parameterization scheme for aerosol indirect effects for observations with different  
386 spatial resolution and different sizes of the study area over eastern China.



387

388 **Figure 2. (a) Schematic diagram of study area and buffer size patterns applied in this study. (b) scheme of**  
 389 **CALIPSO-MODIS coincidence methodology. When CALIPSO detects the presence of aerosol and cloud fields,**  
 390 **we look for MODIS retrievals within a buffer size from the CALIPSO target. The temporal coincidence is**  
 391 **insured by the coordinated satellite orbits.**

### 392 **3 Results**

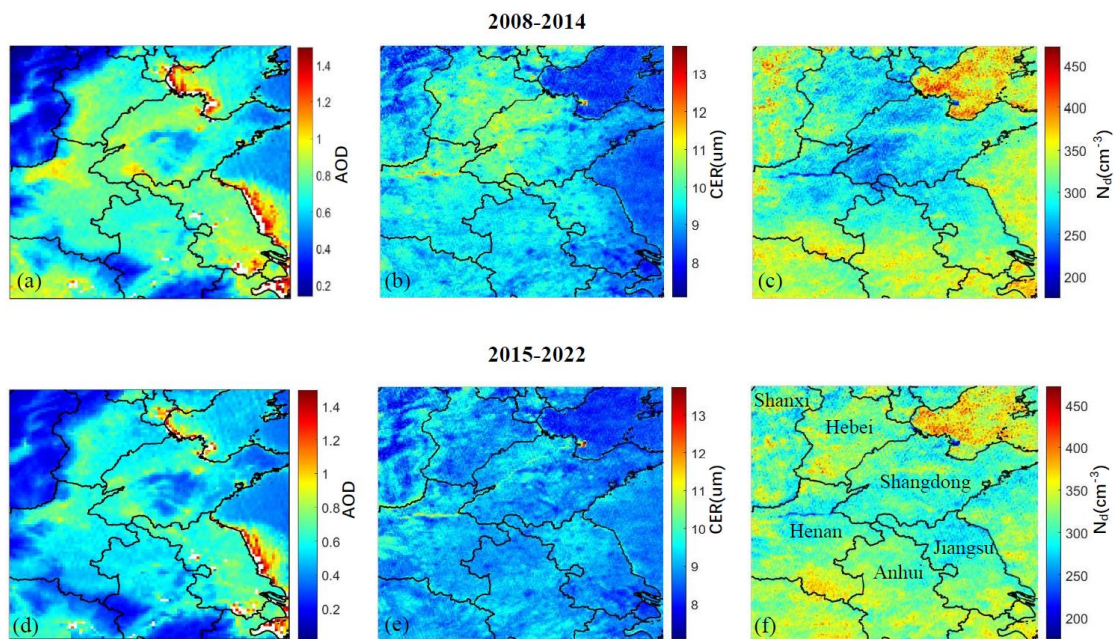
#### 393 **3.1 Spatial variations of aerosol and cloud parameters**

394 Figure 3 illustrates the spatial distributions of AOD and cloud properties (CER and  $N_d$ ) across the study  
 395 region, averaged for the periods 2008-2014 and 2015-2022. The AOD spatial patterns (Fig. 3a,d) show  
 396 similar spatial distributions during both periods, but with notably reduced values during the latter.  
 397 Pronounced spatial gradients in AOD are evident during both periods. The lowest AOD values occur over  
 398 the mountainous regions of Shanxi province in the northwest, while elevated concentrations appear in  
 399 the southeastern areas encompassing the Hebei and Shandong provinces. This geographical contrast  
 400 arises from the mountain ranges that demarcate the heavily industrialized, densely populated North China  
 401 Plain (NCP) in the east - characterized by substantial anthropogenic emissions - from the relatively  
 402 pristine western regions. Under prevailing southeasterly wind conditions, these topographic barriers  
 403 effectively block transport of atmospheric pollutants which accumulate along their windward slopes

404 (Sundström et al., 2012). The concentration of heavy industries and power generation facilities in the  
 405 NCP are primarily responsible for the observed high AOD concentrations, together with meteorological  
 406 and geographical conditions. Additionally, lower AOD values appear in southern Anhui and central  
 407 Shandong relative to the surrounding regions.

408 The CER spatial distributions (Fig. 3b,e) reveal distinct differences between the two periods. During  
 409 2008-2014, larger cloud droplets predominated in the northern sectors, particularly throughout Hebei and  
 410 western Shandong. Notably, the spatial correspondence between AOD and CER maxima aligns with the  
 411 anti-Twomey effect, suggesting that the high aerosol loading promoted cloud droplet growth rather than  
 412 suppression - consistent with findings from Wang et al. (2014) and Liu et al. (2018). The 2015-2022  
 413 period shows markedly reduced CER values (typically  $<10 \mu\text{m}$ ) with enhanced spatial homogeneity.

414 Similarly,  $N_d$  exhibits contrasting spatial patterns between the two periods (Fig. 3c,f). The earlier  
 415 timeframe shows depressed  $N_d$  values in central regions surrounded by elevated concentrations  
 416 peripherally. This pattern reverses during 2015-2022, with increases of  $N_d$  in the central area  
 417 accompanied by overall reduction of the cloud droplet concentrations in the surrounding regions.

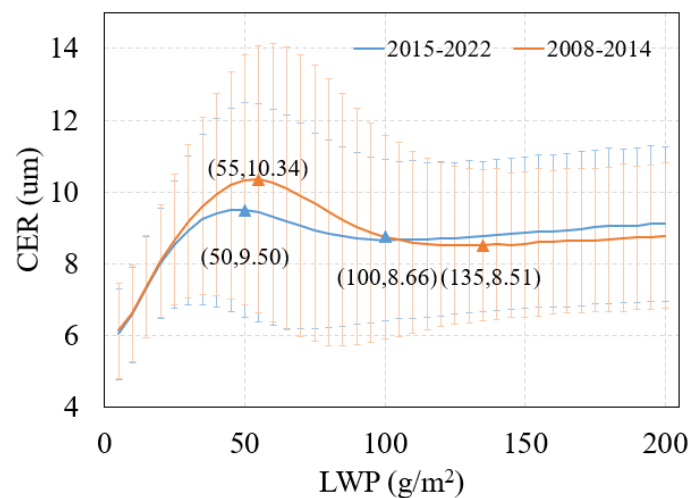


418  
 419 **Figure 3. Spatial distributions of AOD (a, d), CER (b, e) and  $N_d$  (c, f), averaged over the years 2008-2014 (top**  
 420 **row) and 2015-2022 (bottom row) over the study area. The lines are provincial borders and the names of**  
 421 **provinces mentioned in the text are indicated in Fig. (f).**

### 422 3.2 Sensitivity of CER to AOD stratified by LWP

423 Before analyzing the influence of AOD on CER, the relationship between CER and LWP should be

424 investigated. The values of the LWP were divided into 40 subsets with a width of  $5 \text{ g/m}^2$ , and then the  
 425 average value of CER in each subset was calculated and plotted as function of LWP (Figure 4).  
 426 The variation of CER with LWP shows three regimes. For LWP smaller than  $55 \text{ g/m}^2$  (period 1) or  $50$   
 427  $\text{g/m}^2$  (period 2), CER increased rapidly with the increase of LWP. This first LWP regime is referred to as  
 428 a rapid growth regime (LWP1). The second LWP regime, referred to as a decreasing regime (LWP2),  
 429 applies to the LWP range from  $55 \text{ g/m}^2$  to  $135 \text{ g/m}^2$  (period 1) or  $50\text{-}100 \text{ g/m}^2$  (period 2) and CER  
 430 decreased with the increase of LWP. When LWP was greater than  $135 \text{ g/m}^2$  (period 1) or  $100 \text{ g/m}^2$  (period  
 431 2), CER increased with increasing LWP but at a much slower rate than during the first regime; the third  
 432 LWP regime is therefore referred to as a slow growth regime (LWP3). These results show that CER is  
 433 very sensitive to the changes in LWP, which is consistent with the study of Liu et al. (2021). Specifically,  
 434 CER exhibited a three-stage variation with LWP: rapid growth when  $\text{LWP} < 50 \text{ g/m}^2$  (with the fastest  
 435 change rate), a stable state during  $50\text{-}150 \text{ g/m}^2$ , and slow growth when  $\text{LWP} > 150 \text{ g/m}^2$  (at a rate much  
 436 lower than the first stage). This highlighted the necessity of fixing LWP conditions to accurately  
 437 investigate the impact of AOD on CER. To separate the effects of changing LWP on CER from those of  
 438 changing AOD on CER, relations between CER and AOD were evaluated for constant LWP  
 439 (McComiskey et al., 2012), for each of the three regimes mentioned above, by using double-logarithmic  
 440 plots of AOD versus CER. The number of CER observations in the third regime is too small to achieve  
 441 statistically meaningful results, therefore the sensitivity of CER to AOD was only analyzed for the rapid  
 442 growth and decreasing regimes.



443  
 444 **Figure 4. Variation of CER with LWP over the study area. Here all CER data were averaged in LWP bins,**  
 445 **from 0 to 200  $\text{g/m}^2$  with a width of  $5 \text{ g/m}^2$ . The red line is a fit to the data during 2008-2014 and the blue line**  
 446 **for the data during 2015-2022. The numbers in parentheses indicate the (LWP, CER) values for the inflection**

447 points between the regimes. The error bars (the vertical lines) denote the standard deviations, indicating the  
448 variability of CER around the average at each LWP value.

### 449 3.2.1 Rapid CER growth regime

450 For the first LWP regime, the  $S_{CER}$  is negative (as shown in Figure 5). This aligns with the Twomey effect  
451 (Twomey, 1977): an increase in aerosols raises the number of CCN, and with constant LWP, less water  
452 vapor is available per cloud droplet, reducing CER, increasing cloud albedo, and ultimately cooling the  
453 atmosphere. This indicates that, in the rapid growth regime, the interaction between AOD and CER in  
454 the target region is in agreement with the Twomey effect. The data in Figure 5a show that during period  
455 1,  $S_{CER}$  varies with buffer size and that the variations are different for different study areas. The value of  
456  $|S_{CER}|$  is smallest for the largest study area ( $10^\circ \times 10^\circ$ ) and decreases with buffer size to a minimum for  
457 buffer size of 150 km and then increases. For the smallest study area ( $4^\circ \times 4^\circ$ ), the sensitivity exhibits a  
458 much stronger negative correlation, with its magnitude decreasing as the buffer size expands, especially  
459 for  $50 \text{ km} < \text{buffer size} < 100 \text{ km}$ . For the 2 intermediate study areas, the sensitivities are initially similar  
460 (except for the smallest buffer size) and diverge for  $\text{buffer size} > 100 \text{ km}$ . The data show that the value of  
461  $|S_{CER}|$  overall becomes smaller as study area increases. The decrease of  $|S_{CER}|$  with increasing study area  
462 is mechanistically tied to scale-dependent aerosol indirect effect theory and meteorological confounding  
463 (Quaas et al., 2009; McComiskey & Feingold, 2012). The correlation coefficients R (bottom of Figure 5  
464 a) are similar for all four study areas at small buffer sizes, increase fast with buffer size to a maximum  
465 for a buffer size of about 50 km and then decrease and diverge. The largest decrease is observed for study  
466 area of  $10^\circ \times 10^\circ$ . In this study, the optimal scale for each study area is indicated in Figure 5 with a red  
467 solid square. A plot of the optimal scale versus the size of the study area in Figure 6 (curve LWP1-period1)  
468 shows that, as the study area size increased from  $6^\circ \times 6^\circ$  to  $10^\circ \times 10^\circ$ , the optimal scale decreased from  
469 100 km to 30 km.

470 As compared with period 1, in period 2 (Figure 5b) the value of the  $|S_{CER}|$  also decreases as the buffer  
471 size increases. However, the scale sensitivity analysis for period 2 revealed two distinct characteristics  
472 different from period 1: (1) the four  $S_{CER}$  curves for different study areas are much closer than during  
473 period 1; (2) with the exception of the study area of  $10^\circ \times 10^\circ$ , the values of the  $|S_{CER}|$  for the other three  
474 study areas are significantly reduced (closer to zero), indicating a corresponding weakening of aerosol-  
475 cloud interaction intensity against the background of decreased aerosol concentrations. Particularly

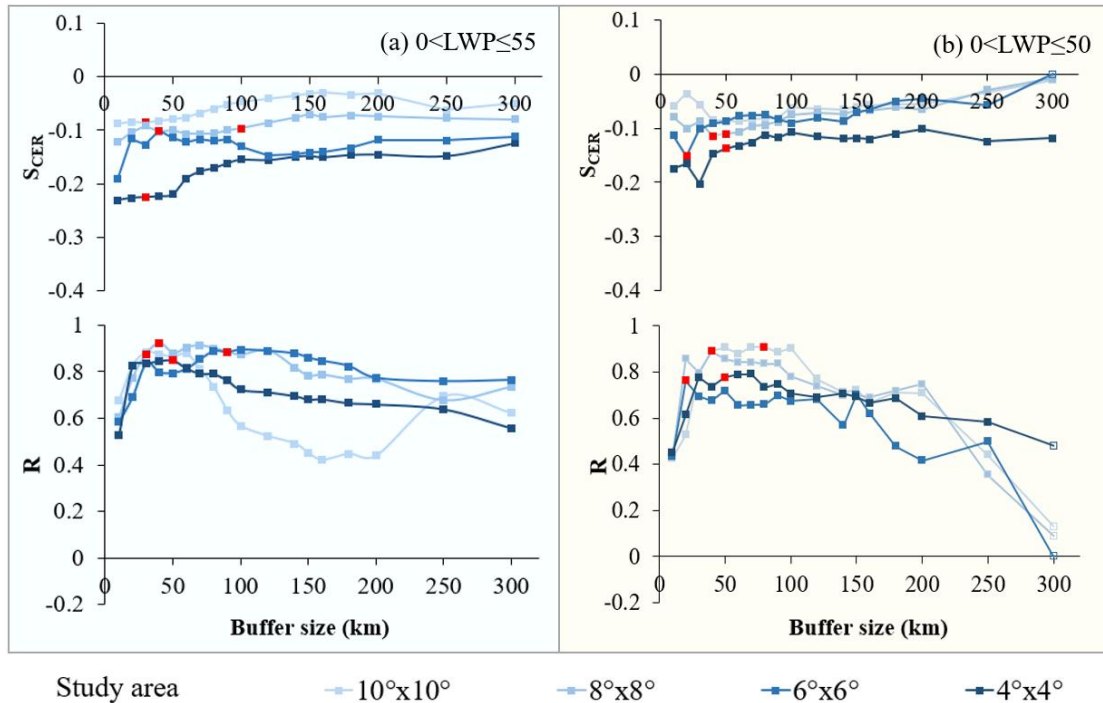
476 noteworthy is that during period 1, the R values for the  $10^{\circ}\times 10^{\circ}$  study area showed a sharp declining  
477 trend when the buffer size exceeds 60 km, while in period 2 this happened for buffer size larger than 110  
478 km and the R value curves for all study areas significantly expanded their high-value ranges. Also for  
479 period 2, the R values for the study areas of  $10^{\circ}\times 10^{\circ}$  and  $8^{\circ}\times 8^{\circ}$  are very similar, in contrast to period 1  
480 when only the R values for the study areas of  $10^{\circ}\times 10^{\circ}$  decreases fast. Across different study areas, the  
481 optimal scale (Curve LWP1-peirod2) shows a behavior opposite to that during period 1: as the study area  
482 size increased from  $6^{\circ}\times 6^{\circ}$  to  $10^{\circ}\times 10^{\circ}$ , the optimal scale increased from 20 km to 80 km. It is noted that  
483 for a study area of  $4^{\circ}\times 4^{\circ}$  the optical scale was 50 km in both periods. For the first LWP regime,  $S_{CER}$   
484 estimates and correlation coefficients R by period and optimal buffer size across  $4^{\circ}\times 4^{\circ}$  to  $10^{\circ}\times 10^{\circ}$  study  
485 areas are given in Supplement Table S1.

### 486 3.2.2 Decreasing CER regime

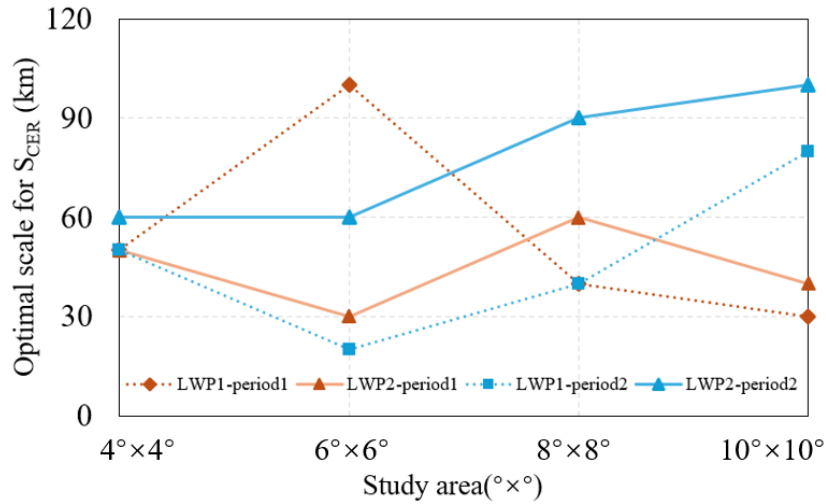
487 During the second LWP regime (Figure 7), the AOD and CER were also negatively correlated ( $S_{CER}<0$ )  
488 during both periods, but the values of  $S_{CER}$  vary stronger with the size of study area: the curve dispersion  
489 increases in the second LWP regime, the values of  $|S_{CER}|$  are larger overall, and the relatively concentrated  
490 trend in the period 1 shifts to more scattered fluctuations in the period 2. During period 1, for the largest  
491 ( $10^{\circ}\times 10^{\circ}$ ) study area: the value of  $|S_{CER}|$  (Figure 7a) decreases with increasing buffer size, nearing zero  
492 at ~150 km, briefly turning slightly positive, then slowly falling below zero by 220 km. For the three  
493 smaller study areas, the  $S_{CER}$  values were all negative and  $|S_{CER}|$  overall decreased with increasing buffer  
494 size. Through the sensitivity of  $S_{CER}$  to buffer size across varying study areas during period 1, the value  
495 of  $|S_{CER}|$  for a given buffer size becomes smaller with increasing study area size. Additionally, across all  
496 study areas,  $|S_{CER}|$  initially increases with the increase of the buffer size, then decreases, and gradually  
497 stabilizes thereafter. The data in Figure 6 (Curve LWP2-peirod1), show that, the optimal size varies  
498 between 30 km and 60 km with no clear dependence on the size of the study area.

499 Compared with period 1, the value of  $|S_{CER}|$  in period 2 (Figure 7b) also decreased overall with increasing  
500 buffer size, and at the same buffer size,  $|S_{CER}|$  decreased as study area increased. However, the scale  
501 sensitivity analysis for period 2 revealed two distinct characteristics: (1) the four curves for different  
502 study areas are closer than during period 1; (2) the  $|S_{CER}|$  for the study area of  $10^{\circ}\times 10^{\circ}$  was overall larger,  
503 while the values of the  $S_{CER}$  curves for the study areas of  $4^{\circ}\times 4^{\circ}$  and  $6^{\circ}\times 6^{\circ}$  were significantly reduced and

504 that for the study area of  $8^\circ \times 8^\circ$  was slightly reduced. The reduction may be attributed to weakened  
 505 aerosol-cloud interactions resulting from decreased regional aerosol concentrations (Jia et al., 2022; Li  
 506 et al., 2024; Zhao et al., 2025). The variation of the optimal scale (Curve LWP2-period2) with the size of  
 507 the study area is similar to that during period 1 in the rapid growth LWP regime: as the study area size  
 508 increased from  $6^\circ \times 6^\circ$  to  $10^\circ \times 10^\circ$ , the optimal scale increased from 60 km to 100 km. For the second  
 509 LWP regime,  $S_{CER}$  estimates and correlation coefficients R between CER and AOD by period and optimal  
 510 buffer size across  $4^\circ \times 4^\circ$  to  $10^\circ \times 10^\circ$  study areas are given in Supplement Table S1.  
 511 Through comparative analysis of  $S_{CER}$  data distribution across different LWP regimes under different  
 512 aerosol conditions (i.e. high AOD and decreasing AOD), we found that the  $|S_{CER}|$  in the second LWP  
 513 regime is significantly larger than that in first LWP regime except for the study area of  $10^\circ \times 10^\circ$  for buffer  
 514 size  $>100$  m, where  $S_{CER}$  curves corresponding to different study areas show greater dispersion. This  
 515 pattern highlights the dominant role of LWP in regulating aerosol-cloud interaction sensitivity, with AOD  
 516 variations further modulating the magnitude of such differences. Sample sizes of CER and AOD for the  
 517 first LWP regime across both study periods, all buffer sizes and study areas, are presented in Supplement  
 518 Tables S3–S6.

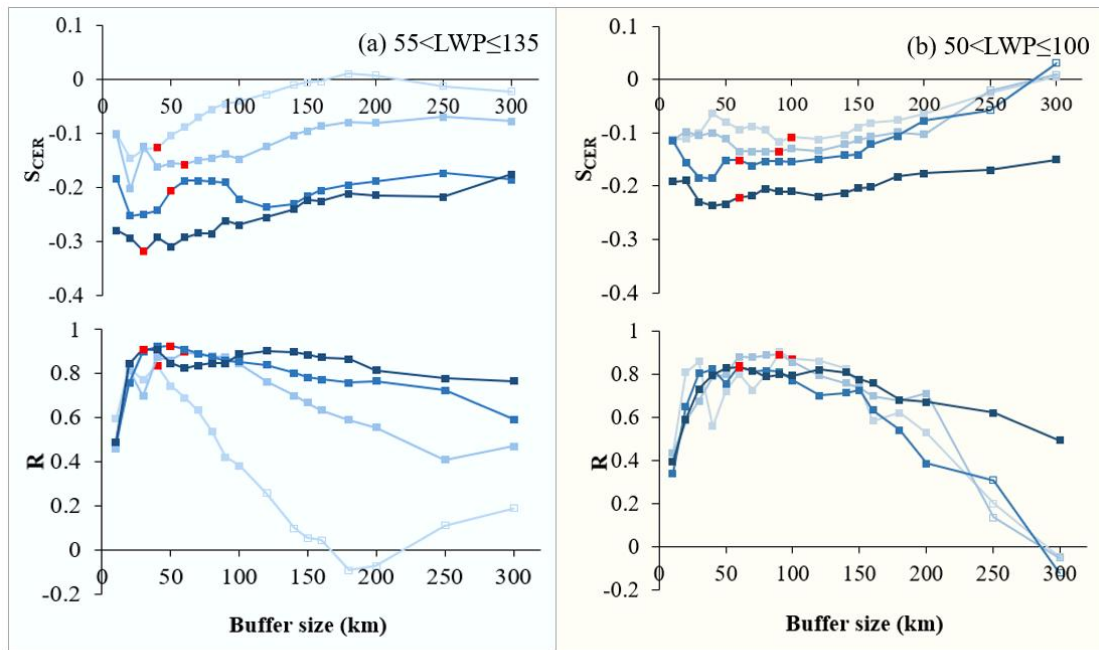


519 Study area  $10^\circ \times 10^\circ$   $8^\circ \times 8^\circ$   $6^\circ \times 6^\circ$   $4^\circ \times 4^\circ$   
 520 Figure 5. Variation of  $S_{CER}$  (top) and correlation coefficient R (bottom) with buffer size for different study  
 521 areas (see legend at the bottom) for (a) the LWP regime with  $0 < LWP \leq 55$  g/m<sup>2</sup> over the years of 2008-2014 and  
 522 (b) the LWP regime with  $0 < LWP \leq 50$  g/m<sup>2</sup> over the years of 2015-2022. Filled squares indicate that the results  
 523 are significant at the 0.01 level and open squares indicate that the results are not statistically significant. The  
 524 red solid squares indicate the optimal buffer sizes for each study area, as shown in the Supplement Table S1.



525  
526  
527  
528  
529  
530

Figure 6. Relationship between optimal scale for SCER and the size of the study area. Here LWP1-period1 and LWP2-period1 indicate the optimal scale in period 2008-2014 for the first LWP regime and that for the second LWP regime, respectively. LWP1-period2 and LWP2-period2 indicate the optimal scale in period 2015-2022 for the first LWP regime and that for the second LWP regime, respectively.



Study area      —□— 10°x10°      —□— 8°x8°      —■— 6°x6°      —■— 4°x4°

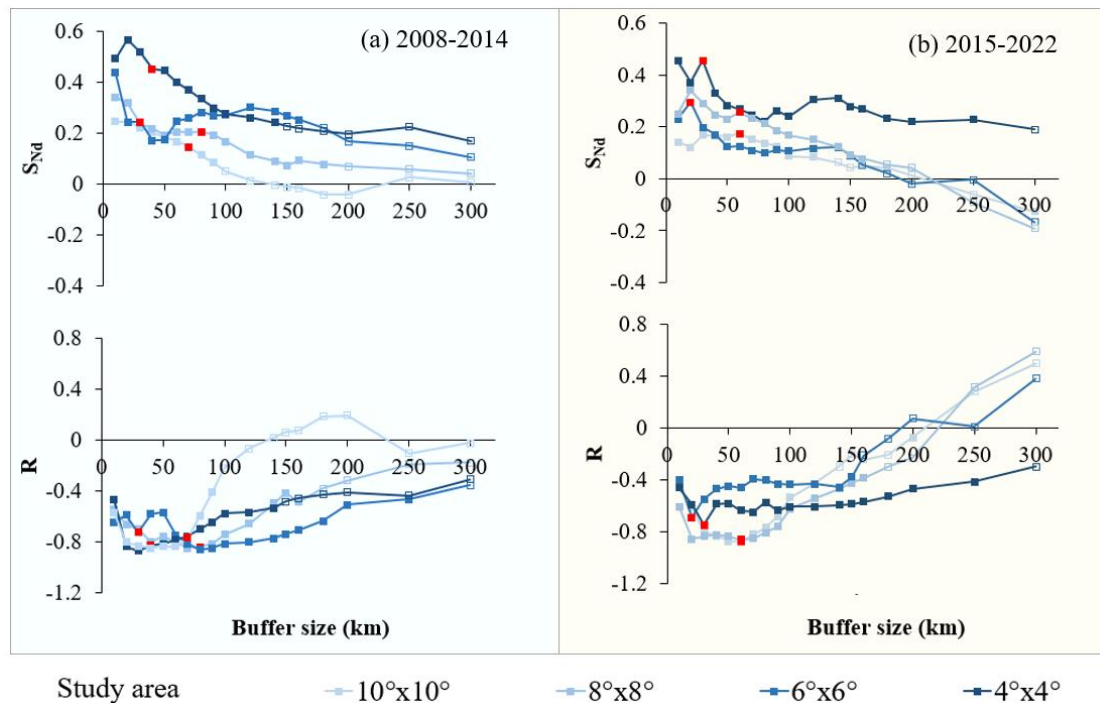
531  
532  
533  
534  
535  
536  
537

Figure 7. Variation of SCER (top) and correlation coefficient R (bottom) with buffer size for different study areas (see legend at the bottom) for (a) the LWP regime with  $55 < LWP \leq 135$  g/m<sup>2</sup> over the years of 2008-2014 and (b) the LWP regime with  $50 < LWP \leq 100$  g/m<sup>2</sup> over the years of 2015-2022. The filled squares indicates that the results are significant at the 0.01 level and the open squares indicates that the results are not statistically significant. The red solid squares indicate the optimal buffer sizes for each study area, as shown in the Supplement Table S1.

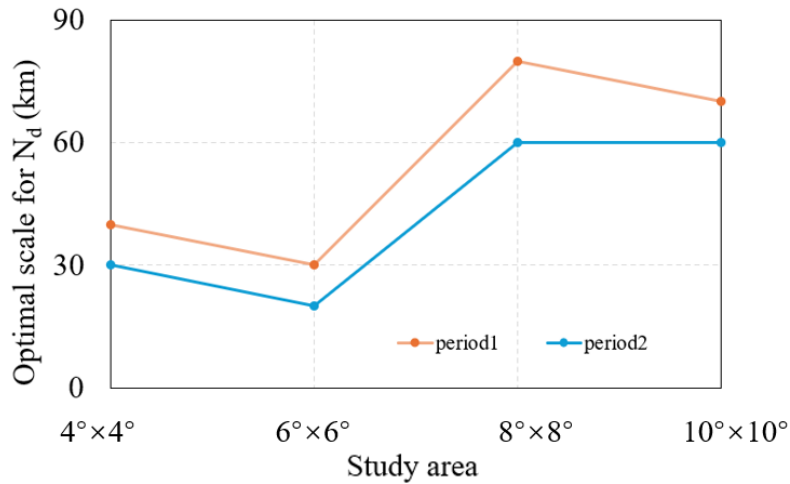
### 538 3.3 Sensitivity of $N_d$ to AOD

539 Eq. (2) shows that the value of the sensitivity of  $N_d$  to AOD is determined by the slope of a linear fit to a  
540 log-log plot of  $N_d$  versus AOD. To investigate  $S_{N_d}$ , we used correlated data pairs for each of the 7 years  
541 during periods 1 and 2, binned the data in AOD intervals with a bin width of 0.02, and the  $N_d$  data in  
542 each AOD bin were averaged. The variation of  $S_{N_d}$  with buffer size for different study areas over the  
543 target region is presented in Figure 8, for both periods. The data in Figure 8 show that, in contrast to  $S_{CER}$ ,  
544  $S_{N_d}$  is predominantly positive ( $p < 0.01$ ) during both periods, and decreases with increasing buffer size.  
545 During period 1, for the study area of  $6^\circ \times 6^\circ$ , the  $S_{N_d}$  initially decreases very fast to a minimum at a buffer  
546 size of 40 to 50 km, followed by an increase to a maximum at a buffer size of 120 km. For buffer size  $\geq$   
547 120 km, the  $S_{N_d}$  values are similar for the two smallest study areas and substantially larger than for the  
548 two larger study areas. During period 2, we can see an initial increase of  $S_{N_d}$  for the study area of  $6^\circ \times 6^\circ$   
549 and  $8^\circ \times 8^\circ$ , and variation of  $S_{N_d}$  for the study area of  $10^\circ \times 10^\circ$  and  $4^\circ \times 4^\circ$ . After that, the  $S_{N_d}$  for the study  
550 area of  $4^\circ \times 4^\circ$  and  $6^\circ \times 6^\circ$  decreases very fast to a minimum for a buffer size of 80 km, followed by an  
551 increase to a maximum for a buffer size of 140 km. The variation of R with buffer size for each of the  
552 two periods shows that the optimal buffer sizes are larger when the study area is larger. Specifically, these  
553 optimal sizes in the  $8^\circ \times 8^\circ$  and  $10^\circ \times 10^\circ$  study areas are larger than those in the  $4^\circ \times 4^\circ$  and  $6^\circ \times 6^\circ$  areas  
554 (Figure 9), reflecting different characteristics in aerosol-cloud interactions in different AOD conditions.  
555 The estimates of  $S_{N_d}$  and correlation coefficients R between  $N_d$  and AOD, stratified by optimal buffer  
556 size, for study areas ranging from  $4^\circ \times 4^\circ$  to  $10^\circ \times 10^\circ$  during the two periods are presented in the  
557 Supplement Table S2. It is noted that  $S_{CER}$  and  $N_d$  exhibit distinct anomalies in large buffer zones, which  
558 may be associated with key factors including aerosol distribution, meteorological heterogeneity, cloud  
559 type transitions, and satellite retrieval limitations.  
560 The chemical composition of aerosols, which directly affects AOD and CCN activation efficiency,  
561 underwent significant changes between the two periods due to policy interventions. During 2008–2014,  
562 aerosols over eastern China were dominated by sulfate, which accounted for 30%–40% of the  $PM_{2.5}$  mass  
563 (Huang et al., 2014; Zheng et al., 2018). Given the strong hygroscopicity of sulfate-dominated aerosols  
564 (Zhang et al., 2012; Liu et al., 2023), their CCN activation efficiency was likely high, which may have  
565 provided a critical physical basis for the aerosol-cloud indirect effect (Lee et al., 2009). In the period of  
566 2015–2022, driven by policies such as the Air Pollution Prevention and Control Action Plan (Zheng et

567 al., 2018), the chemical composition of aerosols underwent a structural transition. Specifically, the mass  
 568 fraction of sulfate dropped sharply to 15%–25% with an absolute concentration reduction of more than  
 569 50%, while the relative proportions of nitrate, carbonaceous aerosols (i.e., organic carbon (OC) and black  
 570 carbon (BC)), and secondary organic aerosols (SOA) showed an increasing trend (Huang et al., 2014;  
 571 Zheng et al., 2018). As these components generally exhibit weaker hygroscopicity compared with sulfate  
 572 (Zhang et al., 2012; Liu et al., 2023), such a compositional shift might have led to a decrease in CCN  
 573 activation efficiency under the same AOD conditions, thereby potentially weakening the sensitivity of  
 574 cloud droplet number concentration to AOD and altering the intensity and mode of aerosol-cloud  
 575 interactions to a certain extent (Lee et al., 2009).



576 Study area       $10^{\circ} \times 10^{\circ}$        $8^{\circ} \times 8^{\circ}$        $6^{\circ} \times 6^{\circ}$        $4^{\circ} \times 4^{\circ}$   
 577 **Figure 8.** Variation of  $S_{Na}$  (top) and correlation coefficient  $R$  (bottom) with buffer size for different study areas  
 578 (see legend **at the bottom**) for the LWP regime with  $0 < LWP \leq 200 \text{ g/m}^2$  over the years of 2008-2014 (a) and  
 579 2015-2022 (b). The **filled squares** indicates that the results are significant at the 0.01 level and the **open squares**  
 580 indicates that the results are not statistically significant. The red solid square indicates the optimal buffer size  
 581 for each study area, as shown in **the Supplement Table S2**.



582

583

584

**Figure 9. Relationship between optimal scale for  $N_d$  and the size of the study area. Here **period1** and **period2** indicate the optimal scale in period 2008-2014 and the optimal scale in period 2015-2022, respectively.**

585

## **4 Discussion**

586

### **4.1 The importance of **liquid water path** constraint**

587

LWP is a critical parameter governing cloud radiative properties (Murray-Watson et al., 2022). The quantification of albedo effects strongly depends on the spatial scale and the LWP. Neglecting LWP constraints in aerosol-cloud interaction studies can weaken microphysical signals, leading to underestimation of radiative forcing (McComiskey et al., 2012). To address this, we first systematically investigated the dynamic relationship between CER and LWP before analyzing CER sensitivity to AOD. The results demonstrate pronounced CER sensitivity to LWP variations, which can be categorized into three distinct **regimes (Figure 4)**:

594

**In the first** LWP regime, CER increases rapidly with LWP, **i.e. the evolution of CER is predominantly driven by changes in LWP**. This dominance may lead to overestimation of the influence of the AOD on CER (Liu et al., 2021).

597

**In the second** LWP regime, CER decreases with increasing LWP. **In** this regime, the regulatory effect of LWP on CER weakens significantly, and CER variations become increasingly governed by aerosol-related processes, indicating the growing dominance of aerosol indirect effects.

600

The third regime contains an insufficient number of CER observations to yield statistically significant results, **which excludes the** analysis of the sensitivity of CER to AOD.

602

**Comparative analysis of scale-conditioned  $S_{CER}$  across LWP regimes in periods 1 and 2 revealed**

603 markedly enhanced sensitivity of  $S_{CER}$  to AOD in the second LWP regime. There is a trade-off between  
604 AOD and LWP when the amount of water vapor is insufficient and CER becomes smaller. As suggested  
605 by Costantino et al. (2013), the LWP response to aerosol invigoration is influenced by two competing  
606 mechanisms: a drying effect caused by enhanced entrainment of dry air at cloud top (dominant in  
607 optically thin clouds) and a moistening effect from precipitation suppression (dominant in optically thick  
608 clouds). For larger LWP, the supply of cloud water is sufficient, and the increase in aerosol number  
609 concentrations significantly affects the distribution of cloud droplet number concentrations and sizes,  
610 enhancing the sensitivity of CER to AOD. For small aerosol concentrations, the values of  $|S_{CER}|$  (Figure  
611 5b, 7b) decreased overall with expanding buffer size within the same study area. For fixed buffer size,  
612  $|S_{CER}|$  decreased as the study area increased, and the ranges of  $|S_{CER}|$  values across different study area  
613 showed a convergent pattern, typically remaining small (close to zero). During the high AOD period  
614 (2008–2014), anthropogenic emissions and dust transport provided abundant CCN, laying the material  
615 foundation for aerosol-cloud interactions. This enhanced the synergistic effect of “sufficient liquid water  
616 + abundant CCN” in the second LWP regime, amplifying the difference in  $S_{CER}$  between the two LWP  
617 regimes. In the period of decreasing AOD (2015–2022), following the implementation of clean air  
618 policies (de Leeuw et al., 2021; 2023), CCN concentration decreased (Wang et al, 2023), weakening the  
619 direct impact of aerosols on CER. However, the LWP-driven microphysical differences persisted, so  $S_{CER}$   
620 in the second regime remained significantly smaller than that in the first regime, albeit with a smaller  
621 difference. Additionally, the complexity of aerosol types during the high AOD period (e.g., mixing of  
622 anthropogenic pollutants and natural dust) may have adjusted the value of  $S_{CER}$ , but did not alter the  
623 dominant role of LWP. This aligns with the theory that “aerosol indirect effects are jointly regulated by  
624 concentration and type” (Liu et al., 2017).

625 The larger  $S_{CER}$  observed at larger spatial scales (Figures 5 and 7) may be attributed to meteorological  
626 confounding effects. In addition, clouds with larger LWP are usually associated with strong updrafts  
627 (such as convective clouds), and stronger turbulence and vertical transport will bring more aerosols into  
628 the clouds, increasing CCN concentration and a decrease in particle size, making them more sensitive to  
629 changes in AOD (Jones et al., 2009; Han et al., 2022; Fan et al., 2025). Therefore, this phenomenon is  
630 the result of the combined action of cloud microphysical processes (CCN activation, cloud droplet  
631 competition growth) and dynamic processes (updrafts, turbulent mixing). If the characteristics of aerosols

632 (such as composition) change in the second LWP regime, this sensitivity may be further amplified.  
633 Consequently, the LWP-stratified  $S_{CER}$  quantification framework enables precise characterization of  
634 scale-dependent aerosol-cloud interactions, providing robust physical insights for climate effect  
635 assessments and effectively reducing uncertainties in future climate projections.

636 The central hypothesis of this study—that LWP is relatively consistent between the two periods (2008–  
637 2014 and 2015–2022), supporting valid comparisons of the spatial sensitivity of AOD-CER  
638 relationships—is well-supported by the following analysis. The differences in the mean, median, 25th,  
639 and 50th percentiles of LWP between the two periods are all less than 5%, indicating a stable overall  
640 water vapor supply level. The spatial patterns of high-LWP regions (e.g., southeastern areas) and low-  
641 LWP regions (e.g., the mountainous areas in northern Shanxi) remained stable across the two periods  
642 (see Supplement Figure S1), demonstrating LWP spatial distribution characteristics are highly consistent.  
643 The sample proportions of LWP in the rapid growth regime are 59.30% (period 1: 0–55 g/m<sup>2</sup>) and 55.36%  
644 (period 2: 0–50 g/m<sup>2</sup>), while those in the decreasing regime are 29.64% (period 1: 55–135 g/m<sup>2</sup>) and  
645 24.59% (period 2: 50–100 g/m<sup>2</sup>), suggesting that there is no systematic temporal shift in the LWP  
646 distribution. Meanwhile, short-term fluctuations are smoothed by multi-year averaging and large-sample  
647 statistics, resulting in a weak indirect impact of aerosols on LWP (LWP only increased by 5.6%, much  
648 smaller than the 24% decrease in AOD). Additionally, LWP-stratified analysis further isolates  
649 interference. The validation of the core hypothesis provides a reliable premise for accurately quantifying  
650 the impact of aerosol concentration changes on the sensitivity of cloud parameters and their spatial scale  
651 dependence.

#### 652 4.2 Scale dependence of cloud parameters sensitivities to aerosol variations

653 Extensive studies have demonstrated a significant spatial scale dependence of aerosol indirect effects  
654 (McComiskey et al., 2012; Possner et al., 2016; Glotfelty et al., 2020; Ekman et al., 2023). Failure to  
655 explicitly define the scale-dependent behavior of aerosol indirect effects may introduce systematic biases  
656 and inconsistencies in subsequent process analyses. Based on satellite observations, this study confirms  
657 statistically significant negative correlations between CER and AOD, as well as positive correlations  
658 between  $N_d$  and AOD during periods with different aerosol concentrations, aligning with classical  
659 aerosol-cloud interaction theory (Quaas et al., 2009). Analysis of scale-conditioned  $S_{CER}$  and  $S_{N_d}$  reveals

660 that for fixed buffer size, an increase in the size of the study area leads to a systematic reduction in  $S_{CER}$   
661 (less negative) and  $S_{Nd}$ , corroborating the nonlinear attenuation of aerosol signals with spatial domain  
662 expansion (Quaas et al., 2009). The results from this study suggest that AOD-cloud property correlations  
663 in large study areas are susceptible to meteorological confounding effects (Quaas et al., 2010; Boucher  
664 and Quaas, 2012; Gryspeerdt et al., 2014; Liu et al., 2024). Theoretically, aerosol regulation of cloud  
665 microphysics is strongly local: smaller domains (e.g.,  $4^\circ \times 4^\circ$ ) feature homogeneous meteorological  
666 conditions (humidity, updrafts), preserving undiluted aerosol-cloud interaction signals and yielding larger  
667  $|S_{CER}|$  (pronounced Twomey effect). In contrast, expanded domains (e.g.,  $10^\circ \times 10^\circ$ ) encompass  
668 heterogeneous meteorological conditions (circulation differences, boundary layer variability) that  
669 independently modulate cloud droplet growth. For example, strong updrafts enhance liquid water supply,  
670 offsetting aerosol-induced radius reduction (Altartatz et al., 2014), weakening aerosol-CER correlations  
671 and reducing  $|S_{CER}|$ . Consistent with Grandey & Stier (2010), large-scale domains introduce “dilution  
672 bias” via non-target meteorological variability. This scale-dependent confounding mechanism elucidates  
673 uncertainties in aerosol indirect effect assessments at regional scales.

674 Multi-scale spatial analysis identifies different optimal buffer sizes for  $S_{CER}$  and  $S_{Nd}$  in different periods.  
675 These findings align closely with satellite-based aerosol indirect effect studies (Wang et al., 2015; Liu et  
676 al., 2017), providing critical scale benchmarks for satellite product validation. Wang et al. (2015) reported  
677 an inverse “Twomey” effect between aerosols and CER in eastern China by analyzing aerosol and CER  
678 within a 50 km buffer zone around CALIOP samples. Similarly, Liu et al. (2017) systematically examined  
679 the response mechanisms of warm cloud macro- and microphysical parameters to increasing AOD in the  
680 Yangtze River Delta region, also using CALIOP samples within a 50 km buffer zone. Present study  
681 further shows that, as aerosol concentrations decrease,  $S_{CER}$  values across different study areas with the  
682 same buffer size exhibit convergence characteristics, with generally smaller  $S_{CER}$  (closer to zero). This  
683 indicates a significant weakening of aerosol-cloud interaction intensity and reduced spatial extent  
684 dependency in low aerosol loading conditions. This phenomenon is consistent with the simulated  
685 behavior of aerosol-limited cloud regimes, where aerosol-cloud interactions are quantitatively modulated  
686 by moisture availability and lose their sensitivity to large-scale dynamical stability, leading to a weaker  
687 and more homogeneous effect (Zhao et al., 2025).

688 By systematically quantifying the scale-response characteristics of aerosol indirect effects, this work not

689 only elucidates the dynamic scale behavior of aerosol-cloud interactions but, more critically, establishes  
690 criteria for determining optimal buffer size in regional aerosol indirect effect studies. Such advancements  
691 provide actionable insights for refining parameterization schemes in climate models, thereby enhancing  
692 their predictive reliability.

### 693 **4.3 Contrasting sensitivity patterns of cloud parameters in response to AOD**

694 A comprehensive comparison of the sensitivity  $S_{CER}$  and  $S_{Nd}$  reveals that the responses of CER and  $N_d$  to  
695 AOD exhibit distinct yet inherently interconnected characteristics. These characteristics are jointly  
696 modulated by spatial scale and LWP regimes (Figs. 5, 7, 8; Supplements Tables 1–2), which profoundly  
697 reflect the core microphysical mechanisms of aerosol-cloud interactions. Details are elaborated as  
698 follows:

#### 699 **4.3.1 Core differences in response modes between $S_{CER}$ and $N_d$ to AOD**

700  $S_{CER}$  is consistently negative across both periods and all LWP regimes ( $-0.33 < S_{CER} < 0$ ) (Figs. 5, 7;  
701 Supplement Table 1), indicating that an increase in AOD leads to a decrease in CER. This aligns with the  
702 core principle of the Twomey effect (Twomey, 1977; Feingold et al., 2001). The values of  $|S_{CER}|$  are larger  
703 in the second LWP regime than in the first regime, reflecting stronger aerosol modulation of cloud  
704 microphysical properties when liquid water is abundant (McComiskey & Feingold, 2012). In contrast,  
705  $S_{Nd}$  maintains a significant positive correlation with AOD across all scenarios ( $0 < S_{Nd} < 1$ ) (Fig. 8;  
706 Supplement Table 2), confirming that higher AOD directly promotes CCN activation and thereby  
707 increases cloud droplet number concentration (Andreae, 2009).  $S_{Nd}$  is larger in small-scale study areas  
708 (e.g.,  $4^\circ \times 4^\circ$ ) and small buffer zones, with a maximum value of 0.45 in the first period, indicating greater  
709 sensitivity of cloud droplet number to aerosol loading at fine spatial scales.

#### 710 **4.3.2 Synergistic modulation of AOD and spatial scale**

711 Using the LWP interval corresponding to  $S_{Nd}$  ( $0 < LWP \leq 200 \text{ g/m}^2$ ) as a benchmark, comparisons  
712 between the two periods (incorporating average values of  $S_{CER}$  across two LWP regimes) reveal distinct  
713 characteristics:

714 For the small-scale study area ( $4^\circ \times 4^\circ$ ): In period 1, the average  $|S_{CER}|$  across two LWP regimes is 0.271  
715 (0.2232 for the 0–55 g/m<sup>2</sup> LWP regime, 0.3189 for the 55–135 g/m<sup>2</sup> LWP regime) and  $S_{Nd}=0.4496$ , both  
716 significantly higher than those in period 2 (average  $|S_{CER}|=0.154$ , with 0.0863 for 0–50 g/m<sup>2</sup> LWP regime  
717 and 0.2212 for 50–100 g/m<sup>2</sup> LWP regime;  $S_{Nd}=0.2903$ ). The negative correlation between AOD and CER  
718 is more significant in period 1, as sufficient CCN in small-scale areas amplifies both cloud droplet  
719 number increase and size reduction, enhancing the Twomey effect.

720 For the medium-to-large scale study areas ( $6^\circ \times 6^\circ$ ,  $8^\circ \times 8^\circ$ ,  $10^\circ \times 10^\circ$ ): In period 1, the average  $|S_{CER}|$  across  
721 two LWP regimes is 0.1683 (0.1305 for 0–55 g/m<sup>2</sup>, 0.2061 for 55–135 g/m<sup>2</sup>), 0.13065 (0.1026 for 0–55  
722 g/m<sup>2</sup>, 0.1587 for 55–135 g/m<sup>2</sup>), and 0.1067 (0.0858 for 0–55 g/m<sup>2</sup>, 0.0885 for 55–135 g/m<sup>2</sup>), respectively,  
723 all higher than the corresponding values in period 2 (0.1516, 0.1246, 0.0985). However,  $S_{Nd}$  in period 1  
724 (0.2430, 0.2050, 0.1430) is lower than that in period 2 (0.2960, 0.2680, 0.1740), with no significant  
725 difference in the negative correlation between AOD and CER between the two periods.

726 This characteristic indicates that meteorological confounding effects are enhanced at larger scales,  
727 weakening the regulation of  $S_{Nd}$  by aerosols, while at small scales the aci is directly driven by AOD levels.

### 728 **4.3.3 Implications for aerosol indirect effects**

729 The differences and interconnections between  $S_{CER}$  and  $S_{Nd}$  highlight that aerosol indirect effects are  
730 dominated by coupled microphysical processes: Aerosol-induced increases in CCN first enhance  $N_d$   
731 through positive  $S_{Nd}$ , and then reduce CER through negative  $S_{CER}$  under constant LWP conditions. The  
732 scale-dependent attenuation of both sensitivities and their modulation by LWP indicate that quantifying  
733 aerosol indirect effects requires full consideration of spatial scales and the key role of liquid water,  
734 providing observational basis for optimizing climate model parameterization schemes.

### 735 **4.4 Limitations and future perspectives**

736 This study has three significant limitations. Firstly, similar to most previous studies (Wang et al., 2015;  
737 Liu et al., 2021), this study only utilized MODIS data with a resolution of 10 km to explore scale effects,  
738 ignoring finer or coarser resolution data. Therefore, using a 10 km buffer size as the minimum  
739 observation unit, this limitation makes the indirect effects of aerosols on smaller scales still unknown,  
740 which may lead to inaccurate evaluation of aerosol indirect effects. Therefore, future research can

741 improve the sensitivity of aerosol indirect effects to scale changes by using observation data with higher  
742 accuracy or model simulations. Secondly, the current research focuses on the influence of buffer size and  
743 study areas, the potential impact of spatial aggregation methods (especially zoning directionality) on the  
744 quantitative results of aerosol indirect effects has not been systematically evaluated. Future research  
745 should further investigate the sensitivity of aerosol indirect effects to zoning direction. Moreover, the  
746 current study employs a uniform buffer size for both aerosol and cloud parameters, failing to account for  
747 potential interaction effects arising from discrepancies of buffer size between them. Therefore, clarifying  
748 scale dependence will avoid directly extrapolating local observation results to a larger study area when  
749 downscaling climate models or formulating regional environmental policies.

## 750 **5 Conclusions**

751 Based on MODIS and CALIOP satellite observations of aerosol and cloud parameters over land in eastern  
752 China, a comparative analysis was conducted of the sensitivity of cloud microphysical parameters (CER  
753 and  $N_d$ ) to variations in AOD during two characteristic periods: 2008–2014 (period 1, high AOD) and  
754 2015–2022 (period 2, decreasing AOD). Through systematic analysis of the relationship between CER  
755 and LWP and their response mechanisms to AOD across these two periods, the following key conclusions  
756 were drawn:

757 Firstly, CER exhibited three distinct regimes with varying LWP. During the rapid growth regime (LWP  
758  $< 55/50$  g/m<sup>2</sup>), CER showed significant negative sensitivity to AOD ( $S_{CER}$ ), consistent with the Twomey  
759 effect; during the decreasing regime (LWP = 55-135/50-100 g/m<sup>2</sup>),  $S_{CER}$  remained negative but with  
760 enhanced sensitivity; and during the slow growth regime (LWP  $> 135/100$  g/m<sup>2</sup>), the rate of CER change  
761 significantly decreased. These findings confirmed that LWP is a crucial, regulatory factor influencing the  
762 CER response to AOD.

763 Secondly, scale dependence analysis led to the conclusion that characteristics in aerosol-cloud interaction  
764 are significantly scale-dependent, with systematic variations of both  $S_{CER}$  and  $S_{N_d}$  with changes in buffer  
765 size and study area. The results of the study show that  $S_{CER}$  systematically increased as buffer size  
766 increased and became negligible for buffer sizes larger than 150-200 km, while the optimal buffer sizes  
767 varied substantially with the size of the study area in the range from  $6^\circ \times 6^\circ$  to  $10^\circ \times 10^\circ$ : increased as study  
768 area increased during period 2, but decreased in period 1 for regime 2. Particularly noteworthy is the

769 enhanced consistency of  $S_{CER}$  across different study areas and the significant increase in  $S_{CER}$  during  
770 period 2, reflecting weaker aerosol-cloud interactions due to declining regional aerosol concentrations.  
771 Finally, the sensitivity of  $N_d$  to AOD ( $S_{Nd}$ ) exhibited distinct characteristics compared to  $S_{CER}$ :  $S_{Nd}$  showed  
772 a significant positive correlation ( $p < 0.01$ ) and demonstrated nonlinear attenuation with increasing buffer  
773 size and study area. The optimal buffer size for  $S_{Nd}$  was smaller during period 2 than during period 1 and  
774 increased with the study area size, being substantially larger for study areas of  $8^\circ \times 8^\circ$  and  $10^\circ \times 10^\circ$  than  
775 for study areas of  $4^\circ \times 4^\circ$  and  $6^\circ \times 6^\circ$  areas. These findings not only deepen our understanding of aerosol  
776 indirect effects but also provide an important observational basis for improving aerosol-cloud  
777 parameterization schemes in climate models. The results emphasize that both the phased characteristics  
778 of LWP and spatial scale effects must be considered when assessing aerosol indirect effects.

#### 779 **Data availability**

780 All data used in this study are publicly available. The satellite data from the MODIS instrument used in  
781 this study were obtained from <https://ladsweb.nascom.nasa.gov/search/> (last access: 02 July 2025). The  
782 satellite data from CALIOP were obtained from <https://subset.larc.nasa.gov/calipso/login.php> (last  
783 access: 02 July 2025).

#### 784 **Author contributions**

785 YL, LT and GL designed the research. YL and LT led the analyses. YL and GL wrote the manuscript  
786 with major input from JH, and further input from all other authors. All authors contributed to interpreting  
787 the results and to the finalization and revision of the manuscript.

#### 788 **Competing interests**

789 The authors declare that they have no conflict of interest.

#### 790 **Acknowledgements**

791 The authors greatly appreciate NASA CloudSat Data Processing Center that provided the data used in  
792 this study. This work was supported by the National Natural Science Foundation of China (Grant No.  
793 42001290), the National Natural Science Foundation of China (Grant No. 42271299), the Natural Science

794 Foundation Project of Xiamen (Grant No. 3502Z202472037) and the Chinese Academy of Sciences  
795 President's International Fellowship Initiative, Grant No. 2025PVA0014\_Y1.

796 **References**

- 797 Albrecht, B. A.: Aerosols, cloud microphysics, and fractional cloudiness, *Science*, 245, 1227-1230, 1989.
- 798 Bellouin, N., Quaas, J., Gryspeerdt, E., Kinne, S., Stier, P., Watson-Parris, D., et al.: Bounding global  
799 aerosol radiative forcing of climate change. *Reviews of Geophysics*, 58, e2019RG000660.  
800 <https://doi.org/10.1029/2019RG000660>, 2020.
- 801 Altaratz, O., Koren, I., Remer, L.A., Hirsch, E.: Review: Cloud invigoration by aerosols—Coupling  
802 between microphysics and dynamics. *Atmospheric Research*, 140-141, 38-60, 2014.
- 803 Andreae, M. O.: Correlation between cloud condensation nuclei concentration and aerosol optical  
804 thickness in remote and polluted regions, *Atmos. Chem. Phys.*, 9, 543-556, [https://doi.org/10.5194/acp-](https://doi.org/10.5194/acp-9-543-2009)  
805 9-543-2009, 2009.
- 806 Baum, B. A., et al.: MODIS cloud-top property refinement for Collection 6, *J. Appl. Meteorol. Climatol.*,  
807 51(6), 1145-1163, 2012.
- 808 Bender, F.A.M., Frey, L., McCoy, D.T., Grosvenor, D.P., Mohrmann, J.K.: Assessment of aerosol–  
809 cloud–radiation correlations in satellite observations, climate models and reanalysis. *Climate Dynamics*,  
810 52, 4371-4392, 2019.
- 811 Boucher, O., Quaas, J.: Water vapour affects both rain and aerosol optical depth. *Nature Geoscience*, 6(1),  
812 4-5. <https://doi.org/10.1038/ngeo1692>, 2012.
- 813 Bréon, F. M., Tanré, D., Generoso, S.: Aerosol effect on cloud droplet size monitored from satellite,  
814 *Science*, 295(5556):834-8. doi: 10.1126/science.1066434, 2002.
- 815 Bulgin, C. E., Palmer, P.I., Thomas, G.E., Arnold, C.P.G., Campmany, E., Carboni, E., Grainger, R. G.,  
816 Poulsen, C., Siddans, R., Lawrence, B.N.: Regional and seasonal variations of the Twomey indirect effect  
817 as observed by the ATSR-2 satellite instrument, *Geophysical Research Letters*, 35, 2, 2008.
- 818 Cai, H., Yang, Y., Chen, Q.: Distribution Characteristics of Cloud Types and Cloud Phases over China  
819 and Their Relationship with Cloud Temperature, *Remote Sensing*, 14(21), 2022.  
820 <https://doi.org/10.3390/rs14215601>

821 Chen, G., W.-C.Wang, and J.-P. Chen, 2015: Aerosol–stratocumulus–radiation interactions over  
822 southeast Pacific. *J. Atmos. Sci.*, 72, 2612–2621, <https://doi.org/10.1175/JAS-D-14-0319.1>.

823 Chen, Y.-C., Christensen, M. W., Stephens, G. L., and Seinfeld, J. H.: Satellite-based estimate of global  
824 aerosol-cloud radiative forcing by marine warm clouds, *Nat. Geosci.*, 7, 643–646,  
825 <https://doi.org/10.1038/ngeo2214>, 2014.

826 Christensen, M. W., Chen, Y.-C., and Stephens, G. L.: Aerosol indirect effect dictated by liquid clouds,  
827 *J. Geophys. Res.*, 121, 14636–14650, <https://doi.org/10.1002/2016JD025245>, 2016.

828 Costantino, L. and Bréon, F. M.: Analysis of aerosol-cloud interaction from multi-sensor satellite  
829 observations. *Geophys. Res. Lett.*, 37, L11801, doi:10.1029/2009GL041828, 2010.

830 Costantino, L. and Bréon, F. M.: Aerosol indirect effect on warm clouds over South-East Atlantic, from  
831 co-located MODIS and CALIPSO observations, *Atmos. Chem. Phys.*, 13: 69–88, 2013.

832 **Dagan, G., Yeheskel, N., Williams, A. I. L.: Radiative forcing from aerosol–cloud interactions enhanced**  
833 **by large-scale circulation adjustments, *Nature geoscience*, 16, 1092–1098, 2023.**

834 de Leeuw, G., R. van der A, J. Bai, Y. Xue, C. Varotsos, Z. Li, C. Fan, X. Chen, I. Christodoulakis, J.  
835 Ding, X. Hou, G. Kouremadas, D. Li, J. Wang, M. Zara, K. Zhang, Y. Zhang.: Air Quality over China.  
836 *Remote Sens.* 2021, 13, 3542. <https://doi.org/10.3390/rs13173542>, 2021.

837 de Leeuw, G., Fan, C, Li, Z., Dong, J., Li, Y., Ou, Y., and Zhu, S. (2022). Spatiotemporal variation and  
838 provincial scale differences of the AOD across China during 2000–2021. *Atmospheric Pollution*  
839 *Research* 13 (2022) 101359 (14 pp). <https://doi.org/10.1016/j.apr.2022.101359>.

840 de Leeuw, G., Kang, H., Fan, C., Li, Z., Fang, C., Zhang, Y. (2023). Meteorological and anthropogenic  
841 contributions to changes in the Aerosol Optical Depth (AOD) over China during the last decade. *Atm.*  
842 *Env.*, 301, 119676. <https://doi.org/10.1016/j.atmosenv.2023.119676>.

843 Ekman, A. M. L., Eva Nygren, Alejandro Baró Pérez, Matthias Schwarz, Gunilla Svensson, Nicolas  
844 Bellouin.: Influence of horizontal resolution and complexity of aerosol–cloud interactions on marine  
845 stratocumulus and stratocumulus-to-cumulus transition in HadGEM3-GC3.1, *Quart. J Royal Met Soc.*,  
846 149, 755, 2049–2066, <https://doi.org/10.1002/qj.4494>, 2023.

847 Fan J, Wang Y, Rosenfeld D, et al.: Review of aerosol–cloud interactions: Mechanisms, significance, and  
848 challenges. *Journal of the Atmospheric Sciences*,73(11): 4221–4252, 2016.

849 Fan, J., Zhang, Y., Li, Z., Yan, H., Prabhakaran, T., Rosenfeld, D., & Khain, A.: Unveiling aerosol  
850 impacts on deep convective clouds: Scientific concept, modeling, observational analysis, and future  
851 direction, *Journal of Geophysical Research: Atmospheres*, 130, e2024JD041931. <https://doi.org/10.1029/2024JD041931>, 2025.

853 Feingold, G., Remer, L. A., Ramaprasad, J., Kaufman, Y. J.: Analysis of smoke impact on clouds in  
854 Brazilian biomass burning regions: an extension of Twomey's approach, *J. Geophys. Res.*, 106 (D19),  
855 22907-22922, 2001.

856 Feingold, G. Modeling of the first indirect effect: analysis of measurement requirements, *Geophys. Res. Lett.*, 30, 1997, doi:10.1029/2003GL017967, 2003.

858 Feingold, G., Goren, T., and Yamaguchi, T.: Quantifying albedo susceptibility biases in shallow clouds,  
859 *Atmos. Chem. Phys.*, 22, 3303–3319, <https://doi.org/10.5194/acp-22-3303-2022>, 2022.

860 Grandey, B.S., Stier, P.: A critical look at spatial scale choices in satellite-based aerosol indirect effect  
861 studies. *Atmos. Chem. Phys.*, 10, 11459-11470, 2010.

862 Gryspeerdt, E., Stier, P., and Partridge, D. G.: Satellite observations of cloud regime development: the  
863 role of aerosol processes, *Atmos. Chem. Phys.*, 14, 1141-1158, doi:10.5194/acp-14-1141-2014, 2014.

864 Gryspeerdt, E., Povey, A. C., Grainger, R. G., Hasekamp, O., Hsu, N. C., Mulcahy, J. P., Sayer, A. M.,  
865 and Sorooshian, A.: Uncertainty in aerosol–cloud radiative forcing is driven by clean conditions, *Atmos. Chem. Phys.*, 23, 4115-4122, <https://doi.org/10.5194/acp-23-4115-2023>, 2023.

867 Gryspeerdt, E., McCoy, D. T., Crosbie, E., Moore, R. H., Nott, G. J., Painemal, D., Small-Griswold, J.,  
868 Sorooshian, A., and Ziemba, L.: The impact of sampling strategy on the cloud droplet number  
869 concentration estimated from satellite data, *Atmos. Meas. Tech.*, 15, 3875–3892, 2022,  
870 <https://doi.org/10.5194/amt-15-3875-2022>, 2022.

871 Glotfelty, T., Kiran Alapaty, Jian He, Patrick Hawbecker, Xiaoliang Song, and Guang Zhang. Studying  
872 Scale Dependency of Aerosol–Cloud Interactions Using Multiscale Cloud Formulations, 77, 11, 2020.

873 Grosvenor, D. P., Sourdeval, O., Zuidema, P., Ackerman, A., Alexandrov, M. D., Bennartz, R., Boers,  
874 R., Cairns, B., Chiu, J. C., Christensen, M., Deneke, H., Diamond, M., Feingold, G., Fridlind, A.,  
875 Hünerbein, A., Knist, C., Kollias, P., Marshak, A., McCoy, D., Merk, D., Painemal, D., Rausch, J.,  
876 Rosenfeld, D., Russchenberg, H., Seifert, P., Sinclair, K., Stier, P., Diedenhoven, B. V., Wendisch, M.,

877 Werner, F., Wood, R., Zhang, Z., and Quaas, J.: Remote sensing of droplet number concentration in  
878 warm clouds: A review of the current state of knowledge and perspectives, *Rev. Geophys.*, 56, 409–453,  
879 <https://doi.org/10.1029/2017RG000593>, 2018.

880 Han, X., Zhao, B., Lin, Y., Chen, Q., Shi, H., Jiang, Z., et al.: Type-dependent impact of aerosols on  
881 precipitation associated with deep convective cloud over East Asia, *Journal of Geophysical Research:*  
882 *Atmospheres*, 127, e2021JD036127. <https://doi.org/10.1029/2021JD036127>, 2022.

883 Hassan, T., Zhang, K., Li, J., Singh, B., Zhang, S., Wang, H., and Ma, P.: Impacts of spatial heterogeneity  
884 of anthropogenic aerosol emissions in a regionally refined global aerosol–climate model, *Geosci. Model*  
885 *Dev.*, 17, 3507-3532, 2024.

886 Huang, R. J., Zhang, Y. L., Bozzetti, C., et al. High secondary aerosol contribution to particulate pollution  
887 during haze events in China, *Nature*, 514, 218–222, 2014.

888 Jia, H. L., Ma, X. Y., Quaas, J., Yin, Y., Qiu, T.: Is positive correlation between cloud droplet effective  
889 radius and aerosol optical depth over land due to retrieval artifacts or real physical processes?  
890 *Atmospheric Chemistry and Physics*, 19, 13, 8879-8896, 2019.

891 Jia, H., Quaas, J., Gryspeerdt, E., Böhm, C., & Sourdeval, O.: Addressing the difficulties in quantifying  
892 droplet number response to aerosol from satellite observations, *Atmospheric Chemistry and Physics*,  
893 22(11), 7353–7372. <https://doi.org/10.5194/acp-22-7353-2022>, 2022.

894 Jones, T. A., Christopher, S. A., & Quaas, J.: A six year satellite-based assessment of the regional  
895 variations in aerosol indirect effects. *Atmospheric Chemistry and Physics*, 9, 4091, 2009.

896 Koren, I., Kaufman, Y. J., Rosenfeld, D., Remer, L. A., Rudich, Y.: Aerosol invigoration and  
897 restructuring of Atlantic convective clouds. *Geophys. Res. Lett.*, 32 (14), L14828, 2005.

898 Kaufman, Y.J. and Fraser, R.S.: The effect of smoke particles on clouds and climate forcing. *Science*,  
899 1997. 277(5332): p. 1636-1639.

900 Kaufman, Y. J., Remer, L., Tanré, D., Li, R., Kleidman, R., Mattoo, S., Levy, R., Eck, T., Holben, B.,  
901 Ichoku, C., Martins, J., and Koren, I.: A critical examination of the residual cloud contamination and  
902 diurnal sampling effects on MODIS estimates of aerosol over ocean, *IEEE Trans. Geosci. Remote Sens.*,  
903 43, 2886–2897, 2005.

904 Kaufman, Y.J., Remer, L.A., Tanré, D., Li, R.R., Kleidman, R., Mattoo, S., Levy, R.C., Eck, T.F., Holben,  
905 B.N., Ichoku, C., Member, IEEE, Martins, J.V., and Koren, I.: A Critical Examination of the Residual

906 Cloud Contamination and Diurnal Sampling Effects on MODIS Estimates of Aerosol Over Ocean, IEEE  
907 TRANSACTIONS ON GEOSCIENCE AND REMOTE SENSING, 43, 12, 2005.

908 Kim, S. W., S. C. Yoon, J. Y. Kim, and S. Y. Kim (2007), Seasonal and monthly variations of columnar  
909 aerosol optical properties over East Asia determined from multi-year MODIS, LIDAR, and AERONET  
910 Sun/sky radiometer measurements, *Atmos. Environ.*, 41(8), 1634–1651,  
911 doi:10.1016/j.atmosenv.2006.10.044.

912 King, M. D., Tsay, S. C., Platnick, S. E., Wang, M., and Liou, K. N.: Cloud Retrieval Algorithms for  
913 MODIS: Optical Thickness, Effective Particle Radius, and Thermodynamic Phase, MODIS Algorithm  
914 Theoretical Basis Document, available at: [http://eosps.nasa.gov/sites/default/files/atbd/atbd\\_mod05.pdf](http://eosps.nasa.gov/sites/default/files/atbd/atbd_mod05.pdf),  
915 1997.

916 King, M. D., Menzel, W. P., Kaufman, Y. J., Tanré, D., Gao, B. C., Platnick, S., Ackerman, S. A., Remer,  
917 L. A., Pincus, R., and Hubanks, P. A.: Cloud and aerosol properties, precipitable water, and profiles of  
918 temperature and water vapor from MODIS, *IEEE T. Geosci. Remote*, 41, 442–458,  
919 doi:10.1109/TGRS.2002.808226, 2003.

920 Lebsock, M., Morrison, H., Gettelman, A.: Microphysical implications of cloud-precipitation covariance  
921 derived from satellite remote sensing. *Journal of Geophysical Research: Atmosphere*, 118, 6521–6533,  
922 2013.

923 Levy, R. C., Mattoo, S., Munchak, L. A., Remer, L. A., Sayer, A. M., Patadia, F., and Hsu, N. C.: The  
924 Collection 6 MODIS aerosol products over land and ocean, *Atmos. Meas. Tech.*, 6, 2989–3034,  
925 <https://doi.org/10.5194/amt-6-2989-2013>, 2013.

926 Levy, R. C., Remer, L. A., Kleidman, R. G., Mattoo, S., Ichoku, C., Kahn, R., and Eck, T. F.: Global  
927 evaluation of the Collection 5 MODIS dark-target aerosol products over land, *Atmos. Chem. Phys.*, 10,  
928 10399–10420, doi:10.5194/acp-10-10399-2010, 2010.

929 Lee, S. S., Donner, L. J., Phillips, V. T. J. Impacts of aerosol chemical composition on microphysics and  
930 precipitation in deep convection, *Atmospheric Research*, 94, 220–237, 2009.

931 Lee, H.-H., Zheng, X., Qiu, S., and Wang, Y.: Numerical case study of the aerosol–cloud interactions in  
932 warm boundary layer clouds over the eastern North Atlantic with an interactive chemistry module, *Atmos.*  
933 *Chem. Phys.*, 25, 6069–6091, <https://doi.org/10.5194/acp-25-6069-2025>, 2025.

934 Leung, G. R., Saleeby, S. M., Sokolowsky, G. A., Freeman, S. W., and van den Heever, S. C.: Aerosol-  
935 cloud impacts on aerosol detrainment and rainout in shallow maritime tropical clouds, *Atmos. Chem.*  
936 *Phys.*, 23, 5263–5278, <https://doi.org/10.5194/acp-23-5263-2023>, 2023.

937 Li, G. H., Wang, Y., Zhang, R. Y.: Implementation of a two-moment bulk microphysics scheme to the  
938 WRF model to investigate aerosol-cloud interaction, *Journal of Geophysical Research-Atmospheres*, 113,  
939 D15, <https://doi.org/10.1029/2007JD009361>, 2008.

940 Li, Z., et al.: Aerosol and monsoon climate interactions over Asia, *Rev. Geophys.*, 54, 866–929,  
941 [doi:10.1002/2015RG000500](https://doi.org/10.1002/2015RG000500), 2016.

942 Li, Y., Liu, X., and Cai, H.: Numerical simulation of aerosol concentration effects on cloud droplet size  
943 spectrum evolutions of warm stratiform clouds in Jiangxi, China, *Atmos. Chem. Phys.*, 24, 13525–13540,  
944 <https://doi.org/10.5194/acp-24-13525-2024>, 2024.

945 Liu, Y., Lin, T., Zhang, J., Wang, F., Huang, Y., Wu, X., Ye, H., Zhang, G., Cao, X., and de Leeuw, G.:  
946 Opposite effects of aerosols and meteorological parameters on warm clouds in two contrasting regions  
947 over eastern China, *Atmos. Chem. Phys.*, 24, 4651–4673, <https://doi.org/10.5194/acp-24-4651-2024>,  
948 2024.

949 Liu, Q., Duan, S. Y., He, Q. S., Chen, Y. H., Zhang, H., Cheng, N. X., Huang, Y. W., Chen, B., Zhan, Q.  
950 Y., Li, J. Z.: The variability of warm cloud droplet radius induced by aerosols and water vapor in  
951 Shanghai from MODIS observations, *Atmospheric Research*, 253, 105470, 2021.

952 Liu, Q., Shen, X., Li, L., et al. Impacts of Aerosol Chemical Composition on Cloud Condensation Nuclei  
953 (CCN) Activity during Wintertime in Beijing, China. *Remote Sens.*, 15, 4119, 2023.

954 Liu, T. Q., Liu, Q., Chen, Y. H., Wang, W. C., Zhang, H., Li, D., Sheng, J.: Effect of aerosols on the  
955 macro- and micro-physical properties of warm clouds in the Beijing-Tianjin-Heibe region. *Science of*  
956 *the Total Environmen*, 720, 137618, 2020.

957 Liu, Y., Zhang, J., Zhou, P., Lin, T., Hong, J., Shi, L., Yao, F., Wu, J., Guo, H., and de Leeuw, G.:  
958 Satellite-based estimate of the variability of warm cloud properties associated with aerosol and  
959 meteorological conditions, *Atmos. Chem. Phys.*, 18, 18187-18202, [https://doi.org/10.5194/acp-18-](https://doi.org/10.5194/acp-18-18187-2018)  
960 18187-2018, 2018.

961 Liu, Y., de Leeuw, G., Kerminen, V.-M., Zhang, J., Zhou, P., Nie, W., Qi, X., Hong, J., Wang, Y., Ding,  
962 A., Guo, H., Krüger, O., Kulmala, M., and Petäjä, T.: Analysis of aerosol effects on warm clouds over

963 the Yangtze River Delta from multi-sensor satellite observations, *Atmos. Chem. Phys.*, 17, 5623-5641,  
964 <https://doi.org/10.5194/acp-17-5623-2017>, 2017.

965 Liu, Z., Vaughan, M., Winker, D., Kittaka, C., Getzewich, B., Kuehn, R., Omar, A., Powell, K., Trepte,  
966 C., and Hostetler, C.: The CALIPSO lidar cloud and aerosol discrimination: Version 2 algorithm and  
967 initial assessment of performance, *J. Atmos. Ocean. Tech.*, 26, 1198–1213, 2009.

968 Ma, X., Jia, H., Yu, F., and Quaas, J.: Opposite aerosol index-cloud droplet effective radius correlations  
969 over major industrial regions and their adjacent oceans, *Geophys. Res. Lett.*, 45, 5771–5778,  
970 <https://doi.org/10.1029/2018GL077562>, 2018.

971 Ma, P.-L., P. J. Rasch, M. Wang, H. Wang, S. J. Ghan, R. C. Easter, W. I. Gustafson Jr., X. Liu, Y.  
972 Zhang, and H.-Y. Ma (2015), How does increasing horizontal resolution in a global climate model  
973 improve the simulation of aerosol-cloud interactions?, *Geophys. Res. Lett.*, 42, 5058–5065,  
974 doi:10.1002/2015GL064183.

975 Marchant, B., et al.: MODIS Collection 6 shortwave-derived cloud phase classification algorithm and  
976 comparisons with CALIOP, *Atmos. Meas. Tech. Discuss.*, 8, 11893–11924, 2015.

977 Matheson, M. A., Coakley Jr., J. A., and Tahnk, W. R.: Aerosol and cloud property from relationships  
978 for summer stratiform clouds in the northeastern Atlantic from advanced very high resolution radiometer  
979 observations, *J. Geophys. Res.*, 110, D24204, doi:10.1029/2005JD006165, 2005.

980 McComiskey, A., & Feingold, G: The scale problem in quantifying aerosol indirect effects. *Atmospheric*  
981 *Chemistry and Physics*, 12, 1031. <https://doi.org/10.5194/acp-12-1031-2012>, 2012.

982 Meskhidze, N., Nenes, A.: Effects of ocean ecosystem on marine aerosol-cloud interaction. *Adv.*  
983 *Meteorol*, doi:10.1155/2010/239808, 2010.

984 Mohebalhojeh, M., Frederick, S., Riemer, N., & West, M. (2026). A Metric for Quantifying Spatial  
985 Heterogeneity in Gridded Atmospheric Fields. *Earth and Space Science* (preprint).

986 Murray-Watson, R. J. and Gryspeerdt, E.: Stability-dependent increases in liquid water with droplet  
987 number in the Arctic, *Atmos. Chem. Phys.*, 22, 5743–5756, <https://doi.org/10.5194/acp-22-5743-2022>,  
988 2022.

989 McComiskey, A., G. Feingold, A. S. Frisch, D. D. Turner, M. A. Miller, J. C. Chiu, Q. Min, and J. A.  
990 Ogren (2009), An assessment of aerosol-cloud interactions in marine stratus clouds based on surface  
991 remote sensing, *J. Geophys. Res.*, 114, D09203, doi:10.1029/2008JD011006.

992 Platnick, S., et al., MODIS Cloud optical properties: User guide for the Collection 6/6.1 level-2  
993 MOD06/MYD06 product and associated level-3 data sets. v1.1, July 2018.

994 Proestakis, E., Amiridis, V., Marinou, E., Georgoulas, A. K., Solomos, S., Kazadzis, S., Chimot, J., Che,  
995 H., Alexandri, G., Biniotoglou, I., Daskalopoulou, V., Kourtidis, K. A., de Leeuw, G., and van der A, R.  
996 J.: Nine-year spatial and temporal evolution of desert dust aerosols over South and East Asia as revealed  
997 by CALIOP, *Atmos. Chem. Phys.*, 18, 1337-1362, <https://doi.org/10.5194/acp-18-1337-2018>, 2018.

998 Possner A., Zubler, E. M., Lohmann, U., and Schär, C.: The resolution dependence of cloud effects  
999 and ship-induced aerosol-cloud interactions in marine stratocumulus, *J. Geophys. Res. Atmos.*, 121,  
1000 4810–4829, doi:10.1002/2015JD024685, 2016.

1001 Pandey, S. K., Vinoj, V., Panwar, A.: The short-term variability of aerosols and their impact on cloud  
1002 properties and radiative effect over the Indo-Gangetic Plain. *Atmospheric Pollution Research*, 11, 630-  
1003 638, 2020.

1004 Platnick, S., Meyer, K. G., King, M. D., Wind, G., Amarasinghe, N., Marchant, B., Arnold, G. T., Zhang,  
1005 Z., Hubanks, P. A., Holz, R. E., Yang, P., Ridgway, W. L., Riedi, J.: The MODIS cloud optical and  
1006 microphysical products: Collection 6 updates and examples from Terra and Aqua. *IEEE Trans Geosci*  
1007 *Remote Sens.* Jan;55(1):502-525. doi: 10.1109/TGRS.2016.2610522, 2017.

1008 Quaas, J., Boucher, O., Bellouin, N., Kinne, S.: Satellite-based estimate of the direct and indirect aerosol  
1009 climate forcing, *J. Geophys. Res.*, 113, D05204, doi:10.1029/2007JD008962, 2008.

1010 Quaas, J., Stevens, B., Stier, P., and Lohmann, U.: Interpreting the cloud cover – aerosol optical depth  
1011 relationship found in satellite data using a general circulation model, *Atmos. Chem. Phys.*, 10, 6129-  
1012 6135, <https://doi.org/10.5194/acp-10-6129-2010>, 2010.

1013 Quaas, J., Boucher, O., and Lohmann, U.: Constraining the total aerosol indirect effect in the LMDZ and  
1014 ECHAM4 GCMs using MODIS satellite data, *Atmos. Chem. Phys.*, 6, 947–955,  
1015 <https://doi.org/10.5194/acp-6-947-2006>, 2006.

1016 Quaas, J., Ming, Y., Menon, S., Takemura, T., Wang, M., Penner, J. E., Gettelman, A., Lohmann, U.,  
1017 Bellouin, N., Boucher, O., Sayer, A. M., Thomas, G. E., McComiskey, A., Feingold, G., Hoose, C.,  
1018 Kristjánsson, J. E., Liu, X., Balkanski, Y., Donner, L. J., Ginoux, P. A., Stier, P., Grandey, B., Feichter,  
1019 J., Sednev, I., Bauer, S. E., Koch, D., Grainger, R. G., Kirkevåg, A., Iversen, T., Seland, Ø., Easter, R.,  
1020 Ghan, S. J., Rasch, P. J., Morrison, H., Lamarque, J.-F., Iacono, M. J., Kinne, S., and Schulz, M.: Aerosol

1021 indirect effects – general circulation model intercomparison and evaluation with satellite data, *Atmos.*  
1022 *Chem. Phys.*, 9, 8697–8717, <https://doi.org/10.5194/acp-9-8697-2009>, 2009.

1023 Rao, S., Dey, S.: Consistent signal of aerosol indirect and semi-direct effect on water clouds in the  
1024 oceanic regions adjacent to the Indian subcontinent. *Atmospheric Research*, 232, 2020.

1025 Remer, L. A., Kaufman, Y. J., Tanre, D., Mattoo, S., Chu, D. A., Martins, J. V., Li, R. R., Ichoku, C.,  
1026 Levy, R. C., Kleidman, R. G., Eck, T. F., Vermote, E., and Holben, B. N.: The MODIS aerosol algorithm,  
1027 products, and validation, *J. Atmos. Sci.*, 62, 947–973, <https://doi.org/10.1175/JAS3385.1>, 2005.

1028 Rosenfeld, D., Zhu, Y. N., Wang, M. H., Zheng, Y. T., Goren, T., Yu, S. C.: Aerosol-driven droplet  
1029 concentrations dominate coverage and water of oceanic low-level clouds, *Science*, 363, 6427, 2019.

1030 Sarna, K. and Russchenberg, H. W. J.: Ground-based remote sensing scheme for monitoring aerosol–  
1031 cloud interactions, *Atmos. Meas. Tech.*, 9, 1039–1050, <https://doi.org/10.5194/amt-9-1039-2016>, 2016.

1032 Saponaro, G., Kolmonen, P., Sogacheva, L., Rodriguez, E., Virtanen, T., de Leeus, G.: Estimates of the  
1033 aerosol indirect effect over the Baltic Sea region derived from 12 years of MODIS observations, *Atmos.*  
1034 *Chem. Phys.*, 17, 3133-3143, 2017.

1035 Stephens, G., Vane, D. G., Boain, R. J., Mace, G. G., Sassen, K., Wang, Z., Illingworth, A. J., O’Connor,  
1036 E. J., Rossow, W. B., Durden, S. L., Miller, S. D., Austin, R. T., Benedetti, A., and Mitrescu, C.: The  
1037 CloudSat Science Team: The CloudSat mission and the A-Train, *B. Am. Meteorol. Soc.*, 83, 1771–1790,  
1038 2002.

1039 Sourdeval, O., Laurent C.-Labonnote, Anthony J. Baran, Johannes Mülmenstädt, Gérard Brogniez.: A  
1040 methodology for simultaneous retrieval of ice and liquid water cloud properties. Part 2: Near-global  
1041 retrievals and evaluation against A-Train products, *Quarterly Journal of the Royal Meteorological*  
1042 *Society*, 142, 701, 3063-3081, 2016.

1043 Sundström, A.-M., Kolmonen, P., Sogacheva, L., and de Leeuw, D.: Aerosol retrievals over China with  
1044 the AATSR dual view algorithm, *Remote Sens. Environ.*, 116, 189–198, 2012.

1045 Theodore L. Anderson, Robert J. Charlson, David M. Winker, John A. Ogren, and Kim Holmén.:  
1046 Mesoscale Variations of Tropospheric Aerosols, *Journal of the Atmospheric Sciences*, 60, 1,  
1047 [https://doi.org/10.1175/1520-0469\(2003\)060<0119:MVOTA>2.0.CO;2](https://doi.org/10.1175/1520-0469(2003)060<0119:MVOTA>2.0.CO;2), 2003.

1048 Tang, J., Wang, P., Mickley, L. J., Xia, X., Liao, H., Yue, X., et al.: Positive relationship between liquid  
1049 cloud droplet effective radius and aerosol optical depth over Eastern China from satellite data.  
1050 Atmospheric Environment, 84, 244-253. <https://doi.org/10.1016/j.atmosenv.2013.08.024>, 2014.

1051 Tao, W. K., Chen, J. P., Li, Z., Wang, C. E., Zhang, C. D.: Impact of aerosols on convective clouds and  
1052 precipitation, Reviews of Geophysics, 50(2), 2012.

1053 Twomey, S. Pollution and the planetary albedo, Atmos. Environ., 1974, 41, 120-125.

1054 Twomey, S.: The influence of pollution on the shortwave albedo of clouds, J. Atmos. Sci. 34(7), 1149-  
1055 1152, 1977.

1056 Wang, F., Guo, J., Zhang, J., Wu, Y., Zhang, X., Deng, M., and Li, X.: Satellite observed aerosol-induced  
1057 variability in warm cloud properties under different meteorological conditions over eastern China, Atmos.  
1058 Environ., 84, 122–132, 2014.

1059 Wang, F., Guo, J., Zhang, J., Wu, Y., Zhang, X., Deng, M., Li, X.: Satellite observed aerosol-induced  
1060 variability in warm cloud properties under different meteorological conditions over eastern China, Atmos.  
1061 Environ., 84, 122-132, 2014.

1062 Wang, Y., Wang, Y., Song, X., Shang, Y., Zhou, Y., Huang, X., Li, Z.: The impact of particulate pollution  
1063 control on aerosol hygroscopicity and CCN activity in North China, Environmental Research Letters, 18,  
1064 074028, 2023.

1065 Winker, D. M., Pelon, J. R., and McCormick, M. P.: The CALIPSO mission: Spaceborne lidar for  
1066 observation of aerosols and clouds, Proc. SPIE, Lidar Remote Sensing for Industry and Environment  
1067 Monitoring III, 4893, doi:10.1117/12.466539, 2003.

1068 Winker, D. M., Hunt, W. H., and McGill, M. J.: Initial performance assessment of CALIOP, Geophys.  
1069 Res. Lett., 34, L19803, doi:10.1029/2007GL030135, 2007.

1070 Winker, D. M., Vaughan, M. A., Omar, A., Hu, Y., Powell, K. A., Liu, Z. Y., Hunt, W. H., Young, S.  
1071 A.: Overview of the CALIPSO Mission and CALIOP Data Processing Algorithms, Journal of  
1072 Atmospheric and Oceanic Technology, 26 (11), 2310-2323, 2009. doi:10.1175/2009JTECHA1281.1.

1073 Winker, D. M., Pelon, J., Coakley Jr, J. A., Ackerman, S. A., Charlson, R. J., Colarco, P. R., Flamant, P.,  
1074 Fu, Q., Hoff, R. M., Kittaka, C., Kubar, T. L., Le Treut, H., McCormick, M. P., Mégie, G., Poole, L.,  
1075 Powell, K., Trepte, C., Vaughan, M. A., and Wielicki, B. A.: The CALIPSO Mission. Bulletin of  
1076 American Meteorological Society, 91(9), 1211-1230, 2010.

1077 Wang, F., Guo, J., Zhang, J., Huang, J., Min, M., Chen, T., Liu, H., Deng, M., Li, X.: Multi-sensor  
1078 quantification of aerosol-induced variability in warm clouds over eastern China, *Atmos. Environ.*, 113:  
1079 1-9, 2015. <http://dx.doi.org/10.1016/j.atmosenv.2015.04.063>.

1080 Yuan, T., Li, Z., Zhang, R., and Fan, J.: Increase of cloud droplet size with aerosol optical depth: an  
1081 observation and modeling study, *J. Geophys. Res.*, 113, D04201, doi:10.1029/2007JD008632, 2008.

1082 Zhang, L., Li, J., Li, J., Li, R., Zhang, W., Lei, M., et al.: Studying the impacts of meteorological factors  
1083 on distribution of cloud horizontal scales based on active satellite, *Journal of Geophysical Research:  
1084 Atmospheres*, 129, e2024JD041844, <https://doi.org/10.1029/2024JD041844>, 2024.

1085 Zhang, Q., Meng, J., Quan, J., et al. Impact of aerosol composition on cloud condensation nuclei activity,  
1086 *Atmos. Chem. Phys.*, 12, 3783–3790, 2012.

1087 Zhao, J., Ma, X., Quaas, J., and Yang, T.: How meteorological conditions influence aerosol-cloud  
1088 interactions under different pollution regimes, *Atmos. Chem. Phys.*, 25, 17701–17723,  
1089 <https://doi.org/10.5194/acp-25-17701-2025>, 2025.

1090 Zheng, B., Tong, D., Li, M., Liu, F., Hong, C., Geng, G., Li, H., Li, X., Peng, L., Qi, J., Yan, L., Zhang,  
1091 Y., Zhao, H., Zheng, Y., He, K., and Zhang, Q.: Trends in China's anthropogenic emissions since 2010  
1092 as the consequence of clean air actions, *Atmos. Chem. Phys.*, 18, 14095–14111,  
1093 <https://doi.org/10.5194/acp-18-14095-2018>, 2018.

1094 Zheng, X., Dong, X., Xi, B., Logan, T., and Wang, Y.: Distinctive aerosol–cloud–precipitation  
1095 interactions in marine boundary layer clouds from the ACE-ENA and SOCRATES aircraft field  
1096 campaigns, *Atmos. Chem. Phys.*, 24, 10323–10347, <https://doi.org/10.5194/acp-24-10323-2024>, 2024.

1097 Zheng, X., Xi, B., Dong, X., Logan, T., Wang, Y., and Wu, P.: Investigation of aerosol–cloud interactions  
1098 under different absorptive aerosol regimes using Atmospheric Radiation Measurement (ARM) southern  
1099 Great Plains (SGP) ground-based measurements, *Atmos. Chem. Phys.*, 20, 3483–3501,  
1100 <https://doi.org/10.5194/acp-20-3483-2020>, 2020.

1101  
1102  
1103  
1104

1105 **Supplement**

1106 **Table S1. Estimates of  $S_{CER}$ , computed using Eq. (1), and correlation coefficients R between CER and AOD,**  
 1107 **stratified by LWP, and optimal buffer size (see text), for study areas varying from  $4^\circ \times 4^\circ$  to  $10^\circ \times 10^\circ$ , during**  
 1108 **the periods 2008-2014 and 2015-2022. Statistically significant data points are indicated with \* (p value < 0.01).**

Years	LWP ( $g/m^2$ )	Study area	Optimal scale (km)	$S_{CER}$	R
2008-2014	0-55	$10^\circ \times 10^\circ$	30	-0.0858	0.8828*
		$8^\circ \times 8^\circ$	40	-0.1026	0.9220*
		$6^\circ \times 6^\circ$	100	-0.1305	0.8939*
		$4^\circ \times 4^\circ$	50	-0.2232	0.8459*
	55-135	$10^\circ \times 10^\circ$	40	-0.1275	0.8377*
		$8^\circ \times 8^\circ$	60	-0.1587	0.8978*
		$6^\circ \times 6^\circ$	30	-0.2061	0.9245*
		$4^\circ \times 4^\circ$	50	-0.3189	0.9096*
2015-2022	0-50	$10^\circ \times 10^\circ$	80	-0.0885	0.9082*
		$8^\circ \times 8^\circ$	40	-0.1138	0.8886*
		$6^\circ \times 6^\circ$	20	-0.1517	0.7618*
		$4^\circ \times 4^\circ$	50	-0.0863	0.6403*
	50-100	$10^\circ \times 10^\circ$	100	-0.1084	0.8717*
		$8^\circ \times 8^\circ$	90	-0.1354	0.8910*
		$6^\circ \times 6^\circ$	60	-0.1514	0.8384*
		$4^\circ \times 4^\circ$	60	-0.2212	0.8318*

1109 **Table S2. Estimates of  $S_{Na}$ , computed using Eq. (2), and correlation coefficients R between  $N_a$  and AOD,**  
 1110 **stratified by optimal buffer size (see text) for study areas varying from  $4^\circ \times 4^\circ$  to  $10^\circ \times 10^\circ$ , during the periods**  
 1111 **2008-2014 and 2015-2022. Statistically significant data points are indicated with \* (p value < 0.01).**  
 1112

Years	Study area	Optimal scale (km)	$S_{Na}$	R
2008-2014	$10^\circ \times 10^\circ$	70	0.1434	-0.8507*
	$8^\circ \times 8^\circ$	80	0.2045	-0.8646*
	$6^\circ \times 6^\circ$	30	0.2430	-0.8741*
	$4^\circ \times 4^\circ$	40	0.4496	-0.8523*
2015-2022	$10^\circ \times 10^\circ$	60	0.1742	-0.8788*
	$8^\circ \times 8^\circ$	60	0.2682	-0.8638*
	$6^\circ \times 6^\circ$	20	0.2964	-0.6900*
	$4^\circ \times 4^\circ$	30	0.2903	-0.7478*

1113

1114

1115

1116

1117

1118

1119  
1120

**Table S3. Sample sizes of cloud droplet effective radius (CER) and aerosol optical depth (AOD) across different buffer sizes, study areas (LWP regime 1, 2008–2014).**

Buffer sizes	Sample sizes of CER in LWP regime 1				Sample sizes of AOD in LWP regime 1			
	10°×10°	8°×8°	6°×6°	4°×4°	10°×10°	8°×8°	6°×6°	4°×4°
10	25054	16133	8551	3879	47846	32406	18711	8808
20	41667	26507	14077	6376	64878	42949	24462	11377
30	54960	34885	18421	8346	76569	50055	28274	13047
40	66170	42147	22136	9966	86291	56006	31523	14482
50	76207	48769	25738	11593	94726	61227	34272	15664
60	85194	54539	28946	12979	102262	65860	36741	16695
70	93413	59681	31788	14192	108792	69756	38749	17519
80	100728	64370	34330	15317	114357	73103	40498	18246
90	107291	68535	36552	16270	119187	76077	42016	18893
100	113457	72525	38761	17155	123607	78839	43496	19469
120	124793	79882	42945	18964	131449	83807	46217	20534
140	134597	86324	46525	20462	138140	88001	48518	21557
150	138760	89086	48145	21141	141012	89985	49570	21991
160	142693	91808	49602	21734	143725	91767	50570	22436
180	150015	96789	52326	22860	148480	94870	52385	23155
200	156655	101246	54894	23983	153084	97946	53963	23921
250	169423	109475	59449	26008	162530	104346	56987	25388
300	178015	115051	62656	27442	170117	109006	59332	26453

1121  
1122  
1123

**Table S4. Sample sizes of cloud droplet effective radius (CER) and aerosol optical depth (AOD) across different buffer sizes, study areas (LWP regime 2, 2008–2014).**

Buffer sizes	Sample sizes of CER in LWP regime 2				Sample sizes of AOD in LWP regime 2			
	10°×10°	8°×8°	6°×6°	4°×4°	10°×10°	8°×8°	6°×6°	4°×4°
10	22338	14357	7737	3715	47846	32406	18711	8808
20	35406	22471	11964	5697	64878	42949	24462	11377
30	45473	28805	15162	7187	76569	50055	28274	13047
40	54074	34078	17839	8368	86291	56006	31523	14482
50	61579	38732	20290	9444	94726	61227	34272	15664
60	68173	43017	22553	10424	102262	65860	36741	16695
70	74272	46909	24584	11230	108792	69756	38749	17519
80	79999	50507	26412	11950	114357	73103	40498	18246
90	85339	53806	28177	12654	119187	76077	42016	18893
100	90440	56944	29812	13329	123607	78839	43496	19469
120	99758	62598	32673	14486	131449	83807	46217	20534
140	108723	68273	35600	15795	138140	88001	48518	21557
150	112740	70969	36864	16426	141012	89985	49570	21991
160	116558	73463	38046	16974	143725	91767	50570	22436
180	123653	78031	40203	17917	148480	94870	52385	23155
200	129864	81813	42186	18674	153084	97946	53963	23921
250	142429	89112	46079	20120	162530	104346	56987	25388

300 152460 95213 49452 21369 170117 109006 59332 26453

1124

1125

1126

**Table S5. Sample sizes of cloud droplet effective radius (CER) and aerosol optical depth (AOD) across different buffer sizes, study areas (LWP regime 1, 2015–2022).**

Buffer sizes	Sample sizes of CER in LWP regime 1				Sample sizes of AOD in LWP regime 1			
	10°×10°	8°×8°	6°×6°	4°×4°	10°×10°	8°×8°	6°×6°	4°×4°
10	25054	16133	8551	3879	47846	32406	18711	8808
20	41667	26507	14077	6376	64878	42949	24462	11377
30	54960	34885	18421	8346	76569	50055	28274	13047
40	66170	42147	22136	9966	86291	56006	31523	14482
50	76207	48769	25738	11593	94726	61227	34272	15664
60	85194	54539	28946	12979	102262	65860	36741	16695
70	93413	59681	31788	14192	108792	69756	38749	17519
80	100728	64370	34330	15317	114357	73103	40498	18246
90	107291	68535	36552	16270	119187	76077	42016	18893
100	113457	72525	38761	17155	123607	78839	43496	19469
120	124793	79882	42945	18964	131449	83807	46217	20534
140	134597	86324	46525	20462	138140	88001	48518	21557
150	138760	89086	48145	21141	141012	89985	49570	21991
160	142693	91808	49602	21734	143725	91767	50570	22436
180	150015	96789	52326	22860	148480	94870	52385	23155
200	156655	101246	54894	23983	153084	97946	53963	23921
250	169423	109475	59449	26008	162530	104346	56987	25388

1127

1128

1129

**Table S6. Sample sizes of cloud droplet effective radius (CER) and aerosol optical depth (AOD) across different buffer size, study areas (LWP regime 2, 2015–2022).**

Buffer sizes	Sample sizes of CER in LWP regime 2				Sample sizes of AOD in LWP regime 2			
	10°×10°	8°×8°	6°×6°	4°×4°	10°×10°	8°×8°	6°×6°	4°×4°
10	6548	6548	5449	2803	12892	12892	12892	5961
20	24886	16258	8833	4421	46067	30536	17623	8079
30	32260	20786	11214	5490	55767	36685	20780	9408
40	38784	24739	13284	6440	63457	41493	23310	10474
50	44831	28399	15176	7183	70030	45443	25423	11419
60	50181	31609	16909	7816	75667	48900	27138	12122
70	54865	34476	18456	8415	80872	51807	28559	12723
80	58946	37042	19776	8901	85308	54361	29846	13245
90	62835	39437	21006	9359	89202	56659	31024	13706
100	66623	41757	22165	9796	92939	58931	32143	14126
120	73427	46010	24248	10605	99298	62674	34081	14927
140	79486	49854	26210	11312	104540	65994	36013	15617
150	82336	51650	26988	11633	107089	67545	36876	15939
160	85055	53440	27893	11942	109626	69104	37718	16261
180	89669	56388	29401	12520	114187	72088	39380	16889

200	93898	58986	30700	13034	117969	74508	40596	17401
250	102933	64417	33649	14040	125590	79489	43005	18271
300	109964	68913	35755	14701	132000	83404	45012	18913

1130

1131

1132

**Table S7. Sample sizes of cloud droplet number concentration (N<sub>a</sub>) and aerosol optical depth (AOD) across different buffer sizes and study areas during 2008-2014.**

Buffer sizes	Sample sizes of N <sub>a</sub>				Sample sizes of AOD			
	10°×10°	8°×8°	6°×6°	4°×4°	10°×10°	8°×8°	6°×6°	4°×4°
10	47846	32406	18711	8808	50686	32611	17320	8053
20	64878	42949	24462	11377	70102	45066	23944	11084
30	76569	50055	28274	13047	84442	54334	28822	13435
40	86291	56006	31523	14482	96186	62056	32857	15309
50	94726	61227	34272	15664	106166	68620	36473	16906
60	102262	65860	36741	16695	114950	74328	39638	18292
70	108792	69756	38749	17519	122840	79508	42510	19478
80	114357	73103	40498	18246	129763	84048	45038	20599
90	119187	76077	42016	18893	135810	87931	47225	21548
100	123607	78839	43496	19469	141407	91543	49256	22436
120	131449	83807	46217	20534	151353	98040	53031	24145
140	138140	88001	48518	21557	159758	103516	56167	25517
150	141012	89985	49570	21991	163180	105820	57561	26100
160	143725	91767	50570	22436	166373	108000	58769	26661
180	148480	94870	52385	23155	172007	111773	60981	27665
200	153084	97946	53963	23921	176658	114922	62862	28696
250	162530	104346	56987	25388	185393	120627	66331	30409
300	170117	109006	59332	26453	191138	124592	68823	31481

1133

1134

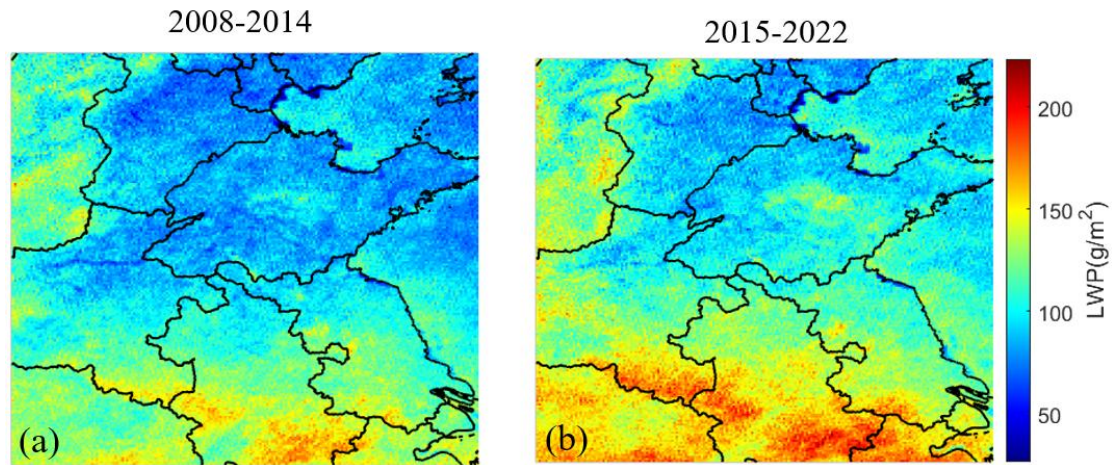
1135

**Table S8. Sample sizes of cloud droplet number concentration (N<sub>a</sub>) and aerosol optical depth (AOD) across different buffer sizes and study areas during 2015-2022.**

Buffer sizes	Sample sizes of N <sub>a</sub>				Sample sizes of AOD			
	10°×10°	8°×8°	6°×6°	4°×4°	10°×10°	8°×8°	6°×6°	4°×4°
10	37182	23994	13048	6149	31621	21503	12892	5961
20	51313	32990	17755	8252	46067	30536	17623	8079
30	61921	39800	21327	9788	55767	36685	20780	9408
40	70663	45351	24213	11063	63457	41493	23310	10474
50	78059	50080	26808	12118	70030	45443	25423	11419
60	84354	53975	28967	13015	75667	48900	27138	12122
70	89675	57448	30881	13832	80872	51807	28559	12723
80	94620	60671	32636	14556	85308	54361	29846	13245
90	99042	63497	34138	15155	89202	56659	31024	13706
100	102936	65993	35444	15703	92939	58931	32143	14126
120	110590	70884	38002	16787	99298	62674	34081	14927
140	116487	74472	40007	17549	104540	65994	36013	15617

150	119140	76230	41049	17958	107089	67545	36876	15939
160	121506	77846	41958	18265	109626	69104	37718	16261
180	125788	80845	43582	18935	114187	72088	39380	16889
200	129613	83370	44887	19538	117969	74508	40596	17401
250	136752	87967	47756	20784	125590	79489	43005	18271
300	141896	91273	49807	21431	132000	83404	45012	18913

1136



1137

1138

1139

1140

**Figure S1. Spatial distributions of LWP averaged over the years 2008-2014 (a) and 2015-2022 (b) over the study area. The lines are provincial borders and the names of provinces mentioned in the text are indicated in Fig. 3(f).**

# Spatial-scale dependence of aerosol indirect effects over land in eastern China: A comparative analysis

Yuqin Liu<sup>1,2</sup>, Tao Lin<sup>1,2</sup>, Jiahua Zhang<sup>3</sup>, Fu Wang<sup>4</sup>, Meixia Lin<sup>1,2</sup>, Yuan Chen<sup>1,2</sup>, Yiyi Huang<sup>1,2</sup>, Hongkai Geng<sup>1,2</sup>, Xin Cao<sup>1,2</sup>, Gerrit de Leeuw<sup>5,6</sup>

1 State Key Laboratory of Regional and Urban Ecology, Institute of Urban Environment, Chinese Academy of Sciences, Xiamen 361021, China

2 Fujian Key Laboratory of Digital Technology for Territorial Blank Analysis and Simulation, Fuzhou 350108, China

3 Key Laboratory of Digital Earth Sciences, The Aerospace Information Research Institute, Chinese Academy of Sciences, Beijing 100094, China

4 CMA Earth System Modeling and Prediction Centre (CEMC), Beijing 100081, China

5 Royal Netherlands Meteorological Institute (KNMI), R&D Satellite Observations, 3730AE De Bilt, The Netherlands

6 State Key Laboratory of Remote Sensing and Digital Earth & Key Laboratory of Satellite Remote Sensing of Ministry of Ecology and Environment, Aerospace Information Research Institute, Chinese Academy of Sciences, Beijing 100101, China

Correspondence to: Tao Lin ([tlin@iue.ac.cn](mailto:tlin@iue.ac.cn)); Gerrit de Leeuw ([gerrit.de.leeuw@knmi.nl](mailto:gerrit.de.leeuw@knmi.nl), ORCID: 0000-0002-1649-6333)

## Abstract

This study aims to reveal the sensitivity patterns of the sensitivity of aerosol indirect effects to spatial scales and investigate the regulatory role of the liquid water path (LWP) in aerosol-cloud cloud-aerosol interactions over land in eastern China. Using MODIS and CALIOP satellite observations, we systematically analyzed the relationships between aerosol optical depth (AOD) and cloud properties (cloud droplet effective radius, CER; cloud droplet number concentration,  $N_d$ ) during Regulatory effects of liquid water path (LWP) on cloud droplet effective radius (CER) and the interaction between aerosol optical depth (AOD) and cloud properties were systematically investigated. MODIS and CALIOP observed aerosols and clouds over eastern China in two periods: 2008–2014 (period 1 period 1, high AOD) and 2015–2022 (period 2 period 2, decreasing AOD). The results show two distinct regimes of the variation of CER variation with LWP: a rapid growth regime ( $LWP < 55/50$  g/m<sup>2</sup>) and a decreasing

33 regime (LWP = 55-135/50-100 g/m<sup>2</sup>) (thresholds vary by period). The sensitivity of CER to AOD ( $S_{CER}$ )  
34 ~~show exhibited~~ a negative correlation, with stronger sensitivity in the decreasing LWP regime than in the  
35 rapid growth regime. and the  $S_{CER}$  in the LWP regime 2 shows larger than that in LWP regime 1. Here,  
36 ~~the~~ spatial scale (characterized ~~is described~~ by buffer size and study area) significantly modulated these  
37 sensitivities: ~~Overall,~~  $|S_{CER}|$  and the positive sensitivity of  $N_d$  to AOD ( $S_{N_d}$ ) both decreased ~~s~~ with  
38 increasing spatial scale. ~~The~~ optimal buffer sizes ~~show notable variations in the ranges~~ from 6°×6° to  
39 10°×10°: increasing ~~as study areas increase~~ with study area in period 2, but decreasing in period 1 for the  
40 decreasing LWP regime ~~2~~. Compared with period 1,  $|S_{CER}|$  ~~decreases in period 2~~ exhibits  
41 ~~significantly decreases~~ in period 2 significantly reduced, reflecting the ~~weaker weakened of~~ aerosol-cloud  
42 interactions for due to declining aerosol concentrations. Additionally, ~~the sensitivity of  $N_d$  (cloud droplet~~  
43 ~~number concentration) to AOD ( $S_{N_d}$ ) shows a positive correlation, with  $S_{N_d}$  decreases as spatial scale~~  
44 increases. ~~The~~ optimal buffer sizes for  $S_{N_d}$  are show larger in the 8°×8° and 10°×10° regions study areas  
45 than ~~that in the~~ 4°×4° and 6°×6° areas areas. This study reveals ~~s~~ the scale-dependence of aerosol-cloud  
46 interactions, providing critical observational support for optimizing climate model parameterization  
47 schemes.

48 **Keywords:** Aerosol, Cloud, Liquid water path, Scale effect, Satellite, Eastern China

## 50 1 Introduction

51 Aerosol particles, depending on their chemical composition and size, can serve as cloud condensation  
52 nuclei (CCN) in liquid clouds or as ice nucleating particles (INP) in ice clouds. When CCN are activated,  
53 they can alter the microphysical properties of clouds and affect precipitation, indirectly impacting the  
54 Earth's radiative budget through aerosol-cloud interactions (aci) (Tao et al., 2012; Fan et al., 2016;  
55 Rosenfeld et al., 2019; Rao and Dey, 2020; Bellouin et al., 2020; [Dagan et al., 2023](#)). An increase in CCN  
56 concentrations results in a larger number of cloud droplets ( $N_d$ ), and if the cloud liquid water path (LWP)  
57 remains constant, it leads to a reduction in the cloud droplet effective radius (CER) ([Twomey, 1974](#);  
58 [Feingold et al., 2004](#)~~33~~). The reduced CER leads to an increased reflection of solar radiation, i.e. a higher  
59 cloud albedo, and enhances radiative forcing due to aerosol-cloud interaction (RFaci). The impact of  
60 increasing aerosol particle numbers on cloud properties, while maintaining a constant LWP, is commonly  
61 known as the “Twomey” effect (Twomey, 1977; Feingold, et al., 2001; Matheson et al., 2005; Koren et

62 al., 2005; Meskhidze and Nenes, 2010; Costantino et al., 2010; 2013). Another aspect of RFaci involves  
63 quick adjustments, which could also cause changes in other cloud characteristics due to the rise in  $N_d$  and  
64 the decrease of CER. For example, this may lead to a reduction in precipitation efficiency, causing an  
65 increase in the LWP and cloud cover. As a result, the reflection of solar radiation is intensified (Albrecht,  
66 1989). These two effects of aci are often categorized as the cloud albedo effect and the cloud lifetime  
67 effect (Quaas et al., 2008).

68 Extensive research on the impact of aerosols on the microphysical properties of clouds has been  
69 conducted utilizing satellite observations ([Liu et al., 2017](#); [Jia et al., 2022](#)), aircraft measurements ([Jia et](#)  
70 [al., 2019](#); [Zheng et al., 2024](#)), ground-based monitoring ([Sarna et al., 2016](#); [Zheng et al., 2020](#)), and  
71 numerical simulations ([Lee et al., 2025](#); [Li et al., 2008](#)). Among these, satellite-based instruments have  
72 become a vital observational tool for studying aerosol-cloud interactions due to their wide spatial  
73 coverage and high spatiotemporal resolution. However, optical satellite sensors such as the Moderate  
74 Resolution Imaging Spectroradiometer (MODIS) cannot effectively penetrate cloud layers ([King et al.,](#)  
75 [2003](#); [Kaufman et al., 2005](#); [Remer et al., 2005](#)), making it difficult to directly retrieve the optical  
76 properties of aerosols underneath clouds. Currently, aerosol data are mainly obtained in cloud-free  
77 conditions as determined using cloud detection methods. This limitation results in significant spatial  
78 mismatches between aerosol and cloud properties, often requiring ~~aggregation of~~ satellite data ~~to be~~  
79 ~~aggregated~~ over large-scale grids for statistical analysis to determine relationships between aerosol and  
80 cloud parameters. The discrepancy between this large-scale analysis and the actual process scale  
81 frequently leads to biases in quantifying aerosol indirect effects, thereby significantly increasing the  
82 uncertainty in radiative forcing estimates (Lebsock et al., 2013; Altaratz et al., 2014; Ma et al., 2015;  
83 Possner et al., 2016; Bender et al., 2018).

84 In recent years, studies based on multi-source satellite data or multi-instrument joint observations have  
85 demonstrated that aerosol particles significantly influence cloud microphysical properties (Saponaro et  
86 al., 2017; Liu et al., 2018; Pandey et al., 2020). Numerous studies have validated the existence of the  
87 Twomey effect (Jones et al., 2009; Christensen et al., 2016; Jia et al., 2019). However, ~~also studies have~~  
88 ~~been published with findings some studies have reported findings that~~ contradicting the Twomey effect,  
89 particularly over land, where an increase in [aerosol optical depth \(AOD\)](#) results in an increase in CER  
90 (Feingold et al., 2001; Yuan et al., 2008; Grandey and Stier, 2010; Tang et al., 2014; Wang et al., 2015;

91 Ma et al., 2018; Jia et al., 2019; Liu et al., 2020). These inconsistent findings highlight the complexity  
92 and regional variability of aci mechanisms, and further in-depth research is needed to reveal the  
93 underlying processes.

94 Currently, researchers usually use grid methods (such as  $1^\circ \times 1^\circ$ ,  $2^\circ \times 2^\circ$ , etc.) to study the aerosol  
95 indirect effects in large areas (Bréon, 2002; Kaufman et al., 2005; Bulgin et al., 2008; Quaas et al., 2008).  
96 For instance, Grandey and Stier (2010) estimated the relationship between aerosols and CER on a global  
97 scale ( $60^\circ\text{N}\sim 60^\circ\text{S}$ ) using multiple spatial resolutions ( $1^\circ \times 1^\circ$ ,  $4^\circ \times 4^\circ$ ,  $8^\circ \times 8^\circ$ ,  $15^\circ \times 15^\circ$ , and  $60^\circ \times 60^\circ$ ). They  
98 ~~found~~ concluded that the ~~aerosol indirect effect~~ sensitivity of retrieved CER to AOD generally  
99 exhibited ~~sed~~ positive values over land and negative values over oceans, and pointed out that using grids  
100 larger than  $4^\circ \times 4^\circ$  could introduce significant errors due to the spatial variability of aerosol and cloud  
101 parameters. Additionally, the study highlighted that, when using grids larger than  $4^\circ \times 4^\circ$  to investigate  
102 the relationship between aerosols and CER, significant errors could be introduced in calculating the  
103 aerosol indirect effect index due to the spatial variability of aerosol and cloud parameters.

104 For studies focusing on smaller regions, researchers often employ a moving window or a fixed area  
105 referred to as a buffer zone methods, within which. ~~These approaches assume a uniform~~ the distribution  
106 of aerosol concentrations is assumed to be uniform. ~~within the window or buffer zone with a certain~~  
107 ~~area and construct s~~ Spatially matched samples are constructed by averaging AOD and cloud parameters  
108 within the window or buffer zone ~~defined area~~. Notably, t The choice of the window or buffer size in these  
109 methods is often arbitrary, and existing studies rarely systematically explore how varying sizes affect the  
110 detection of aerosol-cloud interaction (aci) signals is influenced by the size of the area. For example,  
111 Yuan et al. (2008) used a  $100\text{ km} \times 100\text{ km}$  moving window to calculate the mean values of ~~aerosol~~  
112 ~~optical depth (AOD)~~ and cloud properties to, ~~investigat~~ ing the relationship between aerosols and CER  
113 across seven global regions. Their results indicated that only two of these regions, near the coasts of the  
114 Gulf of Mexico and the South China Sea, exhibited a positive correlation between CER and AOD.  
115 Similarly, Jones et al. (2009) utilized multi-source remote sensing data and applied a point spread  
116 function to derive the mean ~~compute aerosol AOD and cloud properties~~ within a 20 km range, which was  
117 designed to match the native 20 km resolution of the corresponding cloud properties (cloud optical  
118 thickness ~~cloud optical depth, COTD; cloud liquid water path, LWP; cloud droplet effective radius, CER;~~  
119 cloud top pressure, CTP). Their study examined the influence of aerosol types, cloud conditions, and

120 atmospheric factors on aerosol indirect effects across six different oceanic regions globally, finding that  
121 the sensitivity of cloud properties to AOD varied substantially with regional characteristics. In addition,  
122 significant progress has been made in research utilizing observations from the based-on-Cloud-Aerosol  
123 Lidar with Orthogonal Polarization (CALIOP) data (Winker et al., 2007). For instance, Costantino et al.  
124 (2010) used CALIOP data to investigated the aerosol influence on investigated the relationship between  
125 aerosols and CER in stratocumulus clouds over the coastal regions of Namibia and Angola. They  
126 performed the analysis by co-locating an aerosol index (based on AOD and the Ångström exponent) with  
127 CER by calculating aerosol and CER within a 150 km buffer zone around CALIOP observations at  
128 samples. They found that there was no correlation between aerosol load and CER when aerosol and cloud  
129 layers were clearly separated, but a strong correlation when lidar profiles indicated mixing. Costantino  
130 et al. (2013) further analyzed the statistical relationship between aerosol concentrations and cloud  
131 physical parameters by examining aerosol and cloud properties within a 20 km buffer zone around  
132 CALIOP samples, integrating vertical profiles of data of aerosols and clouds data. Their statistics also  
133 clearly showed that aerosol affected cloud micro-physical properties were are affected by aerosols  
134 when aerosol and cloud layers were are mixed, decreasing the CER. It is noted that Not these ably,  
135 while the two studies by Costantino et al. (2010, 2013) reached consistent core conclusions about aci  
136 (i.e., aerosols modulate CER when layers interact), by they adopteding different buffer sizes (150 km vs.  
137 20 km) to target distinct study areas. This demonstrates that the buffer size is tailored to the research  
138 objectives rather than through but a rarely justified through systematic sensitivity analysis. Wang et al.  
139 (2015) revealed an inverse “Twomey” effect between aerosols and CER in eastern China by analyzing  
140 aerosol concentrations and CER within a 50 km buffer zone around CALIOP samples. Their results  
141 showed that high AOD larger CER was associated with high AOD larger CER over eastern China, which  
142 was attributed to the feedback of microphysical processes from intense competitions for vapor in the  
143 presence of high aerosol concentrations and the evaporation of smaller-, less hygroscopic, droplets  
144 associated with more aerosol the combined effects of aerosol type and meteorological conditions.  
145 Similarly, Liu et al. (2017) systematically examined the response mechanisms of warm cloud macro- and  
146 microphysical parameters to increasing AOD in the Yangtze River Delta region, also using CALIOP  
147 samples within a 50 km buffer zone. They found that the relation between cloud properties and AOD  
148 dependded on the aerosol abundance, with a different behaviour for low and high AOD (i.e. AOD <

149 [0.35 and AOD > 0.35](#)). However, both [Wang et al. \(2015\)](#) and [Liu et al. \(2017\)](#) used a fixed 50 km buffer  
150 [zone without justifying the choice or exploring how varying buffer sizes might alter the strength or](#)  
151 [robustness of their findings—a common limitation in regional aci studies.](#) More recently, Liu et al.  
152 (2024) quantified the relative importance of aerosols, meteorological parameters and their interactions  
153 ~~on~~ [for](#) cloud properties in the eastern coastal and inland regions of China, utilizing MODIS 1°×1° aerosol  
154 and cloud product data. [Their study confirmed that CER decreased with the increase in AOD in the](#)  
155 [moderately polluted atmosphere \(0.1 < AOD < 0.3\) over the East China Sea, whereas, in contrast, CER](#)  
156 [increased with increasing AOD in the polluted atmosphere \(AOD > 0.3\) over the Yangtze River Delta.](#)  
157 These studies have provided critical scientific insights into aci at regional scales, [but the lack of](#)  
158 [systematic scale sensitivity analysis—especially for varying window/buffer sizes within the same](#)  
159 [regional domain—leaves uncertainties about the generalizability of their conclusions.](#)  
160 However, the properties and interaction processes of aerosols and clouds ~~exhibit~~ [are spatially](#)  
161 [significantly spatial heterogeneity-heterogeneous](#) and scale ~~dependency~~ [dependent](#) (McComiskey et al.,  
162 2009; McComiskey and Feingold, 2012; Chen et al., 2015; Glotfelty et al., 2020). [McComiskey and](#)  
163 [Feingold \(2012\) explicitly pointed out that the “scale problem” is a major challenge in quantifying](#)  
164 [aerosol indirect effects, as the spatial scale of observation can mask or exaggerate the true interaction](#)  
165 [signals.](#) In previous studies, the definitions of window size and buffer size have often been subjective,  
166 [inadvertently](#) introducing uncertainties into the research on aci. Although studies have explored the  
167 relationship between aerosols and CER across different observational scales, these investigations have  
168 primarily focused on larger spatial scales, leaving a gap in sensitivity analysis of aerosol indirect effects  
169 at smaller regional scales. [For example, Grandey and Stier \(2010\) focused on global-scale grid](#)  
170 [resolutions but did not explore the scale dependence within regional domains; Wang et al. \(2015\) and](#)  
171 [Liu et al. \(2017\) used fixed buffer sizes \(50 km\) without investigating how varying buffer sizes affect the](#)  
172 [results.](#) Therefore, utilizing multi-source remote sensing data to explore whether and how the aerosol  
173 indirect effect depends on observational spatial scales in eastern China is of great significance for  
174 developing parameterization schemes that align with the regional characteristics of aci.  
175 Aerosol properties in China have significantly changed between 2008 and 2022 due to economic  
176 development and the implementation of emission reduction policies. The AOD over China increased  
177 until 2007 to become among the highest worldwide and remained high between 2008 and 2014 with large

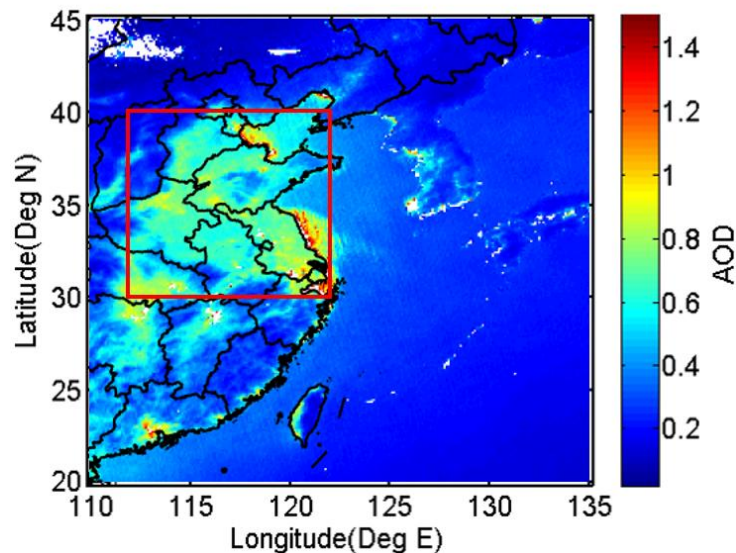
178 interannual variations. The enforcement of emission reduction measures, in particular the implementation  
179 of the 2013-2017 Clean Air Action Plan, resulted in the decline of the AOD between 2014 and 2018 (de  
180 Leeuw et al., 2021; 2022; 2023) and a further decrease resulted in an AOD lower than that in 2000 (de  
181 Leeuw et al., 2023). This distinct two-period variation (high AOD vs. decreasing AOD) provides a unique  
182 opportunity to investigate how changes in aerosol loading modulate the scale dependence of aerosol  
183 indirect effects, a topic that has not been systematically addressed in previous studies. Based on these  
184 observations, in this study we will ~~conducts~~ a comparative analysis of the sensitivity of cloud parameters  
185 (CER and  $N_d$ ) to AOD variation ~~based on using~~ data from two distinct periods: 2008-2014 (~~p~~Period 1,  
186 high AOD) and 2015-2022 (~~p~~Period 2, decreasing AOD). The main objectives ~~is~~ are to  
187 investigate: (1) reveal the sensitivity patterns of the sensitivity of aerosol indirect effects to spatial scales  
188 by investigating how spatial scale modulates the sensitivity of CER to AOD ( $S_{CER}$ ) and the sensitivity of  
189  $N_d$  to AOD ( $S_{N_d}$ ) across the two periods over eastern China during the two periods; the effect of spatial  
190 scale on the sensitivity of CER to AOD ( $S_{CER}$ ) across different time periods in the eastern region of China;  
191 and (2) clarify the regulatory role of LWP in cloud-aerosol interactions by examining the LWP-stratified  
192 responses of  $S_{CER}$  and  $S_{N_d}$  to spatial scale and AOD variations; the effect of spatial scale on the sensitivity  
193 of  $N_d$  to AOD ( $S_{N_d}$ ) across different time periods in the eastern region of China. ~~The results from hrough~~  
194 ~~these two aspects of research,~~ The study aims to reveal the sensitivity patterns of the sensitivity of aerosol  
195 indirect effects to spatial scales, ~~providing~~ provides support for optimizing parameterization schemes and  
196 accurate assessment of regional aerosol effects.

## 197 **2 Method**

### 198 **2.1 Study area**

199 Eastern China (30°N-40°N, 112°E-122°E; Figure 1) has undergone remarkable economic expansion over  
200 the past three decades, which was accompanied by a substantial increase in AOD. Eastern China presents  
201 a unique atmospheric laboratory due to its complex aerosol composition - featuring both anthropogenic  
202 pollutants from industrial emissions and natural mineral dust transported from Central Asian deserts,  
203 particularly during the spring (Proestakis et al., 2018; Liu et al., 2021). The multitude of sources and the  
204 persistent nature of these aerosol particles, which can remain suspended for days to weeks and be  
205 transported over long distances in the absence of precipitation (Kim et al., 2007; Guo et al.,

206 [2013](#)[Costantino et al., 2013](#); [Li et al., 2021](#); [Leung et al., 2023](#)), makes eastern China an ideal study area  
207 for investigating aci. Our research leverages satellite observations to systematically evaluate the  
208 sensitivity of cloud properties ( $S_{CER}$  and  $S_{Nd}$ ) to the AOD variation, [thereby revealing the scale-sensitive](#)  
209 [patterns of aerosol indirect effects and clarifying the regulatory role of LWP in cloud-aerosol interactions](#)  
210 [over this region.](#)



211  
212 **Figure 1.** Map of annual averaged MODIS/AQUA level 2 AOD for all years during the period from 2008 to  
213 2022. The red rectangle ([30°–40°N, 30–40-N and 112°–122°E](#)~~112–122-E~~) indicates the study area.

## 214 2.2 Data used

215 Data used in this study were acquired by the ~~Moderate Resolution Imaging Spectroradiometer~~  
216 ~~(MODIS)~~ instrument aboard NASA’s Aqua satellite, which features an extensive swath width of  
217 approximately 2300 km and comprehensive spectral coverage across multiple bands (King et al.,  
218 2003). The satellite’s equator crossing time is 13:30 (~~LT~~[Local time](#)), i.e. in the early afternoon,  
219 coinciding with optimal development conditions for continental warm cloud systems ([Wang et al.,](#)  
220 [2014](#); [Liu et al., 2024](#)). For aerosol characterization, we utilized the MODIS Collection 6.1 aerosol  
221 product (MOD04), generated from cloud-screened pixels with a native resolution of 500 m at nadir  
222 and subsequently aggregated to 10 km grid cells (Remer et al., 2005; Levy et al., 2010). AOD  
223 retrieval over land uses radiances measured at the top of the atmosphere (TOA) at wavelengths of  
224 0.47, 0.66, and 2.13  $\mu\text{m}$  (Remer et al., 2005). [The MODIS AOD \(at 550 nm\) Level 2 products \(10](#)  
225 [km  \$\times\$  10 km\) has been validated against ground-based remote sensing data](#)~~—~~ and the results show  
226 [that 69.4-0% of the MODIS AOD data fall within the expected uncertainty of  \$\pm \(0.05 + 15 \%\)\$  over](#)

227 [land \(Levy et al., 2013\)](#). In this study, AOD larger than 1.5 was excluded from further analysis to  
228 mitigate potential retrieval overestimation. ~~This threshold is justified~~[was selected based on two key](#)  
229 [considerations: \(1\) Christensen et al. \(2017\) used MOD06 C6 data \(1 km × 1 km\) and reported that](#)  
230 [“large aerosol optical depths remain in the MODIS-observed pixels near cloud edges, due primarily](#)  
231 [to 3D effects \(Várnai and Marshak, 2009\) and the swelling of aerosols by higher relative humidity”;](#)  
232 [\(2\) the threshold of 1.5 aligns with widely adopted thresholds in regional aerosol-cloud interaction](#)  
233 [studies over eastern China, where high AOD often coincides with complex surface conditions \(e.g.,](#)  
234 [urbanization, heterogeneous land cover\) that exacerbate retrieval biases \(Wang et al., 2015; Liu et](#)  
235 [al., 2017, 2024\)](#).

236  
237 The cloud properties ~~analysed-used~~ in this study, including ~~CDR~~[CER](#), LWP, ~~cloud-optical-thickness~~  
238 ~~(COT)~~, ~~cloud-top-pressure~~(CTP), and cloud phase infrared (CPI) index, were derived from the [Collection](#)  
239 [6.1 MODIS Level 2 cloud product \(MYD06\) \(King et al., 2003\)](#). The retrieval of these cloud  
240 characteristics utilizes six spectral channels spanning wavelengths from the visible to the near-infrared  
241 (0.66, 0.86, 1.24, 1.64, 2.12, and 3.75  $\mu\text{m}$ ) as described by King et al. (1997). [Uncertainties in the MODIS](#)  
242 [C6.1 cloud parameters over land originate from instrument calibration, atmospheric correction, land](#)  
243 [surface properties, and model assumptions \(Platnick et al., 2017, 2018\)](#). For COT, these include scene-  
244 [dependent Level 1B data errors \(1.5%–30%\), land surface albedo errors \( \$\pm 15\%\$ \), and atmospheric](#)  
245 [correction errors \( \$\pm 20\%\$ \)](#). The C6.1 algorithm addresses some prior limitations by inheriting C6’s  
246 [optimized lookup table design, which reduces interpolation errors to 0.1%–0.2% for near-nadir views](#)  
247 [and corrects C5’s overestimation of thin-cloud COT \(Platnick et al., 2017\)](#). CER uncertainties, stemming  
248 [from solar irradiance error \( \$\sim 4\%\$  at 3.7  \$\mu\text{m}\$ \), atmospheric correction, and scattering differences, are](#)  
249 [mitigated as C6.1 retains C6’s separate multi-band reporting, thereby eliminating C5’s systematic bias](#)  
250 [\(Platnick et al., 2017\)](#). LWP uncertainty is linked to COT/CER retrieval errors and cloud-phase  
251 [classification accuracy; the latter is improved by C6’s voting-based phase algorithm \(preserved in C6.1\),](#)  
252 [which reduces misclassification over complex surfaces like vegetation and deserts \(Marchant et al., 2015;](#)  
253 [Platnick et al., 2017\)](#). For CTP (1 km resolution), uncertainties from viewing angles and cloud structure  
254 [are partially countered in C6.1 by assigning fill values when the 1 km retrieval fails, avoiding surface](#)  
255 [parameter defaults. For land clouds above 3 km, CTP accuracy reaches  \$\sim 50\$  hPa \(Baum et al., 2012\)](#).

256 [Finally, CPI adopts C6's weighted voting logic \(replacing C5's sequential tree\), with C6.1 maintaining](#)  
257 [an enhanced Phase Agreement Fraction against CALIOP/POLDER data, which reduces uncertainties](#)  
258 [from weak thin-cloud signals and complex land interference \(Marchant et al., 2015; Platnick et al.,](#)  
259 [2017\).~~the ,EThe-~~](#)

260 Following the methodology of Platnick et al. (2017), CER and COT measurements at 3.7  $\mu\text{m}$  ~~are-were~~  
261 ~~employed-used~~ to estimate  $N_d$  through adiabatic approximation principles (Quaas et al., 2006). Previous  
262 investigations have demonstrated that implementing filters based on cloud adiabaticity ~~produces~~  
263 ~~produced~~ minimal effects on  $S_{Nd}$  estimates while significantly reducing the available dataset by up to  
264 63.00% (Gryspeerd et al., 2022). Therefore, such filtering procedures were not adopted in the current  
265 analysis. ~~It should be noted that-Instead,~~  $N_d$  calculations are initially performed at the native pixel  
266 resolution (approximately 1 km) prior to spatial aggregation, thereby avoiding potential biases associated  
267 with deriving  $N_d$  from nonlinear combinations of CER and COT at coarser resolutions (Feingold et al.,  
268 2022). To maintain data quality, the analysis ~~incorporates-incorporated~~ several quality control measures:  
269 only single-phase liquid clouds (CPI = 1) with CTP exceeding 700 hPa and LWP ~~below-smaller than~~ 200  
270  $\text{g m}^{-2}$  are considered, consistent with the typical atmospheric distribution of aerosols in the lower  
271 troposphere (Michibata et al., 2014). Pixels with CER values smaller than 4  $\mu\text{m}$  or COT values smaller  
272 than 4 ~~are-were~~ excluded due to increased retrieval uncertainties (Sourdeval et al., 2016). Additionally,  
273 observations ~~wereare~~ restricted to solar zenith angles  $<65.00^\circ$  and sensor zenith angles  $<41.40^\circ$ . This  
274 constraint ~~wasis~~ intended to reduce the influence of well-documented biases, as elaborated in Grosvenor  
275 et al. (2018).

276 [CALIPSO \(Cloud-Aerosol Lidar and Infrared Pathfinder Satellite Observations\) operates within the A-](#)  
277 [Train constellation alongside the Aqua satellite and other NASA Earth-observing platforms. The primary](#)  
278 [instrument aboard CALIPSO is the Cloud-Aerosol Lidar with Orthogonal Polarization \(CALIOP\).](#)  
279 [CALIOP is a two-wavelength, polarization-sensitive lidar specifically designed to provide high-](#)  
280 [resolution vertical profiles of aerosols and clouds on a global scale \(Winker et al., 2009\). The mission](#)  
281 [and its lidar instrument are described in Winker et al. \(2009\), and the associated Level 1 data products](#)  
282 [are detailed in Winker et al. \(2010\). This\).~~The Aqua satellite operates within the A Train constellation~~  
283 ~~alongside CALIPSO \(Cloud-Aerosol Lidar and Infrared Pathfinder Satellite Observations\) and other~~  
284 ~~NASA Earth-observing platforms \(Stephens et al., 2002\). As the primary instrument aboard CALIPSO,~~](#)

285 ~~the Cloud Aerosol Lidar with Orthogonal Polarization (CALIOP) is a two-wavelength, polarization-~~  
286 ~~sensitive lidar specifically designed to provide high-resolution vertical profiles of aerosols and clouds on~~  
287 ~~a global scale (Winker et al., 2009). As a key instrument aboard CALIPSO, the Cloud Aerosol Lidar~~  
288 ~~with Orthogonal Polarization (CALIOP) represents the first space-based polarization-sensitive lidar~~  
289 ~~system specifically designed for atmospheric profiling of aerosols and clouds (Winker et al., 2003). This~~  
290 advanced sensor features an exceptionally narrow ground footprint of 70 m diameter for each laser pulse.  
291 The vertical resolution of CALIOP's products varies with altitude: 30 m within 0-8.2 km, 60 m between  
292 8.2-20.2 km, and 180 m from 20.2-30.1 km, while maintaining a consistent 5 km horizontal resolution  
293 along the track direction (Liu et al., 2009).

294 The coordinated A-Train configuration ensures near-simultaneous observations (within 1-2 minutes)  
295 between MODIS/Aqua and CALIOP/CALIPSO for identical atmospheric targets (Stephens et al., 2002).

296 This temporal synchronization guarantees data consistency when extracting coincident measurements,  
297 ~~avoiding interferences such as aerosol diffusion and cloud evolution caused by observational time lags—~~  
298 ~~an advantage unparalleled by positioning methods like random grid points and ground-based stations.~~

299 For spatial compatibility, we resampled the higher-resolution MODIS cloud products (CDER, LWP, and  
300  $N_d$  at 1 km native resolution) to match CALIOP's 5 km along-track scale, while directly utilizing the 5  
301 km-resolution CTP and CPI parameters. In cases where CALIOP detected aerosol presence, we  
302 computed spatial averages of MODIS aerosol and cloud retrieval products across multiple observation  
303 scales (detailed in Section 2.4) centred on CALIOP targets. This approach ~~assumes~~ reasonable  
304 homogeneity of aerosol properties between adjacent clear and cloudy regions (Anderson et al., 2003;  
305 Quaas et al., 2008). Table 1 ~~provides a comprehensively documents~~ documented overview of the aerosol  
306 and cloud datasets including the parameters used from each product, the resolution, and the data source,  
307 ~~employed-used~~ in this investigation study, including their respective parameters, resolutions, and sources.

314  
315  
316  
317  
318  
319  
320  
321  
322

**Table 1. Aerosol and cloud products, parameters, horizontal resolutions, and their sources applied in the present study.**

<b>Product</b>	<b>Parameters</b>	<b>Horizontal resolution</b>	<b>Data source</b>		
Aerosol (MYD04 Level 2 Collection <a href="#">56</a> )	Latitude	10 km	MODIS		
	Longitude	10 km			
	Scan_Start_Time	10 km			
	AOD at 550 nm	10 km			
Cloud (MYD06 Level 2 Collection <a href="#">56</a> )	Latitude	5 km			
	Longitude	5 km			
	Scan_Start_Time	5 km			
	CER at 3.7 um and 2.1 um	1 km			
	LWP at 3.7 um	1 km			
	COT at 3.7 um	1 km			
	Cloud multi-layer flag	1 km			
	Cloud_Phase_Infrared_Day	5 km			
	Cloud_TOP_Pressure_Day	5 km			
	Sensor_Zenith_Day	5 km			
	Solar_Zenith_Day	5 km			
	Aerosol (05kmALay)	Latitude		5 km	CALIOP
		Longitude		5 km	
Profile_Time		5 km			

323 **2.3 Calculation of sensitivities**

324 Variations in aerosol loading significantly influence cloud optical properties (such as COT) and  
325 microphysical parameters (such as CER). Under specific environmental conditions, aerosol particles can  
326 transform into CCN or INP, a process primarily determined by their chemical composition and ambient  
327 temperature ([Bellouin et al., 2020](#)). When these nuclei are activated, water vapor condenses on their  
328 surfaces to form cloud droplets or ice particles. As the concentration of aerosol particles increases, the

329 number of CCN or INP may rise correspondingly, leading to an increase in the number of cloud droplets.  
330 Notably, under conditions where the liquid water content in clouds remains constant (i.e., LWP), the same  
331 amount of water vapor is distributed across more cloud droplets, resulting in a reduction in the size of  
332 individual droplets. Specifically, as aerosol concentration increases, the CER decreases, while cloud  
333 albedo increases. On the basis of findings of Kaufman and Fraser (1997), Feingold et al. (2001) pointed  
334 out that the sensitivity of cloud microphysical properties (e.g., CER) to changes in the number  
335 concentration of aerosol particles (e.g., using AOD as a measure) can be described by the following  
336 formula:

$$337 \quad S_{\text{CER}} = \left. \frac{d \ln r_e}{d \ln \alpha} \right|_{\text{LWP}} \quad -0.33 < S < 0 \quad (1)$$

338 Where  $r_e$  represents the CER and  $\alpha$  represents the AOD. Following Andreae (2009), AOD and CCN  
339 are correlated and AOD varies with CCN following a power law relationship. Eq. (1) describes the  
340 relative change of CER with the relative change of the AOD for constant LWP. It is noted that this  
341 formulation differs from that used in recent studies (e.g., Bellouin et al., 2020) where S is expressed in  
342 terms of  $N_d$  with no restriction in LWP. The sensitivity S of CER to AOD can be determined as the slope  
343 of a linear fit to a log-log plot of CER versus AOD. [The effect of aerosols on CER is analyzed by](#)  
344 [comparing the difference in  \$S\_{\text{CER}}\$  and correlation coefficients between AOD and CER under different](#)  
345 [spatial scales \(Section 2.4\) and LWPs \(Section 3.2\).](#)

346 [Here](#)In this study, the variation in  $N_d$  with CCN is referred to as the susceptibility  $S_{N_d}$ . Following the  
347 method of Gryspeerd et al. (2023), the sensitivity,  $S_{N_d}$ , of a cloud property,  $N_d$ , to  $\alpha$  is defined here as

$$348 \quad S_{N_d} = d \ln N_d / d \ln \alpha \quad 0 < S < 1 \quad (2)$$

349 [Relations between CER and  \$N\_d\$  and AOD are determined through Eq. 1 and Eq. 2 and correlation](#)  
350 [coefficients R. The significance of these relations is determined by using the student's t test, i.e. the](#)  
351 [results are statistically significant when the p value is smaller than 0.01, where p is defined as the](#)  
352 [probability of obtaining a result equal to or "more extreme" than what was actually observed.](#)

353 [This method quantifies the sensitivity of CER and  \$N\_d\$  to AOD variations via linear regression in log-log](#)  
354 [space, using Eq. 1 and Eq. 2, respectively. Its core assumptions, uncertainties, and limitations are highly](#)  
355 [consistent: both rely on AOD as an aerosol proxy variable, assume constant cloud liquid water content](#)  
356 [and a linear sensitivity relationship, and depend on the reliability of satellite-retrieved parameters](#)  
357 [\(Feingold et al., 2001; Gryspeerd et al., 2023\). However, AOD cannot distinguish aerosol size and](#)

358 hygroscopicity, retrieval errors are substantial in clean conditions, and linear fitting fails to capture  
359 nonlinear/non-monotonic responses. Both methods are constrained by satellite retrieval biases, limited  
360 scenario applicability (only valid for specific homogeneous clouds and aerosol types), the omission of  
361 key modulating factors (dynamical conditions, aerosol type) and feedback processes, and can only assess  
362 first-order direct effects. Reliability requires scenario constraints and uncertainty analysis; the only  
363 nuances come from the target variable (CER vs.  $N_d$ ), which do not alter the shared methodological  
364 limitations.

365  
366 ~~Relations between CER and  $N_d$  and AOD are determined through Eq. 1 and Eq. 2 and correlation~~  
367 ~~coefficients  $R$ . The significance of these relations is determined by using the student's  $t$  test, i.e. the~~  
368 ~~results are statistically significant when the  $p$  value is smaller than 0.01, where  $p$  is defined as the~~  
369 ~~probability of obtaining a result equal to or "more extreme" than what was actually observed.~~

370  
371 ~~in log-log space in some~~

## 373 2.4 Research design for scale effects analysis

374 This study was conducted at multiple spatial scales to examine the scale dependence of  $S_{CER}$  and  $S_{N_d}$  in  
375 delineating aci (Fig. 2). Here, the spatial scales are described by two parameters: study area size (the  
376 geographic scope of the analysis) and buffer size (the local spatial extent around each observation point  
377 for aggregating aerosol and cloud data). To this end, the study area was divided into four congruent square  
378 research areas all centered at the same geographical location (35°N, 117°E) over Eastern China. Hence,  
379 spatial extent varies from the whole study area as defined in Section 2.1 (30°N-40°N, 112°E-122°E-) to  
380 successively smaller areas simulated by decreasing the study area in steps of 2° to 4°×4° as illustrated in  
381 Figure 2a.

382 Buffer size refers here to a circular spatial domain centered at each CALIOP-detected point in the study  
383 area where CALIOP detected the presence of aerosols. Within this circular domain, MODIS-retrieved  
384 cloud and aerosol data (AOD, CER,  $N_d$ , LWP) are spatially averaged to construct matched aerosol-cloud

385 ~~datasets at different local scales. As previously noted, this approach relies on the assumption that aerosol~~  
386 ~~properties are reasonably homogeneous between adjacent clear and cloudy regions (Anderson et al., 2003;~~  
387 ~~Quaas et al., 2008), and this premise is supported by the short-range transport of aerosols (e.g., 10–300~~  
388 ~~km) and the near-simultaneous observations (1–2 minutes) by MODIS and CALIOP within the A-Train~~  
389 ~~constellation. This approach assumes that aerosol properties are reasonably homogeneous between~~  
390 ~~adjacent clear and cloudy regions (Anderson et al., 2003; Quaas et al., 2008), which is a~~  
391 ~~reasonable plausible approximation considering the short range transport of aerosols (e.g., 10 – 300 km)~~  
392 ~~and the near simultaneous observations (1 – 2 minutes) by MODIS and CALIOP within the A Train~~  
393 ~~constellation.~~

394 Buffer zones with sizes increasing from 10 to ~~300~~ 300 km (10 km, 20 km, 30 km, 40 km, 50 km,  
395 60 km, 70 km, 80 km, 90 km, 100 km, 120 km, 140 km, 150 km, 160 km, 180 km, 200 km, 250 km,  
396 and 300 km) were determined within the whole study area by using CALIOP data, ~~i.e. data points~~  
397 ~~where CALIOP detected the presence of aerosol and cloud fields. To justify the selection of this~~  
398 ~~buffer size gradient, we compared the horizontal extent of clouds with the spatial homogeneity of~~  
399 ~~aerosols across the study domain.~~ Previous observations indicate that the typical horizontal scale of  
400 cloud clusters ranges from tens to hundreds of kilometers (Zhang et al., 2024; Cai et al., 2022),  
401 supported by CloudSat/CALIPSO satellite data showing power-law distributed cloud scales (10-  
402 1000 km fitting range) covering major cloud types (Zhang et al., 2024) and regional evidence of  
403 consistent multi-season, multi-latitude cloud extents (Cai et al., 2022).

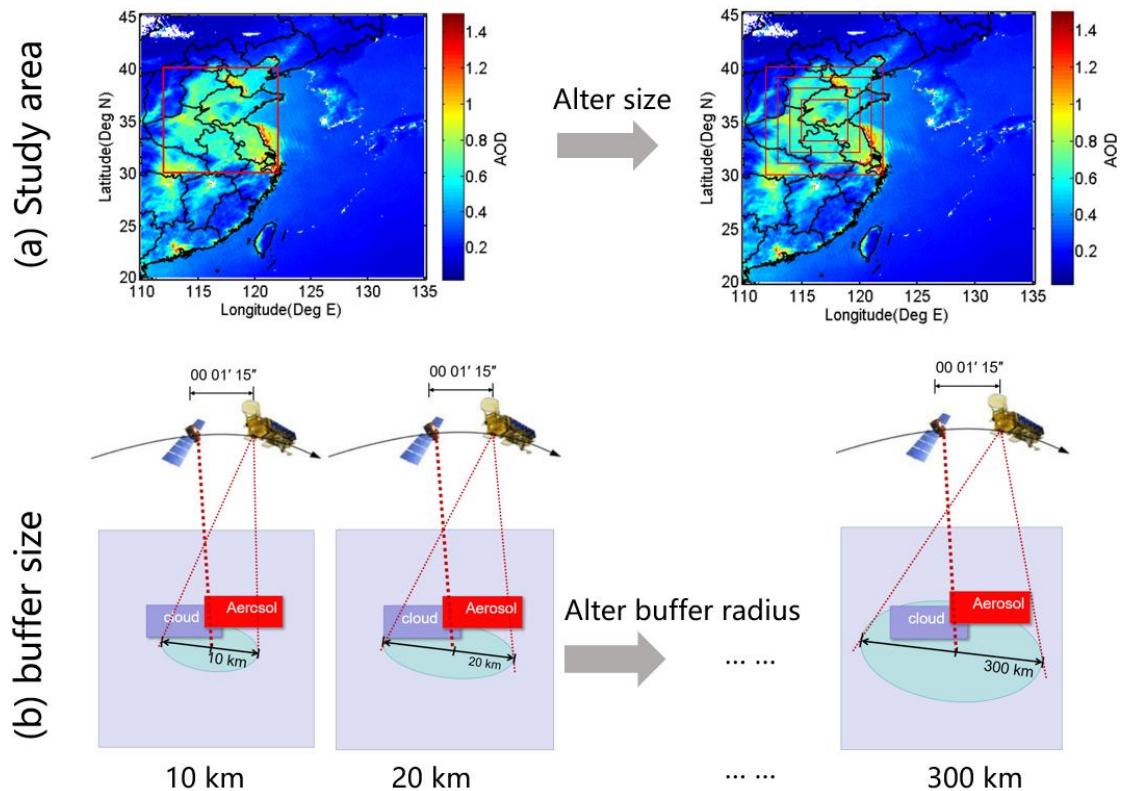
404 Meanwhile, aerosol spatial homogeneity varies with distance: local-scale aerosols ( $\leq 50$  km) exhibit  
405 high homogeneity due to consistent sources and stable diffusion, while regional-scale aerosols ( $>$   
406 100 km) show enhanced heterogeneity from multi-source mixing and atmospheric transport (Hassan  
407 et al., 2024; Mohebalhojeh et al., 2026). ~~Specifically, urban hotspot emissions maintain local~~  
408 ~~homogeneity (Hassan et al., 2024), and a spatial heterogeneity metric quantifies low normalized~~  
409 ~~heterogeneity for local scale ( $\leq 50$  km) emissions (e.g., urban NO) versus high heterogeneity for~~  
410 ~~regional scale ( $> 100$  km) emissions (e.g., agricultural NH<sub>3</sub>) (Mohebalhojeh et al., 2026).~~ Thus, the  
411 10–300 km buffer ~~gradient~~ range covers both cloud characteristic scales and the aerosol  
412 homogeneity transition range, ensuring that MODIS data averaging effectively captures cloud-  
413 aerosol coupling.

414 This range avoids insufficient MODIS pixel coverage caused by due to excessively small buffer sizes (<  
415 10 km). It also prevents conflation between regional meteorological variations and local aci signals  
416 arising from overly large buffer sizes (> 300 km), as synoptic-scale circulation and other regional  
417 meteorological changes may interfere with local aci signals (Quaas et al., 2010). Meanwhile, this range  
418 aligns with the 50 - 150 km buffer sizes widely adopted in regional aci studies (Wang et al., 2015; Liu et  
419 al., 2017; 2024), enabling cross-validation of results and ensuring that MODIS data averaging effectively  
420 captures cloud-aerosol coupling.

421 MODIS-retrieved cloud and aerosol data were averaged over a buffer area around each CALIOP  
422 data point with a radius varying from 10 km to 300 km. Thus, a dataset including aerosol and cloud  
423 properties was constructed with different buffer sizes. The effect of buffer size on the sensitivity of  
424 CER and  $N_d$  to variations in AOD was determined in each study area varying from  $4^\circ \times 4^\circ$  to  $10^\circ \times 10^\circ$ .

425 To this end, for each buffer size, the averaged AOD and cloud parameters were paired to calculate  
426 the sensitivities  $S_{CER}$  (Eq. 1) and  
427  $S_{N_d}$  (Eq. 2), as well as their correlation coefficients (R) between cloud properties (e.g., CER,  $N_d$ ) and  
428 AOD. The optimal buffer size for each study area is defined as the one maximizing the correlation  
429 coefficient (R) between cloud properties (e.g., CER,  $N_d$ ) and AOD. This definition is adopted based on  
430 two core considerations. The optimal buffer size for each study area is defined as the buffer size where  
431 the correlation coefficient (R) between the cloud properties (e.g., CER) and AOD is maximized (i.e., the  
432 most statistically robust aci signal). This optimal size quantifies the local spatial scale at which aerosol  
433 and cloud properties are most tightly coupled, providing a critical benchmark for future aci  
434 parameterization in climate models. Firstly, it aligns with the statistical principle that a higher R value  
435 indicates a stronger linear correlation between the two variables in the log-log space, minimizing the  
436 interference of random noise and non-aerosol confounding factors on the sensitivity estimation (Quaas  
437 et al., 2006; Gryspeerdt et al., 2022). This ensures that the derived  $S_{CER}$  can reliably reflect the intrinsic  
438 relationship between aerosol loading and cloud droplet effective radius, rather than spurious correlations  
439 caused by inappropriate spatial scales. Secondly, this definition also facilitates comparability with  
440 existing literature, as it aligns with the methodological framework of satellite-based aerosol-cloud  
441 interaction studies (Saponaro et al., 2017; Liu et al., 2021+). In these studies, the optimal spatial scale is  
442 typically identified by maximizing the statistical robustness of variable correlations.

443 The dataset was used to study the characteristics of aerosol indirect effects as function of buffer size and  
 444 study area, for two different periods: one with a high aerosol content (2008-2014) and another one with  
 445 a decreasing aerosol content (2015-2022). This approach enabled the determination of the optimal buffer  
 446 size for aerosol indirect effects as function of the size of the study area, ultimately leading to the  
 447 development of a parameterization scheme for aerosol indirect effects for observations with different  
 448 spatial resolution and different sizes of the study area over eastern China.



449  
 450 **Figure 2. (a) Schematic diagram of study area and buffer size patterns applied in this study. (b) scheme of**  
 451 **CALIPSO-MODIS coincidence methodology. When CALIPSO detects the presence of aerosol and cloud fields,**  
 452 **we look for MODIS retrievals within a buffer size from the CALIPSO target. The temporal coincidence is**  
 453 **insured by the coordinated satellite orbits.**

### 454 3 Results

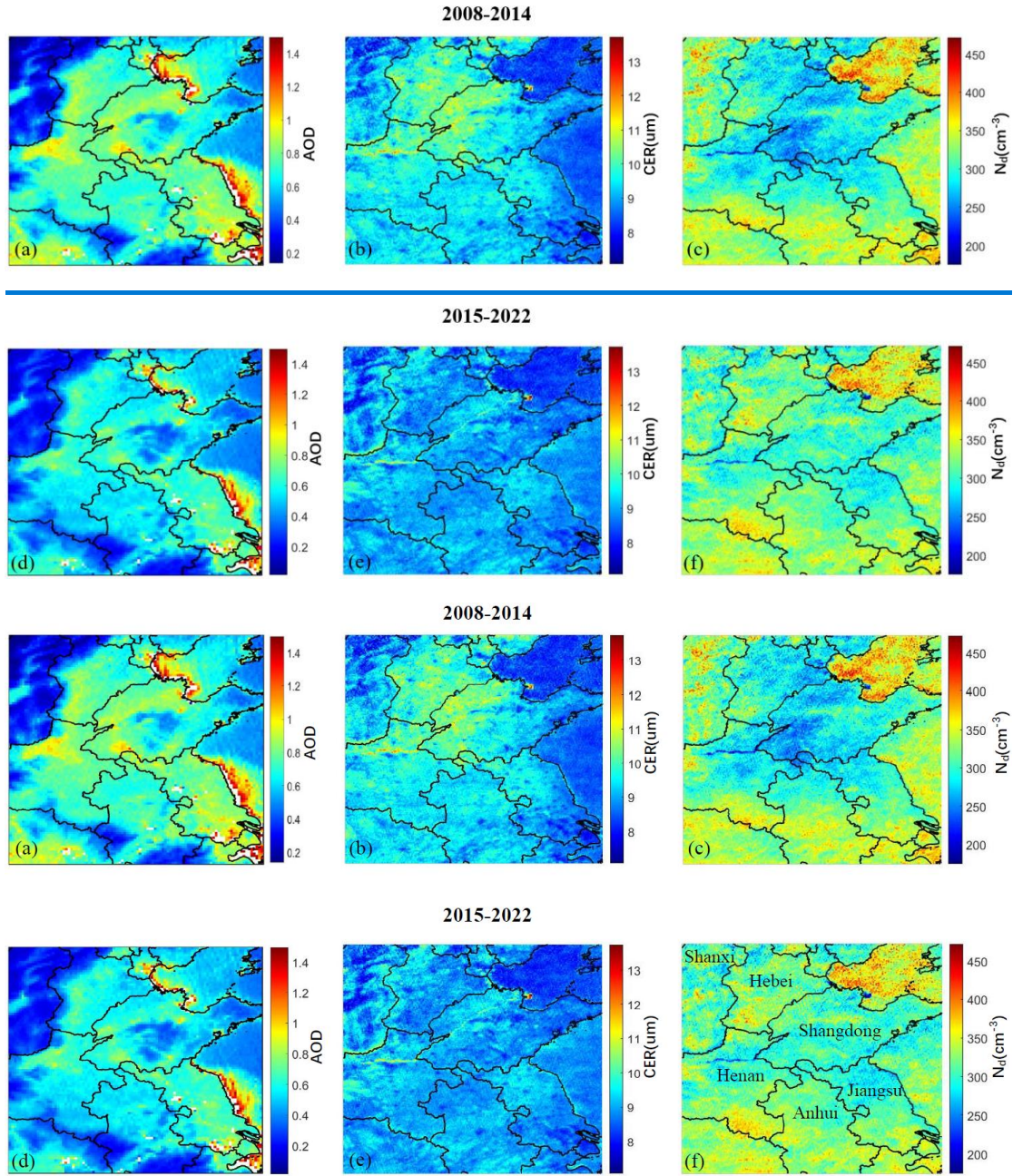
#### 455 3.1 Spatial variations of aerosol and cloud parameters

456 Figure 3 illustrates the spatial distributions of AOD and cloud properties (CER and  $N_d$ ) across the study  
 457 region, averaged for the periods 2008-2014 and 2015-2022. The AOD spatial patterns (Fig. 3a,d) show  
 458 similar spatial distributions during both periods, but with notably reduced values during the latter.  
 459 Pronounced spatial gradients in AOD are evident during both periods. The lowest AOD values occur over

460 the mountainous regions of Shanxi province in the northwest, while elevated concentrations appear in  
461 the southeastern areas encompassing the Hebei and Shandong provinces. This geographical contrast  
462 arises from the mountain ranges that demarcate the heavily industrialized, densely populated North China  
463 Plain (NCP) in the east - characterized by substantial anthropogenic emissions - from the relatively  
464 pristine western regions. Under prevailing southeasterly wind conditions, these topographic barriers  
465 effectively block transport of atmospheric pollutants which accumulate along their windward slopes  
466 (Sundström et al., 2012). The concentration of heavy industries and power generation facilities in the  
467 NCP are primarily responsible for the observed high AOD concentrations, together with meteorological  
468 and geographical conditions. Additionally, lower AOD values appear in southern Anhui and central  
469 Shandong relative to the surrounding regions.

470 The CER spatial distributions (Fig. 3b,e) reveal distinct differences between the two periods. During  
471 2008-2014, larger cloud droplets predominated in the northern sectors, particularly throughout Hebei and  
472 western Shandong. Notably, the spatial correspondence between AOD and CER maxima aligns with the  
473 anti-Twomey effect, suggesting that the high aerosol loading promoted cloud droplet growth rather than  
474 suppression - consistent with findings from Wang et al. (2014) and Liu et al. (2018). The 2015-2022  
475 period shows markedly reduced CER values (typically  $<10 \mu\text{m}$ ) with enhanced spatial homogeneity.

476 Similarly,  $N_d$  exhibits contrasting spatial patterns between the two periods (Fig. 3c,f). The earlier  
477 timeframe shows depressed  $N_d$  values in central regions surrounded by elevated concentrations  
478 peripherally. This pattern reverses during 2015-2022, with increases of  $N_d$  in the central area  
479 accompanied by overall reduction of the cloud droplet concentrations in the surrounding regions.



480

481

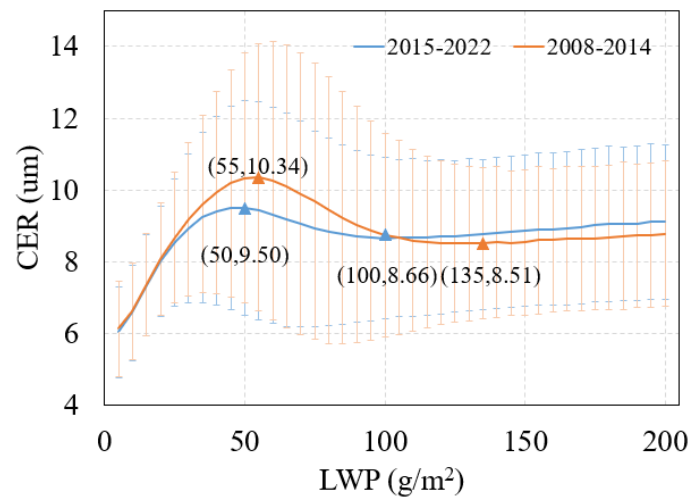
482 **Figure 3. Spatial distributions of AOD (a, d), CER (b, e) and  $N_d$  (c, f), averaged over the years 2008-2014 (top**  
 483 **row) and 2015-2022 (bottom row) over the study area. The lines are provincial borders and the names of**  
 484 **provinces mentioned in the text are indicated in Fig. (f).**

485 **3.2 Sensitivity of CER to AOD stratified by LWP**

486 Before analyzing the influence of AOD on CER, the relationship between CER and LWP should be  
 487 investigated. The values of the LWP were divided into 40 subsets with a width of  $5 \text{ g/m}^2$ , and then the  
 488 average value of CER in each subset was calculated and plotted as function of LWP (Figure 4).

489 The variation of CER with LWP shows three regimes. For LWP smaller than  $55 \text{ g/m}^2$  (period 1) or 50

490  $\text{g/m}^2$  (period 2), CER increased rapidly with the increase of LWP. This first LWP regime is referred to as  
 491 ~~the~~ rapid growth regime (LWP1)~~phase of CER~~. The second LWP regime, referred to as a decreasing  
 492 regime (LWP2), ~~occurred-applies to when~~ the LWP ranged from  $55 \text{ g/m}^2$  to  $135 \text{ g/m}^2$  (period 1) or  $50$ -  
 493  $100 \text{ g/m}^2$  (period 2) and CER decreased with the increase of LWP. When LWP was greater than  $135 \text{ g/m}^2$   
 494 (period 1) or  $100 \text{ g/m}^2$  (period 2), CER increased with increasing LWP but at a much slower rate than  
 495 during the first regime; the third LWP regime is therefore referred to as ~~the~~ slow growth regime (LWP3).  
 496 These results show that CER is very sensitive to the changes in LWP, which is consistent with the study  
 497 of Liu et al. (2021). ~~Their~~ The results of Liu et al. showed that CER was very sensitive to the changes  
 498 in LWP, which was consistent with the study of Liu et al. (2021). Specifically, CER exhibited a three-  
 499 stage variation with LWP: rapid growth when  $\text{LWP} < 50 \text{ g/m}^2$  (with the fastest change rate), a stable state  
 500 during  $50\text{--}150 \text{ g/m}^2$ , and slow growth when  $\text{LWP} > 150 \text{ g/m}^2$  (at a rate much lower than the first stage).  
 501 This highlighted the necessity of fixing LWP conditions to accurately investigate the impact of AOD on  
 502 CER. To separate the effects of changing LWP on CER from those of changing AOD on CER, relations  
 503 between CER and AOD were evaluated for constant LWP (McComiskey et al., 2012), for each of the  
 504 three regimes mentioned above, by using double-logarithmic plots of AOD versus CER. The number of  
 505 CER observations in the third regime is too small to achieve statistically meaningful results, therefore  
 506 the sensitivity of CER to AOD was only analyzed for the rapid growth and decreasing regimes.



507  
 508 **Figure 4. Variation of CER with LWP over the study area. Here all CER data were averaged in LWP bins,**  
 509 **from 0 to 200  $\text{g/m}^2$  with a width of  $5 \text{ g/m}^2$ . The red line is a fit to the data during 2008-2014 and the blue**  
 510 **line is for the data during 2015-2022. The numbers in parentheses indicate the (LWP, CER) values for the**  
 511 **inflection points between the regimes. The error bars (the vertical lines) denote the standard deviations,**  
 512 **indicating the variability of CER around the average at each LWP value.**

### 513 3.2.1 Rapid CER growth regime

514 For the first, ~~rapid CER growth~~LWP regime, the  $S_{CER}$  is negative (as shown in Figure 5). This aligns with  
515 the Twomey effect (Twomey, 1977): The an increase of in aerosols implies an increase in raises the  
516 number of CCN ~~for which, and withat~~ constant LWP, less water vapor is available per cloud droplet,  
517 ~~causing reducing CER~~the CER to become smaller, increasing ~~the albedo of the cloud~~ albedo, and  
518 ultimately cooling the atmosphere. This indicates that, in ~~regime 1~~the rapid growth regime, the interaction  
519 between AOD and CER in the target region is in agreement with the Twomey effect. The data in Figure  
520 5a show that during ~~p~~Period 1,  $S_{CER}$  varies with buffer size and that the variations are different for  
521 different study areas. The value of  $|S_{CER}|$  is smallest for the largest study area ( $10^\circ \times 10^\circ$ ) and decreases  
522 with buffer size to a minimum for buffer size of 150 km and then increases. For the smallest study area  
523 ( $4^\circ \times 4^\circ$ ), the sensitivity exhibits a much stronger negative correlation, with its magnitude decreasing as  
524 the buffer size expands~~the sensitivity is much stronger negative and decreases as buffer size increases,~~  
525 especially for  $50 \text{ km} < \text{buffer size} < 100 \text{ km}$ . For the 2 intermediate study areas, the sensitivities are  
526 initially similar (except for the smallest buffer size) and diverge for buffer size  $> 100 \text{ km}$ . ~~–~~ The data show  
527 that the value of  ~~$|S_{CER}|$~~  $S_{CER}$  overall becomes smaller as study area increases. The decrease of  $|S_{CER}|$  in  
528 with larger~~increasing~~ study areas is mechanistically tied to scale-dependent aerosol indirect effect theory  
529 and meteorological confounding (Quaas et al., 2009; McComiskey & Feingold, 2012). The correlation  
530 coefficients  $R$  (bottom of Figure 5 a) are similar for all four study areas at small buffer sizes, increase  
531 fast with buffer size to a maximum for a buffer size of about 50 km and then decrease and diverge. The  
532 largest decrease is observed for study area of  $10^\circ \times 10^\circ$ . In this study, the optimal scale for  $S_{CER}$  in a study  
533 area is defined as the buffer size with the highest correlation coefficient  $R$  between  $S_{CER}$  and AOD. ~~–~~ The  
534 optimal scale for each study area is indicated in Figure 5 with a red solid square. A plot of the optimal  
535 scale versus the size of the study area in Figure 6 (curve LWP1-~~period~~P1) shows that, as the study area  
536 size ~~is~~ increased from  $6^\circ \times 6^\circ$  to  $10^\circ \times 10^\circ$ , the optimal scale decreased from 100 km to 30 km.

537 As compared with period 1, in period 2 (Figure 5b) the value of the  ~~$|S_{CER}|$~~  $S_{CER}$  also de~~decreases~~increases  
538 as the buffer size increases. However, the scale sensitivity analysis for period 2 revealed two distinct  
539 characteristics different from period 1: (1) the four  $S_{CER}$  curves for different study areas are much closer  
540 than during period 1; (2) with the exception of the study area of  $10^\circ \times 10^\circ$ , the values of the  $|S_{CER}|$  ~~$S_{CER}$~~   
541 curves for the other three study areas are significantly reduced (closer to zero), indicating a corresponding

542 weakening of aerosol-cloud interaction intensity against the background of decreased aerosol  
543 concentrations. Particularly noteworthy is that during period 1, the R values for the ~~study area of~~  $10^{\circ} \times 10^{\circ}$   
544 ~~study area displays~~ showed a sharp ~~attenuation~~ declining trend when the buffer size exceeds 60 km, while  
545 in period 2 this happened for buffer size larger than 110 km and the R value curves for ~~other all~~ study  
546 areas ~~are markedly lower than for period 1, with~~ significantly expanded their high-value ranges  
547 ~~significantly expanded~~. Also for period 2, the R values for the study areas of  $10^{\circ} \times 10^{\circ}$  and  $8^{\circ} \times 8^{\circ}$  are very  
548 similar, in contrast to period 1 when only the R values for the study areas of  $10^{\circ} \times 10^{\circ}$  decreases fast. ~~In~~  
549 ~~period 2, the R values for the study area of  $4^{\circ} \times 4^{\circ}$  show a behavior similar to that for the study area of~~  
550  ~~$10^{\circ} \times 10^{\circ}$  in period 1.~~ Across different study areas, the optimal scale (Curve LWP1-~~peirod2P2~~) showed  
551 ~~shows~~ a behavior opposite to that during ~~period 1P1~~: as the study area size ~~is~~ increased from  $6^{\circ} \times 6^{\circ}$  to  
552  $10^{\circ} \times 10^{\circ}$ , the optimal scale increased from 20 km to 80 km. It is noted that for a study area of  $4^{\circ} \times 4^{\circ}$  the  
553 optical scale was 50 km in both ~~periods~~ periods P1 and P2. ~~The estimates of  $S_{CER}$  and correlation~~  
554 ~~coefficients R between CER and AOD, stratified by LWP period and optimal buffer size, for study areas~~  
555 ~~ranging from  $4^{\circ} \times 4^{\circ}$  to  $10^{\circ} \times 10^{\circ}$  during the 2008–2014 period in rapid LWP regime are presented in~~  
556 ~~Appendix A1.~~ For the first LWP regime,  $S_{CER}$  estimates and correlation coefficients R by period and  
557 ~~optimal buffer size across  $4^{\circ} \times 4^{\circ}$  to  $10^{\circ} \times 10^{\circ}$  study areas are given in Supplement Table S1.~~

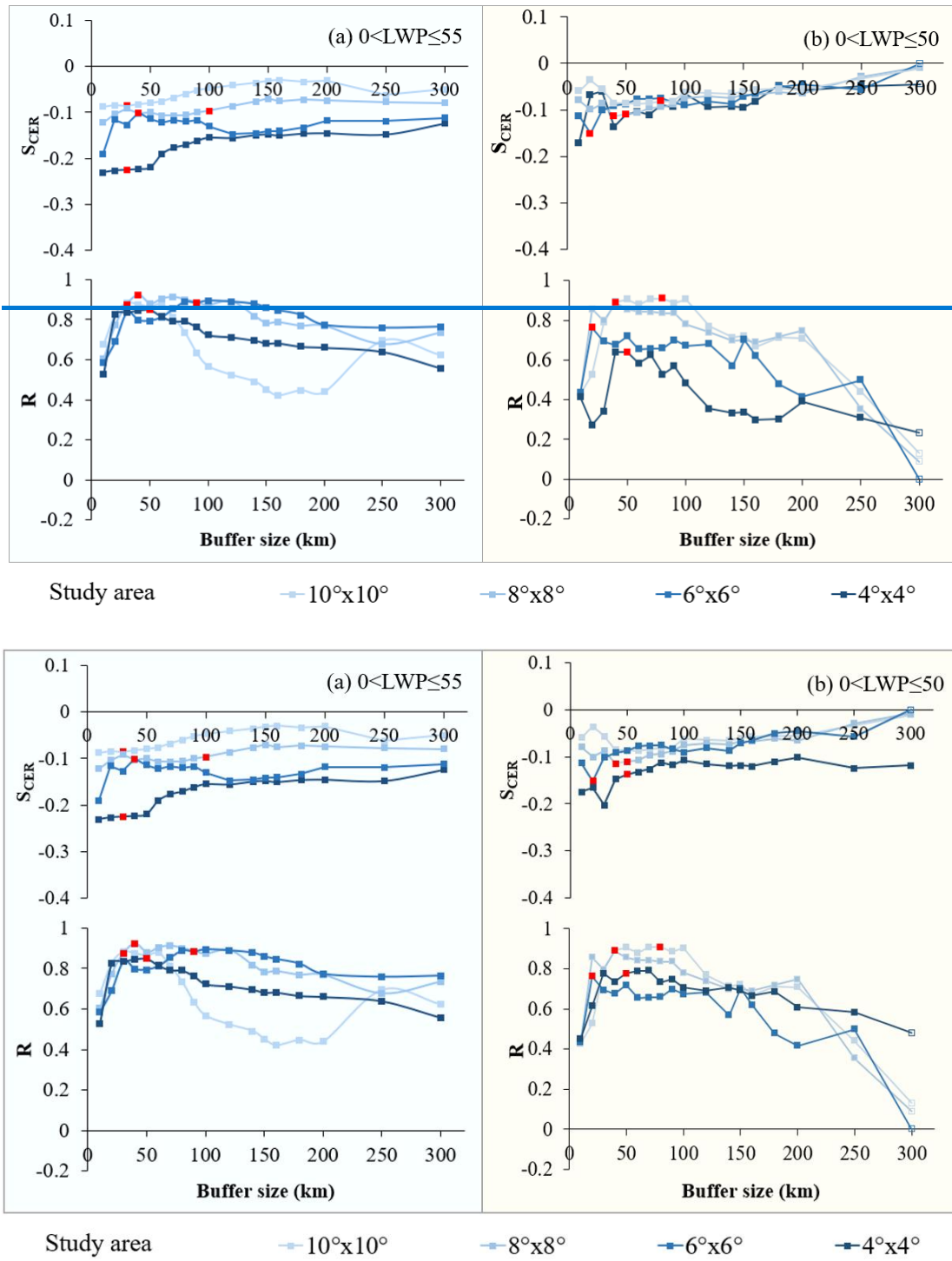
### 558 3.2.2 Decreasing CER regime

559 During the second LWP regime (Figure 7), the AOD and CER were also negatively correlated ( $S_{CER} < 0$ )  
560 during both periods, but the values of  $S_{CER}$  vary stronger with the size of study area: ~~the curve dispersion~~  
561 ~~increases in the second LWP regime, the values of  $|S_{CER}|$   ~~$S_{CER}$  negative values are stronger~~ larger overall,  
562 ~~and the relatively concentrated trend in the earlier period 1 shifts to more scattered fluctuations in the~~  
563 ~~second LWP regime~~ period 2. During period 1, for the largest ( $10^{\circ} \times 10^{\circ}$ ) study area: ~~the value of  $|S_{CER}|$   ~~$S_{CER}$~~~~   
564 ~~(Figure 7a) decreases~~ rises with increasing buffer size, nearing zero at ~150 km, briefly turning slightly  
565 ~~positive, then slowly falling below zero by 220 km.~~ for the largest study area of  $10^{\circ} \times 10^{\circ}$  the value of  
566  ~~$S_{CER}$  decrease with increasing buffer size to close to zero for a buffer size of about 150 m and reach a~~  
567 ~~small positive value before it slowly decreases to below zero for a buffer size of 220 m.~~ For the three  
568 smaller study areas, the  $S_{CER}$  values were all negative and  ~~$|S_{CER}|$  overall~~ ~~decreased~~ increased ~~decreased~~  
569 with increasing buffer size. Through the sensitivity of  $S_{CER}$  to buffer size across varying study areas~~

570 during period 1, the value of  $|S_{CER}|S_{CER}$  for a given buffer size becomes smaller with increasing study  
571 area size. Additionally, across all study areas,  $|S_{CER}|S_{CER}$  initially ~~decreases~~increases with the increase of  
572 the buffer size, then ~~decrease~~increases, and gradually stabilizes thereafter. The data in Figure 6 (Curve  
573 LWP2-~~peirod~~P1), show that, the optimal size varies between 30 km and 60 km with no clear dependence  
574 on the size of the study area.

575 Compared with ~~the~~ period 1, the value of  $|S_{CER}|S_{CER}$  in period 2 (Figure 7b) also decreased—overall with  
576 increasing buffer size, and at the same buffer size,  $|S_{CER}|S_{CER}$  decreased—~~(less negative)~~ as study area  
577 increased. However, the scale sensitivity analysis for period 2 revealed two distinct characteristics: (1)  
578 the four curves for different study areas are closer than during period 1; (2) the  $|S_{CER}|S_{CER}$  for the study  
579 area of  $10^\circ \times 10^\circ$  was overall ~~smaller (more negative)~~larger, while the values of the  $S_{CER}$  curves for the  
580 study areas of  $4^\circ \times 4^\circ$  and  $6^\circ \times 6^\circ$  were significantly reduced and that for the study area of  $8^\circ \times 8^\circ$  was  
581 slightly reduced. The reduction may be attributed to weakened ~~cloud-aerosol~~aerosol-cloud interactions  
582 resulting from decreased regional aerosol concentrations ([Jia et al., 2022](#); [Li et al., 2024](#); [Zhao et al.,](#)  
583 [2025](#)). The variation of the optimal scale (Curve LWP2-~~period~~P2) with the size of the study area is  
584 similar to that during ~~P2~~period 1 in the rapid growth LWP regime: as the study area size ~~is~~ increased  
585 from  $6^\circ \times 6^\circ$  to  $10^\circ \times 10^\circ$ , the optimal scale increased from 60 km to 100 km. The estimates of  $S_{CER}$  and  
586 correlation coefficients R between CER and AOD, stratified by LWP period and optimal buffer size, for  
587 study areas ranging from  $4^\circ \times 4^\circ$  to  $10^\circ \times 10^\circ$  in decreasing LWP regime during the 2015–2022 period  
588 are presented in xA1. For the second LWP regime,  $S_{CER}$  estimates and correlation coefficients R between  
589 CER and AOD by period and optimal buffer size across  $4^\circ \times 4^\circ$  to  $10^\circ \times 10^\circ$  study areas are given in  
590 Supplement Table S1.

591 Through comparative analysis of  $S_{CER}$  data distribution across different LWP regimes under different  
592 aerosol conditions (i.e. high AOD and decreasing AOD), we found that the  $|S_{CER}|S_{CER}$  in the second LWP  
593 regime is significantly larger than that in first LWP regime except for the study area of  $10^\circ \times 10^\circ$  for buffer  
594 size  $>100$  m, where  $S_{CER}$  curves corresponding to different study areas show greater dispersion. This  
595 pattern highlights the dominant role of LWP in regulating aerosol-cloud interaction sensitivity, with AOD  
596 variations further modulating the magnitude of such differences. Sample sizes of CER and AOD for the  
597 first LWP regime across both study periods, all buffer sizes and study areas, are presented in Supplement  
598 Tables S3–S6.



601 **Figure 5.** Variation of  $SCER$  (top) and correlation coefficient  $R$  (bottom) with buffer size for different study areas (see legend [below the figures at the bottom](#)) for (a) the LWP regime with  $0 < LWP \leq 55$   $g/m^2$  over the years  
602 of 2008-2014 and (b) the LWP regime with  $0 < LWP \leq 50$   $g/m^2$  over the years of 2015-2022. **Solid-Filled** squares  
603 indicate that the results are significant at the 0.01 level and **hollow-open** squares indicate that the results are  
604 not statistically significant. The red solid squares indicate the optimal buffer sizes for each study area, as  
605 shown in the [Supplement-Table Sx, Table A1.](#)  
606  
607

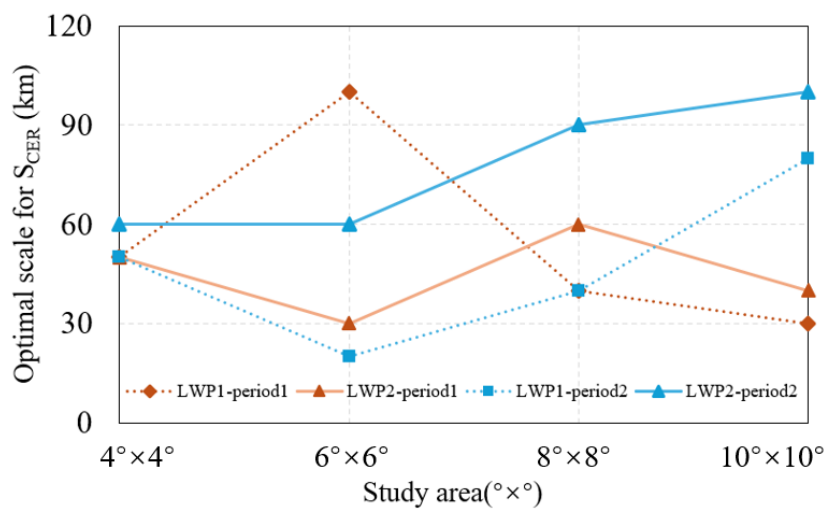
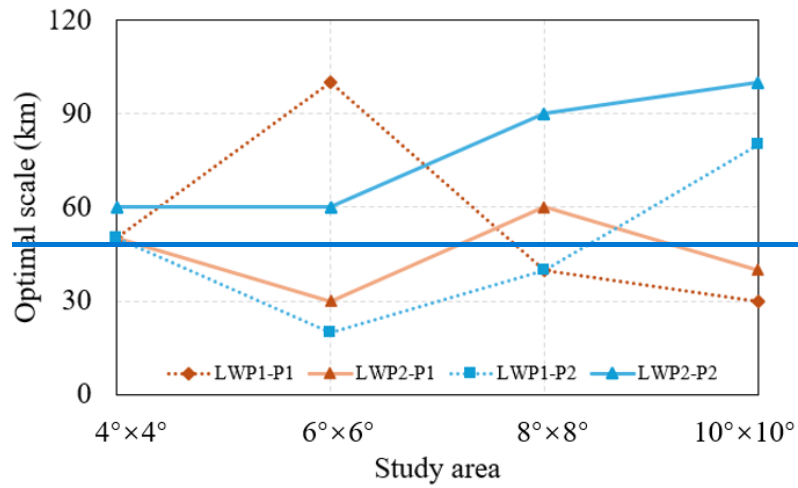
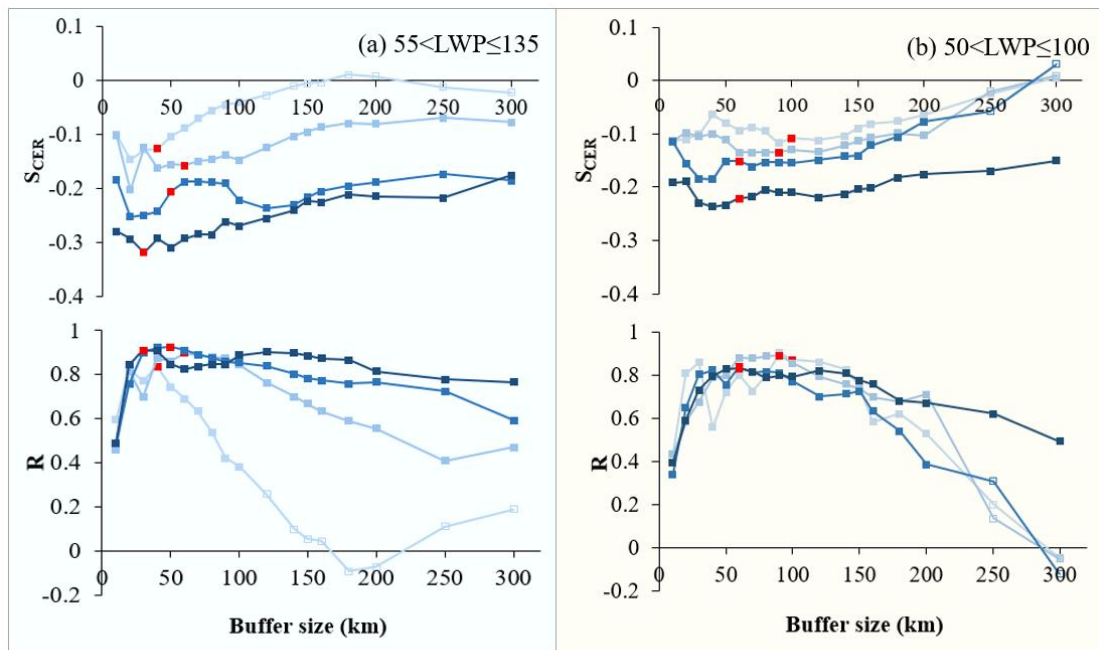


Figure 6. Relationship between optimal scale for  $S_{CER}$  and the size of the study area. Here LWP1-period1 and LWP2-period1 indicate the optimal scale in period 2008-2014 for the first LWP regime and that for the second LWP regime, respectively. LWP1-period2 and LWP2-period2 indicate the optimal scale in period 2015-2022 for the first LWP regime and that for the second LWP regime, respectively.



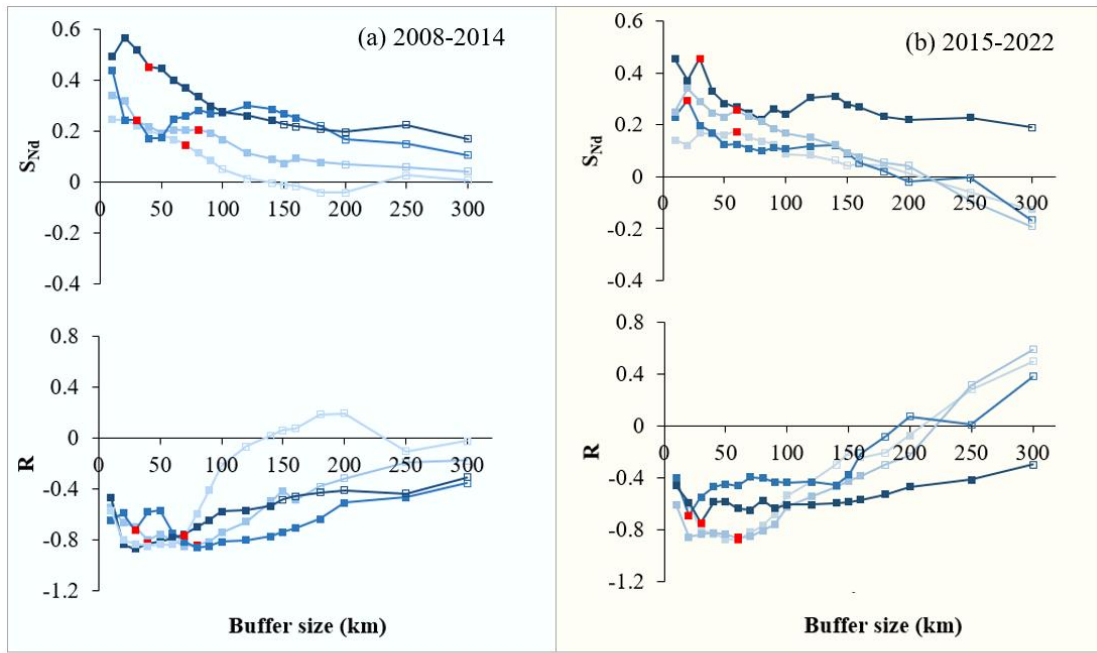
Study area       $10^{\circ} \times 10^{\circ}$        $8^{\circ} \times 8^{\circ}$        $6^{\circ} \times 6^{\circ}$        $4^{\circ} \times 4^{\circ}$

615  
616 **Figure 7.** Variation of  $S_{CER}$  (top) and correlation coefficient  $R$  (bottom) with buffer size for different study  
617 areas (see legend [below the figures at the bottom](#)) for (a) the LWP regime with  $55 < LWP \leq 135$   $g/m^2$  over the  
618 years of 2008-2014 and (b) the LWP regime with  $50 < LWP \leq 100$   $g/m^2$  over the years of 2015-2022. The **solid**  
619 **filled squares** indicates that the results are significant at the 0.01 level and the **hollow-open squares** indicates  
620 that the results are not statistically significant. The red solid squares indicate the optimal buffer sizes for each  
621 study area, as shown in [the Supplement Supplement Table Sx, Table A1](#).

### 622 3.3 Sensitivity of $N_d$ to AOD

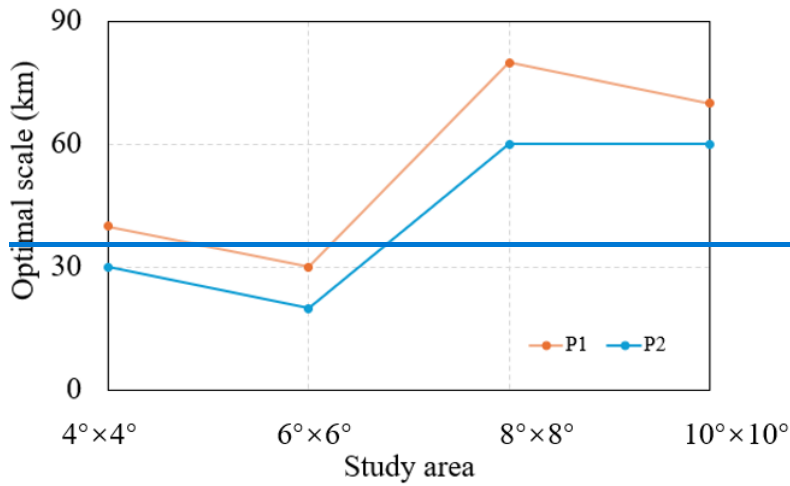
623 Eq. (2) shows that the value of the sensitivity of  $N_d$  to AOD is determined by the slope of a linear fit to a  
624 log-log plot of  $N_d$  versus AOD. To investigate  $S_{N_d}$ , we used correlated data pairs for each of the 7 years  
625 during periods 1 and 2, binned the data in AOD intervals with a bin width of 0.02, and the  $N_d$  data in  
626 each AOD bin were averaged. The variation of  $S_{N_d}$  with buffer size for different study areas over the  
627 target region is presented in Figure 8, for both periods. The data in Figure 8 show that, in contrast to  $S_{CER}$ ,  
628  $S_{N_d}$  is predominantly positive ( $p < 0.01$ ) during both periods, and decreases with increasing buffer size,  
629 **except for the smallest study area during Period 1 and for spatial extends up to 30 km in period 2, when**  
630  **$S_{N_d}$  may initially increase or vary.** During **P**period 1, for the study area of  $6^{\circ} \times 6^{\circ}$ , the  $S_{N_d}$  initially decreases  
631 very fast to a minimum at a buffer size of 40 to 50 km, followed by an increase to a maximum at a buffer  
632 size of 120 km. For buffer size  $\geq 120$  km, the  $S_{N_d}$  values are similar for the two smallest study areas and  
633 substantially larger than for the two larger study areas. During period 2, we can see an initial increase of  
634  $S_{N_d}$  for the study area of  $6^{\circ} \times 6^{\circ}$  and  $8^{\circ} \times 8^{\circ}$ , and variation of  $S_{N_d}$  for the study area of  $10^{\circ} \times 10^{\circ}$  and  $4^{\circ} \times 4^{\circ}$ .

635 After that, the  $S_{Nd}$  for the study area of  $4^\circ \times 4^\circ$  and  $6^\circ \times 6^\circ$  decreases very fast to a minimum for a buffer  
636 size of 80 km, followed by an increase to a maximum for a buffer size of 140 km. The variation of R  
637 with buffer size for each of the two periods shows that the optimal buffer sizes are larger when the study  
638 area is larger, i.e., in the study areas of  $8^\circ \times 8^\circ$  and  $10^\circ \times 10^\circ$  they are larger than in the smaller study areas  
639 of, i.e.,  $4^\circ \times 4^\circ$  and  $6^\circ \times 6^\circ$  (Figure 9). Specifically, these optimal sizes in the  $8^\circ \times 8^\circ$  and  $10^\circ \times 10^\circ$  study  
640 areas are larger than those in the  $4^\circ \times 4^\circ$  and  $6^\circ \times 6^\circ$  areas (Figure 9), reflecting different characteristics in  
641 aerosol-cloud interactions in different AOD conditions. The estimates of  $S_{Nd}$  and correlation coefficients  
642 R between  $N_d$  and AOD, stratified by optimal buffer size, for study areas ranging from  $4^\circ \times 4^\circ$  to  $10^\circ \times 10^\circ$   
643 during the ~~2015–2022~~two periods are presented in the Supplement Table Sx, TableA2. It is noted that  
644  $S_{CER}$  and  $N_d$  exhibit distinct anomalies in large buffer zones, which may be associated with key factors  
645 including aerosol distribution, meteorological heterogeneity, cloud type transitions, and satellite retrieval  
646 limitations.  
647 Notably, the chemical composition of aerosols, which directly affects AOD and CCN activation  
648 efficiency, underwent significant changes between the two periods due to policy interventions. During  
649 2008–2014, aerosols over eastern China were dominated by sulfate, which accounted for 30%–40% of  
650 the  $PM_{2.5}$  mass (Huang et al., 2014; Zheng et al., 2018). Given the strong hygroscopicity of sulfate-  
651 dominated aerosols (Zhang et al., 2012; Liu et al., 2023), their CCN activation efficiency was likely to  
652 remain at a high level, which may have provided a critical physical basis for the aerosol-cloud indirect  
653 effect (Lee et al., 2009). In the period of 2015–2022, driven by policies such as the Air Pollution  
654 Prevention and Control Action Plan (Zheng et al., 2018), the chemical composition of aerosols underwent  
655 a structural transition. Specifically, the mass fraction of sulfate dropped sharply to 15%–25% with an  
656 absolute concentration reduction of more than 50%, while the relative proportions of nitrate,  
657 carbonaceous aerosols (i.e., organic carbon (OC) and black carbon (BC)), and secondary organic aerosols  
658 (SOA) showed an increasing trend (Huang et al., 2014; Zheng et al., 2018). As these components  
659 generally exhibit weaker hygroscopicity compared with sulfate (Zhang et al., 2012; Liu et al., 2023),  
660 such a compositional shift might have led to a decrease in CCN activation efficiency under the same  
661 AOD conditions, thereby potentially weakening the sensitivity of cloud droplet number concentration to  
662 AOD and altering the intensity and mode of aerosol-cloud interactions to a certain extent (Lee et al.,  
663 2009).

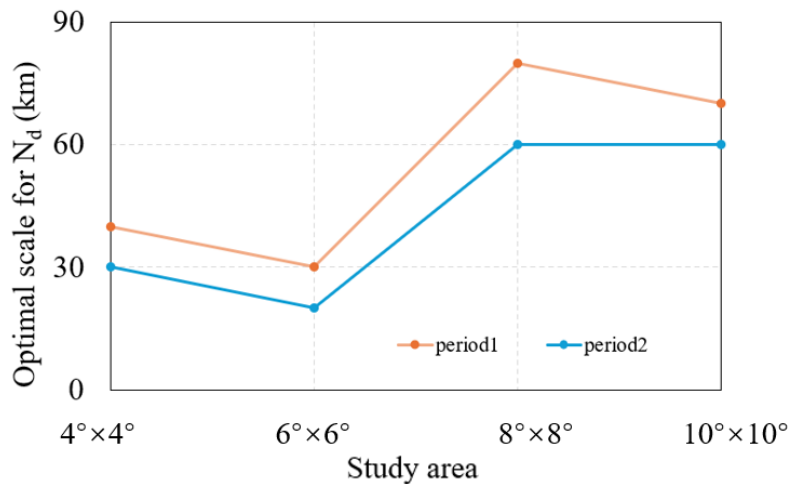


Study area  $10^\circ \times 10^\circ$   $8^\circ \times 8^\circ$   $6^\circ \times 6^\circ$   $4^\circ \times 4^\circ$

664  
 665 **Figure 8.** Variation of  $S_{Nd}$  (top) and correlation coefficient  $R$  (bottom) with buffer size for different study  
 666 areas (see legend [below the figures at the bottom](#)) for the LWP regime with  $0 < LWP \leq 200$  g/m<sup>2</sup> over the  
 667 years of 2008-2014 (a) and 2015-2022 (b). The [filled solid squares](#) indicates that the results are significant  
 668 at the 0.01 level and the [hollow open squares](#) indicates that the results are not statistically significant.  
 669 The red solid square indicates the optimal buffer size for each study area, as shown in [the Supplement](#)  
 670 [Table S Appendix A Supplement, Table 2](#).



671



672  
673 **Figure 9. Relationship between optimal scale for  $N_d$  and the size of the study area. Here [period1](#) and**  
674 **[period2](#) indicate the optimal scale in period 2008-2014 and the optimal scale in period 2015-2022,**  
675 **respectively.**

## 676 4 Discussion

### 677 4.1 The importance of [liquid water path](#) constraint

678 LWP is a critical parameter governing cloud radiative properties (Murray-Watson et al., 2022). The  
679 quantification of albedo effects strongly depends on the spatial scale and the LWP. Neglecting LWP  
680 constraints in aerosol-cloud interaction studies can weaken microphysical signals, leading to  
681 underestimation of radiative forcing (McComiskey et al., 2012). To address this, we first systematically  
682 investigated the dynamic relationship between CER and LWP before analyzing CER sensitivity to AOD.  
683 The results demonstrate pronounced CER sensitivity to LWP variations, which can be categorized into  
684 three distinct [regimes-phases](#) (Figure 4):

685 ~~At-In the small~~ the first LWP regime, CER increases rapidly with LWP, ~~i.e. where the CER~~ evolution of  
686 ~~CER~~ is predominantly driven by ~~changes in~~ LWP ~~changes~~. This dominance may lead to overestimation  
687 of the influence of the AOD on CER (Liu et al., 2021).

688 ~~At-In the the intermediate~~ second LWP regime, CER decreases with increasing LWP. ~~During-In~~ this  
689 regime, the regulatory effect of LWP on CER weakens significantly, and CER variations become  
690 increasingly governed by aerosol-related processes, indicating the growing dominance of aerosol indirect  
691 effects.

692 The third regime contains an insufficient number of CER observations to yield statistically significant  
693 results, ~~which excluding~~ ~~excludes the~~ analysis of the sensitivity of CER to AOD ~~during this regime~~.

694 Comparative analysis of scale-conditioned  $S_{CER}$  across LWP regimes in periods 1 and 2 revealed  
695 markedly enhanced sensitivity of  $S_{CER}$  to AOD ~~during in the second~~ LWP regime-2. There is a trade-off  
696 between AOD and LWP when the amount of water vapor is insufficient and CER becomes smaller. As  
697 suggested by Costantino et al. (2013), the LWP response to aerosol invigoration is influenced by two  
698 competing mechanisms: a drying effect caused by enhanced entrainment of dry air at cloud top (dominant  
699 in optically thin clouds) and a moistening effect from precipitation suppression (dominant in optically  
700 thick clouds). ~~When For larger~~ LWP is larger, the supply of cloud water is sufficient, and the increase in  
701 aerosol number concentrations significantly affects the distribution of cloud droplet number  
702 concentrations and sizes, enhancing the sensitivity of CER to AOD. ~~With reduced~~ For small aerosol  
703 concentrations, the values of  $|S_{CER}|S_{CER}$  (Figure 5b, 7b) ~~exhibited an overall increased~~ decreased overall  
704 with expanding buffer size within the same study area. ~~At a~~ For fixed buffer size,  $|S_{CER}|S_{CER}$   
705 ~~rose~~ increased decreased as the study area increased, and the ranges of  $|S_{CER}|S_{CER}$  values across different  
706 study area ranges showed a convergent pattern, typically remaining small (close to zero). During the high  
707 AOD period (2008–2014), industrial anthropogenic emissions and dust transport provided abundant CCN,  
708 laying the material foundation for aerosol-cloud interactions. This enhanced the synergistic effect of  
709 “sufficient liquid water + abundant CCN” in the second LWP regime, amplifying the difference in  $S_{CER}$   
710 between the two LWP regimes. In the period of decreasing AOD (2015–2022), following the  
711 implementation of clean air policies (de Leeuw et al., 2021; 2023), CCN concentration decreased; (Wang  
712 et al., 2023), weakening the direct impact of aerosols on CER. However, the LWP-driven microphysical  
713 differences persisted, so  $S_{CER}$  in the second regime remained significantly smaller than that in the first  
714 regime, albeit with a reduced magnitude of smaller difference. Additionally, the complexity of aerosol  
715 types during the high AOD period (e.g., mixing of anthropogenic pollutants and natural dust) may have  
716 slightly adjusted the value of  $S_{CER}$ , but did not alter the dominant role of LWP. This aligns with the theory  
717 that “aerosol indirect effects are jointly regulated by concentration and type” (Liu et al., 202417).  
718 The larger  $S_{CER}$  observed at larger spatial scales (Figures 5 and 7) may be attributed to meteorological  
719 confounding effects. The smaller  $S_{CER}$  in the larger scale indicates that  $S_{CER}$  becomes smaller may be due  
720 to meteorological confounding effects. In addition, clouds with larger LWP are usually associated with  
721 strong updrafts (such as convective clouds), and stronger turbulence and vertical transport will bring  
722 more aerosols into the clouds, increasing CCN concentration and a decrease in particle size, making them

723 more sensitive to changes in AOD ([Jones et al., 2009](#); [Han et al., 2022](#); [Fan et al., 2025](#)). Therefore, this  
724 phenomenon is the result of the combined action of cloud microphysical processes (CCN activation,  
725 cloud droplet competition growth) and dynamic processes (updrafts, turbulent mixing). If the  
726 characteristics of aerosols (~~such as composition~~) change in the second LWP regime (~~such as composition~~)  
727 change, this sensitivity may be further amplified. Consequently, the ~~LWP LWP~~-stratified  $S_{CER}$   
728 quantification ~~framework~~ framework enables precise characterization of scale-dependent aerosol-cloud  
729 interactions, providing robust physical insights for climate effect assessments and effectively reducing  
730 uncertainties in future climate projections.

731 The central hypothesis of this study—that LWP is relatively consistent between the two periods (2008–  
732 2014 and 2015–2022), supporting valid comparisons of the spatial sensitivity of AOD-CER  
733 relationships—is well-supported by the following analysis. The differences in the mean, median, 25th,  
734 and 50th percentiles of LWP between the two periods are all less than 5%, indicating a stable overall  
735 water vapor supply level. The spatial patterns of high-LWP regions (e.g., southeastern areas) and low-  
736 LWP regions (e.g., the mountainous areas in northern Shanxi) remained stable across the two periods  
737 (see Supplement Figure S1), demonstrating LWP spatial distribution characteristics are highly consistent.  
738 The sample proportions of LWP in the rapid growth regime are 59.30% (pPeriod 1: 0–55 g/m<sup>2</sup>) and 55.36%  
739 (pPeriod 2: 0–50 g/m<sup>2</sup>), while those in the decreasing regime are 29.64% (pPeriod 1: 55–135 g/m<sup>2</sup>) and  
740 24.59% (pPeriod 2: 50–100 g/m<sup>2</sup>), suggesting that there is no systematic temporal shift in the LWP  
741 probability distribution. Meanwhile, short-term fluctuations are smoothed by multi-year averaging and  
742 large-sample statistics, resulting in a weak indirect impact of aerosols on LWP (LWP only increased by  
743 5.6%, much smaller than the 24% decrease in AOD). Additionally, LWP-stratified analysis further  
744 isolates interference. The validation of the core hypothesis provides a reliable premise for accurately  
745 quantifying the impact of aerosol concentration changes on the sensitivity of cloud parameters and their  
746 spatial scale dependence.

#### 747 **4.2 Scale ~~effect~~ dependence of ~~sensitivity of~~ cloud parameters sensitivities to aerosol variations**

748 Extensive studies have demonstrated a significant spatial scale dependence ~~in~~ of aerosol indirect effects<sub>s</sub>  
749 (McComiskey et al., 2012; Possner et al., 2016; Glotfelty et al., 2020; Ekman et al., 2023). Failure to  
750 explicitly define the scale-dependent behavior of aerosol indirect effects<sub>s</sub> may introduce systematic biases

751 and inconsistencies in subsequent process analyses. Based on satellite observations, this study confirms  
752 statistically significant negative correlations between CER and AOD, as well as positive correlations  
753 between  $N_d$  and AOD during ~~both~~ periods with different aerosol concentrations, aligning with classical  
754 aerosol-cloud interaction theory (Quaas et al., 2009). Analysis of scale-conditioned  $S_{CER}$  and  $S_{N_d}$  reveals  
755 that for fixed buffer size, an increase in the size of the study area leads to a systematic reduction in  $S_{CER}$   
756 (less negative) and  $S_{N_d}$ , corroborating the nonlinear attenuation of aerosol signals with spatial domain  
757 expansion (Quaas et al., 2009). The results from this study ~~verifies-suggest~~ that AOD-cloud property  
758 correlations ~~at-in~~ large study areas are susceptible to meteorological confounding effects (Quaas et al.,  
759 2010; Boucher and Quaas, 2012; Gryspeerd et al., 2014; Liu et al., 2024). Theoretically, aerosol  
760 regulation of cloud microphysics is strongly local: smaller domains (e.g.,  $4^\circ \times 4^\circ$ ) feature homogeneous  
761 meteorological conditions (humidity, updrafts), preserving undiluted aerosol-cloud interaction signals  
762 and yielding larger  $|S_{CER}|$  (pronounced Twomey effect). In contrast, expanded domains (e.g.,  $10^\circ \times 10^\circ$ )  
763 encompass heterogeneous meteorological ~~processes~~conditions (circulation differences, boundary layer  
764 variability) that independently modulate cloud droplet growth. For example, strong updrafts enhance  
765 liquid water supply, offsetting aerosol-induced radius reduction (Altaratz et al., 2014), weakening  
766 aerosol-CER correlations and reducing  $|S_{CER}|$ . Consistent with Grandey & Stier (2010), large-scale  
767 domains introduce “dilution bias” via non-target meteorological variability. This scale-dependent  
768 confounding mechanism elucidates uncertainties in aerosol indirect effect assessments at regional scales.  
769 Multi-scale spatial analysis identifies different optimal buffer sizes for  $S_{CER}$  and  $S_{N_d}$  in different periods.  
770 These findings align closely with satellite-based aerosol indirect effect studies (Wang et al., 2015; Liu et  
771 al., 2017), providing critical scale benchmarks for satellite product validation. Wang et al. (2015)  
772 ~~reported~~revealed an inverse “Twomey” effect between aerosols and CER in eastern China by analyzing  
773 aerosol and CER within a 50 km buffer zone around CALIOP samples. Similarly, Liu et al. (2017)  
774 systematically examined the response mechanisms of warm cloud macro- and microphysical parameters  
775 to increasing AOD in the Yangtze River Delta region, also using CALIOP samples within a 50 km buffer  
776 zone. ~~Present~~The study further ~~reveals~~shows that, ~~as under~~ decreasing aerosol concentrations decrease,  
777  $S_{CER}$  values across different study areas ~~at-with~~ the same buffer size exhibit convergence characteristics,  
778 with generally smaller  $S_{CER}$  (closer to zero). This indicates a significant weakening of aerosol-cloud  
779 interaction intensity and reduced spatial extent dependency ~~under-in~~ low aerosol loading conditions. This

780 phenomenon is consistent with the simulated behavior of aerosol-limited cloud regimes, where aerosol-  
781 cloud interactions are quantitatively modulated by moisture availability and lose their sensitivity to large-  
782 scale dynamical stability, leading to a weaker and more homogeneous effect (Zhao et al., 2025). Notably,  
783 ~~These findings mechanistically align with the conclusion of Ma et al. (2015) that spatially aggregated~~  
784 ~~pollutant emissions at higher resolutions amplify aerosol effects, demonstrating a nonlinear coupling~~  
785 ~~between the spatial resolution dependency of aerosol effects and their concentration gradients.~~

786 By systematically quantifying the scale-response characteristics of aerosol indirect effects, this work not  
787 only elucidates the dynamic scale behavior of aerosol-cloud interactions but, more critically, establishes  
788 criteria for determining optimal buffer size in regional aerosol indirect effect studies. Such advancements  
789 provide actionable insights for refining parameterization schemes in climate models, thereby enhancing  
790 their predictive reliability.

### 791 **4.3 Contrasting sensitivity patterns of cloud parameters in response to AOD**

792 A comprehensive comparison of the sensitivity  $S_{CER}$  and  $S_{Nd}$  reveals that the responses of CER and  $N_d$  to  
793 AOD exhibit distinct yet inherently interconnected characteristics. These characteristics are jointly  
794 modulated by spatial scale and LWP regimes (Figs. 5, 7, 8; ~~Supplementary Tables~~SupplementsAppendix  
795 1–2), which profoundly reflect the core microphysical mechanisms of aerosol-cloud interactions. Details  
796 are elaborated as follows:

#### 797 **4.3.1 Core differences in response modes between $S_{CER}$ and $N_d$ to AOD**

798  $S_{CER}$  is consistently negative across both periods and all LWP regimes ( $-0.33 < S_{CER} < 0$ ) (Figs. 5, 7;  
799 Supplement 1), indicating that an increase in AOD leads to a decrease in CER. This aligns with the core  
800 principle of the Twomey effect (Twomey, 1977; Feingold et al., 2001). The values of  $|S_{CER}|$  are larger in  
801 the second LWP regime than in the first regime, reflecting stronger aerosol modulation of cloud  
802 microphysical properties when liquid water is abundant (McComiskey & Feingold, 2012). In contrast,  
803  $S_{Nd}$  maintains a significant positive correlation with AOD across all scenarios ( $0 < S_{Nd} < 1$ ) (Fig. 8;  
804 Supplement 2), confirming that higher AOD directly promotes CCN activation and thereby increases  
805 cloud droplet number concentration (Andreae, 2009).  $S_{Nd}$  is larger in small-scale study areas (e.g.,  $4^\circ \times 4^\circ$ )  
806 and small buffer zones, with a maximum value of 0.45 in the first period, indicating greater sensitivity

807 of cloud droplet number to aerosol loading at fine spatial scales.~~larger~~

### 808 4.3.2 Synergistic modulation of AOD and spatial scale

809 Using the LWP interval corresponding to  $S_{Nd}$  ( $0 < LWP \leq 200 \text{ g/m}^2$ ) as ~~the~~ benchmark, comparisons  
810 between the two periods (incorporating average values of  $S_{CER}$  across two LWP regimes) reveal distinct  
811 characteristics:

812 For the small-scale study area ( $4^\circ \times 4^\circ$ ): In period 1, the average  $|S_{CER}|$  across two LWP regimes is 0.271  
813 ( $-0.2232$  for the  $0\text{--}55 \text{ g/m}^2$  LWP regime,  $-0.3189$  for the  $55\text{--}135 \text{ g/m}^2$  LWP regime) and  $S_{Nd}=0.4496$ ,  
814 both significantly higher than those in period 2 (average  $|S_{CER}|=0.154$ , with  $-0.0863$  for  $0\text{--}50 \text{ g/m}^2$  LWP  
815 regime and  $-0.2212$  for  $50\text{--}100 \text{ g/m}^2$  LWP regime;  $S_{Nd}=0.2903$ ). The negative correlation between AOD  
816 and CER is more significant in period 1, as sufficient CCN in small-scale areas amplifies both cloud  
817 droplet number increase and size reduction, enhancing the Twomey effect.

818 For the medium-to-large scale study areas ( $6^\circ \times 6^\circ$ ,  $8^\circ \times 8^\circ$ ,  $10^\circ \times 10^\circ$ ): In period 1, the average  $|S_{CER}|$  across  
819 two LWP regimes is 0.1683 ( $-0.1305$  for  $0\text{--}55 \text{ g/m}^2$ ,  $-0.2061$  for  $55\text{--}135 \text{ g/m}^2$ ), 0.13065 ( $-0.1026$  for  $0\text{--}$   
820  $55 \text{ g/m}^2$ ,  $-0.1587$  for  $55\text{--}135 \text{ g/m}^2$ ), and 0.1067 ( $-0.0858$  for  $0\text{--}55 \text{ g/m}^2$ ,  $-0.0885$  for  $55\text{--}135 \text{ g/m}^2$ ),  
821 respectively, all higher than the corresponding values in period 2 (0.1516, 0.1246, 0.0985). However,  $S_{Nd}$   
822 in period 1 (0.2430, 0.2050, 0.1430) is lower than that in period 2 (0.2960, 0.2680, 0.1740), with no  
823 significant difference in the negative correlation between AOD and CER between the two periods.

824 This characteristic indicates that meteorological confounding effects are enhanced at larger scales,  
825 weakening the regulation of  $S_{Nd}$  by aerosols, while at small scales the ~~aci~~ is ~~remain~~ directly driven by  
826 AOD levels.

### 827 4.3.3 Implications for aerosol indirect effects

828 The differences and interconnections between  $S_{CER}$  and  $S_{Nd}$  highlight that aerosol indirect effects are  
829 dominated by coupled microphysical processes: Aerosol-induced increases in CCN first enhance  $N_d$   
830 through positive  $S_{Nd}$ , and then reduce CER through negative  $S_{CER}$  under constant LWP conditions. The  
831 scale-dependent attenuation of both sensitivities and their modulation by LWP indicate that quantifying  
832 aerosol indirect effects requires full consideration of spatial scales and the key role of liquid water,  
833 providing observational basis for optimizing climate model parameterization schemes.

#### 834 **4.3.4 Limitations and ~~implications~~future perspectives**

835 This study has three significant limitations. Firstly, similar to most previous studies (Wang et al., 2015;  
836 Liu et al., 2021), this study only utilized MODIS data with a resolution of 10 km to explore scale effects,  
837 ignoring finer or coarser resolution data. Therefore, using a 10 km buffer size as the minimum  
838 observation unit, this limitation makes the indirect effects of aerosols on smaller scales still unknown,  
839 which may lead to inaccurate evaluation of aerosol indirect effects. Therefore, future research can  
840 improve the sensitivity of aerosol indirect effects to scale changes by using observation data with higher  
841 accuracy or model simulations. Secondly, the current research focuses on the influence of buffer size and  
842 study areas, the potential impact of spatial aggregation methods (especially zoning directionality) on the  
843 quantitative results of aerosol indirect effects has not been systematically evaluated. Future research  
844 should further investigate the sensitivity of aerosol indirect effects to zoning direction. Moreover, the  
845 current study employs a uniform buffer size for both aerosol and cloud parameters, failing to account for  
846 potential interaction effects arising from discrepancies of buffer size between them. Therefore, clarifying  
847 scale dependence will avoid directly extrapolating local observation results to a larger study area when  
848 downscaling climate models or formulating regional environmental policies.

#### 849 **5 Conclusions**

850 Based on MODIS and CALIOPS satellite observations of aerosol and cloud parameters over land in  
851 eastern China, ~~this study conducted~~ a comparative analysis was conducted of the sensitivity of cloud  
852 microphysical parameters (CER and  $N_d$ ) to variations in AOD during two characteristic periods: 2008–  
853 2014 (period 1, high AOD) and 2015–2022 (period 2, decreasing AOD).~~period 1 (2008–2014) and period~~  
854 2 (2015–2022). Through systematic analysis of the relationship between CER and LWP and their response  
855 mechanisms to AOD across these two periods, the following key conclusions were drawn:

856 Firstly, CER exhibited three distinct ~~regimes~~ phases with varying LWP. During the rapid growth regime  
857 ( $LWP < 55/50 \text{ g/m}^2$ ), CER showed significant negative sensitivity to AOD ( $S_{CER}$ ), consistent with the  
858 Twomey effect; during the ~~decreasing~~ liming regime ( $LWP = 55\text{--}135/50\text{--}100 \text{ g/m}^2$ ),  $S_{CER}$  remained  
859 negative but with enhanced sensitivity; and during the slow growth regime ( $LWP > 135/100 \text{ g/m}^2$ ), the  
860 rate of CER change significantly decreased. These findings confirmed that LWP is a crucial regulatory  
861 factor influencing the CER response to AOD.

862 Secondly, scale dependence analysis ~~revealed~~ led to the conclusion significant scale dependent that  
863 characteristics in aerosol-cloud interaction are significantly scale-dependent, with systematic variations  
864 of both  $S_{CER}$  and  $S_{Nd}$  exhibiting systematic variations with changes in buffer size and study area. The  
865 results of the study show~~ed~~ that  $S_{CER}$  systematically ~~decreases~~ increased as buffer size ~~increases~~ increased  
866 and ~~becomes~~ became negligible for buffer sizes larger than 150-200 km, while the optimal buffer sizes  
867 varied~~y~~ substantially with the size of the study area in the range from  $6^{\circ} \times 6^{\circ}$  to  $10^{\circ} \times 10^{\circ}$ : ~~increasing~~  
868 increased as study area ~~increases~~ increased during period 2, but ~~decreasing~~ decreased in period 1 for  
869 regime 2. Particularly noteworthy ~~is~~ was the enhanced consistency of  $S_{CER}$  across different study areas  
870 and the significantly ~~decreased~~ increased in  $S_{CER}$  during period 2, reflecting weaker aerosol-cloud  
871 interactions due to declining regional aerosol concentrations.

872 Finally, the sensitivity of  $N_d$  to AOD ( $S_{Nd}$ ) exhibited distinct characteristics compared to  $S_{CER}$ :  $S_{Nd}$  showed  
873 a significant positive correlation ( $p < 0.01$ ) and demonstrated nonlinear attenuation with increasing buffer  
874 size and study area. The optimal buffer size for  $S_{Nd}$  was smaller during period 2 than during period 1 and  
875 increased with the study area size, being substantially larger for study areas of  $8^{\circ} \times 8^{\circ}$  and  $10^{\circ} \times 10^{\circ}$  than  
876 for study areas of  $4^{\circ} \times 4^{\circ}$  and  $6^{\circ} \times 6^{\circ}$  areas. These findings not only deepen our understanding of aerosol  
877 indirect effects but also provide an important observational basis for improving aerosol-cloud  
878 parameterization schemes in climate models. The results emphasize that both the phased characteristics  
879 of LWP and spatial scale effects must be considered when assessing aerosol indirect effects.

#### 880 **Data availability**

881 All data used in this study are publicly available. The satellite data from the MODIS instrument used in  
882 this study were obtained from <https://ladsweb.nascom.nasa.gov/search/> (last access: 02 July 2025). The  
883 satellite data from CALIOP were obtained from <https://subset.larc.nasa.gov/calipso/login.php> (last  
884 access: 02 July 2025).

#### 885 **Author contributions**

886 YL, LT and GL designed the research. YL and LT led the analyses. YL and GL wrote the manuscript  
887 with major input from JH, and further input from all other authors. All authors contributed to interpreting  
888 the results and to the finalization and revision of the manuscript.

889 **Competing interests**

890 The authors declare that they have no conflict of interest.

891 **Acknowledgements**

892 The authors greatly appreciate NASA CloudSat Data Processing Center that provided the data used in  
893 this study. This work was supported by the National Natural Science Foundation of China (Grant No.  
894 42001290), the National Natural Science Foundation of China (Grant No. 42271299), ~~and~~ the Natural  
895 Science Foundation Project of Xiamen (Grant No. 3502Z202472037) ~~and~~. ~~Gerrit de Leeuw is supported~~  
896 ~~by~~ the [Chinese Academy of Sciences President's International Fellowship Initiative, Grant No.](#)  
897 [2025PVA0014\\_Y1](#) ~~Chinese Academy of Sciences President's International Fellowship Initiative. Grant~~  
898 ~~No. 2025PVA0014.~~

899 **References**

- 900 Albrecht, B. A.: Aerosols, cloud microphysics, and fractional cloudiness, *Science*, 245, 1227-1230, 1989.
- 901 Bellouin, N., Quaas, J., Gryspeerdt, E., Kinne, S., Stier, P., Watson-Parris, D., et al.: Bounding global  
902 aerosol radiative forcing of climate change. *Reviews of Geophysics*, 58, e2019RG000660.  
903 <https://doi.org/10.1029/2019RG000660>, 2020.
- 904 Altaratz, O., Koren, I., Remer, L.A., Hirsch, E.: Review: Cloud invigoration by aerosols—Coupling  
905 between microphysics and dynamics. *Atmospheric Research*, 140-141, 38-60, 2014.
- 906 Andreae, M. O.: Correlation between cloud condensation nuclei concentration and aerosol optical  
907 thickness in remote and polluted regions, *Atmos. Chem. Phys.*, 9, 543-556, [https://doi.org/10.5194/acp-](https://doi.org/10.5194/acp-9-543-2009)  
908 [9-543-2009](https://doi.org/10.5194/acp-9-543-2009), 2009.
- 909
- 910 [Baum, B. A., et al.: MODIS cloud-top property refinement for Collection 6, \*J. Appl. Meteorol. Climatol.\*,](#)  
911 [51\(6\), 1145-1163, 2012.](#)
- 912 Bender, F.A.M., Frey, L., McCoy, D.T., Grosvenor, D.P., Mohrmann, J.K.: Assessment of aerosol–  
913 cloud–radiation correlations in satellite observations, climate models and reanalysis. *Climate Dynamics*,  
914 52, 4371-4392, 2019.

915 Boucher, O., Quaas, J.: Water vapour affects both rain and aerosol optical depth. *Nature Geoscience*, 6(1),  
916 4-5. <https://doi.org/10.1038/ngeo1692>, 2012.

917 Bréon, F. M., Tanré, D., Generoso, S.: Aerosol effect on cloud droplet size monitored from satellite,  
918 *Science*, 295(5556):834-8. doi: 10.1126/science.1066434, 2002.

919 Bulgin, C. E., Palmer, P.I., Thomas, G.E., Arnold, C.P.G., Campmany, E., Carboni, E., Grainger, R. G.,  
920 Poulsen, C., Siddans, R., Lawrence, B.N.: Regional and seasonal variations of the Twomey indirect effect  
921 as observed by the ATSR-2 satellite instrument, *Geophysical Research Letters*, 35, 2, 2008.

922 [Cai, H., Yang, Y., Chen, Q.: Distribution Characteristics of Cloud Types and Cloud Phases over China  
923 and Their Relationship with Cloud Temperature, \*Remote Sensing\*, 14\(21\), 2022.  
924 <https://doi.org/10.3390/rs14215601>](#)

925 Chen, G., W.-C.Wang, and J.-P. Chen, 2015: Aerosol–stratocumulus–radiation interactions over  
926 southeast Pacific. *J. Atmos. Sci.*, 72, 2612–2621, <https://doi.org/10.1175/JAS-D-14-0319.1>.

927 Chen, Y.-C., Christensen, M. W., Stephens, G. L., and Seinfeld, J. H.: Satellite-based estimate of global  
928 aerosol-cloud radiative forcing by marine warm clouds, *Nat. Geosci.*, 7, 643–646,  
929 <https://doi.org/10.1038/ngeo2214>, 2014.

930 Christensen, M. W., Chen, Y.-C., and Stephens, G. L.: Aerosol indirect effect dictated by liquid clouds,  
931 *J. Geophys. Res.*, 121, 14636–14650, <https://doi.org/10.1002/2016JD025245>, 2016.

932 Costantino, L. and Bréon, F. M.: Analysis of aerosol-cloud interaction from multi-sensor satellite  
933 observations. *Geophys. Res. Lett.*, 37, L11801, doi:10.1029/2009GL041828, 2010.

934 Costantino, L. and Bréon, F. M.: Aerosol indirect effect on warm clouds over South-East Atlantic, from  
935 co-located MODIS and CALIPSO observations, *Atmos. Chem. Phys.*, 13: 69-88, 2013.

936 [Dagan, G., Yeheskel, N., Williams, A. I. L.: Radiative forcing from aerosol–cloud interactions enhanced  
937 by large-scale circulation adjustments, \*Nature geoscience\*, 16, 1092-1098, 2023.](#)

938 de Leeuw, G., R. van der A, J. Bai, Y. Xue, C. Varotsos, Z. Li, C. Fan, X. Chen, I. Christodoulakis, J.  
939 Ding, X. Hou, G. Kouremadas, D. Li, J. Wang, M. Zara, K. Zhang, Y. Zhang.: Air Quality over China.  
940 *Remote Sens.* 2021, 13, 3542. <https://doi.org/10.3390/rs13173542>, 2021.

941 de Leeuw, G., Fan, C, Li, Z., Dong, J., Li, Y., Ou, Y., and Zhu, S. (2022). Spatiotemporal variation and  
942 provincial scale differences of the AOD across China during 2000–2021. *Atmospheric Pollution  
943 Research* 13 (2022) 101359 (14 pp). <https://doi.org/10.1016/j.apr.2022.101359>.

944 de Leeuw, G., Kang, H., Fan, C., Li, Z., Fang, C., Zhang, Y. (2023). Meteorological and anthropogenic  
945 contributions to changes in the Aerosol Optical Depth (AOD) over China during the last decade. *Atm.*  
946 *Env.*, 301, 119676. <https://doi.org/10.1016/j.atmosenv.2023.119676>.

947 Ekman, A. M. L., Eva Nygren, Alejandro Baró Pérez, Matthias Schwarz, Gunilla Svensson, Nicolas  
948 Bellouin.: Influence of horizontal resolution and complexity of aerosol–cloud interactions on marine  
949 stratocumulus and stratocumulus-to-cumulus transition in HadGEM3-GC3.1, *Quart. J Royal Met Soc.*,  
950 149, 755, 2049-2066, <https://doi.org/10.1002/qj.4494>, 2023.

951 Fan J, Wang Y, Rosenfeld D, et al.: Review of aerosol-cloud interactions: Mechanisms, significance, and  
952 challenges. *Journal of the Atmospheric Sciences*,73(11): 4221-4252, 2016.

953 [Fan, J., Zhang, Y., Li, Z., Yan, H., Prabhakaran, T., Rosenfeld, D., & Khain, A.: Unveiling aerosol](#)  
954 [impacts on deep convective clouds: Scientific concept, modeling, observational analysis, and future](#)  
955 [direction. \*Journal of Geophysical Research: Atmospheres\*, 130, e2024JD041931. \[https://doi.org/10.1029/\]\(https://doi.org/10.1029/2024JD041931\)](#)  
956 [2024JD041931, 2025.](#)

957 Feingold, G., Remer, L. A., Ramaprasad, J., Kaufman, Y. J.: Analysis of smoke impact on clouds in  
958 Brazilian biomass burning regions: an extension of Twomey’s approach, *J. Geophys. Res.*, 106 (D19),  
959 22907-22922, 2001.

960 [Feingold, G. Modeling of the first indirect effect: analysis of measurement requirements. \*Geophys. Res.\*](#)  
961 [Lett., 30, 1997, doi:10.1029/2003GL017967, 2003.](#)

962 Feingold, G., Goren, T., and Yamaguchi, T.: Quantifying albedo susceptibility biases in shallow clouds,  
963 *Atmos. Chem. Phys.*, 22, 3303–3319, <https://doi.org/10.5194/acp-22-3303-2022>, 2022.

964 Grandey, B.S., Stier, P.: A critical look at spatial scale choices in satellite-based aerosol indirect effect  
965 studies. *Atmos. Chem. Phys.*, 10, 11459-11470, 2010.

966 Gryspeerdt, E., Stier, P., and Partridge, D. G.: Satellite observations of cloud regime development: the  
967 role of aerosol processes, *Atmos. Chem. Phys.*, 14, 1141-1158, doi:10.5194/acp-14-1141-2014, 2014.

968 Gryspeerdt, E., Povey, A. C., Grainger, R. G., Hasekamp, O., Hsu, N. C., Mulcahy, J. P., Sayer, A. M.,  
969 and Sorooshian, A.: Uncertainty in aerosol–cloud radiative forcing is driven by clean conditions, *Atmos.*  
970 *Chem. Phys.*, 23, 4115-4122, <https://doi.org/10.5194/acp-23-4115-2023>, 2023.

971 Gryspeerdt, E., McCoy, D. T., Crosbie, E., Moore, R. H., Nott, G. J., Painemal, D., Small-Griswold, J.,  
972 Sorooshian, A., and Ziemba, L.: The impact of sampling strategy on the cloud droplet number

973 concentration estimated from satellite data, *Atmos. Meas. Tech.*, 15, 3875–3892, 2022,  
974 <https://doi.org/10.5194/amt-15-3875-2022>, 2022.

975 Glotfelty, T., Kiran Alapaty, Jian He, Patrick Hawbecker, Xiaoliang Song, and Guang Zhang. Studying  
976 Scale Dependency of Aerosol–Cloud Interactions Using Multiscale Cloud Formulations, 77, 11, 2020.

977 Grosvenor, D. P., Sourdeval, O., Zuidema, P., Ackerman, A., Alexandrov, M. D., Bennartz, R., Boers,  
978 R., Cairns, B., Chiu, J. C., Christensen, M., Deneke, H., Diamond, M., Feingold, G., Fridlind, A.,  
979 Hünerbein, A., Knist, C., Kollias, P., Marshak, A., McCoy, D., Merk, D., Painemal, D., Rausch, J.,  
980 Rosenfeld, D., Russchenberg, H., Seifert, P., Sinclair, K., Stier, P., Diedenhoven, B. V., Wendisch, M.,  
981 Werner, F., Wood, R., Zhang, Z., and Quaas, J.: Remote sensing of droplet number concentration in  
982 warm clouds: A review of the current state of knowledge and perspectives, *Rev. Geophys.*, 56, 409–453,  
983 <https://doi.org/10.1029/2017RG000593>, 2018.

984 [Han, X., Zhao, B., Lin, Y., Chen, Q., Shi, H., Jiang, Z., et al.: Type-dependent impact of aerosols on](#)  
985 [precipitation associated with deep convective cloud over East Asia, \*Journal of Geophysical Research:\*](#)  
986 [\*Atmospheres\*, 127, e2021JD036127. <https://doi.org/10.1029/2021JD036127>, 2022.](#)

987 [Hassan, T., Zhang, K., Li, J., Singh, B., Zhang, S., Wang, H., and Ma, P.: Impacts of spatial heterogeneity](#)  
988 [of anthropogenic aerosol emissions in a regionally refined global aerosol–climate model, \*Geosci. Model\*](#)  
989 [\*Dev.\*, 17, 3507-3532, 2024.](#)

990 [Huang, R. J., Zhang, Y. L., Bozzetti, C., et al. High secondary aerosol contribution to particulate pollution](#)  
991 [during haze events in China, \*Nature\*, 514, 218–222, 2014.](#)

992

993 Jia, H. L., Ma, X. Y., Quaas, J., Yin, Y., Qiu, T.: Is positive correlation between cloud droplet effective  
994 radius and aerosol optical depth over land due to retrieval artifacts or real physical processes?  
995 *Atmospheric Chemistry and Physics*, 19, 13, 8879-8896, 2019.

996 [Jia, H., Quaas, J., Gryspeerdt, E., Böhm, C., & Sourdeval, O.: Addressing the difficulties in quantifying](#)  
997 [droplet number response to aerosol from satellite observations, \*Atmospheric Chemistry and Physics\*,](#)  
998 [22\(11\), 7353–7372. <https://doi.org/10.5194/acp-22-7353-2022>, 2022.](#)

999 Jones, T. A., Christopher, S. A., & Quaas, J.: A six year satellite-based assessment of the regional  
1000 variations in aerosol indirect effects. *Atmospheric Chemistry and Physics*, 9, 4091, 2009.

1001 Koren, I., Kaufman, Y. J., Rosenfeld, D., Remer, L. A., Rudich, Y.: Aerosol invigoration and  
1002 restructuring of Atlantic convective clouds. *Geophys. Res. Lett.*, 32 (14), L14828, 2005.

1003 Kaufman, Y.J. and Fraser, R.S.: The effect of smoke particles on clouds and climate forcing. *Science*,  
1004 1997. 277(5332): p. 1636-1639.

1005 [Kaufman, Y. J., Remer, L., Tanré, D., Li, R., Kleidman, R., Mattoo, S., Levy, R., Eck, T., Holben, B.,](#)  
1006 [Ichoku, C., Martins, J., and Koren, I.: A critical examination of the residual cloud contamination and](#)  
1007 [diurnal sampling effects on MODIS estimates of aerosol over ocean, \*IEEE Trans. Geosci. Remote Sens.\*,](#)  
1008 [43, 2886–2897, 2005.](#)

1009 Kaufman, Y.J., Remer, L.A., Tanré, D., Li, R.R., Kleidman, R., Mattoo, S., Levy, R.C., Eck, T.F., Holben,  
1010 B.N., Ichoku, C., Member, IEEE, Martins, J.V., and Koren, I.: A Critical Examination of the Residual  
1011 Cloud Contamination and Diurnal Sampling Effects on MODIS Estimates of Aerosol Over Ocean, *IEEE*  
1012 *TRANSACTIONS ON GEOSCIENCE AND REMOTE SENSING*, 43, 12, 2005.

1013 Kim, S. W., S. C. Yoon, J. Y. Kim, and S. Y. Kim (2007), Seasonal and monthly variations of columnar  
1014 aerosol optical properties over East Asia determined from multi-year MODIS, LIDAR, and AERONET  
1015 Sun/sky radiometer measurements, *Atmos. Environ.*, 41(8), 1634–1651,  
1016 doi:10.1016/j.atmosenv.2006.10.044.

1017 King, M. D., Tsay, S. C., Platnick, S. E., Wang, M., and Liou, K. N.: Cloud Retrieval Algorithms for  
1018 MODIS: Optical Thickness, Effective Particle Radius, and Thermodynamic Phase, MODIS Algorithm  
1019 Theoretical Basis Document, available at: [http://eosps.nasa.gov/sites/default/files/atbd/atbd\\_mod05.pdf](http://eosps.nasa.gov/sites/default/files/atbd/atbd_mod05.pdf),  
1020 1997.

1021

1022 King, M. D., Menzel, W. P., Kaufman, Y. J., Tanré, D., Gao, B. C., Platnick, S., Ackerman, S. A., Remer,  
1023 L. A., Pincus, R., and Hubanks, P. A.: Cloud and aerosol properties, precipitable water, and profiles of  
1024 temperature and water vapor from MODIS, *IEEE T. Geosci. Remote*, 41, 442–458,  
1025 doi:10.1109/TGRS.2002.808226, 2003.

1026 Lebsock, M., Morrison, H., Gettelman, A.: Microphysical implications of cloud-precipitation covariance  
1027 derived from satellite remote sensing. *Journal of Geophysical Research: Atmosphere*, 118, 6521–6533,  
1028 2013.

1029 [Levy, R. C., Mattoo, S., Munchak, L. A., Remer, L. A., Sayer, A. M., Patadia, F., and Hsu, N. C.: The](#)  
1030 [Collection 6 MODIS aerosol products over land and ocean, \*Atmos. Meas. Tech.\*, 6, 2989-3034,](#)  
1031 <https://doi.org/10.5194/amt-6-2989-2013>, 2013.

1032 Levy, R. C., Remer, L. A., Kleidman, R. G., Mattoo, S., Ichoku, C., Kahn, R., and Eck, T. F.: Global  
1033 evaluation of the Collection 5 MODIS dark-target aerosol products over land, *Atmos. Chem. Phys.*, 10,  
1034 10399–10420, doi:10.5194/acp-10-10399-2010, 2010.

1035 [Lee, S. S., Donner, L. J., Phillips, V. T. J. Impacts of aerosol chemical composition on microphysics and](#)  
1036 [precipitation in deep convection, \*Atmospheric Research\*, 94, 220–237, 2009.](#)

1037 [Lee, H.-H., Zheng, X., Qiu, S., and Wang, Y.: Numerical case study of the aerosol–cloud interactions in](#)  
1038 [warm boundary layer clouds over the eastern North Atlantic with an interactive chemistry module, \*Atmos.\*](#)  
1039 [Chem. Phys., 25, 6069–6091, <https://doi.org/10.5194/acp-25-6069-2025>, 2025.](#)

1040 [Leung, G. R., Saleeby, S. M., Sokolowsky, G. A., Freeman, S. W., and van den Heever, S. C.: Aerosol–](#)  
1041 [cloud impacts on aerosol detrainment and rainout in shallow maritime tropical clouds, \*Atmos. Chem.\*](#)  
1042 [Phys., 23, 5263–5278, <https://doi.org/10.5194/acp-23-5263-2023>, 2023.](#)

1043 [Li, G. H., Wang, Y., Zhang, R. Y.: Implementation of a two-moment bulk microphysics scheme to the](#)  
1044 [WRF model to investigate aerosol-cloud interaction, \*Journal of Geophysical Research-Atmospheres\*, 113,](#)  
1045 [D15, <https://doi.org/10.1029/2007JD009361>, 2008.](#)

1046 [Li, Z., et al.: Aerosol and monsoon climate interactions over Asia, \*Rev. Geophys.\*, 54, 866–929,](#)  
1047 [doi:10.1002/2015RG000500, 2016.](#)

1048 [Li, Y., Liu, X., and Cai, H.: Numerical simulation of aerosol concentration effects on cloud droplet size](#)  
1049 [spectrum evolutions of warm stratiform clouds in Jiangxi, China, \*Atmos. Chem. Phys.\*, 24, 13525–13540,](#)  
1050 <https://doi.org/10.5194/acp-24-13525-2024>, 2024.

1051

1052 Liu, Y., Lin, T., Zhang, J., Wang, F., Huang, Y., Wu, X., Ye, H., Zhang, G., Cao, X., and de Leeuw, G.:  
1053 Opposite effects of aerosols and meteorological parameters on warm clouds in two contrasting regions  
1054 over eastern China, *Atmos. Chem. Phys.*, 24, 4651–4673, <https://doi.org/10.5194/acp-24-4651-2024>,  
1055 2024.

1056 Liu, Q., Duan, S. Y., He, Q. S., Chen, Y. H., Zhang, H., Cheng, N. X., Huang, Y. W., Chen, B., Zhan, Q.  
1057 Y., Li, J. Z.: The variability of warm cloud droplet radius induced by aerosols and water vapor in  
1058 Shanghai from MODIS observations, *Atmospheric Research*, 253, 105470, 2021.

1059 [Liu, Q., Shen, X., Li, L., et al. Impacts of Aerosol Chemical Composition on Cloud Condensation Nuclei](#)  
1060 [\(CCN\) Activity during Wintertime in Beijing, China. \*Remote Sens.\*, 15, 4119, 2023.](#)

1061 Liu, T. Q., Liu, Q., Chen, Y. H., Wang, W. C., Zhang, H., Li, D., Sheng, J.: Effect of aerosols on the  
1062 macro- and micro-physical properties of warm clouds in the Beijing-Tianjin-Hebei region. *Science of*  
1063 *the Total Environmen*, 720, 137618, 2020.

1064 Liu, Y., Zhang, J., Zhou, P., Lin, T., Hong, J., Shi, L., Yao, F., Wu, J., Guo, H., and de Leeuw, G.:  
1065 Satellite-based estimate of the variability of warm cloud properties associated with aerosol and  
1066 meteorological conditions, *Atmos. Chem. Phys.*, 18, 18187-18202, [https://doi.org/10.5194/acp-18-](https://doi.org/10.5194/acp-18-18187-2018)  
1067 [18187-2018](https://doi.org/10.5194/acp-18-18187-2018), 2018.

1068 Liu, Y., de Leeuw, G., Kerminen, V.-M., Zhang, J., Zhou, P., Nie, W., Qi, X., Hong, J., Wang, Y., Ding,  
1069 A., Guo, H., Krüger, O., Kulmala, M., and Petäjä, T.: Analysis of aerosol effects on warm clouds over  
1070 the Yangtze River Delta from multi-sensor satellite observations, *Atmos. Chem. Phys.*, 17, 5623-5641,  
1071 <https://doi.org/10.5194/acp-17-5623-2017>, 2017.

1072 Liu, Z., Vaughan, M., Winker, D., Kittaka, C., Getzewich, B., Kuehn, R., Omar, A., Powell, K., Trepte,  
1073 C., and Hostetler, C.: The CALIPSO lidar cloud and aerosol discrimination: Version 2 algorithm and  
1074 initial assessment of performance, *J. Atmos. Ocean. Tech.*, 26, 1198–1213, 2009.

1075 Ma, X., Jia, H., Yu, F., and Quaas, J.: Opposite aerosol index-cloud droplet effective radius correlations  
1076 over major industrial regions and their adjacent oceans, *Geophys. Res. Lett.*, 45, 5771–5778,  
1077 <https://doi.org/10.1029/2018GL077562>, 2018.

1078 Ma, P.-L., P. J. Rasch, M. Wang, H. Wang, S. J. Ghan, R. C. Easter, W. I. Gustafson Jr., X. Liu, Y.  
1079 Zhang, and H.-Y. Ma (2015), How does increasing horizontal resolution in a global climate model  
1080 improve the simulation of aerosol-cloud interactions?, *Geophys. Res. Lett.*, 42, 5058–5065,  
1081 [doi:10.1002/2015GL064183](https://doi.org/10.1002/2015GL064183).

1082 [Marchant, B., et al.: MODIS Collection 6 shortwave-derived cloud phase classification algorithm and](#)  
1083 [comparisons with CALIOP, \*Atmos. Meas. Tech. Discuss.\*, 8, 11893–11924, 2015.](#)

1084 Matheson, M. A., Coakley Jr., J. A., and Tahnk, W. R.: Aerosol and cloud property from relationships  
1085 for summer stratiform clouds in the northeastern Atlantic from advanced very high resolution radiometer  
1086 observations, *J. Geophys. Res.*, 110, D24204, doi:10.1029/2005JD006165, 2005.

1087 McComiskey, A., & Feingold, G: The scale problem in quantifying aerosol indirect effects. *Atmospheric*  
1088 *Chemistry and Physics*, 12, 1031. <https://doi.org/10.5194/acp-12-1031-2012>, 2012.

1089 Meskhidze, N., Nenes, A.: Effects of ocean ecosystem on marine aerosol-cloud interaction. *Adv.*  
1090 *Meteorol*, doi:10.1155/2010/239808, 2010.

1091 [Mohebalhojeh, M., Frederick, S., Riemer, N., & West, M. \(2026\). A Metric for Quantifying Spatial](#)  
1092 [Heterogeneity in Gridded Atmospheric Fields. \*Earth and Space Science\* \(preprint\).](#)

1093 Murray-Watson, R. J. and Gryspeerdt, E.: Stability-dependent increases in liquid water with droplet  
1094 number in the Arctic, *Atmos. Chem. Phys.*, 22, 5743–5756, <https://doi.org/10.5194/acp-22-5743-2022>,  
1095 2022.

1096 McComiskey, A., G. Feingold, A. S. Frisch, D. D. Turner, M. A. Miller, J. C. Chiu, Q. Min, and J. A.  
1097 Ogren (2009), Anassessment of aerosol-cloud interactions in marine stratus clouds based on surface  
1098 remote sensing, *J. Geophys. Res.*, 114, D09203,doi:10.1029/2008JD011006.

1099 [Platnick, S., et al., MODIS Cloud optical properties: User guide for the Collection 6/6.1 level-2](#)  
1100 [MOD06/MYD06 product and associated level-3 data sets. v1.1, July 2018.](#)

1101 [Proestakis, E., Amiridis, V., Marinou, E., Georgoulas, A. K., Solomos, S., Kazadzis, S., Chimot, J., Che,](#)  
1102 [H., Alexandri, G., Biniotoglou, I., Daskalopoulou, V., Kourtidis, K. A., de Leeuw, G., and van der A, R.](#)  
1103 [J.: Nine-year spatial and temporal evolution of desert dust aerosols over South and East Asia as revealed](#)  
1104 [by CALIOP, \*Atmos. Chem. Phys.\*, 18, 1337-1362, https://doi.org/10.5194/acp-18-1337-2018, 2018.](#)

1105 Possner A., ~~E. M.~~ Zubler, ~~E. M.~~ U. Lohmann, ~~U.~~ and ~~C.~~ Schär, ~~C.~~ (2016).: -The resolution dependence  
1106 of cloud effects  
1107 and ship-induced aerosol-cloud interactions in marine stratocumulus, *J. Geophys. Res. Atmos.*, 121,  
1108 4810–4829, doi:10.1002/2015JD024685, [2016.](#)

1109 Pandey, S. K., Vinoj, V., Panwar, A.: The short-term variability of aerosols and their impact on cloud  
1110 properties and radiative effect over the Indo-Gangetic Plain. *Atmospheric Pollution Research*, 11, 630-  
1111 638, 2020.

1112 Platnick, S., Meyer, K. G., King, M. D., Wind, G., Amarasinghe, N., Marchant, B., Arnold, G. T., Zhang,  
1113 Z., Hubanks, P. A., Holz, R. E., Yang, P., Ridgway, W. L., Riedi, J.: The MODIS cloud optical and  
1114 microphysical products: Collection 6 updates and examples from Terra and Aqua. *IEEE Trans Geosci*  
1115 *Remote Sens. Jan*;55(1):502-525. doi: 10.1109/TGRS.2016.2610522, 2017.

1116 Quaas, J., Boucher, O., Bellouin, N., Kinne, S.: Satellite-based estimate of the direct and indirect aerosol  
1117 climate forcing, *J. Geophys. Res.*, 113, D05204, doi:10.1029/2007JD008962, 2008.

1118 Quaas, J., Stevens, B., Stier, P., and Lohmann, U.: Interpreting the cloud cover – aerosol optical depth  
1119 relationship found in satellite data using a general circulation model, *Atmos. Chem. Phys.*, 10, 6129-  
1120 6135, <https://doi.org/10.5194/acp-10-6129-2010>, 2010.

1121 Quaas, J., Boucher, O., and Lohmann, U.: Constraining the total aerosol indirect effect in the LMDZ and  
1122 ECHAM4 GCMs using MODIS satellite data, *Atmos. Chem. Phys.*, 6, 947–955,  
1123 <https://doi.org/10.5194/acp-6-947-2006>, 2006.

1124 Quaas, J., Ming, Y., Menon, S., Takemura, T., Wang, M., Penner, J. E., Gettelman, A., Lohmann, U.,  
1125 Bellouin, N., Boucher, O., Sayer, A. M., Thomas, G. E., McComiskey, A., Feingold, G., Hoose, C.,  
1126 Kristjánsson, J. E., Liu, X., Balkanski, Y., Donner, L. J., Ginoux, P. A., Stier, P., Grandey, B., Feichter,  
1127 J., Sednev, I., Bauer, S. E., Koch, D., Grainger, R. G., Kirkevåg, A., Iversen, T., Seland, Ø., Easter, R.,  
1128 Ghan, S. J., Rasch, P. J., Morrison, H., Lamarque, J.-F., Iacono, M. J., Kinne, S., and Schulz, M.: Aerosol  
1129 indirect effects – general circulation model intercomparison and evaluation with satellite data, *Atmos.*  
1130 *Chem. Phys.*, 9, 8697–8717, <https://doi.org/10.5194/acp-9-8697-2009>, 2009.

1131 Rao, S., Dey, S.: Consistent signal of aerosol indirect and semi-direct effect on water clouds in the  
1132 oceanic regions adjacent to the Indian subcontinent. *Atmospheric Research*, 232, 2020.

1133 Remer, L. A., Kaufman, Y. J., Tanre, D., Mattoo, S., Chu, D. A., Martins, J. V., Li, R. R., Ichoku, C.,  
1134 Levy, R. C., Kleidman, R. G., Eck, T. F., Vermote, E., and Holben, B. N.: The MODIS aerosol algorithm,  
1135 products, and validation, *J. Atmos. Sci.*, 62, 947–973, <https://doi.org/10.1175/JAS3385.1>, 2005.

1136 Rosenfeld, D., Zhu, Y. N., Wang, M. H., Zheng, Y. T., Goren, T., Yu, S. C.: Aerosol-driven droplet  
1137 concentrations dominate coverage and water of oceanic low-level clouds, *Science*, 363, 6427, 2019.

1138 [Sarna, K. and Russchenberg, H. W. J.: Ground-based remote sensing scheme for monitoring aerosol–](#)  
1139 [cloud interactions. \*Atmos. Meas. Tech.\*, 9, 1039–1050, <https://doi.org/10.5194/amt-9-1039-2016>, 2016.](#)

1140 Saponaro, G., Kolmonen, P., Sogacheva, L., Rodriguez, E., Virtanen, T., de Leeus, G.: Estimates of the  
1141 aerosol indirect effect over the Baltic Sea region derived from 12 years of MODIS observations, *Atmos.*  
1142 *Chem. Phys.*, 17, 3133-3143, 2017.

1143 Stephens, G., Vane, D. G., Boain, R. J., Mace, G. G., Sassen, K., Wang, Z., Illingworth, A. J., O'Connor,  
1144 E. J., Rossow, W. B., Durden, S. L., Miller, S. D., Austin, R. T., Benedetti, A., and Mitrescu, C.: The  
1145 CloudSat Science Team: The CloudSat mission and the A-Train, *B. Am. Meteorol. Soc.*, 83, 1771–1790,  
1146 2002.

1147 Sourdeval, O., Laurent C.-Labonnote, Anthony J. Baran, Johannes Mülmenstädt, Gérard Brogniez.: A  
1148 methodology for simultaneous retrieval of ice and liquid water cloud properties. Part 2: Near-global  
1149 retrievals and evaluation against A-Train products, *Quarterly Journal of the Royal Meteorological*  
1150 *Society*, 142, 701, 3063-3081, 2016.

1151 Sundström, A.-M., Kolmonen, P., Sogacheva, L., and de Leeuw, D.: Aerosol retrievals over China with  
1152 the AATSR dual view algorithm, *Remote Sens. Environ.*, 116, 189–198, 2012.

1153 Theodore L. Anderson, Robert J. Charlson, David M. Winker, John A. Ogren, and Kim Holmén.:  
1154 Mesoscale Variations of Tropospheric Aerosols, *Journal of the Atmospheric Sciences*, 60, 1,  
1155 [https://doi.org/10.1175/1520-0469\(2003\)060<0119:MVOTA>2.0.CO;2](https://doi.org/10.1175/1520-0469(2003)060<0119:MVOTA>2.0.CO;2), 2003.

1156 Tang, J., Wang, P., Mickley, L. J., Xia, X., Liao, H., Yue, X., et al.: Positive relationship between liquid  
1157 cloud droplet effective radius and aerosol optical depth over Eastern China from satellite data.  
1158 *Atmospheric Environment*, 44, 244-253. <https://doi.org/10.1016/j.atmosenv.2013.08.024>, 2014.

1159 Tao, W. K., Chen, J. P., Li, Z., Wang, C. E., Zhang, C. D.: Impact of aerosols on convective clouds and  
1160 precipitation, *Reviews of Geophysics*, 50(2), 2012.

1161 [Twomey, S. Pollution and the planetary albedo, \*Atmos. Environ.\*, 1974, 41, 120-125.](#)

1162 Twomey, S.: The influence of pollution on the shortwave albedo of clouds, *J. Atmos. Sci.* 34(7), 1149-  
1163 1152, 1977.

1164 Wang, F., Guo, J., Zhang, J., Wu, Y., Zhang, X., Deng, M., and Li, X.: Satellite observed aerosol-induced  
1165 variability in warm cloud properties under different meteorological conditions over eastern China, *Atmos.*  
1166 *Environ.*, 48, 122–132, 2014.

1167 Wang, F., Guo, J., Zhang, J., Wu, Y., Zhang, X., Deng, M., Li, X.: Satellite observed aerosol-induced  
1168 variability in warm cloud properties under different meteorological conditions over eastern China, *Atmos.*  
1169 *Environ.*, 84, 122-132, 2014.

1170 [Wang, Y., Wang, Y., Song, X., Shang, Y., Zhou, Y., Huang, X., Li, Z.: The impact of particulate pollution](#)  
1171 [control on aerosol hygroscopicity and CCN activity in North China, \*Environmental Research Letters\*, 18,](#)  
1172 [074028, 2023.](#)

1173 Winker, D. M., Pelon, J. R., and McCormick, M. P.: The CALIPSO mission: Spaceborne lidar for  
1174 observation of aerosols and clouds, *Proc. SPIE, Lidar Remote Sensing for Industry and Environment*  
1175 *Monitoring III*, 4893, doi:10.1117/12.466539, 2003.

1176 [Winker, D. M., Hunt, W. H., and McGill, M. J.: Initial performance assessment of CALIOP, \*Geophys.\*](#)  
1177 [\*Res. Lett.\*, 34, L19803, doi:10.1029/2007GL030135, 2007.](#)

1178 [Winker, D. M., Vaughan, M. A., Omar, A., Hu, Y., Powell, K. A., Liu, Z. Y., Hunt, W. H., Young, S.](#)  
1179 [A.: Overview of the CALIPSO Mission and CALIOP Data Processing Algorithms, \*Journal of\*](#)  
1180 [\*Atmospheric and Oceanic Technology\*, 26 \(11\), 2310-2323, 2009. doi:10.1175/2009JTECHA1281.1.](#)

1181 [Winker, D. M., Pelon, J., Coakley Jr, J. A., Ackerman, S. A., Charlson, R. J., Colarco, P. R., Flamant, P.,](#)  
1182 [Fu, Q., Hoff, R. M., Kittaka, C., Kubar, T. L., Le Treut, H., McCormick, M. P., Mégie, G., Poole, L.,](#)  
1183 [Powell, K., Trepte, C., Vaughan, M. A., and Wielicki, B. A.: The CALIPSO Mission. \*Bulletin of\*](#)  
1184 [\*American Meteorological Society\*, 91\(9\), 1211-1230, 2010.](#)

1185 Wang, F., Guo, J., Zhang, J., Huang, J., Min, M., Chen, T., Liu, H., Deng, M., Li, X.: Multi-sensor  
1186 quantification of aerosol-induced variability in warm clouds over eastern China, *Atmos. Environ.*, 113:  
1187 1-9, 2015. <http://dx.doi.org/10.1016/j.atmosenv.2015.04.063>.

1188 Yuan, T., Li, Z., Zhang, R., and Fan, J.: Increase of cloud droplet size with aerosol optical depth: an  
1189 observation and modeling study, *J. Geophys. Res.*, 113, D04201, doi:10.1029/2007JD008632, 2008.

1190 [Zhang, L., Li, J., Li, J., Li, R., Zhang, W., Lei, M., et al.: Studying the impacts of meteorological factors](#)  
1191 [on distribution of cloud horizontal scales based on active satellite, \*Journal of Geophysical Research:\*](#)  
1192 [\*Atmospheres\*, 129, e2024JD041844, <https://doi.org/10.1029/2024JD041844>, 2024.](#)

1193 [Zhang, Q., Meng, J., Quan, J., et al. Impact of aerosol composition on cloud condensation nuclei activity,](#)  
1194 [\*Atmos. Chem. Phys.\*, 12, 3783–3790, 2012.](#)

1195 [Zhao, J., Ma, X., Quaas, J., and Yang, T.: How meteorological conditions influence aerosol-cloud](#)  
1196 [interactions under different pollution regimes, Atmos. Chem. Phys., 25, 17701–17723,](#)  
1197 <https://doi.org/10.5194/acp-25-17701-2025>, 2025.

1198 [Zheng, B., Tong, D., Li, M., Liu, F., Hong, C., Geng, G., Li, H., Li, X., Peng, L., Qi, J., Yan, L., Zhang,](#)  
1199 [Y., Zhao, H., Zheng, Y., He, K., and Zhang, Q.: Trends in China's anthropogenic emissions since 2010](#)  
1200 [as the consequence of clean air actions, Atmos. Chem. Phys., 18, 14095–14111,](#)  
1201 <https://doi.org/10.5194/acp-18-14095-2018>, 2018.

1202 [Zheng, X., Dong, X., Xi, B., Logan, T., and Wang, Y.: Distinctive aerosol–cloud–precipitation](#)  
1203 [interactions in marine boundary layer clouds from the ACE-ENA and SOCRATES aircraft field](#)  
1204 [campaigns, Atmos. Chem. Phys., 24, 10323–10347, https://doi.org/10.5194/acp-24-10323-2024](#), 2024.

1205 [Zheng, X., Xi, B., Dong, X., Logan, T., Wang, Y., and Wu, P.: Investigation of aerosol–cloud interactions](#)  
1206 [under different absorptive aerosol regimes using Atmospheric Radiation Measurement \(ARM\) southern](#)  
1207 [Great Plains \(SGP\) ground-based measurements, Atmos. Chem. Phys., 20, 3483–3501,](#)  
1208 <https://doi.org/10.5194/acp-20-3483-2020>, 2020.

1209  
1210  
1211  
1212  
1213  
1214  
1215  
1216  
1217  
1218  
1219  
1220

1221 [Supplement Appendices](#)

1222 **Table SA1.** Estimates of  $S_{CER}$ , computed using Eq. (1), and correlation coefficients  $R$  between CER and AOD,  
1223 stratified by LWP, and optimal buffer size (see text), for study areas varying from  $4^{\circ} \times 4^{\circ}$  to  $10^{\circ} \times 10^{\circ}$ , during

1224

the periods 2008-2014 and 2015-2022. Statistically significant data points are indicated with \* (p value &lt; 0.01).

Years	LWP (g/m <sup>2</sup> )	Study area	Optimal scale (km)	S <sub>CER</sub>	R
2008-2014	0-55	10°×10°	30	-0.0858	0.8828*
		8°×8°	40	-0.1026	0.9220*
		6°×6°	100	-0.1305	0.8939*
		4°×4°	50	-0.2232	0.8459*
	55-135	10°×10°	40	-0.1275	0.8377*
		8°×8°	60	-0.1587	0.8978*
		6°×6°	30	-0.2061	0.9245*
		4°×4°	50	-0.3189	0.9096*
2015-2022	0-50	10°×10°	80	-0.0885	0.9082*
		8°×8°	40	-0.1138	0.8886*
		6°×6°	20	-0.1517	0.7618*
		4°×4°	50	-0.0863	0.6403*
	50-100	10°×10°	100	-0.1084	0.8717*
		8°×8°	90	-0.1354	0.8910*
		6°×6°	60	-0.1514	0.8384*
		4°×4°	60	-0.2212	0.8318*

1225

1226

[Table SA2](#). Estimates of S<sub>Nd</sub>, computed using Eq. (2), and correlation coefficients R between N<sub>d</sub> and AOD,

1227

stratified by optimal buffer size (see text) for study areas varying from 4°×4° to 10°×10°, during the periods

1228

2008-2014 and 2015-2022. Statistically significant data points are indicated with \* (p value &lt; 0.01).

Years	Study area	Optimal scale (km)	S <sub>Nd</sub>	R
2008-2014	10°×10°	70	0.1434	-0.8507*
	8°×8°	80	0.2045	-0.8646*
	6°×6°	30	0.2430	-0.8741*
	4°×4°	40	0.4496	-0.8523*
2015-2022	10°×10°	60	0.1742	-0.8788*
	8°×8°	60	0.2682	-0.8638*
	6°×6°	20	0.2964	-0.6900*
	4°×4°	30	0.2903	-0.7478*

1229

1230

1231

1232

1233

1234

1235

1236

1237

1238

1239  
 1240  
 1241  
 1242  
 1243  
 1244  
 1245  
 1246  
 1247  
 1248  
 1249  
 1250  
 1251  
 1252  
 1253

**Table S3. Sample sizes of cloud droplet effective radius (CER) and aerosol optical depth (AOD) across different buffer sizes, study areas (LWP regime 1, 2008–2014).**

<u>Buffer sizes</u>	<u>Sample sizes of CER in LWP regime 1</u>				<u>Sample sizes of AOD in LWP regime 1</u>			
	<u>10°×10°</u>	<u>8°×8°</u>	<u>6°×6°</u>	<u>4°×4°</u>	<u>10°×10°</u>	<u>8°×8°</u>	<u>6°×6°</u>	<u>4°×4°</u>
<u>10</u>	<u>25054</u>	<u>16133</u>	<u>8551</u>	<u>3879</u>	<u>47846</u>	<u>32406</u>	<u>18711</u>	<u>8808</u>
<u>20</u>	<u>41667</u>	<u>26507</u>	<u>14077</u>	<u>6376</u>	<u>64878</u>	<u>42949</u>	<u>24462</u>	<u>11377</u>
<u>30</u>	<u>54960</u>	<u>34885</u>	<u>18421</u>	<u>8346</u>	<u>76569</u>	<u>50055</u>	<u>28274</u>	<u>13047</u>
<u>40</u>	<u>66170</u>	<u>42147</u>	<u>22136</u>	<u>9966</u>	<u>86291</u>	<u>56006</u>	<u>31523</u>	<u>14482</u>
<u>50</u>	<u>76207</u>	<u>48769</u>	<u>25738</u>	<u>11593</u>	<u>94726</u>	<u>61227</u>	<u>34272</u>	<u>15664</u>
<u>60</u>	<u>85194</u>	<u>54539</u>	<u>28946</u>	<u>12979</u>	<u>102262</u>	<u>65860</u>	<u>36741</u>	<u>16695</u>
<u>70</u>	<u>93413</u>	<u>59681</u>	<u>31788</u>	<u>14192</u>	<u>108792</u>	<u>69756</u>	<u>38749</u>	<u>17519</u>
<u>80</u>	<u>100728</u>	<u>64370</u>	<u>34330</u>	<u>15317</u>	<u>114357</u>	<u>73103</u>	<u>40498</u>	<u>18246</u>
<u>90</u>	<u>107291</u>	<u>68535</u>	<u>36552</u>	<u>16270</u>	<u>119187</u>	<u>76077</u>	<u>42016</u>	<u>18893</u>
<u>100</u>	<u>113457</u>	<u>72525</u>	<u>38761</u>	<u>17155</u>	<u>123607</u>	<u>78839</u>	<u>43496</u>	<u>19469</u>
<u>120</u>	<u>124793</u>	<u>79882</u>	<u>42945</u>	<u>18964</u>	<u>131449</u>	<u>83807</u>	<u>46217</u>	<u>20534</u>
<u>140</u>	<u>134597</u>	<u>86324</u>	<u>46525</u>	<u>20462</u>	<u>138140</u>	<u>88001</u>	<u>48518</u>	<u>21557</u>
<u>150</u>	<u>138760</u>	<u>89086</u>	<u>48145</u>	<u>21141</u>	<u>141012</u>	<u>89985</u>	<u>49570</u>	<u>21991</u>
<u>160</u>	<u>142693</u>	<u>91808</u>	<u>49602</u>	<u>21734</u>	<u>143725</u>	<u>91767</u>	<u>50570</u>	<u>22436</u>
<u>180</u>	<u>150015</u>	<u>96789</u>	<u>52326</u>	<u>22860</u>	<u>148480</u>	<u>94870</u>	<u>52385</u>	<u>23155</u>
<u>200</u>	<u>156655</u>	<u>101246</u>	<u>54894</u>	<u>23983</u>	<u>153084</u>	<u>97946</u>	<u>53963</u>	<u>23921</u>
<u>250</u>	<u>169423</u>	<u>109475</u>	<u>59449</u>	<u>26008</u>	<u>162530</u>	<u>104346</u>	<u>56987</u>	<u>25388</u>
<u>300</u>	<u>178015</u>	<u>115051</u>	<u>62656</u>	<u>27442</u>	<u>170117</u>	<u>109006</u>	<u>59332</u>	<u>26453</u>

1254  
 1255  
 1256

**Table S4. Sample sizes of cloud droplet effective radius (CER) and aerosol optical depth (AOD) across different buffer sizes, study areas (LWP regime 2, 2008–2014).**

<u>Buffer sizes</u>	<u>Sample sizes of CER in LWP regime 2</u>				<u>Sample sizes of AOD in LWP regime 2</u>			
	<u>10°×10°</u>	<u>8°×8°</u>	<u>6°×6°</u>	<u>4°×4°</u>	<u>10°×10°</u>	<u>8°×8°</u>	<u>6°×6°</u>	<u>4°×4°</u>

<u>10</u>	<u>22338</u>	<u>14357</u>	<u>7737</u>	<u>3715</u>	<u>47846</u>	<u>32406</u>	<u>18711</u>	<u>8808</u>
<u>20</u>	<u>35406</u>	<u>22471</u>	<u>11964</u>	<u>5697</u>	<u>64878</u>	<u>42949</u>	<u>24462</u>	<u>11377</u>
<u>30</u>	<u>45473</u>	<u>28805</u>	<u>15162</u>	<u>7187</u>	<u>76569</u>	<u>50055</u>	<u>28274</u>	<u>13047</u>
<u>40</u>	<u>54074</u>	<u>34078</u>	<u>17839</u>	<u>8368</u>	<u>86291</u>	<u>56006</u>	<u>31523</u>	<u>14482</u>
<u>50</u>	<u>61579</u>	<u>38732</u>	<u>20290</u>	<u>9444</u>	<u>94726</u>	<u>61227</u>	<u>34272</u>	<u>15664</u>
<u>60</u>	<u>68173</u>	<u>43017</u>	<u>22553</u>	<u>10424</u>	<u>102262</u>	<u>65860</u>	<u>36741</u>	<u>16695</u>
<u>70</u>	<u>74272</u>	<u>46909</u>	<u>24584</u>	<u>11230</u>	<u>108792</u>	<u>69756</u>	<u>38749</u>	<u>17519</u>
<u>80</u>	<u>79999</u>	<u>50507</u>	<u>26412</u>	<u>11950</u>	<u>114357</u>	<u>73103</u>	<u>40498</u>	<u>18246</u>
<u>90</u>	<u>85339</u>	<u>53806</u>	<u>28177</u>	<u>12654</u>	<u>119187</u>	<u>76077</u>	<u>42016</u>	<u>18893</u>
<u>100</u>	<u>90440</u>	<u>56944</u>	<u>29812</u>	<u>13329</u>	<u>123607</u>	<u>78839</u>	<u>43496</u>	<u>19469</u>
<u>120</u>	<u>99758</u>	<u>62598</u>	<u>32673</u>	<u>14486</u>	<u>131449</u>	<u>83807</u>	<u>46217</u>	<u>20534</u>
<u>140</u>	<u>108723</u>	<u>68273</u>	<u>35600</u>	<u>15795</u>	<u>138140</u>	<u>88001</u>	<u>48518</u>	<u>21557</u>
<u>150</u>	<u>112740</u>	<u>70969</u>	<u>36864</u>	<u>16426</u>	<u>141012</u>	<u>89985</u>	<u>49570</u>	<u>21991</u>
<u>160</u>	<u>116558</u>	<u>73463</u>	<u>38046</u>	<u>16974</u>	<u>143725</u>	<u>91767</u>	<u>50570</u>	<u>22436</u>
<u>180</u>	<u>123653</u>	<u>78031</u>	<u>40203</u>	<u>17917</u>	<u>148480</u>	<u>94870</u>	<u>52385</u>	<u>23155</u>
<u>200</u>	<u>129864</u>	<u>81813</u>	<u>42186</u>	<u>18674</u>	<u>153084</u>	<u>97946</u>	<u>53963</u>	<u>23921</u>
<u>250</u>	<u>142429</u>	<u>89112</u>	<u>46079</u>	<u>20120</u>	<u>162530</u>	<u>104346</u>	<u>56987</u>	<u>25388</u>
<u>300</u>	<u>152460</u>	<u>95213</u>	<u>49452</u>	<u>21369</u>	<u>170117</u>	<u>109006</u>	<u>59332</u>	<u>26453</u>

1257

1258

1259

**Table S5. Sample sizes of cloud droplet effective radius (CER) and aerosol optical depth (AOD) across different buffer sizes, study areas (LWP regime 1, 2015–2022).**

<u>Buffer sizes</u>	<u>Sample sizes of CER in LWP regime 1</u>				<u>Sample sizes of AOD in LWP regime 1</u>			
	<u>10°×10°</u>	<u>8°×8°</u>	<u>6°×6°</u>	<u>4°×4°</u>	<u>10°×10°</u>	<u>8°×8°</u>	<u>6°×6°</u>	<u>4°×4°</u>
<u>10</u>	<u>25054</u>	<u>16133</u>	<u>8551</u>	<u>3879</u>	<u>47846</u>	<u>32406</u>	<u>18711</u>	<u>8808</u>
<u>20</u>	<u>41667</u>	<u>26507</u>	<u>14077</u>	<u>6376</u>	<u>64878</u>	<u>42949</u>	<u>24462</u>	<u>11377</u>
<u>30</u>	<u>54960</u>	<u>34885</u>	<u>18421</u>	<u>8346</u>	<u>76569</u>	<u>50055</u>	<u>28274</u>	<u>13047</u>
<u>40</u>	<u>66170</u>	<u>42147</u>	<u>22136</u>	<u>9966</u>	<u>86291</u>	<u>56006</u>	<u>31523</u>	<u>14482</u>
<u>50</u>	<u>76207</u>	<u>48769</u>	<u>25738</u>	<u>11593</u>	<u>94726</u>	<u>61227</u>	<u>34272</u>	<u>15664</u>
<u>60</u>	<u>85194</u>	<u>54539</u>	<u>28946</u>	<u>12979</u>	<u>102262</u>	<u>65860</u>	<u>36741</u>	<u>16695</u>
<u>70</u>	<u>93413</u>	<u>59681</u>	<u>31788</u>	<u>14192</u>	<u>108792</u>	<u>69756</u>	<u>38749</u>	<u>17519</u>
<u>80</u>	<u>100728</u>	<u>64370</u>	<u>34330</u>	<u>15317</u>	<u>114357</u>	<u>73103</u>	<u>40498</u>	<u>18246</u>
<u>90</u>	<u>107291</u>	<u>68535</u>	<u>36552</u>	<u>16270</u>	<u>119187</u>	<u>76077</u>	<u>42016</u>	<u>18893</u>
<u>100</u>	<u>113457</u>	<u>72525</u>	<u>38761</u>	<u>17155</u>	<u>123607</u>	<u>78839</u>	<u>43496</u>	<u>19469</u>
<u>120</u>	<u>124793</u>	<u>79882</u>	<u>42945</u>	<u>18964</u>	<u>131449</u>	<u>83807</u>	<u>46217</u>	<u>20534</u>
<u>140</u>	<u>134597</u>	<u>86324</u>	<u>46525</u>	<u>20462</u>	<u>138140</u>	<u>88001</u>	<u>48518</u>	<u>21557</u>
<u>150</u>	<u>138760</u>	<u>89086</u>	<u>48145</u>	<u>21141</u>	<u>141012</u>	<u>89985</u>	<u>49570</u>	<u>21991</u>
<u>160</u>	<u>142693</u>	<u>91808</u>	<u>49602</u>	<u>21734</u>	<u>143725</u>	<u>91767</u>	<u>50570</u>	<u>22436</u>
<u>180</u>	<u>150015</u>	<u>96789</u>	<u>52326</u>	<u>22860</u>	<u>148480</u>	<u>94870</u>	<u>52385</u>	<u>23155</u>
<u>200</u>	<u>156655</u>	<u>101246</u>	<u>54894</u>	<u>23983</u>	<u>153084</u>	<u>97946</u>	<u>53963</u>	<u>23921</u>
<u>250</u>	<u>169423</u>	<u>109475</u>	<u>59449</u>	<u>26008</u>	<u>162530</u>	<u>104346</u>	<u>56987</u>	<u>25388</u>

1260

1261

1262

**Table S6. Sample sizes of cloud droplet effective radius (CER) and aerosol optical depth (AOD) across different buffer size, study areas (LWP regime 2, 2015–2022).**

<b>Buffer sizes</b>	<b>Sample sizes of CER in LWP regime 2</b>				<b>Sample sizes of AOD in LWP regime 2</b>			
	<b>10°×10°</b>	<b>8°×8°</b>	<b>6°×6°</b>	<b>4°×4°</b>	<b>10°×10°</b>	<b>8°×8°</b>	<b>6°×6°</b>	<b>4°×4°</b>
10	6548	6548	5449	2803	12892	12892	12892	5961
20	24886	16258	8833	4421	46067	30536	17623	8079
30	32260	20786	11214	5490	55767	36685	20780	9408
40	38784	24739	13284	6440	63457	41493	23310	10474
50	44831	28399	15176	7183	70030	45443	25423	11419
60	50181	31609	16909	7816	75667	48900	27138	12122
70	54865	34476	18456	8415	80872	51807	28559	12723
80	58946	37042	19776	8901	85308	54361	29846	13245
90	62835	39437	21006	9359	89202	56659	31024	13706
100	66623	41757	22165	9796	92939	58931	32143	14126
120	73427	46010	24248	10605	99298	62674	34081	14927
140	79486	49854	26210	11312	104540	65994	36013	15617
150	82336	51650	26988	11633	107089	67545	36876	15939
160	85055	53440	27893	11942	109626	69104	37718	16261
180	89669	56388	29401	12520	114187	72088	39380	16889
200	93898	58986	30700	13034	117969	74508	40596	17401
250	102933	64417	33649	14040	125590	79489	43005	18271
300	109964	68913	35755	14701	132000	83404	45012	18913

1263

1264

**Table S7. Sample sizes of cloud droplet number concentration (N<sub>d</sub>) and aerosol optical depth (AOD) across different buffer sizes and study areas during 2008-2014.**

1265

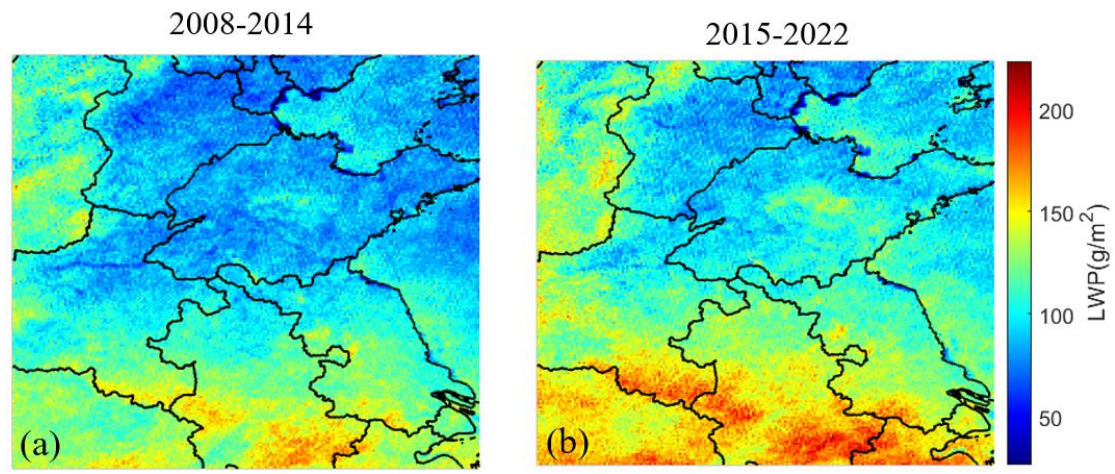
<b>Buffer sizes</b>	<b>Sample sizes of N<sub>d</sub></b>				<b>Sample sizes of AOD</b>			
	<b>10°×10°</b>	<b>8°×8°</b>	<b>6°×6°</b>	<b>4°×4°</b>	<b>10°×10°</b>	<b>8°×8°</b>	<b>6°×6°</b>	<b>4°×4°</b>
10	47846	32406	18711	8808	50686	32611	17320	8053
20	64878	42949	24462	11377	70102	45066	23944	11084
30	76569	50055	28274	13047	84442	54334	28822	13435
40	86291	56006	31523	14482	96186	62056	32857	15309
50	94726	61227	34272	15664	106166	68620	36473	16906
60	102262	65860	36741	16695	114950	74328	39638	18292
70	108792	69756	38749	17519	122840	79508	42510	19478
80	114357	73103	40498	18246	129763	84048	45038	20599
90	119187	76077	42016	18893	135810	87931	47225	21548
100	123607	78839	43496	19469	141407	91543	49256	22436
120	131449	83807	46217	20534	151353	98040	53031	24145
140	138140	88001	48518	21557	159758	103516	56167	25517
150	141012	89985	49570	21991	163180	105820	57561	26100
160	143725	91767	50570	22436	166373	108000	58769	26661
180	148480	94870	52385	23155	172007	111773	60981	27665
200	153084	97946	53963	23921	176658	114922	62862	28696
250	162530	104346	56987	25388	185393	120627	66331	30409
300	170117	109006	59332	26453	191138	124592	68823	31481

1266  
1267  
1268

**Table S8. Sample sizes of cloud droplet number concentration ( $N_d$ ) and aerosol optical depth (AOD) across different buffer sizes and study areas during 2015-2022.**

Buffer sizes	Sample sizes of $N_d$				Sample sizes of AOD			
	$10^\circ \times 10^\circ$	$8^\circ \times 8^\circ$	$6^\circ \times 6^\circ$	$4^\circ \times 4^\circ$	$10^\circ \times 10^\circ$	$8^\circ \times 8^\circ$	$6^\circ \times 6^\circ$	$4^\circ \times 4^\circ$
10	37182	23994	13048	6149	31621	21503	12892	5961
20	51313	32990	17755	8252	46067	30536	17623	8079
30	61921	39800	21327	9788	55767	36685	20780	9408
40	70663	45351	24213	11063	63457	41493	23310	10474
50	78059	50080	26808	12118	70030	45443	25423	11419
60	84354	53975	28967	13015	75667	48900	27138	12122
70	89675	57448	30881	13832	80872	51807	28559	12723
80	94620	60671	32636	14556	85308	54361	29846	13245
90	99042	63497	34138	15155	89202	56659	31024	13706
100	102936	65993	35444	15703	92939	58931	32143	14126
120	110590	70884	38002	16787	99298	62674	34081	14927
140	116487	74472	40007	17549	104540	65994	36013	15617
150	119140	76230	41049	17958	107089	67545	36876	15939
160	121506	77846	41958	18265	109626	69104	37718	16261
180	125788	80845	43582	18935	114187	72088	39380	16889
200	129613	83370	44887	19538	117969	74508	40596	17401
250	136752	87967	47756	20784	125590	79489	43005	18271
300	141896	91273	49807	21431	132000	83404	45012	18913

1269  
1270



1271  
1272  
1273  
1274  
1275

**Figure S1. Spatial distributions of LWP averaged over the years 2008-2014 (a) and 2015-2022 (b) over the study area. The lines are provincial borders and the names of provinces mentioned in the text are indicated in Fig. 3(f).**